12-12-2019 10:00 AM

Spatial and Temporal Characteristics of Temperature-Precipitation Covariability across Canada in a Changing Climate

Harsimrenjit Singh
The University of Western Ontario

Supervisor
Najafi, Reza, M.
The University of Western Ontario

Graduate Program in Civil and Environmental Engineering
A thesis submitted in partial fulfillment of the requirements for the degree in Master of Engineering Science

Abstract

Changes in the regional characteristics of temperature and precipitation can intensify the occurrence and severity of extreme events such as rain-on-snow induced flooding, droughts and wildfires. Analyzing these climate variables in isolation without considering their interdependencies might result in severe underestimation of their combined effects. In this study, copula functions are used to describe the joint behaviour of temperature and precipitation across Canada over a historical period of 1910-present using observations and further till the end of 21st century using three large ensembles of regional climate models. Moreover, given the lack of observation data over Canada, gridded datasets are also evaluated under both univariate and bivariate settings. The importance of preserving the dependence structure is shown through a hydrologic model forced with multivariate bias corrected data. Climate projections are evaluated against observations using a hierarchical Bayesian framework followed by calculation of extreme climate indices over four future warming scenarios corresponding to +1.5, +2.0, +3.0 and +4.0°C mean temperature rise above the pre-industrial period. Finally, an ensemble pooling approach is applied to calculate non-stationary return periods of compound extreme events.

Results show clear signs of accelerated warming and wetting over northern Canada and strong evidence of hot and dry conditions in Prairie Provinces while non-stationary analyses reveal shifts towards warm and wet climate conditions for the rest of southern Canada. Results from the comparison of multiple gridded datasets show that while they represent temperature and precipitation well, their performance in simulating the joint behavior is relatively weak. Hydrological modelling results indicate that the multivariate

bias correction of the input datasets can improve streamflow simulations particularly extreme events compared to the univariate approach. Climate projections show an increase in warm spells in the future accompanied with an increase in extreme precipitation as well for most regions in Canada. The importance of considering the dependence of temperature and precipitation extremes in calculating joint return periods reveals potential future changes in the frequency of compound extremes. Overall, this study provides a comprehensive characterization of the joint behavior of temperature and precipitation over Canada under a changing climate.

Keywords

Compound Events, Copula, Temperature, Precipitation, Joint Variability, Hydrologic Model, Hierarchical Bayesian Model, Multivariate Bias Correction, Regional Climate Models, Large Ensembles.

Lay Summary

Temperature and precipitation are two important climate variables that directly affect societies. Whereas temperature extremes in the form of very hot summers or very cold winters can cause socioeconomic disruptions, precipitation extremes cause floods, snow storms and droughts. These events are not independent from each other and are almost always jointly caused by both temperature and precipitation exceeding some thresholds. Floods caused by rain falling over frozen ground, heatwaves adding to the intensity of droughts and wildfire risk increasing due to extended hot-dry periods are some examples of *compound events* caused by temperature and precipitation jointly. To study this behavior comprehensively for historical and future periods over Canada, state-of-the-art statistical methods are applied, which are able to capture the complete dependence structure of both variables. The analysis of multiple gridded historical data show that they are not very reliable in capturing this dependency. The potential impact of this drawback is revealed by running a hydrologic model, which produces unreliable outputs in comparison to the same model, if run with data from which biases have been removed. Analysis of future temperature and precipitation dependence under climate change is conducted using three large ensembles of regional climate model simulations that project these two variables until the end of the 21st century. The accuracy of projections is validated against observations revealing that methods which correct the dependence structure of simulated temperature and precipitation should be preferred over methods that adjust these variables in isolation. Next, we determine how frequent extreme compound events would occur when the dependence between the variables is considered and how this frequency can change in the future. The study provides comprehensive information on the relationship between

temperature and precipitation and its potential impacts in the future under a changing climate.

Co-Authorship Statement

This Integrated Article dissertation consists of four distinct pieces of work (Chapter 3 – Chapter 6). The following section briefly illustrates the contribution of co-authors to each chapter. All other chapters besides the following were written by the author.

Contributions in Chapter 3

Besides the primary author, two other co-authors have provided contributions to chapter 3, Farshad J Pirani and Mohammad Reza Najafi. The primary author was responsible for majority of the underlying data analysis, statistical modeling, writing the manuscript and generating figures. Pirani's contribution came in the form of preliminary data analysis as well as help in conceptual development of copula framework. Najafi's contributions were in refining the manuscript text by providing constructive feedback and providing guidance to the author in theoretical concepts.

This work is accepted for publication in the journal of *Theoretical and Applied Climatology*.

Contributions in Chapter 4

Najafi helped develop the statistical framework and revised the manuscript. Data analyses, statistical modeling, generating results and writing the manuscript draft were done by Singh. The work was submitted for publication in *Journal of Hydrology* in November 2019.

Contributions in Chapter 5

Najafi's contributions came in the form of manuscript revisions and helping develop the theoretical concepts of the work while Cannon provided bias corrected climate datasets for

the study. Singh was responsible for developing the overall framework, writing the manuscript, modeling and generating results.

This work is under (internal) review.

Contributions in Chapter 6

Similar to Chapter 5.

Contributing Members

Mohammad Reza Najafi, Dept. of Civil and Environmental Engineering, Western University, ON

Alex Cannon, Environment and Climate Change Canada, Victoria, BC

Farshad Jalili Pirani, Dept. of Civil and Environmental Engineering, Western University, ON

Acknowledgement

I will start by acknowledging my supervisor, Dr. Mohammad Reza Najafi who gave me the opportunity to work under his guidance. His method of supervision greatly complemented the way I like to work, by subtly nudging me towards new challenges and giving me opportunities beyond just research. I am also thankful to my research group members for constructive feedbacks throughout these two years.

I would like to thank Western University, as an institution, for providing an excellent infrastructure for a graduate student to thrive. I would also like to thank Alex Cannon from Environment and Climate Change Canada (ECCC) for supplementing majority of the data for this work.

I would also like to thank the open-source community who provide tools, knowledge and a support group making science more accessible to people. This includes open-source software developers, professors all around the world who make their course work public and all the anonymous participants of reputed online communities dedicated to collaborative QnA. I would particularly like to thank Dr. Richard McElreath, whose book Statistical Rethinking greatly influenced my outlook towards research.

I am thankful to the members of the examination committee, Dr. Girma Bitsuamlak, Dr. Wenxing Zhou and Dr. Camila de Souza for reviewing this dissertation.

Finally, I am thankful to my family and friends for supporting me through this journey.

This thesis is dedicated to my parents,

Gurmej Singh and Paramjeet Kaur;

My sister,

Manpreet Kaur;

and to

Simran Gharial.

Table of Contents

Tables

Figures

Acronyms

AHCCD	Adjusted and Homogenized Canadian Climate Data
AIC	Akaike Information Criterion
AICc	Corrected Akaike Information Criterion
ANUSPLIN	Australian National University Splines
AR5	Fifth Assessment Report
ARDA	Agricultural and Rural Development Act
BIC	Bayesian Information Criterion
CanAM4	The Fourth Generation Canadian Atmospheric Global Climate Model
CanESM2	The Second Generation Earth System Model
CanLEAD	Canadian Large Ensembles Adjusted Dataset
CanRCM4	Canadian Regional Climate Model
CaPA	Canadian Precipitation Analysis
C-C Relationship	Clausius-Clapeyron Relationship
CCCma	Canadian Centre for Climate Modelling and Analysis
CCCR	Canada's Changing Climate Report
CDF	Cumulative Distribution Function
CFSR	Climate Forecast System Reanalysis
CMIP5	Coupled Model Inter-comparison Project
CORDEX	The Coordinated Regional climate Downscaling Experiment
CRCM	Canadian Regional Climate Model
CRU-TS	Climatic Research Unit Timeseries
CWD	Consecutive Wet Days

DQM	Detrended Quantile Mapping
E2OBS	EartH2Observe Forcing Data
ECMWF	The European Centre for Medium-Range Weather Forecasts
ERA-40	40-year European Reanalysis
ESS	Effective Sample Size
ETCCDI	Expert Team on Climate Change Detection and Indices
EWEMBI	EartH2Observe, WFDEI and ERA-Interim data Merged and Bias-corrected for ISIMIP
GCM	Global Climate Model
GHG	Greenhouse Gases
GOF Test	Goodness of Fit Test
GPCC	Global Precipitation Climatology Centre
GPGP	Global Precipitation Climatology Project
GRASP	Global Risk Assessment toward Stable Production of Food
HadCM3	Third Hadley Centre Coupled Model
HMC	Hamiltonian Monte Carlo
HRU	Hydrological Response Unit
IPCC	Inter-governmental Panel on Climate Change
ISIMIP	Inter-Sectoral Impact Model Inter-comparison Project
ISIMIP3BASD	ISIMIP-Bias Adjustment and Statistical Downscaling
JRA-25	25-year Japanese Reanalysis
JRA-55	55-year Japanese Reanalysis
KGE	Kling-Gupta Efficiency

MAE	Mean Absolute Error
MBCn	N-dimensional Multivariate Bias Correction
MBCp	Multivariate Bias Correction – Pearson's correlation
MBCr	Multivariate Bias Correction – Spearman's rank correlation
MBE	Mean Absolute Error
MCMC	Markov Chain Monte Carlo
MERRA	Modern-Era Retrospective analysis for Research and Applications
MLE	Maximum Likelihood Estimation
MPL	Maximum Pseudo Likelihood
NARR	North American Regional Reanalysis
NASA	National Aeronautics and Space Administration
NCAR	National Center for Atmospheric Research
NCDA	National Climate Data Archive
NCEP	National Centers for Environmental Prediction
NRCANmet	Natural Resources Canada Meteorological Dataset
NUTS	No U-Turn Sampler
PCIC	Pacific Climate Impacts Consortium
PI Period	Pre-Industrial Period
POD	Probability of Detection
PRCPTOT	Annual total precipitation on wet days
QDM	Quantile Delta Mapping
RCM	Regional Climate Model
RDAS	Regional Data Assimilation System

RMSE	Root Mean Square Error
ROS Events	Rain-on-Snow Events
S14FD	S14 Global Meteorological Forcing Dataset
SRB	Surface Radiation Budget
SWE	Snow Water Equivalent
TNx	Monthly maximum value of daily minimum temperature
TPI	Temperature-Precipitation Index
TXx	Monthly maximum value of daily maximum temperature
US	United States
WSDI	Warm Spell Duration Index

Chapter 1. Introduction

1.1 Temperature and Precipitation Covariability

Understanding of atmospheric processes is the first step towards realizing that temperature and precipitation interact with each other. An increase in temperature causes evaporation, which in turn causes the moisture content of the air to rise and eventually, the excess moisture returns to land in the form of precipitation. At the macro and micro scales however, there are numerous other factors (wind direction, wind speed, topography, ocean temperature, large-scale circulations etc.) intertwined into the process. Thus, one cannot simply deduce a one-to-one causation between changes in temperature leading to changes in precipitation. Indeed, some degree of causation does exist, and studies have shown that the causation is potentially bidirectional (Barbero et al. 2018). Whereas temperature causes changes to precipitation through the evaporation process, precipitation also causes changes in temperature with factors such as increased albedo over the region due to cloud cover and sudden drops in temperature due to precipitation's cooling effect.

Evidence of this two-way causality between temperature and precipitation can be seen in the form of correlation. Correlation may not always imply causation but a causal process driven by physical reasoning can be expected to 'leave its traces' in the data in the form of correlation. This correlation can take several forms such as a purely linear dependence between two variables, which has been the focus of many studies that have analysed the relationship between temperature and precipitation or, the dependence may be non-linear.

Three key statements from Canada's Changing Climate Report (Bush and Lemmen, 2019), are critical to describe the motivation behind studying temperature and precipitation jointly:

- *"It is virtually certain that Canada's climate has warmed and that it will warm further in the future. Both the observed and projected increases in mean temperature in Canada are about twice the corresponding increases in the global mean temperature, regardless of emission scenario."*
- *"There is medium confidence that annual mean precipitation has increased, on average, in Canada, with larger percentage increases in northern Canada."*
- *"The changing frequency of temperature and precipitation extremes can be expected to lead to a change in the likelihood of events such as wildfires, droughts, and floods."*

The report provides further evidence on specific events caused by interactions of temperature and precipitation that, to some degree, were affected by anthropogenic climate change. A few examples of compound events caused by temperature and precipitation covariability are Rain-on-Snow (ROS) floods, droughts caused by extended dry periods happening simultaneously with high temperature, increase in intensity of extreme precipitation events caused by increase in moisture holding capacity of the air because of air temperature rise, and wildfires which are exacerbated by extended periods of low moisture and high temperature increasing the amount of combustible material available to the fire. Collectively, all these events take a heavy toll on Canada every year, in the form of resources that are invested in prevention, mitigation, post-disaster restoration and even

leading to fatalities in extreme cases (See further details on damage caused by combinations of temperature and precipitation extreme events in Chapter 4).

Thus, a deeper understanding of the covariability between temperature and precipitation is required. More importantly, given an inevitable rise in temperatures around the globe, coupled with the fact that Canada is warming at a faster rate compared to the global average, it is critical to identify which regions are expected to bear the brunt of compound events in Canada.

1.2 Research Objectives

The overall objective of this study is to characterize the nonstationary individual and joint behavior of temperature and precipitation under climate change. Under this, the first objective is to perform a complete characterization of historical dependence between the two variables at different temporal scales using ground-based observations. The second objective is to evaluate temperature and precipitation covariability based on global and regional gridded datasets and its implications on hydrologic simulations. The third objective is to assess projected changes in extreme temperature and precipitation and quantify the corresponding uncertainties using large ensembles of regional climate model simulations. And finally, the fourth objective is to assess the non-stationarity in joint projections of temperature and precipitation till the end of 21st century using a large-ensemble pooling approach.

Some of the research questions that are addressed in this study include:

1. How can biases in individual variables be isolated from biases in their dependence structure and further, how can the impacts of these different biases be quantified?

2. Is there an added value for performing multivariate bias correction of climate projections?
3. How can the effect of changes in dependence structure be studied in a non-stationary setting?
4. How can uncertainties across an ensemble of climate projections be studied without loss of information?

Each objective in this research is aimed at addressing existing research gaps within the overall framework and the following section provides a deeper discussion into the motivation behind them.

1.2.1 Characterizing past dependence using historical data

Canada is a relatively under-studied region in terms of joint variability of temperature and precipitation. In one of the earliest studies on this topic in Canada, Isaac and Stuart (1992) highlight examples of analysis conducted over United States but none over Canada. Since then, there have been a few prominent research developments in this area (Tencer et al. 2014; Vincent and Mekis, 2006; Zhang et al. 2011). These developments however have either analysed only the linear relationship between the two variables, compared long term trends or compared concurrent exceedances of univariate thresholds (see further details on these methods in Chapter 2). Although this leads to valuable information about their joint behavior, it does not represent the full dependence structure as the assumption of linearity may not hold in this application. The most robust method of studying the dependence between two variables is to explore the full underlying bivariate distribution which can capture several hidden aspects of the dependency.

In order to achieve this, the first objective is to establish the joint dependency between temperature and precipitation using a set of reliable observation data spread across Canada. To be perceived almost as an exploratory step of research where limited prior knowledge of the dependence structure is available, especially when the assumption of linearity is abandoned, the analysis is conducted for different time scales to identify how dependence changes from one temporal resolution to another, as well as using different statistical methods. This will help establish a *ground truth* of temperature and precipitation covariability using reliable historical data.

1.2.2 Filling in the gaps

The density of stations recording climate data is commonly low. In Canada, most climate stations are concentrated in lower latitudes while stations above 60°N are quite rare (Further details on station density in Canada are provided in Chapter 4). Moreover, these observation data are marred with long temporal gaps and inconsistencies caused by climatic factors such as wind undercatch and non-climatic factors such as human errors and station relocations. To avoid these spatial and temporal gaps, interpolated data, reanalysis and satellite products are commonly used as "observations" in applications such as calculation of weather indices, hydrological modeling and downscaling of climate projections. How well do these datasets represent ground-based observations? In a univariate setting, this question has been addressed to some extent but how well do these data capture the dependence between observed climate variables is still an open question.

In order to address this research gap, gridded "observation" datasets are evaluated under both univariate as well as bivariate settings. Moreover, the potential impacts of the

breakdown of dependence structure between temperature and precipitation on applications driven by these data are identified.

1.2.3 Characterizing future dependence using climate projections

Climate projections generated by General Circulation Models (GCMs) and their corresponding downscaled and bias-corrected products are used to assess potential impacts of climate change in the future. There is great interest in exploring the impacts of an accelerated warming over Canada and, how these changes will interact with changes in future precipitation. To address these questions, a reliable set of future climate projections are needed. GCM bias correction is commonly performed using univariate approaches which are able to correct for biases in individual distributions of temperature and precipitation but can break down the dependence structure of correlated variables. These univariate bias corrected simulations can lead to errors in estimating climate change impacts on hydrologic processes, especially when the impact is the result of two or more interacting variables. Will bias correcting future projections using multivariate bias correction methods create a better understanding of compound events in the future? How will the 21st century look like from the perspective of temperature and precipitation changes?

In order to address these questions, biases in future climate projections are investigated comprehensively, under both univariate and bivariate settings. Next, the likelihood of compound extreme events is explored under an inevitably changing, non-stationary climate.

1.3 Thesis Outline

Chapter 2 covers a brief literature review of existing research on temperature and precipitation covariability, different statistical methods used and their limitations and potential solutions. Sources of future projections of climate are also discussed along with methods of quantifying uncertainty in inferences drawn from the projections.

Chapter 3 addresses research objective 1, in which an adjusted and homogenized observation dataset of temperature and precipitation is analysed and the dependence is characterized using copulas at different time-scales. Non-stationarity in the dependence structure is analysed using long historical records from 1910-2017 and moving-window copula analysis. Further, the response of extreme precipitation to temperature is studied using the Clausius-Clapeyron relationship.

Chapter 4 addresses research objective 2, in which five gridded climate datasets are compared to the observation data used in chapter 3. The comparison is done in both univariate and bivariate settings. Then, the gridded datasets are corrected for biases using univariate and multivariate bias correction methods to study how the respective biases propagate through a hydrological model.

Chapter 5 addresses research objective 3, in which three large ensembles of climate simulations are used, two of which are bias corrected using a novel multivariate bias correction method. In chapter 5, the datasets are compared to a gridded observation data used in chapter 4 following which projections of extreme climate indices are calculated under future warming scenarios. The uncertainty of each individual run of the large ensembles is explored using a hierarchical Bayesian framework.

Objective 4 is covered in chapter 6, where the focus is shifted to characterizing the bivariate structure exhibited by the ensembles. First, the ability of the models to capture dependence exhibited by gridded observations is tested using a formal goodness of fit test for copulas. Then, the joint return periods of extreme events are analysed using a non-stationary framework that pools information across the entire ensemble. The ensemble uncertainty is estimated using a Bayesian method.

1.4 References

Barbero, R., Westra, S., Lenderink, G., & Fowler, H. J. (2018). Temperature-extreme precipitation scaling: a two-way causality?. International Journal of Climatology, 38, e1274-e1279.

Bush E, Lemmen DS (2019) Canada's Changing Climate Report; Government of Canada, Ottawa, ON pp 444

Isaac, G. A., & Stuart, R. A. (1992). Temperature–precipitation relationships for Canadian stations. Journal of climate, 5(8), 822-830.

Tencer, B., Weaver, A., & Zwiers, F. (2014). Joint occurrence of daily temperature and precipitation extreme events over Canada. Journal of Applied Meteorology and Climatology, 53(9), 2148-2162.

Vincent, L. A., & Mekis, E. (2006). Changes in daily and extreme temperature and precipitation indices for Canada over the twentieth century. Atmosphere-Ocean, 44(2), 177-193.

Zhang, X., Vincent, L. A., Hogg, W. D., & Niitsoo, A. (2000). Temperature and precipitation trends in Canada during the 20th century. Atmosphere-ocean, 38(3), 395-429.

Chapter 2. Literature Review

2.1 Quantifying Dependence

2.1.1 Correlation

Studying the presence of correlation is the first step towards identifying a relationship between two variables. Whether the correlation comes from causation or not depends on the researcher's knowledge of the underlying processes. As stated in Chapter 1, understanding of the physical atmospheric processes provides substantial motivation for stating the hypothesis that temperature and precipitation exhibit inter-dependence. Indeed, evidence for this hypothesis has been provided in several studies around the world. The earliest correlation studies between temperature and precipitation were conducted by Blair (1931), Hamrick and Martin (1941), Crutcher (1976), and Madden and Williams (1978). These studies were conducted over the United States at varying temporal scales such as monthly means or seasonal means. The overall outcome from these early studies is that besides significant spatial variations, temperature and precipitation correlation also varies extensively from season to season with usually negative correlations observed in the summer and positive in winter.

Over Canada, Isaac and Stuart (1992) studied the relationship between daily temperature and daily precipitation at 56 locations in Canada. They summarized the results over a 30-year period of 1951-1980 using Temperature-Precipitation Index (TPI), which is used to find the percentage of precipitation occurring below the median daily temperature. They reported higher precipitation occurring at warmer temperatures in winter (indicating a positive correlation) in all regions except the Rocky mountain range and its leeward side

to the east. In warmer months (starting from April and peaking in July), majority of precipitation occurred below the median indicating negative correlation. This general trend of negative correlation in summer and positive correlation in winter has been reported by several studies since in different regions over the globe. For example, Trenberth and Shea (2005) studied this correlation globally, using surface air temperature from the European Reanalysis (ERA-40; Uppala et al. 2005) and precipitation from second version of the Global Precipitation Climatology Project (GPGP2; Adler et al. 2003). They computed correlation using monthly anomalies split coarsely over two seasons (winter and summer) and reported negative correlations over land in summer and positive correlation in winter except in the Rocky Mountains and Mexican highlands.

All these studies used the Pearson correlation coefficient, which accounts for linear dependence between the two variables. The assumption of linearity however does not represent the true mechanism of dependence between most hydrological variables and thus a more robust model is required for modeling the dependence structure.

2.1.2 Multivariate Probability Distributions

The use of multivariate distributions in hydrology is well documented (Favre et al. 2004; Goel et al. 2000; Hosking and Wallis 1988; Pons 1992; Singh 1987). These distributions are multivariate extensions of their univariate parametric counterparts such as normal, log-normal, gamma and exponential. Multivariate models have been used in flood analysis (relating flood peak and flood volume), analysing storms (relating storm duration to storm intensity) and droughts (relating duration and severity of the drought) (Salvadori and Michele, 2007). Hydrological processes usually have heavy tails (i.e. extreme events, which are of most interest), however multivariate normal distribution does not capture this

dependency and thus is not adequate for modeling joint extremes in hydrology (Favre et al. 2004). Although this limitation is overcome by using multivariate extensions of gamma, Pareto or exponential distributions but they have a significant limitation in the choice of the marginal distributions. In any multivariate extension, the marginals have to be of the similar form as well, for example, a bivariate gamma can only be used to jointly model two univariate gamma distributions. Such assumptions are not viable in hydrologic studies since marginals can, and almost always, have different forms.

2.1.3 Joint Quantiles for Studying Compound Extremes

Several studies have analysed concurrent exceedances of lower and upper quantiles of temperature and precipitation to establish how extremes of both variables relate to each other. Tencer at al. (2014) used daily maximum temperature, daily minimum temperature and daily precipitation from Adjusted and Homogenized Canadian Climate Data (AHCCD; Mekis and Vincent, 2011; Vincent et al. 2012) as well as data from three Regional Climate Models (RCMs), the Met Office Hadley Centre's regional climate model, version 3 (HRM3; Jones et al. 2003); the Regional Climate Model, version 3 (RCM3; Giorgi et al. 1993a,b; Pal et al. 2000, 2007); and the Weather Research and Forecasting Model (Skamarock et al. 2005) to evaluate if RCMs exhibit the same dependence as the observation data. They selected thresholds of precipitation extremes (75^{th} percentile of wet days, i.e. days with precipitation > 0.1mm) and temperature extremes (10^{th} and 90^{th} percentiles from both daily maximum and minimum temperature) from the empirical distributions of the data. Further, a compound extreme event was defined as precipitation extreme coinciding with one of the four temperature extremes. They reported significant positive correlation between heavy precipitation and warm nights as well as warm days on

east and west coast of Canada in winter whereas negative correlation was found in summer. Their analysis of the RCM data revealed that an ensemble of models was better able to capture spatial and seasonal patterns in comparison to any single model. Similar procedure has been used by other studies over different regions of the world (Chen and Zhai, 2017; Sedlmeier et al. 2018). Further details on methods used to analyse compound extremes can be found in Hao et al. (2018).

2.1.4 Clausius-Clapeyron (CC) Relationship

In the introduction section of Trenberth et al. (2003), the authors explore a simple yet profound question, *"Why does it rain?"* They focus on the question of the supply of moisture to the air which ultimately causes precipitation. They state that the Clausius-Clapeyron equation can be used to establish a non-linear relationship between intensity of precipitation extremes and temperature rise. The equation is used to define the amount of saturation vapor pressure at a given temperature and its value ranges from $6.0\%K^{-1}$ at 300K to $7.4\%K^{-1}$ at 270K. Given the global mean temperature, an approximate value of $6.8\%K^{-1}$ (often rounded to $7.0\%K^{-1}$) is established as a reasonable rate of how the moisture in the air rises with respect to temperature. Further, the authors argue that since heavy precipitation relies mostly on low-level moisture convergence, its intensity should increase at the same rate, i.e. $7\%K^{-1}$ or even higher due to latent feedbacks (heat radiated by the land back into the atmosphere).

Since then, several studies have used the Clausius-Clapeyron relationship to identify increase in extreme precipitation events with respect to increasing temperature. Pall et al. (2007) tested the CC relationship globally using data from the Third Hadley Centre Coupled Model, HadCM3 (Pope et al. 2000) and reported good agreement at mid-latitudes

(60°N - 60°S). Most of the results however, found a significant departure from the 7%K^{-1} scaling rate. Sub-CC scaling rates (less than 7%K^{-1}) and super-CC scaling rates (more than 7%K^{-1}) have been reported at different time scales on which precipitation is studied with sub-CC rates mostly found at coarser time scales (daily precipitation), while super-CC rates are mostly observed for sub-daily precipitation. Lenderink and van Meijgaard (2008) reported scaling rates up to 14%K^{-1} for large parts of Europe for 1-hourly precipitation. Similar results can be found in other studies (Berg and Haerter, 2011; Lenderink et al 2011; Loriaux et al. 2013; Mishra et al. 2012; Maeda et al. 2012).

2.1.5 Copulas

Copula, introduced by Sklar (1959), provide an ideal tool for characterizing the dependence structure between two or more variables. Copula overcome the limitations of correlation coefficients and multivariate extensions of univariate parametric distributions in several ways. Copula functions can identify all aspects of the multivariate structure including correlation and dependence in tails, while they make calculation of conditional probabilities and joint return periods straight forward. Moreover, they disassociate the dependence structure between variables from their individual forms, thus overcoming the limitation of marginal choices in multivariate extensions of parametric distributions. Copulas have been used widely in hydrology for flood frequency analysis (Favre et al. 2004; Grimaldi and Serinaldi, 2006; Zhang and Singh, 2006; Zhang and Singh, 2007) and multivariate drought analysis (Hao and AghaKouchak, 2013; Kao and Govindaraju, 2010; Shiau 2006). Copulas were first used for temperature and precipitation by Scholzel and Friederichs (2008) where they fit a Gaussian copula to Gamma distributed precipitation and Gumbel distributed temperature at a location in Berlin. They did not draw any

inference from the bivariate model. Cong and Brady (2012) used copulas on monthly temperature and rainfall at a site in Scania, Sweden from 1961-2000. They used five copula families (Normal, Student, Clayton, Frank and Gumbel) and used Akaike Information Criterion (AIC; Akaike, 1974) and Bayesian Information Criterion (BIC; Schwarz, 1978) as their model selection criteria. AghaKouchak et al. (2014) showed the importance of considering dependence between temperature and precipitation by providing evidence of how a 2014 drought in California was a compound event caused by consistently high temperatures along with low precipitation. Similar results were reported by Zscheischler and Seneviratne (2017) by calculating return periods of warm-dry events under the assumption of independence between temperature and precipitation and then calculating the return periods by considering the dependence. They found a significant reduction in the occurrence of the compound extreme when dependence was considered in the model. For future projections, only Rana et al. (2017) have used copulas to characterize the dependence between temperature and precipitation from a multi-model ensemble of 10 Global Climate Models (GCMs) in northwestern United States.

2.2 Large Ensembles

Projection of climate data into the future is performed with the help of General Circulation Models (GCMs) which are three dimensional mathematical representations of atmosphere, land, oceans and the inter-connected physical processes within this system. These models compute climate variables on a grid that extends horizontally over the surface of the earth and vertically into the atmosphere and ocean from a historical period (usually starting at 1850 or 1950) to the end of the 21st century (or longer). The resolution of these grids is

generally very course (100km-500km) due to computational constraints as well as scarcity of historical data at finer scales to define the boundary conditions of the model.

Through early developments by Poincare (1914) and Thompson (1957), it was recognized that errors in the initial conditions of weather forecasting systems grow non-linearly and limit the predictive skill of the model. Lorenz (1963) founded the Chaos Theory in the process of quantifying this predictability limit (Bauer et al. 2015). Thus, it was realized that any single model cannot be expected to provide a reliable estimate of the future climate state, since the model is a "slave" to its initial conditions. To rectify this, Epstein (1969) proposed an approach to treat the atmosphere as a deterministic entity (i.e. governed by a set of fundamental laws) but the state of the atmosphere as probabilistic; they called this approach *"stochastic dynamic"*. Using a Monte Carlo approach, an ensemble of forecasts is generated with varying initial conditions and the spread of the ensemble at any time in the future represents the uncertainty inherent in the system due to the initial conditions of the model. Collins et al. (2011) discuss the two methods of creating an ensemble of models. First, the *multi-model* ensemble is created by pooling different GCMs together such as the Coupled Model Intercomparison Project Phase 5 (CMIP5) which was the basis of the IPCC Fifth Assessment Report (IPCC AR5). The other is the *perturbed-physics* ensemble which is created by running a single GCM multiple times by changing the initial values of uncertain parameters that are too fine to be physically represented at large spatial scales (such as cloud cover) (Murphy et al. 2007).

Multi-model ensembles such as CMIP5 have produced reliable climate change projections which aid policy makers in decision making process for the future however, these models are too coarse to provide reliable estimates at a regional scale. To overcome this, Regional

Climate Models (RCMs) are created at finer resolutions over limited spatial domains using initial conditions and lateral boundary conditions from global reanalysis data or GCMs; this process is termed as *dynamical downscaling* (Giorgi, 2019). Most RCMs are created using *one-way nesting* method where the flow of information between models is only in one direction (from GCM to RCM). The limitations of one-way nesting method are discussed in detail by Scinocca et al. (2016) where they identify two primary issues with the approach and explain how this method is unable to rectify both issues at hand simultaneously. Putting it in authors' words, *"At its core, one-way nesting is a deterministic modeling approach applied to an inherently chaotic system. That is, an RCM's prognostic variables are required to follow a specified time-evolving realization of synoptic scale evolution, or weather, on its lateral boundaries but it is also expected to deviate from that realization in its interior."* They propose a novel framework of coordinating global and regional climate modeling in which an RCM is run with a *"strict physics compatibility"* with a GCM model along with the use of spectral nudging (von Storch et al. 2000). The Canadian Regional Climate Model (CanRCM4) was thus created by the Canadian Centre for Climate Modelling and Analysis (CCCma) under this framework with The Second Generation Earth System Model (CanESM2) as its parent GCM. CanESM2 (and subsequently CanRCM4) is a 50-member large ensemble created using the *perturbed-physics* ensemble approach mentioned earlier. A complete set of details on CanESM2 can be found in Von Salzen (2013).

2.3 Quantifying Uncertainty

It could be argued that providing uncertainty associated with results is as critical as the results themselves. Indeed, there is an inherent flaw in providing *deterministic* answers by

applying *probabilistic* methods to data that has *stochastic* elements. The Fifth Assessment Report (AR5) by the Intergovernmental Panel on Climate Change (IPCC, 2014) presents the results with a qualitative level of confidence (from *very low* to *very high*) and a quantitative likelihood (from *exceptionally unlikely* to *virtually certain*), which are associated with different probability levels. Canada's Changing Climate Report, 2019 (CCCR; Bush and Lemmen, 2019) also uses similar standards of reporting results.

The Bayesian interpretation of probability was introduced by Thomas Bayes and later fully developed by Pierre-Simon Laplace (Bayes, 1763; Laplace, 1774). In a Bayesian world, everything is probabilistic. A *prior* belief, which is formed independently from the data using subjective knowledge on part of the researcher, is updated to a *posterior* belief using evidence from the data. Formally, this statement can be summarized in the following expression,

$$P(\theta|D,h) \propto P(D|\theta,h) * P(\theta,h)$$

Here, h is a hypothesis on which all entities are conditioned and is excluded from further notation hereafter. The term $P(\theta|D)$ refers to the posterior of the model parameter set θ, given the data D, which is proportional to the underlying data creating process (i.e. the likelihood of the model) $P(D|\theta)$ and the prior belief $P(\theta)$ (Gelman et al. 2013). The entity of interest for which uncertainty is to be calculated, becomes a parameter within the Bayesian framework and since every parameter is defined probabilistically, it naturally results in credible interval for the parameter rather than a single deterministic value.

Bayesian uncertainty quantification has been used in several studies such as estimating uncertainty in parameters of hydrological models (Kavetski et al. 2006; Duan et al. 2007;

Najafi et al. 2011; Renard, 2011; Najafi and Moradkhani, 2013; Najafi and Moradkhani, 2014; Najafi and Moradkhani, 2015) and estimating uncertainty in regional climate change projections (Tebaldi et al. 2005). Bayesian methods have also been used in copula analysis, producing posterior estimates of copula parameter that account for uncertainty in the dependence between the variables included in the copula (Madadgar and Moradkhani, 2013).

In this study, Bayesian methods are used whenever dealing with future projections of climate change, in order to provide a credible interval of most likely results, rather than one deterministic value.

2.4 References

Adler, R. F., et al. (2003), The version 2 Global Precipitation Climatology Project (GPCP) monthly precipitation analysis (1979–present), J. Hydrometeorol., 4, 1147–1167.

AghaKouchak, A., Cheng, L., Mazdiyasni, O., and Farahmand, A. (2014), Global warming and changes in risk of concurrent climate extremes: Insights from the 2014 California drought, Geophys. Res. Lett., 41, 8847– 8852, doi:10.1002/2014GL062308.

Akaike H (1974) A new look at the statistical model identification. In Selected Papers of Hirotugu Akaike. Springer, New York, NY pp 215-222

Bauer, P., Thorpe, A. & Brunet, G. The quiet revolution of numerical weather prediction. Nature 525, 47–55 (2015) doi:10.1038/nature14956

Bayes, T. (1763). LII. An essay towards solving a problem in the doctrine of chances. By the late Rev. Mr. Bayes, FRS communicated by Mr. Price, in a letter to John Canton, AMFR S. Philosophical transactions of the Royal Society of London, (53), 370-418.

Berg, P., and J. O. Haerter, 2011: Unexpected increase in precipitation intensity with temperature—A result of mixing of precipitation types? Atmos. Res., 119, 56–61.

Blair TA, 1931. Relations between winter temperature and precipitation. Mon. Wea. Rev., 59, 34-35

Bush, E., & Lemmen, D. S. (Eds.). (2019). Canada's Changing Climate Report. Government of Canada= Gouvernement du Canada.

Chen, Y. & Zhai, P. Simultaneous modulations of precipitation and temperature extremes in Southern parts of China by the boreal summer intraseasonal oscillation.Clim Dyn (2017) 49: 3363. https://doi.org/10.1007/s00382-016-3518-4

Collins, M., Booth, B. B., Bhaskaran, B., Harris, G. R., Murphy, J. M., Sexton, D. M., & Webb, M. J. (2011). Climate model errors, feedbacks and forcings: a comparison of perturbed physics and multi-model ensembles. Climate Dynamics, 36(9-10), 1737-1766.

Cong R and Brady M, "The Interdependence between Rainfall and Temperature: Copula Analyses," The Scientific World Journal, vol. 2012, Article ID 405675, 11 pages, 2012. https://doi.org/10.1100/2012/405675.

Crutcher HL, 1976. A note on correlations of temperature and precipitation within the United States - 1906-1948. To be published by EDS NOAA

Duan, Q., Ajami, N. K., Gao, X., & Sorooshian, S. (2007). Multi-model ensemble hydrologic prediction using Bayesian model averaging. Advances in Water Resources, 30(5), 1371-1386.

Epstein, E. S. Stochastic-dynamic prediction. Tellus 21, 739–759 (1969)

Favre, A.-C., El Adlouni, S., Perreault, L., Thiémonge, N., and Bobée, B. (2004). "Multivariate hydrological frequency analysis using copulas." Water Resour. Res., 40, W01101.10.1029/2003WR00245610.1029/2003WR02456

Gelman, A., Carlin, J. B., Stern, H. S., Dunson, D. B., Vehtari, A., & Rubin, D. B. (2013). Bayesian data analysis. Chapman and Hall/CRC.

Giorgi, F., M. R. Marinucci, and G. T. Bates, 1993a: Development of a second-generation regional climate model (RegCM2). Part I: Boundary-layer and radiative transfer processes. Mon. Wea. Rev., 121, 2794–2813, doi:10.1175/1520-0493(1993)121,2794:DOASGR.2.0.CO;2.

Giorgi, F. (2019). Thirty years of regional climate modeling: Where are we and where are we going next?. Journal of Geophysical Research: Atmospheres, 124(11), 5696-5723.

Goel, N. K., Kurothe, R. S., Mathur, B. S., and Vogel, R. M. (2000). "A derived flood frequency distribution for correlated rainfall intensity and duration." J. Hydrol., 228, 56–67.10.1016/S0022-1694(00)00145-1

Grimaldi, S., & Serinaldi, F. (2006). Asymmetric copula in multivariate flood frequency analysis. Advances in Water Resources, 29(8), 1155-1167.

Hamrick AM, Martin HH, 1941. Fifty years' weather in Kansas City, Mo. 1889-1938. Mon. Wea. Rev. Suppl. No. 44.

Hao, Z., & AghaKouchak, A. (2013). Multivariate standardized drought index: a parametric multi-index model. Advances in Water Resources, 57, 12-18.

Hao, Z., Singh, V.P. and Hao, F., 2018. Compound extremes in hydroclimatology: a review. Water, 10(6), p.718.

Hosking, J. R. M., and Wallis, J. R. (1988). "The effect of intersite dependence on regional flood frequency analysis." Water Resour. Res., 24(2), 588–600.

IPCC, 2014: Climate Change 2014: Synthesis Report. Contribution of Working Groups I, II and III to the Fifth Assessment Report of the

Intergovernmental Panel on Climate Change [Core Writing Team, R.K. Pachauri and L.A. Meyer (eds.)]. IPCC, Geneva, Switzerland, 151 pp

Isaac, G.A. and R.A. Stuart, 1992: Temperature–Precipitation Relationships for Canadian Stations. J. Climate, 5, 822–830, https://doi.org/10.1175/1520-0442(1992)005<0822:TRFCS>2.0.CO;2

Jones, R., D. Hassell, D. Hudson, S. Wilson, G. Jenkins, and J. Mitchell, 2003: Generating high resolution climate change scenarios using PRECIS. UNDP National Communications Unit Workbook, 34 pp.

Kao, S. C., & Govindaraju, R. S. (2010). A copula-based joint deficit index for droughts. Journal of Hydrology, 380(1-2), 121-134.

Karl, T.R., G. Kukla, and J. Gavin, 1984: Decreasing Diurnal Temperature Range in the United States and Canada from 1941 through 1980. J. Climate Appl. Meteor., 23, 1489–1504, https://doi.org/10.1175/1520-0450(1984)023<1489:DDTRIT>2.0.CO;2

Karl, T.R., G. Kukla, and J. Gavin, 1986: Relationship between Decreased Temperature Range and Precipitation Trends in the United States and Canada, 1941–80. J. Climate Appl.

Kavetski, D., Kuczera, G., and Franks, S. W. (2006), Bayesian analysis of input uncertainty in hydrological modeling: 1. Theory, Water Resour. Res., 42, W03407, doi:10.1029/2005WR004368.

Laplace, P.-S. (1774). "'M´emoire sur la Probabilit´e des Causes par les Ev´ ´enements." M´emoires de Math´ematique et de Physique Present´es a´ l'Acad´emie Royale des Sciences, Par Divers Savans, & Lus ˆ dans ses Assembl´ees, 6: 621–656.

Lenderink, G., van Meijgaard, E. Increase in hourly precipitation extremes beyond expectations from temperature changes. Nature Geosci 1, 511–514 (2008) doi:10.1038/ngeo262

Lenderink, G., H. Mok, T. Lee, and G. Van Oldenborgh (2011), Scaling and trends of hourly precipitation extremes in two different climate zones—Hong Kong and the Netherlands, Hydrol. Earth Syst. Sci., 15(9), 3033–3041, doi:10.5194/hessd-8-4701-2011.

Lorenz, E. N. Deterministic non-periodical flow. J. Atmos. Sci. 20, 130–141 (1963) One of the most influential papers establishing the fundamentals of chaos theory applied to numerical weather prediction.

Loriaux, J. M., G. Lenderink, S. R. D. Roode, and A. P. Siebesma (2013), Understanding convective extreme precipitation scaling using observations and an entraining plume model, J. Atmos. Sci., 70(11), 3641–3655, doi:10.1175/JAS-D-12-0317.1.

Madadgar, S., & Moradkhani, H. (2013). A Bayesian framework for probabilistic seasonal drought forecasting. Journal of Hydrometeorology, 14(6), 1685-1705.

Madden, R.A. and J. Williams, 1978: The Correlation between Temperature and Precipitation in the United States and Europe. Mon. Wea. Rev., 106, 142–147, https://doi.org/10.1175/1520-0493(1978)106<0142:TCBTAP>2.0.CO;2

Maeda, E. E., N. Utsumi, and T. Oki, 2012: Decreasing precipitation extremes at higher temperatures in tropical regions. Nat. Hazards, 64, 935–941.

Mekis E, Vincent LA (2011). An overview of the second generation adjusted daily precipitation dataset for trend analysis in Canada. Atmosphere-Ocean 49(2): 163-177

Meteor., 25, 1878–1886, https://doi.org/10.1175/1520-0450(1986)025<1878:RBDTRA>2.0.CO;2Mishra, V., J. M. Wallace, and D. P. Lettenmaier (2012), Relationship between hourly extreme precipitation and local air temperature in the United States, Geophys. Res. Lett., 39, L16403, doi:10.1029/2012GL052790.

Murphy JM, Booth BBB, Collins M, Harris GR, Sexton D, Webb MJ (2007) A methodology for probabilistic predictions of regional climate change from perturbed physics ensembles. Philos Trans R Soc Lond A 365:1993–2028

Najafi, M. R., Moradkhani, H., & Jung, I. W. (2011). Assessing the uncertainties of hydrologic model selection in climate change impact studies. Hydrological processes, 25(18), 2814-2826.

Najafi, M. R., & Moradkhani, H. (2013). Analysis of runoff extremes using spatial hierarchical Bayesian modeling. Water Resources Research, 49(10), 6656-6670.

Najafi, M. R., & Moradkhani, H. (2014). A hierarchical Bayesian approach for the analysis of climate change impact on runoff extremes. Hydrological processes, 28(26), 6292-6308.

Najafi, M. R., & Moradkhani, H. (2015). Multi-model ensemble analysis of runoff extremes for climate change impact assessments. Journal of Hydrology, 525, 352-361.

Pal, J. S., E. E. Small, and E. A. B. Eltahir, 2000: Simulation of regional-scale water and energy budgets: Representation of subgrid cloud and precipitation processes within RegCM. J. Geophys. Res., 105, 29 579–29 594, doi:10.1029/2000JD900415.

Pal et al., 2007: Regional climate modeling for the developing world: The ICTP RegCM3 and RegCNET. Bull. Amer. Meteor. Soc., 88, 1395–1409, doi:10.1175/BAMS-88-9-1395

Pall, P., Allen, M.R. & Stone, D.A. Testing the Clausius–Clapeyron constraint on changes in extreme precipitation under CO2 warming.Clim Dyn (2007) 28: 351. https://doi.org/10.1007/s00382-006-0180-2

Poincare, H. Science and Method (T. Nelson, London, 1914)

Pons, F. A. (1992). "Regional flood frequency analysis based on multivariate log-normal models." Ph.D. thesis, Colorado State Univ., Fort Collins, Colo.

Pope V, Gallani ML, Rowntree P, Stratton R (2000) The impact of new physical parameterizations in the Hadley Centre climate model: HadAM3. Clim Dyn 16:123–146

Rana, A., Moradkhani, H. & Qin, Y. Understanding the joint behavior of temperature and precipitation for climate change impact studies.Theor Appl Climatol (2017) 129: 321. https://doi.org/10.1007/s00704-016-1774-1

Tencer B, Weaver A, Zwiers F (2014). Joint occurrence of daily temperature and precipitation extreme events over Canada. Journal of Applied Meteorology and Climatology 53(9): 2148-2162

Salvadori, G., and Carlo De Michele. "On the use of copulas in hydrology: theory and practice." Journal of Hydrologic Engineering 12, no. 4 (2007): 369-380. https://doi.org/10.1061/(ASCE)1084-0699(2007)12:4(369)

Scholzel C. and Friederichs P., "Multivariate non-normally ¨ distributed random variables in climate research—introduction to the copula approach," Nonlinear Processes in Geophysics, vol. 15, no. 5, pp. 761–772, 2008.

Schwarz G., "Estimating the dimension of a model", The Annals of Statistics, vol. 6, pp 461-464, 1978.

Scinocca, J.F., Kharin, V.V., Jiao, Y., Qian, M.W., Lazare, M., Solheim, L., Flato, G.M., Biner, S., Desgagne, M. and Dugas, B., 2016. Coordinated global and regional climate modeling. Journal of Climate, 29(1), pp.17-35.

Sedlmeier, K., Feldmann, H. & Schädler, G. Compound summer temperature and precipitation extremes over central Europe.Theor Appl Climatol (2018) 131: 1493. https://doi.org/10.1007/s00704-017-2061-5

Shiau, J. T. (2006). Fitting drought duration and severity with two-dimensional copulas. Water resources management, 20(5), 795-815.

Singh, V. P. (1987). Hydrologic frequency modeling, Reidel, Boston.

Skamarock, W. C., J. B. Klemp, J. Dudhia, D. O. Gill, D. M. Barker, W. Wang, and J. G. Powers, 2005: A description of the Advanced Research WRF version 2. NCAR Tech. Note NCAR/TN-4681STR, 88 pp. [Available online at http://www2.mmm.ucar.edu/wrf/users/docs/arw_v2.pdf.]

Sklar M (1959). Fonctions de repartition an dimensions et leurs marges. Publ. inst. statist. univ. Paris 8: 229-231.

Tebaldi, C., R.L. Smith, D. Nychka, and L.O. Mearns, 2005: Quantifying Uncertainty in Projections of Regional Climate Change: A Bayesian Approach to the Analysis of Multimodel Ensembles. J. Climate, 18, 1524–1540, https://doi.org/10.1175/JCLI3363.1

Thompson, P. D. Uncertainty of initial state as a factor in the predictability of large scale atmospheric flow patterns. Tellus 9, 275–295 (1957)

Trenberth, K.E., A. Dai, R.M. Rasmussen, and D.B. Parsons, 2003: The Changing Character of Precipitation. Bull. Amer. Meteor. Soc., 84, 1205–1218, https://doi.org/10.1175/BAMS-84-9-1205

Trenberth, K. E., and Shea, D. J. (2005), Relationships between precipitation and surface temperature, Geophys. Res. Lett., 32, L14703, doi:10.1029/2005GL022760.

Uppala, S.M., Kållberg, P.W., Simmons, A.J., Andrae, U., Bechtold, V.D.C., Fiorino, M., Gibson, J.K., Haseler, J., Hernandez, A., Kelly, G.A. and Li, X., 2005. The ERA-40 re-analysis. Quarterly Journal of the Royal Meteorological Society: A journal of the atmospheric sciences, applied meteorology and physical oceanography, 131(612), pp.2961-3012.

Vincent LA, Wang XL, Milewska EJ, Wan H, Yang F, Swail V (2012). A second generation of homogenized Canadian monthly surface air temperature for climate trend analysis. Journal of Geophysical Research: Atmospheres: 117(D18)

Von Salzen, K., Scinocca, J.F., McFarlane, N.A., Li, J., Cole, J.N., Plummer, D., Verseghy, D., Reader, M.C., Ma, X., Lazare, M. and Solheim, L., 2013. The Canadian fourth generation atmospheric global climate model (CanAM4). Part I: representation of physical processes. Atmosphere-Ocean, 51(1), pp.104-125.

von Storch, H., H. Langenberg, and F. Feser, 2000: A spectral nudging technique for dynamical downscaling purposes. Mon. Wea. Rev., 128, 3664–3673, doi:10.1175/1520-0493(2000)128,3664:ASNTFD.2.0.CO;2.

Zhang, L. S. V. P., & Singh, V. P. (2006). Bivariate flood frequency analysis using the copula method. Journal of hydrologic engineering, 11(2), 150-164.

Zhang, L., & Singh, V. P. (2007). Trivariate flood frequency analysis using the Gumbel–Hougaard copula. Journal of Hydrologic Engineering, 12(4), 431-439.

Chapter 3.

Characterization of Temperature and Precipitation Covariability over Canada using Observed Data

3.1 Introduction

The recently published Canada's Changing Climate Report (CCCR, 2019) states that the global mean surface temperature has increased by 0.6°C in 1986-2005 compared to the pre-industrial period (1850-1900). Future temperature is projected to increase by 1°C under the low emission scenario and 3.7°C under the high emission scenario by the end of the 21st century with respect to the reference period of 1986-2005 (Bush and Lemmen, 2019). Vincent et al. (2015) reported an overall temperature increase of 1.7 °C over Canada from 1948-2012 with the largest increase of 3.3 °C in winter and the lowest of 1.4 °C in summer. They reported a 19% increase in precipitation during the same period. Vincent et al. (2018) reported an increase in the frequency of summer days and hot days, and increases in rainfall accompanied by decreases in snowfall over southern Canada. Changes in temperature and precipitation have resulted in reduced snowpack and Arctic sea-ice (Najafi et al., 2016 ; Najafi et al., 2017a, Min et al., 2008), changes in surface water availability (Najafi et al., 2017b), increased evapotranspiration, increased depth and extent of permafrost thaw, more frequent droughts and flooding, among others (Blankinship and Hart, 2012 ; Warren and Lemen, 2014).

Understanding the interdependencies between temperature and precipitation can improve the prediction of extreme events such as floods and droughts and help better project the impacts of climate change. Information obtained from an isolated study of these climate variables fails to capture the conditional effects of other drivers that are caused by their mutual interactions. This can result in a misrepresentation of the joint physical processes and the possible underestimation of hydrological hazards and risks (Favre et al., 2004; Hao and Singh, 2016). Multivariate analysis approaches based on bivariate normal distributions or other multivariate extensions of student's t and Fischer's F distributions can be used to characterize the dependencies between temperature and precipitation (Anderson, 1984; Johnson and Wichern, 2002). However, these approaches are marred by drawbacks, such as the inability of a bivariate Gaussian distribution to capture the dependence of extremes (i.e. tails of the distribution). Moreover, they require the marginal distributions to belong to the same family as the bivariate distribution and offer no solution for cases beyond the bivariate dimension (Favre et al., 2004). Such homogeneity assumptions across distributions do not always hold.

In this study, we use copula functions (Sklar, 1959), which address the aforementioned restraints. Copulas are flexible family of functions that can bind a multivariate distribution with the constituent univariate marginal distributions irrespective of the homogeneities in the families of distributions (Frees and Valdez, 1998). Copulas have been an integral component of financial modelling, and their applications in hydrology have grown considerably in recent years as they can represent the complex non-linear dependence structures between hydroclimatic variables (Favre et al., 2004; Laux et al., 2011; Lazoglou et al., 2018). Several studies have been conducted to model droughts in a multivariate

framework using copulas (Shiau 2006; Wong et al., 2009). Schoelzel and Friederichs (2008) reported the advantages of copulas over other multivariate methods such as mixture models using ground-based temperature and precipitation observations in Berlin. Beniston (2009) studied the trends of higher and lower quantiles of precipitation and temperature over nine locations in Europe. Using regional climate models, they found a decrease in cold/dry conditions and an increase in wet/warm conditions from 1900 to 2100. Cong and Brady (2012) analyzed the relations between April precipitation and temperature in Sweden from 1960 to 2010 using five copula families. Rana et al. (2017) studied the joint distribution of daily precipitation and temperature using an ensemble of 10 global climate models over the Columbia River Basin in the U.S. They reported that temperature and precipitation have a negative relationship in the dry season whereas in wet seasons, precipitation is mostly independent of temperature changes. Their analyses showed a significant positive trend for both temperature and precipitation in the future. Only a limited number of studies, mostly restricted to regional scales, have explored the joint variability of temperature and precipitation in Canada. Asong et al. (2016) used Generalized Linear Models to study temperature and precipitation over the Canadian Prairies. Gennaretti et al. (2015) and Guerfi et al. (2015) used copulas to model temperature and precipitation over the Canadian Arctic coastal zones and southern Quebec, respectively. Tencer et al. (2014) conducted a pan-Canadian study of temperature and precipitation extremes. They analyzed the joint daily occurrence of extreme precipitation and extreme temperature (higher and lower quantiles) at 293 sites across Canada using non-parametric methods. They found a strong positive relationship between high temperature and precipitation in eastern and southwestern coastal areas in autumn and winter and a strong relationship between

precipitation and low temperature in spring and summer. Other studies have analysed the relationship between temperature and precipitation globally but their analyses have been restricted to exploring the linear associations between the two variables (Dery and Wood, 2005; Trenberth and Shea, 2005). These studies have reported strong positive correlations between the two variables at higher latitudes, especially in winter, however, they also acknowledge the presence of non-linearity in the dependence structure. Another approach to study the association between precipitation and temperature is the theoretical Clausius-Clapeyron (CC) relation, which states that the water holding capacity of the air rises by about 7% for every 1 Kelvin (K) increase in air temperature (Pall et al., 2007). Allen et al. (2010) reported that whereas the global mean precipitation has a scaling rate of about 3.4%, extreme precipitation follows the CC relation more closely.

Previous studies have reported trends in both temperature and precipitation (Vincent et al. 2015; Zhang et al., 2000) which can result in temporal changes in the dependence structure between these climate variables. While characterizing this trend is critical for hazard risk assessments and the design of infrastructure, most studies have focused on temporal variations of the individual variables in isolation assuming that their covariabilities will remain unchanged. Only a few studies have considered non-stationarity in a bivariate framework (Hao and Singh, 2016).

In this study, we use copulas to characterize the joint behaviour of temperature and precipitation in 15 ecozones across Canada at multiple time scales. In addition, CC scaling curves are generated to characterize extreme precipitation response to temperature changes within each zone. Next, we evaluate the non-stationary joint behaviour of temperature and precipitation following the approach proposed by Bender et al. (2014). Primarily, the

novelty of this study lies in the number of candidate copula models we choose to include in the analysis and the non-stationary approach which is not adopted in previous temperature-precipitation copula analysis studies. The study aims to answer the following questions:

- Do temperature and precipitation exhibit significant non-linear relationships over Canada?
- How does precipitation respond to temperature changes over different regions in Canada?
- Is the dependence structure between temperature and precipitation changing over time?

The remainder of the paper is organized as follows: Section 2 describes the study area and observed datasets. Section 3 discusses the methodology including the precipitation and temperature covariability scenarios, the non-stationary approach, copula and the corresponding model selection criteria. Results and conclusions are presented in sections 4 and 5, respectively.

3.2 Study Area and Data

Canada is the second-largest country in the world, covering an area of over 9.9 million km^2. It is surrounded by the Pacific, Atlantic, and Arctic Oceans on the west, east and north, respectively and the US on the south. The extensive variety of geographical features, presence of the oceans, the Great Lakes in southern parts of Ontario, and mountain ranges in the west generate a diverse array of climatic conditions throughout the country. Areas in the north experience polar and sub-Arctic climate conditions, eastern provinces have a

temperate climate and southwestern regions experience hot and humid summer continental climate (Peel et al., 2007). Increases in temperature and changing precipitation patterns have led to a wide range of hydroclimatic impacts in Canada, including reduced snowpack (Najafi et al., 2016 ; Najafi et al., 2017a) and Arctic sea-ice (Min et al., 2008), changes in timing and amount of surface water availability (Najafi et al., 2017b), increased evapotranspiration, increased depth and extent of permafrost thaw, decreased water quality and shorter seasons for northern ice roads, increased loss of forests due to pests and wildfires, more frequent droughts and flooding, and increased risks of food-borne diseases (Blankinship and Hart, 2012 ; Warren and Lemen, 2014).

The study area is divided into 15 ecozones, which were characterized by Wiken (1986) as a way to define, "on a subcontinental scale, the broad mosaics formed by the interaction of macroscale climate, human activity, vegetation, soils, geological, and physiographic features of the country" and were used in the first State of the Environment Report for Canada in 1986 (Bird and Rapport, 1986).

Adjusted and Homogenized Canadian Climate Data (AHCCD) at a daily time scale are used in this study. AHCCD is a corrected version of the historical station records created by removing various non-climatic inconsistencies such as instrument changes, station relocation, wind undercatch, evaporation and wetting losses for precipitation (Mekis and Vincent, 2011) and corrections to temperature for temporal gaps, inhomogeneities and a nation-wide change for time observation (Vincent et al., 2012). Temperature and precipitation records from 107 stations with at least 80% data availability from 1950 to 2010 are considered for the analyses. This time period is selected to provide a balance between the spatial spread of the stations and the length of the dataset. Zones 1 and 11

(Arctic Cordillera and Taiga Cordillera respectively) are excluded from the analyses because of the limited data availability (over 50% missing data). An exception is made for Zone 4 (Taiga Plains) where two stations with 78% available data are selected to avoid excluding the zone. To analyze the non-stationary dependence structure between temperature and precipitation we use 66 AHCCD stations (a subset of the already selected 107) with long historical records (1910 – 2017) and over 80% data availability (Figure 1). The end period of the analysis was extended to 2017 in this case because it was desirable to include the longest possible timespan available. Consequently, non-stationary analyses are conducted over eight zones (zones 6 - 9 and zones 12 - 14).

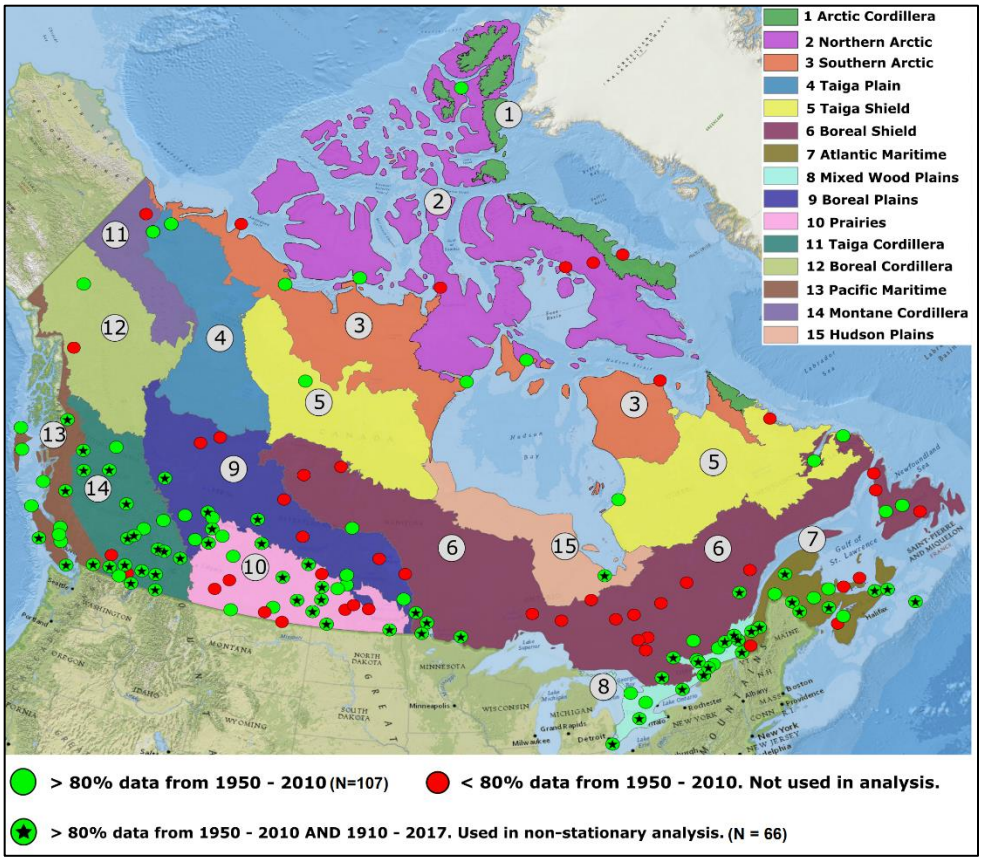

Figure 1 - Ecozones of Canada as defined by Wiken (1986) and the location of the selected Adjusted and Homogenized Canadian Climate Data (AHCCD) Stations. Total of 107 stations are used in the study. A further subset of 66 stations from the selected 107 are used.

3.3 Methods

3.3.1 Copulas

Copulas, first introduced by Sklar (1959), allow for the characterization of the dependence structure between two (or more) variables independent from their marginal distributions (Genest and Favre, 2007; Schmidt, 2007). Sklar's theorem states that given two continuous random variables *X* and *Y*, the joint Cumulative Density Function (CDF) *H(X, Y)* can be written as:

$$H(X,Y) = C[F(X), G(Y)] \qquad (1),$$

where, *F(X)* and *G(Y)* are the marginal distributions of *X* and *Y*, respectively and *C* is the copula function built over uniform marginals, which are the quantile transformations of *X* and *Y*. The determination of the joint CDF *H(X, Y)* then becomes a two-step process of finding the dependence structure *C* and the marginal distributions of *X* and *Y* (Zhang and Singh, 2006). This concept is extendable to multivariate scenarios (Nelsen, 2007).

In this study, multiple families of copulas are used, each having their own unique set of properties which allows for a wide range of models to choose from when identifying the bivariate structure (Favre et al., 2004; Salvadori and Michele, 2004). They include the elliptical, Archimedean, and extreme value copulas, and their rotated versions (90, 180 or survival, and 270). All types of copulas used in this study are listed in Table 1 along with

their corresponding symbols, which are used to reference the respective copula for the remainder of the paper.

Table 1 - The list of copulas used in this study

Symbol	**Copula Name**	**Symbol**	**Copula Name**
C0	Independent	C20	Rotated Joe 90 degrees
C1	t	C21	Rotated BB1 90 degrees
C2	Gaussian	C22	Rotated BB6 90 degrees
C3	Clayton	C23	Rotated BB7 90 degrees
C4	Gumbel	C24	Rotated BB8 90 degrees
C5	Frank	C25	Rotated Clayton 270 degrees
C6	Joe	C26	Rotated Gumbel 270 degrees
C7	BB1	C27	Rotated Joe 270 degrees
C8	BB6	C28	Rotated BB1 270 degrees
C9	BB7	C29	Rotated BB6 270 degrees
C10	BB8	C30	Rotated BB7 270 degrees
C11	Survival Clayton	C31	Rotated BB8 270 degrees
C12	Survival Gumbel	C32	Tawn type 1
C13	Survival Joe	C33	Rotated Tawn type 1 180 degrees
C14	Survival BB1	C34	Rotated Tawn type 1 90 degrees

C15	Survival BB6	C35	Rotated Tawn type 1 270 degrees
C16	Survival BB7	C36	Tawn type 2
C17	Survival BB8	C37	Rotated Tawn type 2 180 degrees
C18	Rotated Clayton 90 degrees	C38	Rotated Tawn type 2 90 degrees
C19	Rotated Gumbel 90 degrees	C39	Rotated Tawn type 2 270 degrees

A brief description of one of some widely used copulas has been provided in Appendix-A1. The two-parameter families of copulas, such as BB1, provide the flexibility of modelling asymmetric upper and lower tail dependencies. Joe (2014) and Nelsen (2007) provide an extensive explanation of all classes of copulas and their characteristics.

Given the high intra-annual variations of temperature and precipitation, it is important to understand their dependence structure at different temporal scales for hazard risk assessments. In this study, analyses are performed at the annual, seasonal and monthly scales based on daily records of temperature and precipitation spatially averaged over the ecozones by taking the arithmetic mean of all stations lying within each zone. In each scenario, accumulated precipitation P_i^* and mean temperature T_i^* are calculated at the corresponding time scale:

$$P_i^* = \sum_{d=1}^{n} P_d \qquad (2),$$

$$T_i^* = \sum_{d=1}^{n} \frac{T_d}{n} \qquad (3),$$

where (*d = 1,..., n*) denotes the number of days in each year, season or month of the year *(i = 1950, 1951, ..., 2010)*. The seasonal analysis is conducted over winter (DJF), spring (MAM), summer (JJA) and fall (SON). Analyses at daily time scales are not shown because of the weak correlations between temperature and precipitation due to the large noise in data at this temporal resolution. The same procedure is repeated for standardized anomalies of temperature and precipitation, which shows negligible changes in the rank correlation. Therefore, values in their original scales are used in the analyses because they provide more realistic interpretations of the regional changes.

3.3.2 Model Selection Criteria

Selection of the most suitable copula is based on the corrected version of the Akaike Information Criterion (AIC_c) (Akaike, 1974), which is defined as:

$$AIC_c = -2\sum_{i=1}^{N} \ln\left[C\left(u_{i,1}, v_{i,2}|\theta\right)\right] + 2k + \frac{2k^2 + 2k}{n - k - 1} \qquad (4),$$

where *k* is the number of parameters of the copula (*k* = 1 for one-parameter and *k* = 2 for two-parameter families) and *n* is the sample size (Schepsmeier et al., 2018). The first term of the right-hand side of Equation 4 is the likelihood function, the second is the penalty for model complexity and the last expression is the small-sample correction. AIC_c is used as a small sample corrected version of *AIC* when the sample size to model parameter ratio (*n/k*) is under 40. It converges to *AIC* as the sample size gets larger (Burnham and Anderson, 2003). The copula model with the lowest AIC_c is selected as it minimizes the information loss between the unknown true copula and the selected model (Burnham and Anderson,

2003). The marginal distributions of temperature and precipitation are selected from a pool of candidate distributions using AIC_c. For precipitation, the candidate distributions are Gamma, Weibull, Exponential and Log-Normal, whereas normal distribution is selected to model temperature.

The selection criteria based on the information theory would only provide a relative score of the models considered raising the question *'What if all the models are wrong?'* since a comparison between all *'wrong'* models would still provide one model with the best relative score (Burnham et al. 2011). Therefore, in this study, an additional goodness of fit test proposed by Genest et al. (2006) is used to evaluate the selected models (see Appendix-A5).

3.3.3 Non-Stationary Dependence Structure

Non-stationary analyses of the dependence structure require long records of climate variables. Considering data availability, the time period of 1910-2017 is selected to analyze the non-stationary covariability between temperature and precipitation over 66 stations in eight ecozones. First, a non-parametric Mann-Kendall trend test is used to evaluate the trends of both temperature and precipitation at each zone. Since the presence of serial correlation can increase the chances of rejecting a no-trend null hypothesis (Zwiers and Von Storch, 1995), the series is pre-whitened before applying the trend test when significant serial correlations exist (at the 95% confidence level). If a significant trend is found in either one of the series, moving-window dependency analysis is conducted following Bender et al. (2014) by considering a window size of 50 years with one-year increments. A stationary copula model is fitted to data in each window using methods described previously. This approach provides a fine balance between sufficiently long

records within each window for a reasonable marginal and copula fitting procedure and total number of windows to detect a change in trend.

3.3.4 Clausius-Clapeyron Relation

The CC scaling coefficient is determined for each ecozone similar to Jones et al. (2010). The daily temperature is divided into 2K bins (with 1K overlap for smoothing). Precipitation over the full 61-year period (1950-2010) is assigned to each bin and the 95^{th}, 99^{th} and 99.9^{th} quantiles within each bin are calculated as representatives of extreme precipitation for the specific average bin temperature. The following equation is used to relate extreme precipitation to temperature changes:

$$P_2 = P_1(1 + a)^{\Delta T} \qquad (8),$$

where P_1 and P_2 are extreme precipitation rates (95^{th}, 99^{th} and 99.9^{th} quantiles) at temperatures T_1 and T_2, respectively. ΔT is the change in temperature ($T_2 - T_1$) and a is the scaling coefficient, which is theoretically equal to 6.8% $°C^{-1}$ at 25°C. To determine this coefficient for each ecozone, a linear regression model is fitted to temperature and logarithm of extreme precipitation as per equation (8).

3.4 Results and Discussions

It is imperative to state that the aim of this study is not to establish a direct one-to-one causal relationship between precipitation and temperature. As stated by Isaac and Stuart (1992) *"temperature-precipitation relationship does not provide strong evidence for any cause and effect. Certainly, stability indices, pressure, upper airflow, and temperature-dew point spreads are more directly related to precipitation-formation mechanisms."* However, temperature is one of the most well-recorded and well-studied climate variables whereas

our capability to predict precipitation is limited due to the complex interactions between multiple factors. Therefore, characterizing the covariability between precipitation and temperature can improve our understanding of precipitation behaviour as well as the joint impact of the two variables.

3.4.1 Dependency of total annual precipitation on mean temperature

The annual temperature series are normally distributed whereas precipitation is described by Gamma and Weibull distributions in all ecozones. Table 2 shows the average rank correlation between temperature and precipitation over time in all zones at the annual time scale. Statistically significant Kendall's rank coefficient values at a significance level of 5% are found in seven zones. Except Zone 9 and Zone 10 (Boreal Plains and Prairies) which exhibit negative correlations, temperature is positively correlated with precipitation in other parts of Canada. The strongest positive relationship is observed around the Hudson Bay, specifically in southern Arctic and Taiga shield ecozones with τ = 0.28 and 0.26, respectively. Relatively stronger positive correlations in northern zones follow the trends reported by Bush (2019) and Environment Canada (2014) of northern Canada getting warmer and wetter at an increasingly higher rate compared to the global average. Copulas for each zone were selected according to the AIC_c model selection criteria and the goodness of fit was evaluated as described in section 3.1.

Table 2 – Kendall's rank correlation coefficients for fifteen ecozones at an annual timescale (1950-2010). The p-values marked with asterisks show statistically significant correlations at a 5% significance level.

Zone	Kendall's Rank	p-value	Number of

	Correlation Coefficient	(5% Significance Level)	stations
1 – Arctic Cordillera	NA	NA	NA
2 – Northern Arctic	0.11	0.23	2
3 – Southern Arctic	0.28	0.00*	3
4 – Taiga Plains	0.19	0.02*	2
5 – Taiga Shield	0.26	0.00*	3
6 – Boreal Shield	0.09	0.47	14
7 – Atlantic Maritime	0.22	0.01*	13
8 – Mixedwood Plains	0.05	0.88	12
9 – Boreal Plains	-0.18	0.04*	9
10 – Prairies	-0.23	0.00*	16
11 – Taiga Cordillera	NA	NA	NA
12 – Boreal Cordillera	0.15	0.08	1
13 – Pacific Maritime	0.09	0.71	12
14 – Montane Cordillera	0.06	0.79	19
15 – Hudson Plains	0.17	0.05*	1

The dependence structure of the two variables is shown for southern Arctic (based on Joe copula) and the Prairies (based on R270 Clayton) with contrasting joint behaviour (Figure 2). The model shows upper tail dependency in the southern Arctic indicating that higher values of temperature tend to correlate with higher precipitation values. The copula density shows a peak at a temperature around -16 °C and precipitation around 350 mm/year. The stations in this zone are not ideally representative of the climate regime of the entire ecozone as they are located on the northern edge resulting in a slight cold bias. Bintanja and Selten (2014) discussed how precipitation in the Arctic region is driven primarily by 'local surface evaporation' thus establishing the direct impact of the Arctic warming on precipitation amounts. Positive correlations and dependency in the upper tails (extremes) between temperature and precipitation suggest that rising temperature could intensify precipitation due to increased evaporation. For the Prairies, the copula peak is observed at a temperature of 3 °C and around 500 mm/year precipitation. There is the presence of higher dependency for low temperatures and high precipitation which is reduced as the temperature gets warmer.

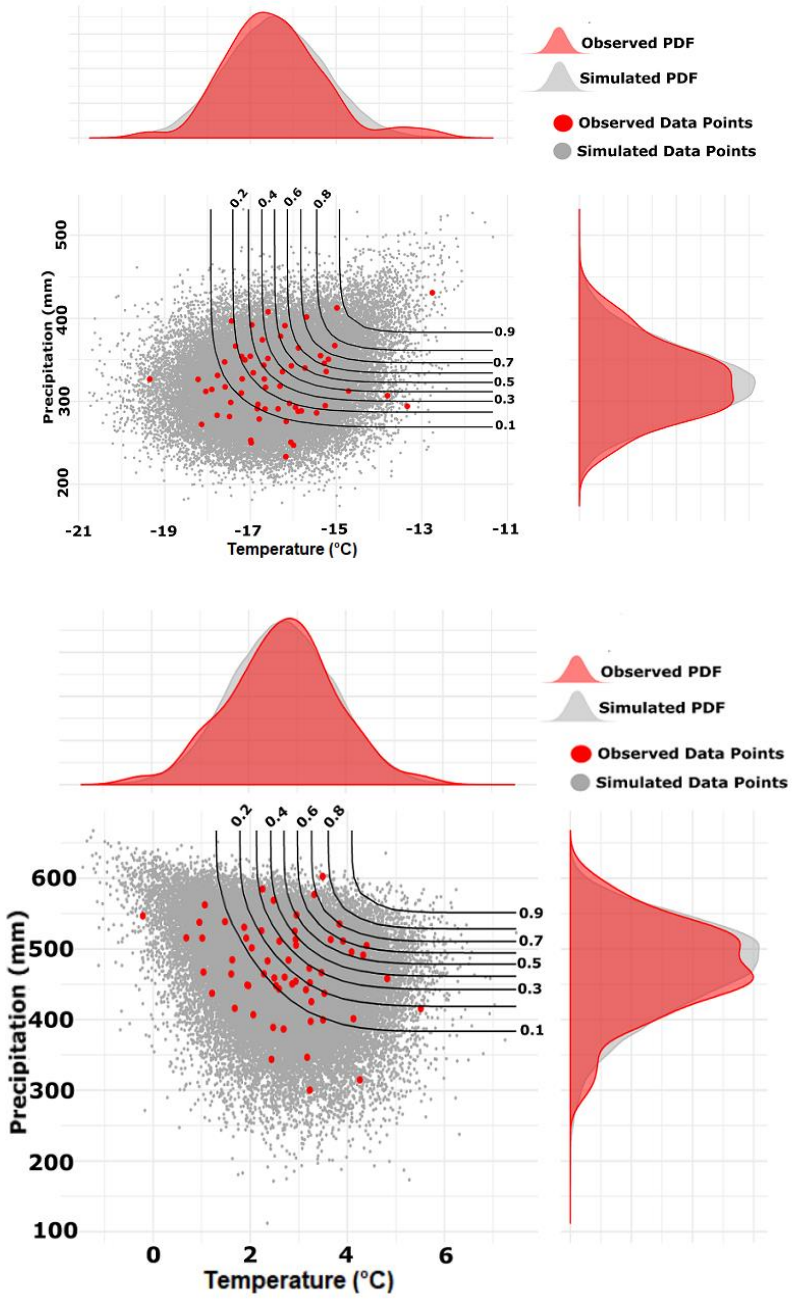

Figure 2 - Joe copula and R270 Clayton copula used to characterize the joint behaviour of temperature and precipitation in the southern Arctic (top) and Prairies zones (bottom), respectively from 1950-2010. Red and grey points are the observed and simulated data overlaid with contours of the joint CDF.

3.4.2 Seasonal Dependency

The northern and southern Arctic zones are the only two zones that maintain a positive correlation between temperature and precipitation throughout the four seasons indicating that the northern regions tend to get wetter with rising temperatures (Figure 3). Zones 9 and 10 (i.e. Boreal Plains and Canadian Prairies) maintain negative correlations throughout all seasons that reflect hot and dry conditions prevalent in the region. More zones exhibit significant correlations in summer than in any other season whereas the magnitude of the correlation is highest in spring and fall, reaching below -0.4 for the Prairies and the Boreal Plains, respectively. Correlations are negligible in winter with only Boreal Plain exhibiting statistical significance.

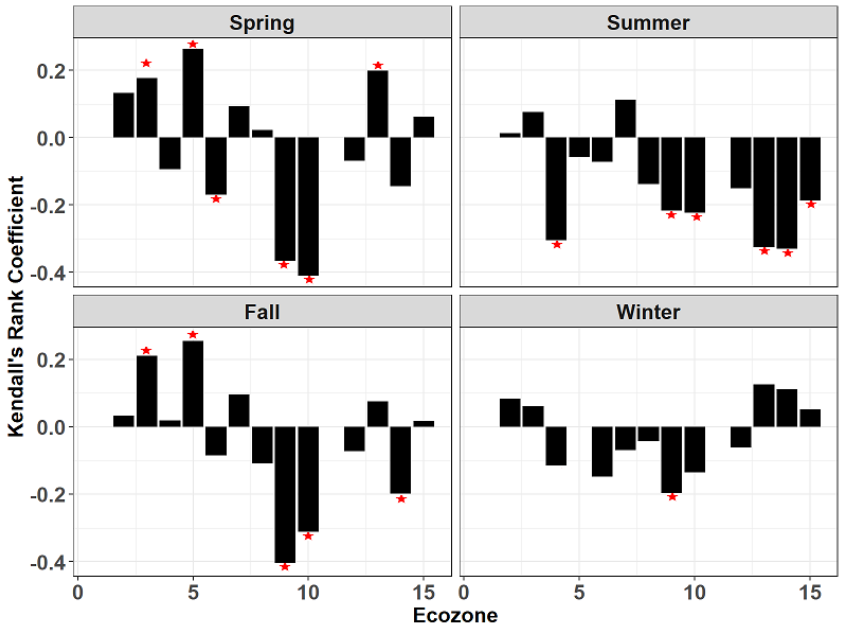

Figure 3 - Kendall's rank coefficients across all zones in each season analysed for 1950-2010. The red asterisk signifies statistically significant correlations at a level of 5%.

Each copula is selected from a pool of candidate models according to the minimum AIC_c score and then evaluated using the goodness of fit test. Copulas selected for each

season passed the goodness of fit test at a significance level of 5% with p-values ranging from 0.44 in winter to 0.72 in spring providing strong evidence that the empirical data follows the selected parametric copula (p-value = 1 indicates a perfect match). The dependence structure in the Boreal Plains is quite similar in all seasons except in the summer (Figure 4). The accumulated precipitation is highest in the summer with the peak copula density at a temperature of 13 °C and 175 mm/season of rain. In all other seasons, the precipitation peak drops below 150 mm/season with the lowest amount in winter at under 100 mm/season. In summer, the dependency between high temperature and low precipitation is evident in the lower tail indicating that hotter summers tend to receive lower than average precipitation. This corresponds to the prevalence of hot and dry conditions, which might exacerbate conditions that can lead to frequent droughts in the region. However, Stewart (2012) showed that drought conditions are not only the result of hot and dry conditions but in fact, cold and dry conditions are common during droughts. They identified 15-month long cold-dry periods using the Standardized Precipitation Index, which occurred during droughts and mostly in late spring. These findings which reflects in the results reported here as well as winter receives the least amount of accumulated precipitation.

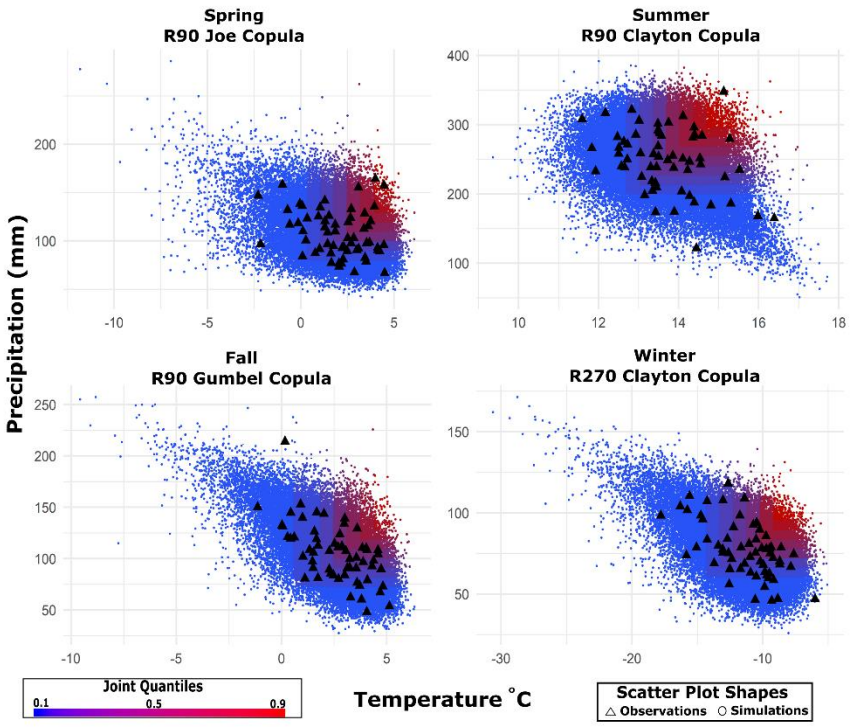

Figure 4 – Copulas selected for the Boreal Plains zone in each season for 1950-2010 based on 9 stations in the zone. Circles and triangles represent copula simulations and observed data, respectively. The colour coding represents the joint quantiles of temperature and precipitation.

3.4.3 Monthly Dependency

The northern and southern Arctic zones (zones 2 and 3) show significantly strong positive correlations from October to March, whereas the Boreal Plains and Prairie zones (9 and 10) show significant negative correlations throughout the year, peaking around the months of August to November (Figure 5). In western zones, including the Pacific Maritime and Montane Cordillera, the dependence shifts from significantly positive in November to February to significantly negative in June to August and September. Majority of the copulas selected for these cases are the ones which exhibit both lower and upper tail dependence (2-parameter copulas) indicating correlation in extremes. Strong concordance (i.e. positive dependence) in winter months suggests a wetting and warming trend whereas

the discordance in summer months hints towards hotter and drier conditions as temperatures rise. This is consistent with Merritt et al. (2006) who reported that winter temperatures are expected to rise by 1.5° - 4.0° C with a corresponding 5-20% increase in precipitation by 2050s. Zhang et al. (2000) reported similar findings with a significant increase in precipitation in all four seasons. They reported increases in snowfall due to increased winter precipitation, which can lead to larger deposits of snow and increases in the magnitude of late winter – early spring flooding. Although this effect can be restricted to higher elevations as other studies have reported reductions in snow water equivalent (Najafi et al., 2017a). Najafi et al. (2017b) attributed the declines in summer runoff in four major river basins in British Columbia to the reduction of April-1st SWE caused by anthropogenic influence. The zones which did not show any significant correlations at the annual and seasonal timescales do not exhibit any relationship at the monthly timescale.

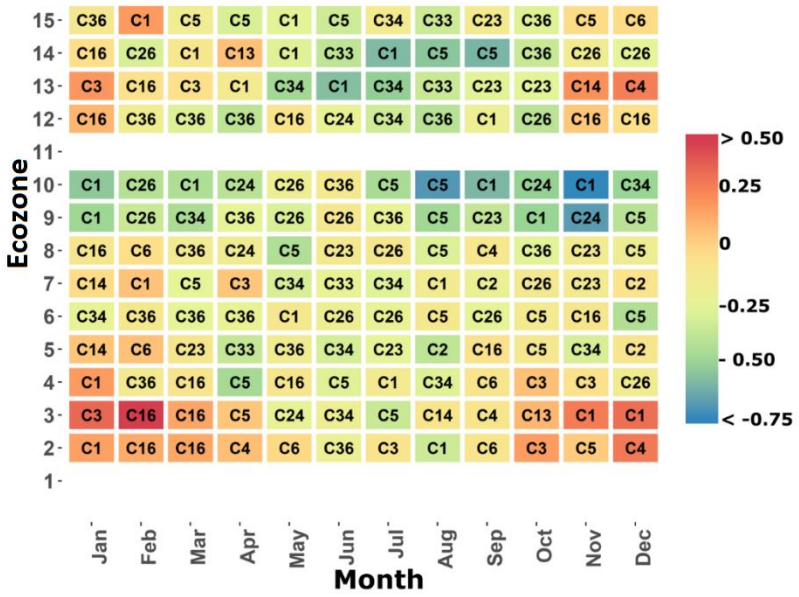

Figure 5 – Kendall's rank correlation coefficient (colour scale) and the corresponding copula (symbol) selected for monthly aggregated data across all zones.

3.4.4 Non-stationary Dependence Structure

The Mann-Kendall trend test analysis is performed on the pre-whitened (if the significant serial correlation is found at a 5% significance level) temperature and precipitation data. Significant temperature trends are found in all zones except for Zone 14 (Montane Cordillera), whereas precipitation trends are statistically insignificant in all zones except for Zone 12 (Boreal Cordillera) (Table 3).

Table 3 – p-values of the Mann-Kendall trend test for temperature and precipitation. Bold numbers represent statistically significant trends at 5% significance level.

Zone	Temperature trend (°C/108 years)	P-value of temperature trend	Precipitation Trend (mm/108 years)	P-value of precipitation trend
6 – Boreal Shield	1.63	0.000*	4.89	0.055
7 – Atlantic Maritime	1.15	0.000*	5.80	0.066
8 – Mixedwood Plains	1.86	0.000*	5.25	0.118
9 – Boreal Plains	1.68	0.000*	0.60	0.398
10 – Prairies	1.88	0.001*	-1.16	0.740
12 – Boreal Cordillera	1.29	0.019*	8.16	0.019*
13 – Pacific Maritime	1.71	0.000*	4.00	0.275
14 – Montane Cordillera	0.87	0.445	0.85	0.056

The non-stationary approach is applied at the seasonal time scale for each zone. The common observation among all zones and seasons is the warming trend over the last century. Copula peak densities (i.e. the mode of the joint probability density function for each 50-year moving window) have shifted to the right on the temperature axis in every case while precipitation shows variations among zones and seasons. Here, we present the results of summer and winter seasons for the Mixed Wood Plains (Zone 8) and Boreal Plains (Zone 9).

Figure 6 shows the peak of the joint distribution for each moving window, which depicts the most probable joint event within the corresponding time period. Results of Zone 8 (i.e. Mixed Wood Plains) show that the region has been getting warmer and wetter in the summer over the last century. Whereas temperature shows an approximate increase of 4% from the first to the last time window, precipitation shows an increase of almost 8% in the same period. In winter, temperature increases are higher compared to the ones in the summer, close to 7%, but precipitation amounts show a steep increase in the 1980s before returning to almost the same levels of the initial window by 2017. Although as discussed previously, Zone 8 does not show significant evidence of dependence between temperature and precipitation, the "warmer and wetter" trend in summer is in line with the joint behaviour observed in almost all other zones. The same was reported by Zhang et al. (2000) who observed that the joint 66^{th} quantiles of temperature and precipitation have been growing larger in southern Canada indicating an increase in wetter and warmer conditions.

Zone 9 (i.e. Boreal Plain) shows a decline in precipitation levels with increasing temperatures in the latter half of the last century. This is similar to the findings of the

seasonal analysis of the 1950-2010 period that showed a strong negative dependence between temperature and precipitation in all seasons particularly in the summer.

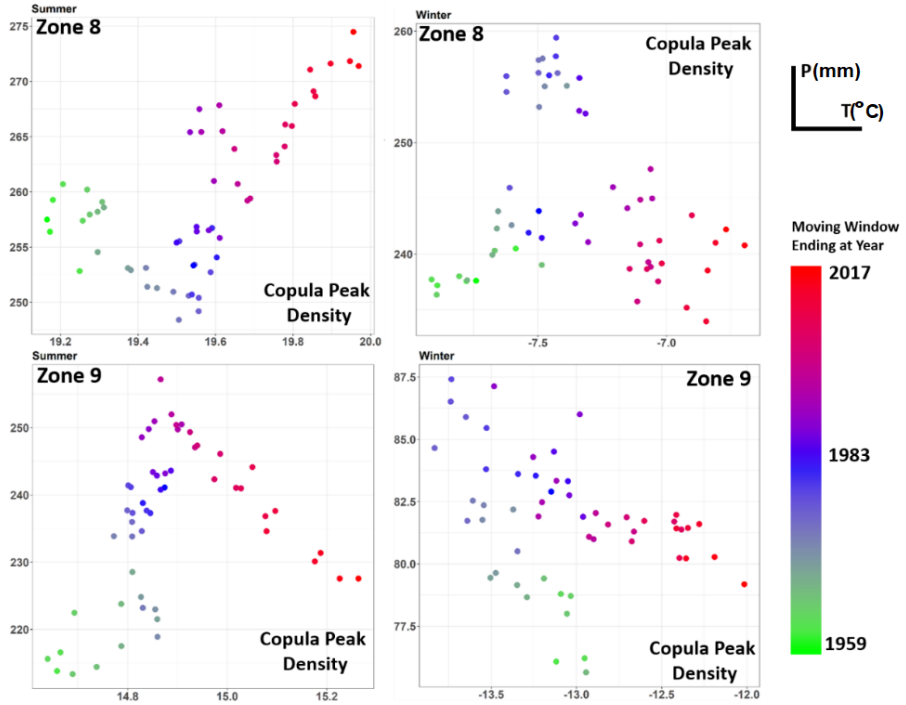

Figure 6 – Results of non-stationary copula analysis in Zone 8 (Mixed Wood Plains) and Zone 9 (Boreal Plains). The scatterplot shows the peak density (i.e. the most probable joint occurrence of temperature and precipitation) at each 50-year moving window from 1900-1959 (the first window) to 1968-2017 (the last window). Precipitation is plotted along the Y-axis and temperature along the X-axis in each figure.

3.4.5 C-C Scaling Curves

The scaling rates of extreme precipitation mostly deviate from the theoretical value of 6.8% $°C^{-1}$. Most regions show lower scaling rates (i.e. sub-CC) except in the north (Table 4). The scaling rates are also proportional to the precipitation amounts in almost all zones with the 95^{th} quantile having the lowest scaling rates in every zone and the 99.9^{th} quantile showing the highest rates (Figure 7). This behaviour is consistent with the results obtained in

previous studies (Jones et al., 2010; Panthou et al., 2014; Singleton and Toumi, 2013; Utsumi et al., 2011). One of the reasons that sub-CC scaling rates are observed is because precipitation is analysed at a daily temporal scale and previous studies have shown that the CC scaling rates decline as the temporal scale is increased from sub-daily to daily. For example, in a multi-time scale study over Quebec, Panthou et al. (2014) reported that as the temporal scale of precipitation increases from shorter to longer durations, the CC scaling rate would decline. Jones et al. (2010) provide another insight into the phenomenon that as the air temperature increases beyond 26°C, there is a reduction in relative humidity in the air. They argue that even though the moisture-holding capacity of the air would theoretically increase with increasing temperature, the amount of moisture available to the air would decline at high temperatures thus causing a decline in extreme precipitation. Super-CC scaling rates (i.e. scaling rates over 6.8%) are observed in the northern regions consistent with Utsumi et al. (2011) who found increases in the global observed extreme precipitation only at high latitudes (> 55° N). To better understand the spatial variability of the scaling rates a station by station analysis was also performed using similar procedure applied for each zone (Figures S7-S9). The results show spatial heterogeneity of the scaling rates and sensitivity to the spatial scale. For example, one of the highest scaling rates (close to +16%) is found on the western coast in zone 13 (Pacific Maritime) while the corresponding zone has one of the lowest scaling rates due to the effects of other stations. The at-site CC ratios range between slightly negative rates (mostly in southwestern region) to approximately +16%. For each extreme quantile of precipitation, there were at least 30 stations with values more than the theoretical scaling rate indicating larger increases in extreme precipitation with rising temperature compared to CC estimates. For other stations,

although the scaling ratio is below the theoretical value, but they still point to increases in intense precipitation rates in a warmer climate.

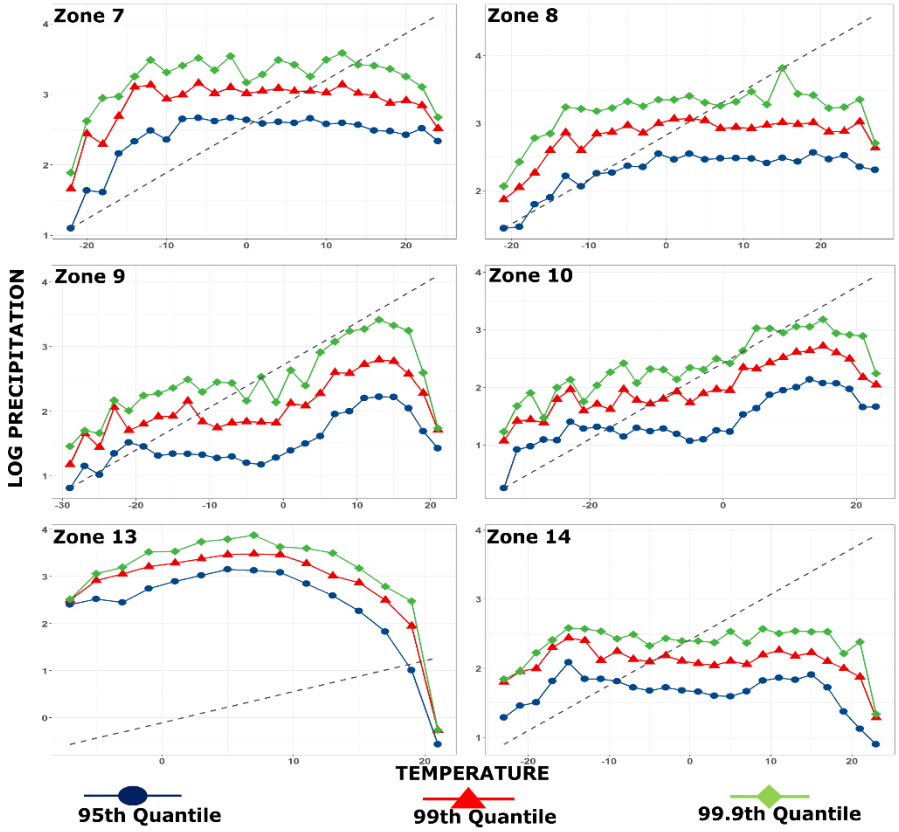

Figure 7 – CC-Scaling curves for extreme precipitation and temperature. Grey dotted line corresponds to the theoretical scaling rate of 7.3% $°C^{-1}$ at 0°C. Blue, red and green lines represent the 95th, 99th and 99.9th quantile of precipitation, respectively.

Table 4 – Scaling rates for extreme precipitation over Canadian ecozones.

Quantile	Zone	**Scaling** ($\%°C^{-1}$)	Zone	**Scaling** ($\%°C^{-1}$)
95th	2	8.82	8	3.04
99th		10.96		3.25

99.9th		12.71		3.81
95th	3	7.62	9	2.57
99th		8.78		3.16
99.9th		10.03		3.72
95th	4	5.13	10	3.03
99th		6.12		3.67
99.9th		8.77		3.81
95th	5	3.01	13	-1.95
99th		3.38		0.16
99.9th		3.65		1.67
95th	6	1.55	14	0.81
99th		1.75		1.02
99.9th		2.81		1.63
95th	7	4.21	15	8.24
99th		4.61		8.31
99.9th		4.65		8.89

3.5 Conclusion

This study characterizes the dependence structure between temperature and precipitation over Canada using copulas. The analyses are conducted over 15 terrestrial ecozones to represent the spatial patterns of the corresponding covariabilities at the annual, seasonal, and monthly temporal scales. AHCCD station data are first spatially and then temporally aggregated within each ecozone of Canada to the respective timescales. The Kendall's rank correlations are calculated and if significant correlations (at 5% significance level) are found, then the non-linear dependency is analyzed using copulas. Further, this procedure is adapted into a moving window copula analysis over long-term historical records dating back to 1910 to reveal the joint trends between temperature and precipitation. C-C scaling curves are built for all zones to find evidence of changes in precipitation that might have occurred due to the gradual rise in temperature over the past decades.

The northern regions show relatively strong positive correlations between temperature and precipitation. In addition, they show upper tail dependencies indicating that warmer periods tend to correlate with wetter periods in these regions. The Canadian Prairies, however, show strong negative dependencies between the two variables, with strong evidence of tail dependence between hot and dry conditions. The moving window analysis shows that while temperature trends are significant throughout southern Canada from 1910-2017, precipitation trends are spatially varied. Temperature increases are highest in the Boreal Plains and Prairies accompanied with negligible changes in precipitation in the Boreal Plains and a non-significant decrease in the Prairies. The consensus is that most regions tend to become warmer and wetter except for the zones in the Canadian Prairies, which show warmer and drier conditions. This is in line with the findings of stationary copulas.

Southeastern Canada and zones around east and west of Hudson Bay show no significant dependencies between temperature and precipitation. In addition, extreme precipitation is studied with respect to temperature changes using the Clausius-Clapeyron scaling relationship. Large deviations from theoretical values are observed in all regions with super-CC scaling rates in the north and sub-CC scaling rates in most of the south, particularly the west coast where negative scaling rates were also observed. The study is limited by the number of observation records, especially in the northern regions of Canada. A potential future work would be extend this analysis to the whole spatial domain by incorporating data from reanalysis products and satellite based datasets.

This study shows the non-linear relationships exhibited by temperature and precipitation across Canada. The findings here can help better understand the effects of these two variables that result in compound scenarios such as the prevalence of warm-wet and hot-dry conditions.

3.6 References

Akaike H (1974) A new look at the statistical model identification. In Selected Papers of Hirotugu Akaike. Springer, New York, NY pp 215-222

Akinremi OO, McGinn SM, Cutforth HW (1999) Precipitation trends on the Canadian prairies. Journal of Climate 12(10): 2996-3003

Allen CD, Macalady AK, Chenchouni H, Bachelet D, McDowell N, Vennetier M, Gonzalez P (2010) A global overview of drought and heat-induced tree mortality reveals emerging climate change risks for forests. Forest ecology and management 259(4): 660-684

Anderson TW (1962). An introduction to multivariate statistical analysis (No. 519.9 A53). New York: Wiley

Asong ZE, Khaliq MN, Wheater HS (2016) Multisite multivariate modeling of daily precipitation and temperature in the Canadian Prairie Provinces using generalized linear models. Climate dynamics 47(9-10): 2901-2921

Barnett TP, Adam JC, Lettenmaier DP (2005) Potential impacts of a warming climate on water availability in snow-dominated regions. Nature 438(7066): 303–309

Bender J, Wahl T, Jensen J (2014) Multivariate design in the presence of non-stationarity. Journal of Hydrology 514: 123-130

Beniston M (2009) Trends in joint quantiles of temperature and precipitation in Europe since 1901 and projected for 2100. Geophysical Research Letters 36(7)

Berkes F, Jolly D (2002) Adapting to climate change: social-ecological resilience in a Canadian western Arctic community. Conservation ecology 5(2): 18

Bintanja R, Selten FM (2014) Future increases in Arctic precipitation linked to local evaporation and sea-ice retreat. Nature 509(7501): 479-482

Bird PM , D Rapport (1986) State of the environment report for Canada, Environment Canada.

Blankinship JC, Hart SC (2012). Consequences of manipulated snow cover on soil gaseous emission and N retention in the growing season: a meta-analysis. Ecosphere 3(1): 1-20

Burke M, Hsiang SM, Miguel E (2015). Global non-linear effect of temperature on economic production. Nature 527(7577): 235-239

Anderson DR, Burnham K (2004). Model selection and multi-model inference. Second NY: Springer-Verlag, 63

Burnham KP, Anderson DR, Huyvaert KP (2011). AIC model selection and multimodel inference in behavioral ecology: some background, observations, and comparisons. Behavioral ecology and sociobiology 65(1): 23-35

Bush E, Lemmen DS (2019) Canada's Changing Climate Report; Government of Canada, Ottawa, ON pp 444

Cong RG, Brady M (2012). The interdependence between rainfall and temperature: copula analyses. The Scientific World Journal, 2012

Déry SJ, Wood EF (2005). Observed twentieth century land surface air temperature and precipitation covariability. Geophysical Research Letters 32(21)

Eastoe EF (2009). A hierarchical model for non-stationary multivariate extremes: a case study of surface-level ozone and NOx data in the UK. Environmetrics: The official journal of the International Environmetrics Society 20(4): 428-444

Environment Canada (2014). Canada's Sixth National Report on Climate Change

Favre AC, El Adlouni S, Perreault L, Thiémonge N, Bobée B (2004). Multivariate hydrological frequency analysis using copulas. Water resources research 40(1)

Filmon G (2004). Firestorm 2003 provincial review, Firestorm 2003 Provincial Review

Frees EW, Valdez EA (1998). Understanding relationships using copulas. North American actuarial journal 2(1): 1-25

Genest C (1987). "Frank's family of bivariate distributions." Biometrika 74.3 (1987): 549-555.

Genest C, Favre AC (2007). Everything you always wanted to know about copula modeling but were afraid to ask. Journal of hydrologic engineering 12(4): 347-368

Genest C, Quessy JF, Rémillard B (2006). Goodness-of-fit procedures for copula models based on the probability integral transformation. Scandinavian Journal of Statistics 33(2): 337-366

Genest C, Rémillard B (2008). Validity of the parametric bootstrap for goodness-of-fit testing in semiparametric models. In Annales de l'IHP Probabilités et statistiques Vol. 44 No. 6 pp 1096-1127

Genest C, Rivest LP (1993). Statistical inference procedures for bivariate Archimedean copulas. Journal of the American statistical Association 88(423): 1034-1043

Gennaretti F, Sangelantoni L, Grenier P (2015). Toward daily climate scenarios for Canadian Arctic coastal zones with more realistic temperature-precipitation interdependence. Journal of Geophysical Research: Atmospheres 120(23): 11-862

Guerfi N, Assani AA, Mesfioui M, Kinnard C (2015). Comparison of the temporal variability of winter daily extreme temperatures and precipitations in southern Quebec (Canada) using the Lombard and copula methods. International Journal of Climatology 35(14): 4237-4246

Hao Z, Singh VP (2016). Review of dependence modeling in hydrology and water resources. Progress in Physical Geography 40(4): 549-578

Hardwick Jones R, Westra S, Sharma A (2010). Observed relationships between extreme sub-daily precipitation, surface temperature, and relative humidity. Geophysical Research Letters 37(22)

Henze N (1996) Empirical-distribution-function goodness-of-fit tests for discrete models. Canadian Journal of Statistics 24(1): 81-93

Isaac GA, Stuart RA (1992). Temperature–precipitation relationships for Canadian stations. Journal of climate 5(8): 822-830

Joe H (2014). Dependence modeling with copulas. Chapman and Hall/CRC

Johnson RA, Wichern DW (2002). Applied multivariate statistical analysis Vol. 5 No. 8. Upper Saddle River NJ Prentice hall

Jonathan P, Ewans K, Randell D (2014). Non-stationary conditional extremes of northern North Sea storm characteristics. Environmetrics 25(3): 172-188

Kao SC, Govindaraju RS (2010). A copula-based joint deficit index for droughts. Journal of Hydrology 380(1-2): 121-134

Khajehei S, Ahmadalipour A, Moradkhani H (2018). An effective post-processing of the North American multi-model ensemble (NMME) precipitation forecasts over the continental US. Climate dynamics 51(1-2): 457-472

Laux P, Vogl S, Qiu W, Knoche HR, Kunstmann H (2011). Copula-based statistical refinement of precipitation in RCM simulations over complex terrain. Hydrology and Earth System Sciences 15(7): 2401-2419

Lazoglou G, Anagnostopoulou C (2019). Joint distribution of temperature and precipitation in the Mediterranean, using the Copula method. Theoretical and Applied Climatology 135(3-4): 1399-1411

Mekis E, Vincent LA (2011). An overview of the second generation adjusted daily precipitation dataset for trend analysis in Canada. Atmosphere-Ocean 49(2): 163-177

Vincent LA, Wang XL, Milewska EJ, Wan H, Yang F, Swail V (2012). A second generation of homogenized Canadian monthly surface air temperature for climate trend analysis. Journal of Geophysical Research: Atmospheres: 117(D18)

Merritt WS, Alila Y, Barton M, Taylor B, Cohen S, Neilsen D (2006). Hydrologic response to scenarios of climate change in sub watersheds of the Okanagan basin, British Columbia. Journal of Hydrology 326(1-4): 79-108

Min SK, Zhang X, Zwiers FW, Agnew T (2008). Human influence on Arctic sea ice detectable from early 1990s onwards. Geophysical Research Letters: 35(21).

Najafi MR, Zwiers FW, Gillett NP (2016). Attribution of the spring snow cover extent decline in the Northern Hemisphere, Eurasia and North America to anthropogenic influence. Climate Change 136(3-4): 571-586.

Najafi MR, ZwiersF, Gillett N (2017a). Attribution of the observed spring snowpack decline in British Columbia to anthropogenic climate change. Journal of Climate 30(11):

4113-4130 Najafi, MR, Zwiers FW, Gillett NP (2017b). Attribution of observed streamflow changes in key British Columbia drainage basins. Geophysical Research Letters 44(21): 11012-11020

Nelsen RB (2007). An introduction to copulas. Springer Science & Business Media

Pachauri Rajendra K et al. Climate change 2014: synthesis report. Contribution of Working Groups I, II and III to the fifth assessment report of the Intergovernmental Panel on Climate Change. IPCC, 2014

Pall P, Allen MR, Stone DA (2007). Testing the Clausius–Clapeyron constraint on changes in extreme precipitation under CO 2 warming. Climate Dynamics 28(4): 351-363

Panthou G, Mailhot A, Laurence E, Talbot G (2014). Relationship between surface temperature and extreme rainfalls: A multi-time-scale and event-based analysis. Journal of hydrometeorology 15(5): 1999-2011

Peel MC, Finlayson BL, McMahon TA Updated world map of the Köppen-Geiger climate classification. Hydrology and Earth System Sciences 11, 1633–1644.

Rana A, Moradkhani H, Qin Y (2017). Understanding the joint behavior of temperature and precipitation for climate change impact studies. Theoretical and Applied Climatology 129(1-2): 321-339

Ulf Schepsmeier et al. (2018). VineCopula: Statistical Inference of Vine Copulas. R package version 2.1.8

Salvadori G, De Michele C (2004). Frequency analysis via copulas: Theoretical aspects and applications to hydrological events. Water resources research 40(12)

Schmidt T (2007). Coping with copulas. Copulas-From theory to application in finance: 3-34

Schoelzel C, Friederichs P (2008). Multivariate non-normally distributed random variables in climate research–introduction to the copula approach. Nonlinear Processes in Geophysics 15(5): 761-772

Shabbar A, Skinner W (2004). Summer Drought Patterns in Canada and the Relationship to Global Sea Surface Temperatures. Journal of Climate 17(14): 2866-2880

Shiau JT (2006). Fitting drought duration and severity with two-dimensional copulas. Water resources management 20(5): 795-815

Singleton A, Toumi R (2013). Super-Clausius–Clapeyron scaling of rainfall in a model squall line. Quarterly Journal of the Royal Meteorological Society 139(671): 334-339

Sklar M (1959). Fonctions de repartition an dimensions et leurs marges. Publ. inst. statist. univ. Paris 8: 229-231.

Stewart RE, Bonsal BR, Harder P, Henson W, Kochtubajda B (2012). Cold and hot periods associated with dry conditions over the Canadian prairies. Atmosphere-Ocean 50(3): 364-372

Stute W, Manteiga WG, Quindimil MP (1993). Bootstrap based goodness-of-fit-tests. Metrika 40(1): 243-256

Tencer B, Weaver A, Zwiers F (2014). Joint occurrence of daily temperature and precipitation extreme events over Canada. Journal of Applied Meteorology and Climatology 53(9): 2148-2162

Trenberth KE, Shea DJ (2005). Relationships between precipitation and surface temperature. Geophysical Research Letters 32(14)

Trömel S, Schönwiese CD (2007). Probability change of extreme precipitation observed from 1901 to 2000 in Germany. Theoretical and Applied Climatology 87(1-4): 29-39

Utsumi N, Seto S, Kanae S, Maeda EE, Oki T (2011). Does higher surface temperature intensify extreme precipitation? Geophysical research letters: 38(16)

Vincent LA et al. (2015). Observed trends in Canada's climate and influence of low-frequency variability modes. Journal of Climate 28(11): 4545-4560

Vincent LA, Zhang X, Mekis É, Wan H, Bush EJ (2018). Changes in Canada's Climate: Trends in Indices Based on Daily Temperature and Precipitation Data. Atmosphere-Ocean 56(5): 332-349

Wahl T, Jain S, Bender J, Meyers SD, Luther ME (2015). Increasing risk of compound flooding from storm surge and rainfall for major US cities. Nature Climate Change 5(12): 1093-1097

Wang W, Wells MT (2000). Model selection and semiparametric inference for bivariate failure-time data. Journal of the American Statistical Association 95(449): 62-72

Warren FJ, Lemmen DS (2014). Canada in a changing climate: Sector perspectives on impacts and adaptation. Ottawa: Natural Resources Canada.

Watson RT, Zinyowera MC, Moss RH, Dokken DJ (1998). The regional impacts of climate change. IPCC, Geneva

Wiken EB (1986). Terrestrial ecozones of Canada, Ecological Land Classification Series No. 19. Environment Canada, Ottawa.

Wong G, Lambert MF, Leonard M, Metcalfe AV (2009). Drought analysis using trivariate copulas conditional on climatic states. Journal of Hydrologic Engineering 15(2): 129-141

Zhang LS, Singh VP (2006). Bivariate flood frequency analysis using the copula method. Journal of hydrologic engineering 11(2): 150-164

Zhang X, Vincent LA, Hogg WD, Niitsoo A (2000). Temperature and precipitation trends in Canada during the 20th century. Atmosphere-ocean 38(3): 395-429

Zwiers FW, Von Storch H (1995). Taking serial correlation into account in tests of the mean. Journal of Climate 8(2): 336-351

Chapter 4.

Evaluation of Gridded Climate Datasets over Canada using Univariate and Bivariate Approaches: Implications for Hydrological Modelling

4.1 Introduction

Extreme weather events commonly occur because of the interactions between temperature and precipitation. For example, precipitation in an unusually warm winter day will likely increase the chances of flooding in snow-packed regions. Similarly, extended periods of low precipitation along with high temperatures in the summer give rise to heatwaves, droughts and wildfires. In 2017, British Columbia spent almost $649 million suppressing wildfires, which also lead to the evacuation of 65,000 people from the fire-affected area (a record 1.2 million hectares) (Service, BC Wildfire, 2019). In July 2018, heatwave caused over 90 deaths in Quebec with temperatures consistently peaking over 35°C for over a week (Pelmorex Weather Networks Inc., 2018). In April 2017, the highest water levels in the last 50 years were recorded in the Ottawa River basin, which lead to flooding in southern Quebec. The flooding damaged 5,371 residences and cost upwards of $228 million (Philips, 2018). Recently, the 2019 spring flood in Quebec proved to be even more disastrous, leaving over 10,000 people homeless (Haines, 2019). Figure 8 shows some of the extreme events that can be directly attributed to the covariability of temperature and

precipitation since 2015 based on *Canada's Top 10 Weather Stories* (Environment and Climate Change Canada, 2018).

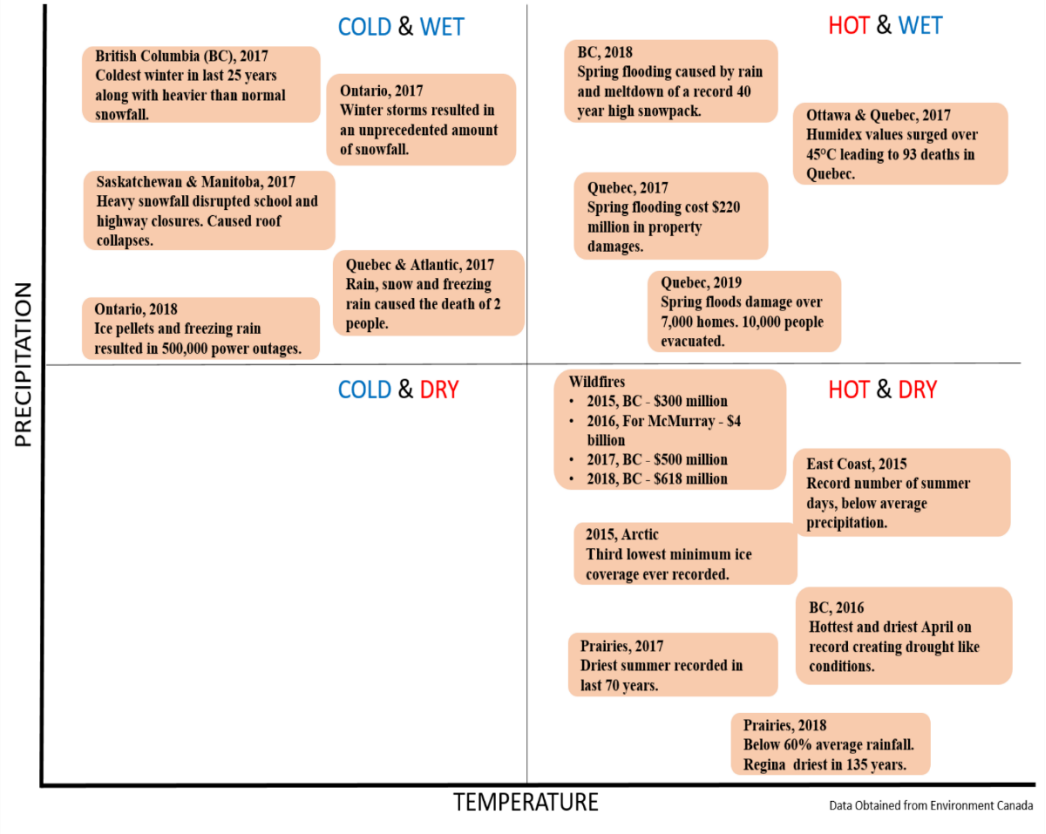

Figure 8 - Extreme Weather events from 2015 – 2019 which can be attributed to temperature and precipitation covariability. The four quadrants depict different conditions created by the possible combinations of temperature and precipitation.

According to the Intergovernmental Panel on Climate Change (IPCC) special report (Seneviratne et al., 2012) compound events can be defined as, *"two or more extreme events occurring simultaneously or successively", or "combinations of events that are not themselves extremes but lead to an extreme event or impact when combined."*. The increasing frequency of extremes and their catastrophic effects on human life and infrastructure have resulted in peaked interest in identification, prediction and mitigation

of compound events. Highlighting shortcomings of the definition of compound events in the IPCC report, Leonard et al. (2014) proposed a more general definition "*A compound event is an extreme impact that depends on multiple statistically dependent variables or events*" and laid out a framework for analysing, modeling and communicating the risks associated with such events. Whereas earlier, most studies performed univariate analysis of extremes, the focus has now shifted towards multivariate analyses considering the joint behaviour of multiple factors. This has been made possible by advances in modeling tools and methodologies for studying multivariate data such as copulas introduced by Sklar (1959).

Copulas are a set of functions that can bind individual marginals with their dependence structure to create multivariate distributions, which allow for easy interpretation of joint return periods and exceedance probabilities. The efficacy of applying copulas to meteorology and climate research was presented by Schoelzel and Friederichs (2008). AghaKouchak et al. (2014) used copulas to show that univariate methods underestimate or overestimate drought return periods as compared to the bivariate study of temperature and precipitation. Zscheischler and Seneviratne (2017) analysed joint quantiles of temperature and precipitation and reported that the likelihood of a hot and dry summer in Russia increased by a factor of 5 when both variables were considered as compared to their individual analysis.

Although advances have been made in tools to analyse multivariate data, the availability and reliability of climate data is still a limiting factor. Hutchinson et al. (2009) provide extensive details about the availability of station data in Canada obtained from the National Climate Data Archive (NCDA). They report the presence of 2000-3000 stations measuring

precipitation and 1500-2200 stations measuring temperature from 1961 to 2003. Over 95% of these stations lie in the southern half of Canada, despite that the density of weather stations in southern Canada is 1 per 2500 km^2. Hutchinson et al. (2009) report several other problems with the data such as missing or incorrect coordinates and elevation along with large temporal gaps in the measurements. Environment and Climate Change Canada has produced a more reliable observation dataset called the Adjusted and Homogenized Canadian Climate Data (AHCCD), which provides temperature and precipitation records at 330 and 460 locations across Canada, respectively (Mekis and Vincent, 2011; Vincent et al. 2012). This gap in climate data is filled by temporally and spatially continuous models created using different interpolation techniques on existing station data or through reanalysis products such as Modern-Era Retrospective analysis for Research and Applications (MERRA) by National Aeronautics and Space Administration (NASA) Global Modeling and Assimilation Office (GMAO) (Rienecker et al. 2011), Climate Forecast System Reanalysis (CFSR) by National Centers for Environmental Prediction (NCEP) (Saha et al. 2010), North American Regional Reanalysis (NARR) by National Centers for Environmental Prediction–National Center for Atmospheric Research (NCEP–NCAR) (Mesinger et al. 2006), Japanese 25-year Reanalysis (JRA-25) by Japanese Meteorological Agency (JMA) (Onogi et al. 2007) and ERA-40 by The European Centre for Medium-Range Weather Forecasts (ECMWF) (Uppala et al. 2005).

Despite their advantages and widespread use, these gridded datasets are only estimates of the truth that are required to be validated. Makshtas et al. (2007) compared five variables (sea level pressure, air temperature at 2m, winds at 10m, specific humidity at 2m and total cloudiness) from NCEP-Reanalysis 1 dataset to station observations over the North Pole

drifting stations for 1954-2006. They reported their results based on seasonal mean error (ME), standard deviation (STD) and correlation coefficient (COR). Decker et al. (2012) compared multiple gridded datasets against observations and reported ECMWF Interim Re-Analysis (ERA-Interim) as the best product for surface air temperature and Global Land Data Assimilation System (GLDAS) from the Goddard Space Flight Center (GSFC) for precipitation. They used measures such as Mean Squared Error (MSE), Root Mean Squared Error (RMSE) along with a performance ranking system as proposed by Brunke et. al. (2003). The following metrics are the most widely used criteria for performance evaluation of gridded datasets: Mean Error (ME), Mean Absolute Error (MAE), RMSE, Mean Squared Error (MSE), correlation, parametric distributions and Extreme Climate Indices (CLIMDEX) among few others (Balmaseda et. al. 2013; Bao and Zhang, 2013; Bosilovich et al. 2008; Henn et al. 2018; Janowiak et al. 1998; Werner et al, 2019; Zhang et al. 2011). Wong et al. (2017) compared precipitation from 7 datasets (ground-based, reanalysis, statistically and dynamically downscaled products) across Canada using similar metrics mentioned previously. Other studies in Canada and around the world have also been limited to the univariate analysis of climate variables (Eum et al. 2014; Islam et al, 2017; Werner et al. 2019), and analyses based on the multivariate behaviour of climate variables are lacking. A few studies have compared outputs from hydrological models forced with gridded datasets. Essout et al. (2016) compared three gridded products over 424 basins in the continental United States. They concluded that even though there were significant differences in temperature and precipitation biases, the overall difference in simulated streamflow was not significant for lumped hydrological modeling.

In this study, the univariate and bivariate characteristics of temperature and precipitation from five gridded datasets are evaluated over Canada. The datasets include NRCANmet, NCEP-CFSR, NCEP-NARR, GRASP and S14FD. Results are presented in the form of bias/error metrics for temperature and precipitation along with bivariate evaluation results in the form of formal goodness of fit test for all datasets under the assumption of a true underlying copula represented by the observation dataset. Finally, a hydrological model is forced with unadjusted and bias-corrected input data using two different bias correction methods (univariate and multivariate bias correction) to ascertain the propagation of uncertainty from univariate and multivariate biases in gridded datasets to streamflow simulations.

4.2 Study Area and Data

The study compares temperature and precipitation from five gridded datasets over Canada (Table 5). Adjusted and Homogenized Canadian Climate Data (AHCCD) is used as a reference for the evaluation of the gridded products. The dataset provides the temperature at 338 locations across Canada which were adjusted for multiple factors including non-climatic shifts, discontinuities and errors arising from a nation-wide change in time observation in July 1961 (Vincent et al. 2012). Precipitation data are available at 464 locations and is adjusted for common gauge related issues like wind undercatch, evaporation and wetting losses (Mekis and Vincent, 2011). Discontinuities in both datasets were removed by combining data from nearby gauging locations. The data were also corrected for non-climatic factors like instrument changes and station relocation. Given the bivariate focus of the study, 160 stations that provide both temperature and precipitation measurements are selected. These data are further filtered based on at least 80% data

availability from 1980-01-01 to 2010-12-31, resulting in 113 stations retained for the analysis. Figure 9 shows the selected AHCCD stations along with their elevations.

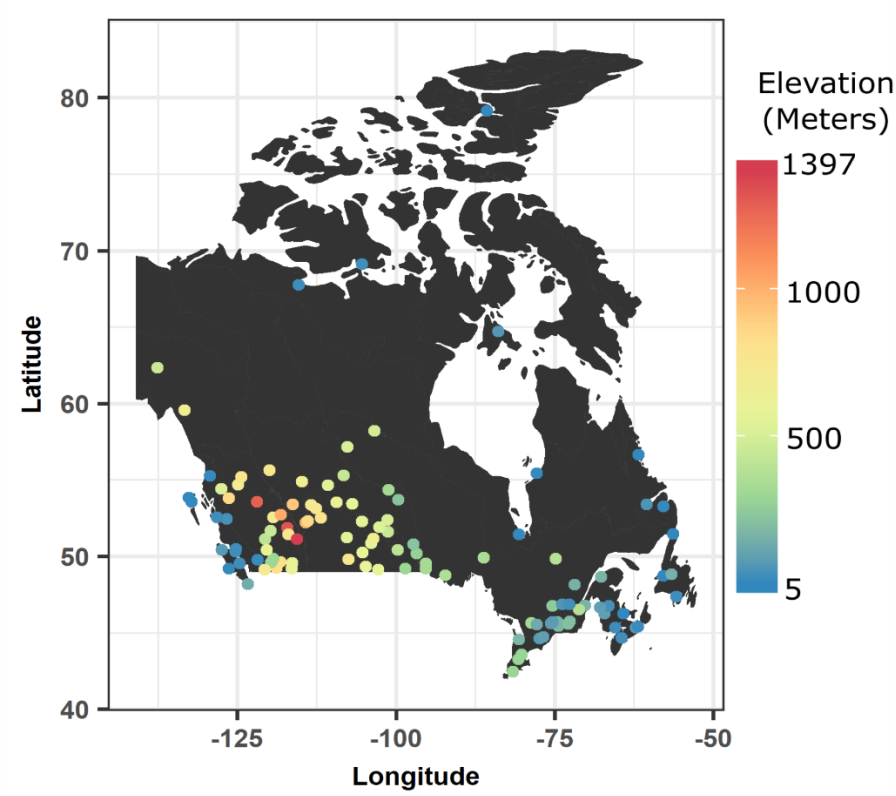

Figure 9 - AHCCD station locations with records of both temperature and precipitation and at least 80% data availability from January 1980 to December 2010.

Natural Resources Canada Meteorological Dataset (NRCANmet)

NRCANmet is a gridded product based on station data from National Climate Data Archive (NCDA), Environment and Climate Change Canada, which is available at a resolution of 30 arc-second (1/12° or ~ 10 km) for 1950 – 2013 (updated from the original time span of 1961-2003). Quality controlled (but not adjusted as in AHCCD) station data were interpolated using the Australian National University Splines (ANUSPLIN) package (Hutchinson et al. 2009), a trivariate thin-plate splines interpolation method that considers

the latitude, longitude and elevation of each site. The dataset is often used as a *source of truth* and has been extensively used in hydrological studies in Canada. Some notable examples include works done by Chen et al. (2011a and 2011b) and Wehner et al. (2011).

NCEP Climate Forecast System Reanalysis (CFSR)

CFSR (Saha et al. 2010) is a global reanalysis product available from 1979 to present at a horizontal resolution of about 35km. The product is a successor to the extensively used Reanalysis-1 dataset produced jointly by National Centers for Environmental Prediction (NCEP) and the National Center for Atmospheric Research (NCAR) (Kalnay et al. 1996). As described by Saha et al. (2010), the novelties of this product include a coupled ocean model, an interactive sea-ice model and assimilation of radiances. The dataset has been used in hydrological studies, as well as evaluation studies (Daggupati et al. 2018; Faramarzi et al. 2015; Rapaić et al. 2015).

Global Risk Assessment toward Stable Production of Food (GRASP)

The GRASP dataset (Iizumi et al. 2014) is created using two different reanalysis products, ERA-40 (Uppala et al. 2005) and JRA-25 (Onogi et al. 2007). It is a global dataset (excluding Antarctica) available at a resolution of 1.125 degrees in both dimensions from 1961–2010. ERA-40 is used to generate the new dataset from 1961-1978 while JRA-25 is used from 1979-2010. Before merging the two datasets to create the new product, the authors match the biases of ERA-40 to JRA-25 followed by the calculation of monthly correction factors based on the corrected ERA-40 dataset. Finally, they apply the correction factors to the two reanalysis products in the respective time-periods as mentioned above. The data was bias-corrected using cumulative distribution function-based downscaling.

GRASP was created with the objective of providing a meteorological forcing dataset for crop modelling.

NCEP North American Regional Reanalysis (NARR)

Mesinger et al. (2006) describe NARR as "long-term, dynamically consistent, high-resolution, high-frequency, atmospheric and land surface hydrology dataset for the North American domain." The dataset is available at a resolution of approximately 32km at the lowest latitude from 1979 to present at 3-hourly intervals. The product is a regional extension of the NCEP Global Reanalysis created using the NCEP Eta Model and the Regional Data Assimilation System (RDAS). Several studies over Canada have used NARR for evaluation/comparison purposes and as forcing to drive hydrological models (Choi et al. 2009; Eum et al. 2014; Woo and Thorne, 2006).

S14 Global Meteorological Forcing Dataset (S14FD)

The S14FD dataset (Iizumi et al. 2017) is created by downscaling and bias correcting the JRA-55 reanalysis available from 1958-2013 at a resolution of ~55km (Kobayashi et al. 2015). JRA-55 is downscaled to a resolution of 0.5°in both dimensions over the 55-year span to obtain S14FD. The 2m air temperature was corrected using the CRU-TS3.22 data (Harris et al. 2014). Monthly precipitation data and dry/wet day frequency were corrected using GPCCv7 and data provided by Motaya et al. (2002), respectively.

Table 5 – Spatial and temporal resolution of the gridded products used in this study.

Dataset	Spatial Resolution	Temporal Resolution

NRCANmet	~10 km in both dimensions	Daily
NCEP-CFSR	~38 km (horizontal)	Sub-Daily (3 hours)
GRASP	1.125˚ in both dimensions	Daily
NCEP-NARR	~32 km (horizontal)	Sub-Daily (3 hours)
S14FD	0.5˚ in both dimensions	Daily

4.3 Methods

All gridded products are evaluated against the AHCCD dataset by comparing the grid records with the closest AHCCD station record. From each gridded product, one grid closest to each of the AHCCD sites is chosen using a simple nearest neighbour algorithm. Mean Bias Error (MBE) is used to evaluate the temperature and precipitation separately. We assess the frequency and magnitude of extreme temperature and precipitation events across each dataset. In addition to the individual analysis of temperature and precipitation, copulas are used to evaluate how well the gridded products mimic the dependence structure of the ground-based data. Furthermore, a hydrological model is forced with temperature and precipitation data from all six datasets to evaluate how the uncertainties, from both univariate and multivariate biases, propagate through the model into the simulated streamflow. The hydrological model is driven under three scenarios: 1) the model is forced with original data from all products, 2) all gridded products are bias-corrected using a univariate bias correction method and 3) the gridded products are bias-corrected using a multivariate bias correction algorithm that corrects for marginal biases as well as the bias

in the dependence structure. The comparison across all scenarios reveals the importance of maintaining the covariability of temperature and precipitation from a hydrological perspective.

The following section describes the metrics used in the validation and comparison process.

4.3.1 Univariate Validation Metrics

Mean Bias Error (MBE) is used to assess the direction and magnitude of biases in temperature and precipitation, respectively.

$$MBE = \frac{\sum_{i=1}^{n}(g_i - o_i)}{n} \qquad (9),$$

where (o_i) represents the observation AHCCD, (g_i) represents the gridded data and n is the total number of data records. Analyses are performed for each season separately i.e. winter (DJF), spring (MAM), summer (JJA) and fall (SON).

The magnitude of extreme precipitation is compared by taking the accumulated precipitation of all days exceeding the 95th quantile of wet days (pr > 1mm) within each year and then averaging it across the 31-year period. This approach is similar to the definition of R95p (Annual total precipitation when RR > 95th percentile) by the Expert Team on Climate Change Detection and Indices (ETCCDI) which is part of the extreme climate indices (Zhang et al. 2011). The magnitude of extreme temperature is analysed by comparing the annual average of 95th quantiles of daily temperature across all datasets.

To evaluate the frequency of extremes in each dataset, we followed the approach proposed by Papalexiou and Montanari (2019). The method involves extracting N highest precipitation extremes from a data record of N years. A discrete data series is then created

by counting the number of extremes that occurred within each year. This method results in a frequency series of length N, where some years have multiple extremes and some years may have none. The frequency series corresponding to gridded datasets are compared to the one from AHCCD using Pearson correlation coefficient. This method is applied to both temperature and precipitation extremes in this study.

4.3.2 Bivariate Validation

Copulas are used for comparing the full dependence structure instead of other measures, such as correlation coefficients (for details on copulas, refer to sections 3.3.1 and Appendix-A1). This provides a more robust assessment of the interrelationships between precipitation and temperature because it is possible that two pairs of data with similar correlation coefficients have different dependence structure especially in their tails or extreme values, which is of most interest in hydrological applications. Figure 10 shows an example where two synthetic datasets have exactly similar rank correlation but different dependence behaviour in their tails.

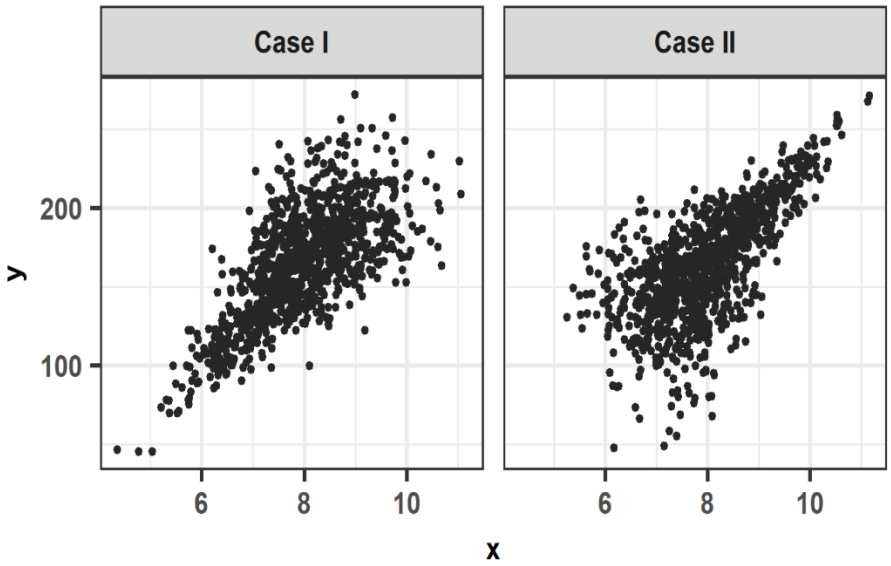

Figure 10 - Two synthetic datasets having the same Kendall's rank correlation ($\tau = 0.50$) but different dependence, especially in the tails. This emphasizes the need to use copulas as a bivariate comparison metric since they capture the full dependence structure including extremes. For example, Case I here corresponds to a Clayton copula with parameter 1.98 and Case II corresponds to Joe copula with parameter 2.91.

In this study, we use the Archimedean family of copulas, which are the most widely used class of copulas in hydrological studies (Grimaldi and Serinaldi 2006; Zhang and Singh, 2006). This family of copulas consist of Clayton, Frank, Joe and Gumbel copula. The copula model selection, for each site, is performed based on the Akaike Information Criterion (AIC) (Akaike, 1974). AIC stems from the field of information theory. Given two candidate models, and one true unknown model, AIC attempts to minimize the Kullback-Leibler divergence (Kullback and Leibler, 1951) of the candidate model to the true model, thus, in turn, minimizing the information loss when the candidate model is used instead of the true model (Burnham and Anderson, 2003). The model that leads to the least loss of information (i.e. lowest AIC score) is selected.

AIC is calculated by taking into consideration the residual sum of squares (RSS) and the number of parameters of the copula function as a penalising factor.

$$AIC = N \log\left(\frac{RSS}{N}\right) + 2p \qquad (10),$$

where N is the number of samples and p is the number of copula parameters.

The fitted model is further evaluated using a formal goodness of fit test for copulas proposed by Genest et al. (2006). See Appendix-A5 for further details.

To identify whether a particular dataset captures the true dependence between temperature and precipitation, we perform the following procedure: Using AIC and GOF test, a parametric copula C_p (from the Archimedean family of copulas) is fitted to the reference data (AHCCD). It is assumed that the copula C_p represents true dependence structure between temperature and precipitation because the observed data are indeed considered the ground truth. Then, the fit of the selected copula is tested on the other datasets and a p-value is calculated based on the null hypothesis $H_0 : C' \epsilon\, C_p$, where C' is the empirical copula of the gridded dataset under evaluation. Based on a 5% significance level, the gridded dataset at a particular location is assigned a binary value of 1 (success) if the null hypothesis is accepted i.e. the gridded dataset is able to capture the *true* dependence structure or 0 (failure) if the null hypothesis is rejected.

4.3.3 Propagation of Univariate and Bivariate Climate Biases to Hydrological Simulations

The covariability between climate variables can have important implications for extreme events such as rain-on-snow, multivariate droughts (Hao and AghaKouchak, 2014), fire weather indices (Vicente-Serrano et al. 2010), among others. Evidence for the variability and trends of compound events, such as extreme warm-wet or extreme warm-dry periods might be misrepresented if the data does not capture such behaviour.

In this study, we use a hydrological model to explore how the univariate and multivariate biases can affect model outputs (i.e. streamflow) and quantify the corresponding uncertainties. The semi-distributed Raven hydrological model (Craig, 2015) is setup and

calibrated over the Kootenay River basin by BC Hydro. The Kootenay basin is predominantly mountainous with elevation ranging from 2130m in the south to 3700m in northern parts. Most of the precipitation in the region takes place in winter and fall with the highest annual magnitude of up to 1000mm and the lowest up to 200mm (Quesnel and Thiessen 1993). Streamflow is dominated by snowmelt from snow deposits and glaciers at high elevations in the north causing relatively low flows in winter and peak flows in the months of May or June.

Raven is a flexible hydrological modeling framework that allows for the development of lumped and semi-distributed models. Some of the features of Raven include discretization of land into Hydrological Response Units (HRUs) and flexibility of using empirical models or physical systems to represent hydrological processes (Shafii, 2017). Gridded records corresponding to each dataset that fall within the basin are spatially averaged to create a single 31-year time series of temperature and precipitation. Then, the hydrologic model is forced with all six datasets (AHCCD and five gridded products) and the simulated streamflow is compared using various summary measures such as average mean and maximum flows within each season. We also use the modified version of Kling-Gupta efficiency (Kling et al. 2012), a statistic proposed in an earlier study by Gupta et al. (2009).

$$KGE' = 1 - \sqrt{(r-1)^2 + (\beta-1)^2 + (\gamma-1)^2} \qquad (11),$$

The metric combines the Pearson correlation coefficient r, the bias ratio β, and the variability ratio γ into one quantifiable value that ranges from -∞ to 1 with 1 being the ideal score. Finally, to validate the frequency of extreme flows, Probability of Detection (POD) of extreme flows is calculated. To calculate POD, a particular day is identified in

the observed flow time series when an extreme event happens (i.e. Q > 95th percentile). Then we check whether the corresponding simulated streamflow also exceeds its 95th percentile or not, the principal being whether simulated streamflow is able to capture the occurrence of a high flow irrespective of bias in its magnitude.

We classify the input data bias into two categories: univariate bias, that represents the biases in temperature and precipitation individually and the multivariate bias that is the bias in their dependence structure. First, the gridded products are bias-corrected using the Quantile Delta Mapping (QDM), a univariate bias correction method (Cannon et al. 2015). Next, the gridded products are bias-corrected using the Multivariate Bias Correction method (MBC) proposed by Cannon (2016).

The QDM bias correction approach preserves relative changes in quantiles of the variable being corrected. The approach builds upon previous approaches such as Quantile Mapping (QM) and Detrended Quantile Mapping (DQM). Cannon et al. (2015) show how their approach accounts for relative changes in all modeled quantiles where earlier approaches (i.e. DQM) only accounts for relative changes in the modeled mean. The MBC approach is a further development of the QDM bias correction method combined with a multivariate linear bias correction algorithm proposed by Bürger et al. (2011). While QDM only corrects for univariate biases the multivariate bias correction algorithm corrects the multivariate structure, but not the univariate structure (unless it is strictly multivariate Gaussian). This approach combines the two methods using an iterative process correcting both univariate and preserving the dependence structure at the same time. The MBC algorithm has two variants, MBCp which relies on the Pearson correlation coefficient and MBCr which relies on the Spearman rank correlation coefficient. In this study, MBCr is

used for bias correction of temperature and precipitation since the bivariate structure of the two variables is not necessarily Gaussian, hence making rank correlation the ideal choice to represent their dependence.

Consequently, three scenarios of simulated streamflow are considered based on the gridded product inputs (Figure 11): streamflow generated using original gridded products (Q_o), streamflow generated after univariate bias correction of gridded products (Q_u), and streamflow generated after multivariate bias correction of gridded products (Q_m). This allows for investigating the propagation of biases in both univariate and multivariate structure of the input data into hydrological model predictions.

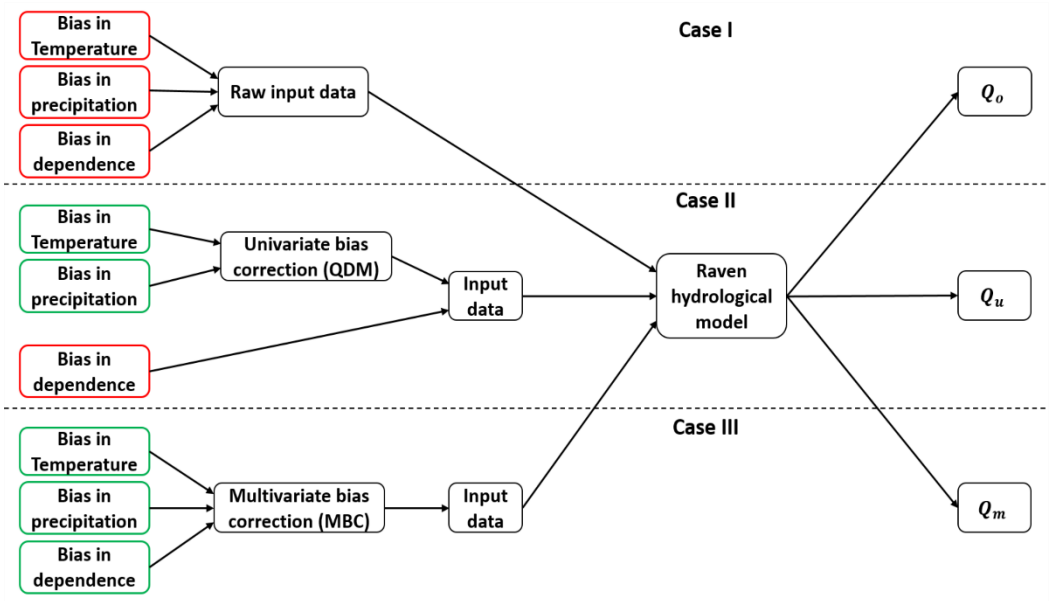

Figure 11 - Hydrologic modeling under three different scenarios to characterize the effects of univariate and multivariate biases in input data.

4.4 Results and Discussions

4.4.1 Univariate Analysis Results

Majority of the 113 locations have cold biases across all products in all seasons (Figure 12). The magnitude of the cold bias is maximum in winter at -10°C as an outlier on the eastern coast. If the outlier is excluded, then all seasons show a similar pattern where maximum cold biases (around -8°C) occur over the Rockies in the west whereas maximum warm biases (around +5°C) occur over the Canadian Prairies. There are significant spatial similarities among the datasets in terms of where warm and cold biases are observed. All products have the highest accuracy in southeastern Canada (southern Ontario) in capturing temperature with the region having the lowest bias on average. On an average, both NCEP products (CFSR and NARR) have the highest warm and cold biases across seasons with NARR being predominantly warmer in all seasons except winter. NRCANmet and S14FD have very similar biases in each case but NRCANmet on the whole performs better than every other dataset. Similar patterns are observed for precipitation biases as well (Figure 13). NRCANmet and S14FD tend to be the most accurate products across all seasons however S14FD proves marginally better than NRCANmet on average. GRASP has some extreme outliers in all seasons except summer with biases reaching over 4mm/day in winter and spring and 6mm/day in fall observed at a couple of location on the western coast. In all seasons, NCEP products display opposite behavior to each other with CFSR predominantly wet and NARR predominantly dry. Maximum wet biases in CFSR are observed over the western mountains while maximum dry biases in NARR are observed over the Canadian Prairies and southern Ontario.

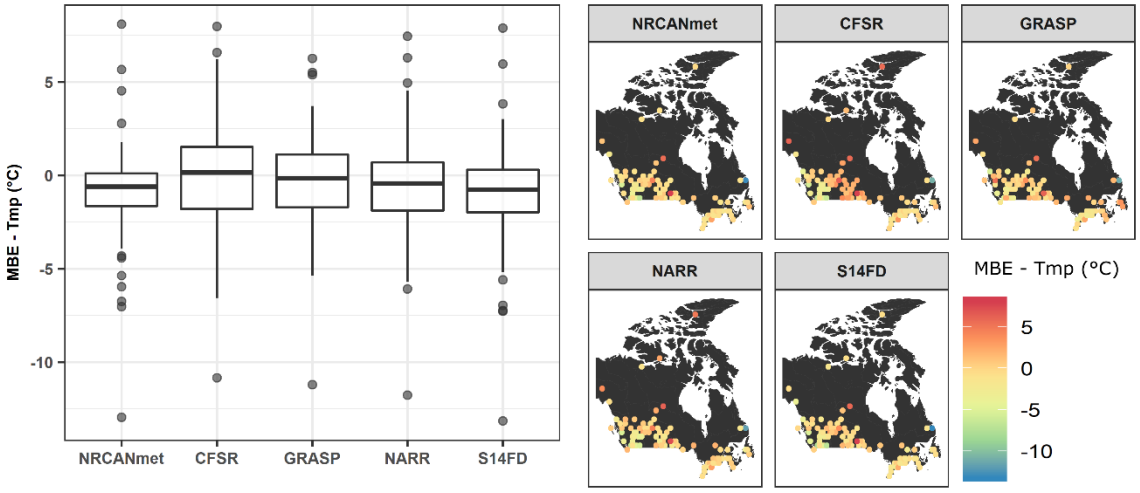
MBE - Tmp (°C)
5
0
-5
-10
NRCANmet
CFSR
GRASP
NARR
S14FD
NRCANmet
CFSR
GRASP
NARR
S14FD
MBE - Tmp (°C)
5
0
-5
-10

(a)

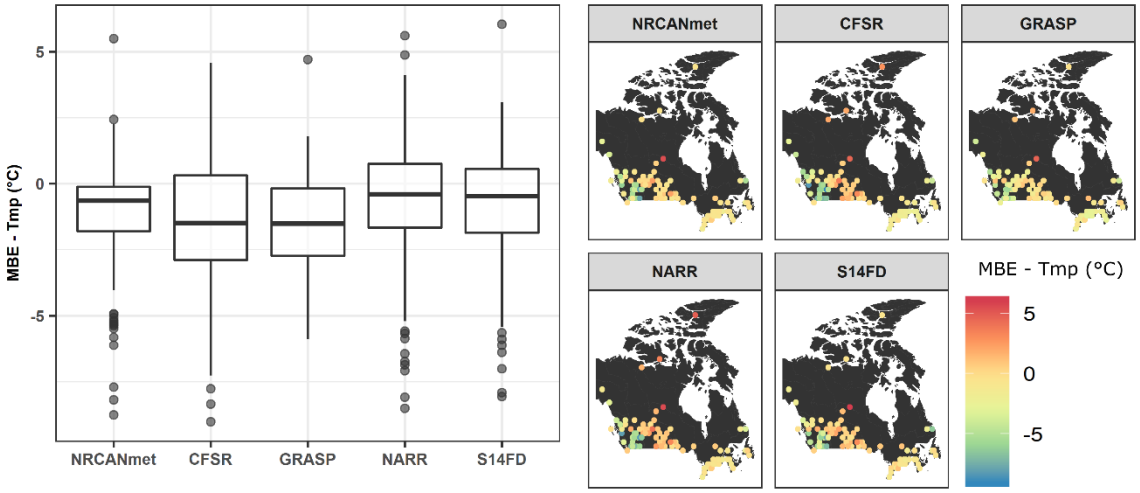
MBE - Tmp (°C)
5
0
-5
NRCANmet
CFSR
GRASP
NARR
S14FD
NRCANmet
CFSR
GRASP
NARR
S14FD
MBE - Tmp (°C)
5
0
-5

(b)

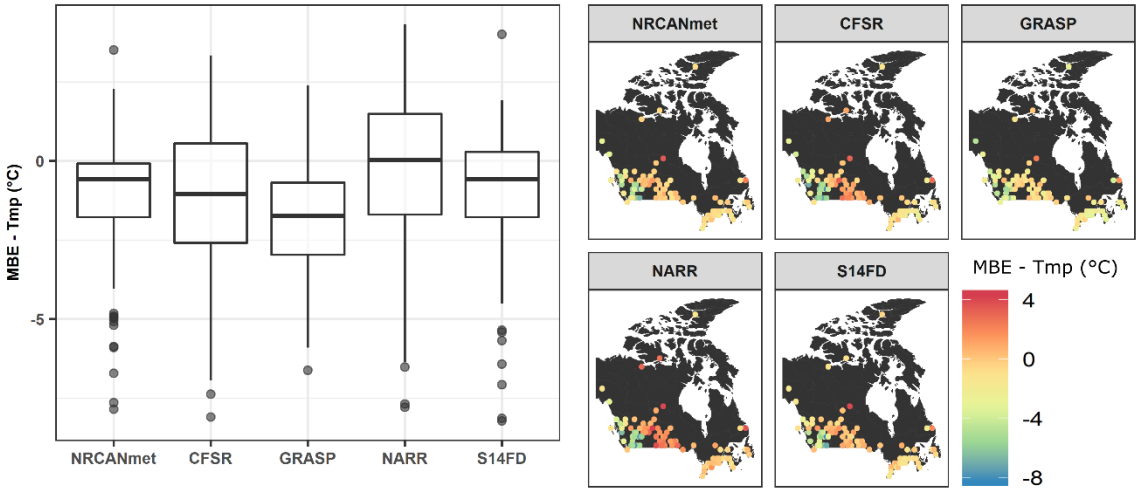

(c)

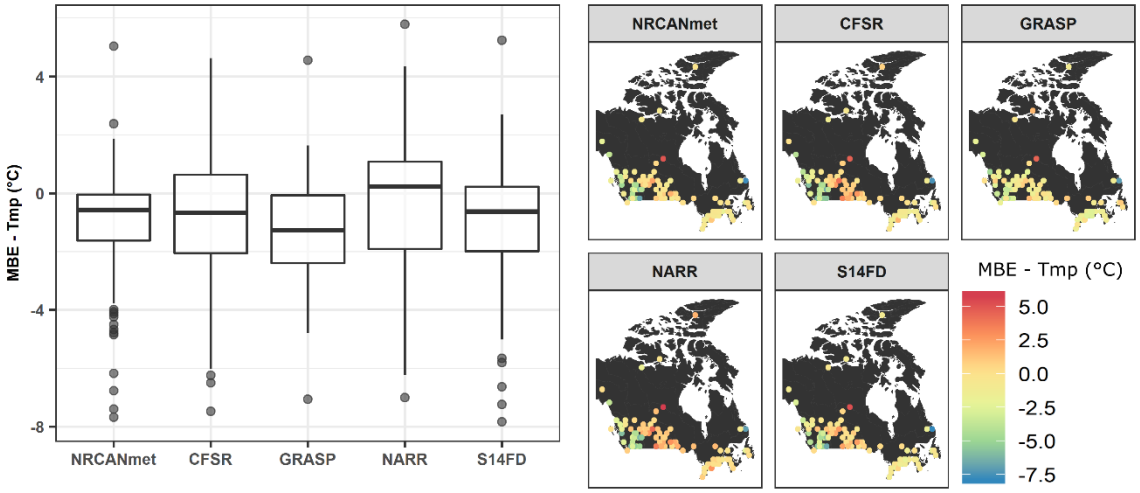

(d)

Figure 12 – Spatial variations and the corresponding range of Mean Bias Error (MBE) values for daily mean temperature for each dataset at the AHCCD locations in (a) winter (DJF) (b) spring (MAM) (c) summer (JJA) and (d) fall (SON) seasons. The boxplots represent the distribution of bias across 113 locations while spatial maps show the bias value at each site.

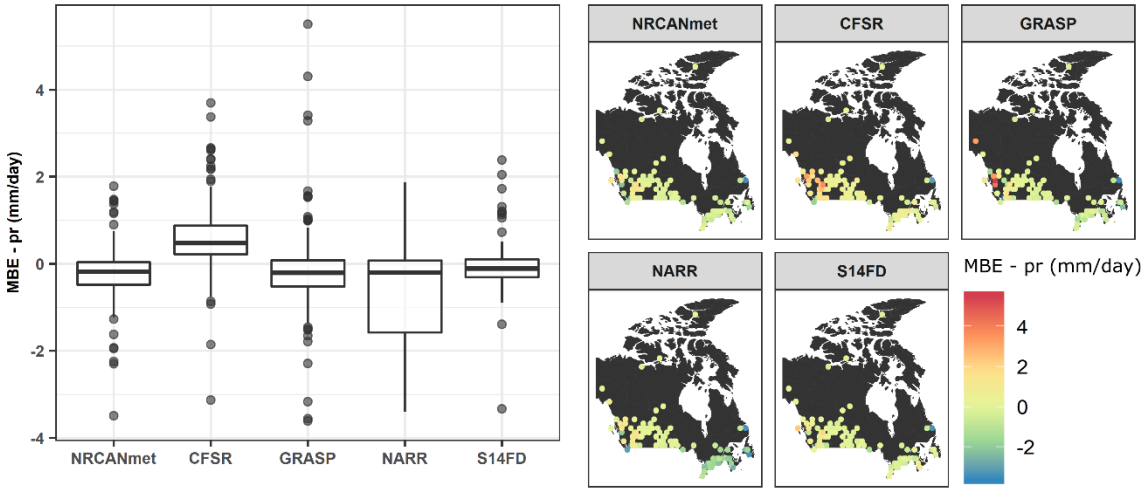
MBE - pr (mm/day)
4
2
0
-2
-4
NRCANmet
CFSR
GRASP
NARR
S14FD
NRCANmet
CFSR
GRASP
NARR
S14FD
MBE - pr (mm/day)
4
2
0
-2

(a)

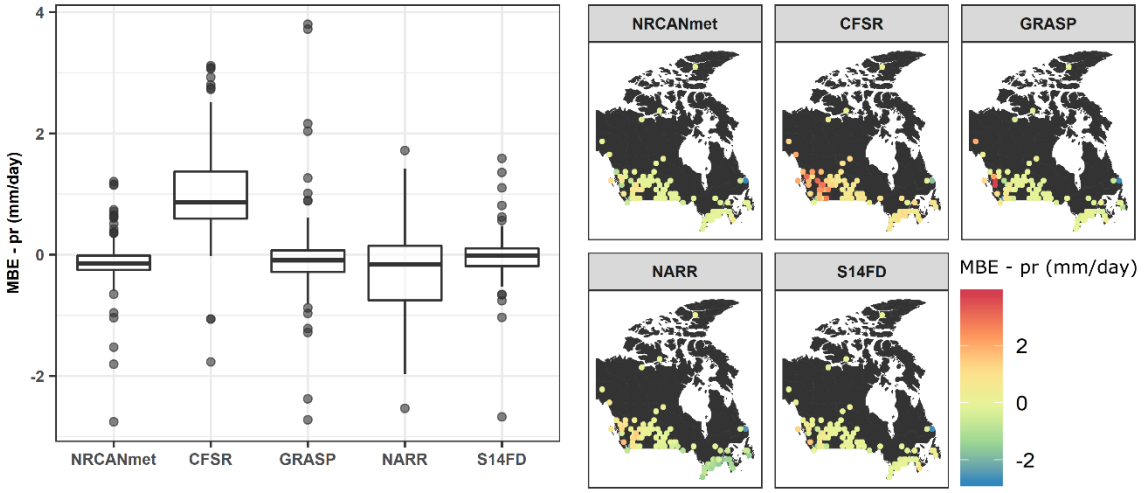
MBE - pr (mm/day)
4
2
0
-2
NRCANmet
CFSR
GRASP
NARR
S14FD
NRCANmet
CFSR
GRASP
NARR
S14FD
MBE - pr (mm/day)
2
0
-2

(b)

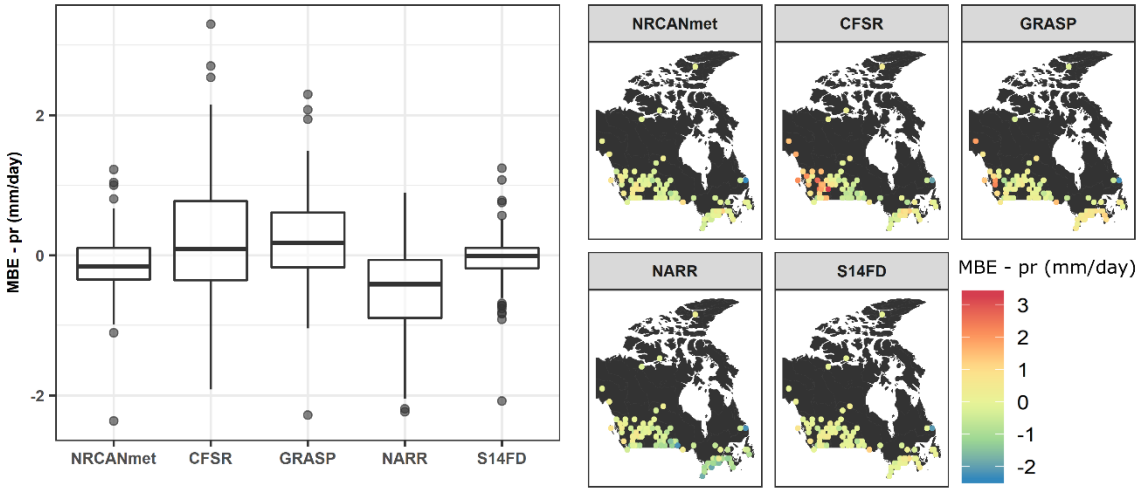

(c)

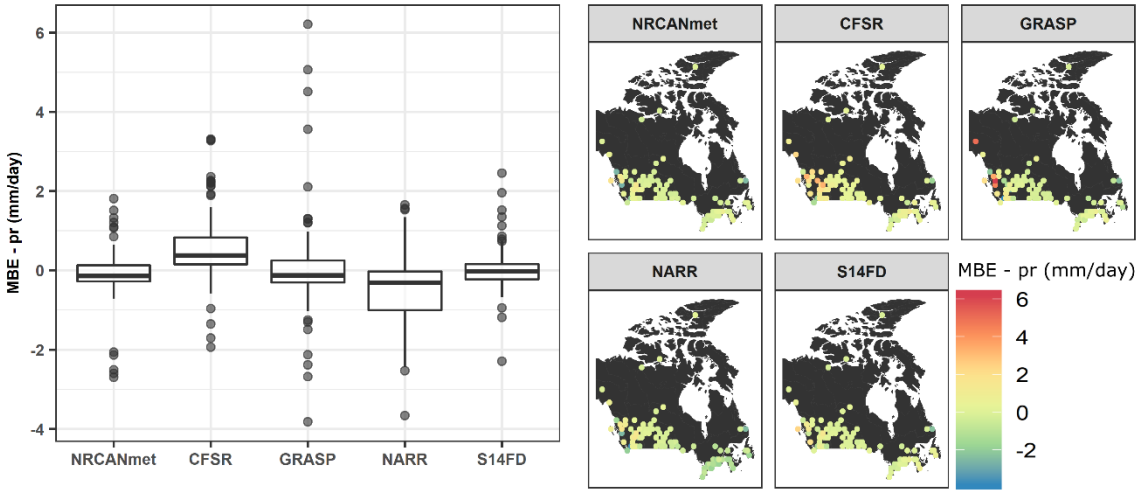

(d)

Figure 13 – Spatial variations and the corresponding range of Mean Bias Error (MBE) values for daily precipitation for each dataset at the AHCCD locations in (a) winter (DJF) (b) spring (MAM) (c) summer (JJA) and (d) fall (SON) seasons. The boxplots represent the distribution of bias across 113 locations while spatial maps show the bias value at each site.

The 95th quantile of temperature (T95) is underestimated by all gridded datasets (Figure 14a) with NARR being the closest to the observation and GRASP being the farthest. NRCANmet and S14FD again exhibit very similar results with the average T95 at just over 20°C while the GRASP estimates the average T95 across the 113 locations at 19.1°C. Regarding the frequency of temperature extremes, NRCANmet has the highest correlation with the observed dataset with 47 locations having correlations of above 0.8 while for all other products the number of sites the number is below 15 with the lowest in NARR. The magnitude of extreme precipitation is best captured by NARR followed by NRCANmet and S14FD (Figure 14b). It is evident from the results that the biases observed in daily time-step in precipitation do not play a large role in extremes. The consistent wet bias in CFSR and dry bias in NARR is not evident in R95p, in fact CFSR slightly underestimates the annual sum of extreme precipitation. GRASP shows a very narrow distribution of extremes across all sites with a few outliers at both ends. Regarding the frequency of extreme precipitation events, NRCANmet outperforms other products, followed by S14FD but the overall value of correlation is much lower than observed for temperature extremes. Only one site across all products shows a correlation above 0.8 while more than 50% of locations across all products show correlations of less than 0.5 indicating that even though the magnitude of extreme events might be captured satisfactorily, their temporal occurrence is not.

According to the univariate analyses, NRCANmet and S14FD can represent temperature and precipitation better than other gridded datasets, with NRCANmet performing marginally better for temperature and S14FD marginally better for precipitation.

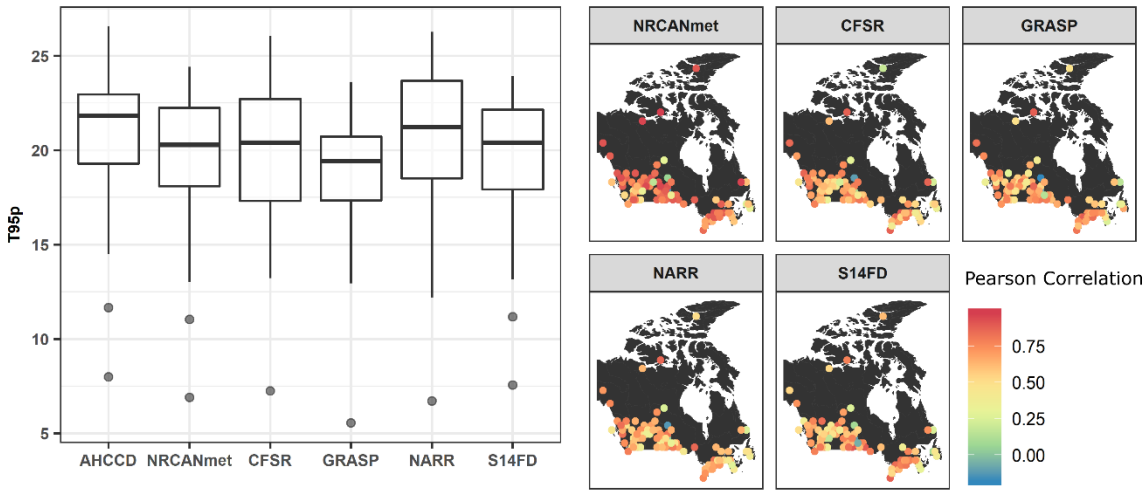

(a)

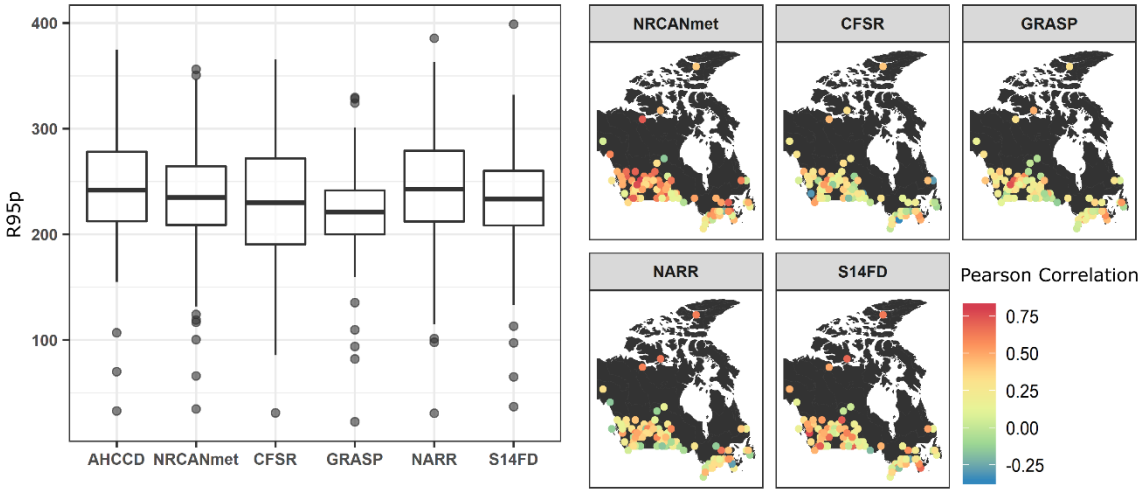

(b)

Figure 14 – Comparison of extreme (a) temperature and (b) precipitation across datasets. Boxplots show the mean (for temperature) and sum (for precipitation) of the respective annual 95th quantile values across each dataset. Spatial plot shows the Pearson correlation coefficient of extreme frequency series from each dataset with respect to the series of station data (AHCCD).

4.4.2 Bivariate Analysis Results

Across all gridded products and four seasons, the number of sites that match the dependence of ground-based observation data is below 50% (except for S14FD in winter at 67 sites) (Figure 15). There is hardly any homogeneity between the datasets in different seasons, and the number of common sites across all products where dependence is captured (or not captured) is less than 15. These sites are located in the southwest (southern Ontario) and east of the Rockies. All datasets struggle the most in capturing dependence between temperature and precipitation in spring. The following are some of the significant dependence features of the ground-based data that gridded products do not capture well:

1. The observed data shows significant dependency between warm and wet events (upper tail) in spring in the north and southwestern regions of Canada (windward side of the Rockies), which the gridded datasets fail to capture.
2. The observed data shows significant dependency between hot and dry events in the Prairies in both spring and summer, which the gridded datasets do not capture.

These dependencies have important hydrologic implications. The northern regions of Canada have warmed by over 2.3°C according to Canada's Changing Climate Report, released by Environment and Climate Change Canada, which is almost 4 times the global average (Bush & Lemmen (2019). The positive dependence between temperature and precipitation in the north indicates that the region can get wetter as it gets warmer, something that the gridded products fail to capture. The western coast of Canada is impacted by numerous snowmelt and rain-on-snow floods in late spring and early winter when precipitation occurs on unusually warm days with snow on the ground. The positive dependence implies that with warming temperature, the amount of precipitation can be

expected to rise, which can further worsen these conditions (Tencer et al. 2014). Gridded datasets, however, fail to capture this warm-wet dependency in southwest Canada. In addition, the Prairies has experienced dramatic droughts amounting to billions of dollars in damages (Garnett, 2002). The strong overall negative dependence between hot and dry events suggests that as the area gets hotter it might get drier thus exacerbating the occurrence and severity of droughts (AghaKouchak et al. 2014). This phenomenon is not captured well by gridded datasets, which can lead to an underestimation of the risk associated with these extreme events.

While NRCANmet characterizes the univariate behaviour of temperature and precipitation relatively well, results suggest that it does not represent the dependency any better than the other datasets. This brings into question the use of NRCANmet as an 'observation' dataset in numerous hydrologic applications, and in bias correction of other products such as global climate models. There is a growing interest in developing multivariate bias correction methods, which correct the dependence between variables along with their univariate characteristics. However, as shown in this study, this 'true' dataset may not be capable of capturing the dependence structure correctly, which undermines the accuracy of bias-corrected products and further inferences drawn from them.

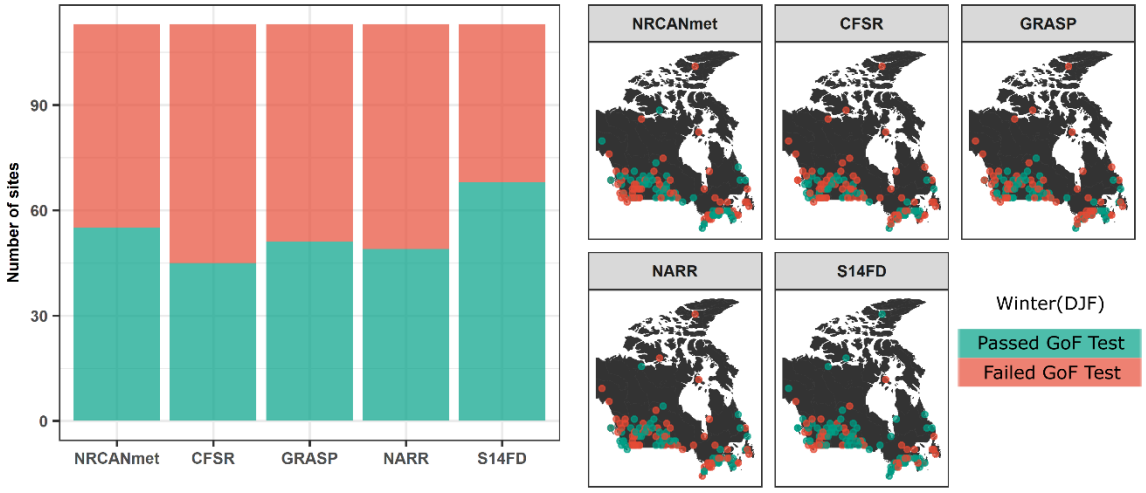
Number of sites
90
60
30
0
NRCANmet
CFSR
GRASP
NARR
S14FD
NRCANmet
CFSR
GRASP
NARR
S14FD
Winter(DJF)
Passed GoF Test
Failed GoF Test

(a)

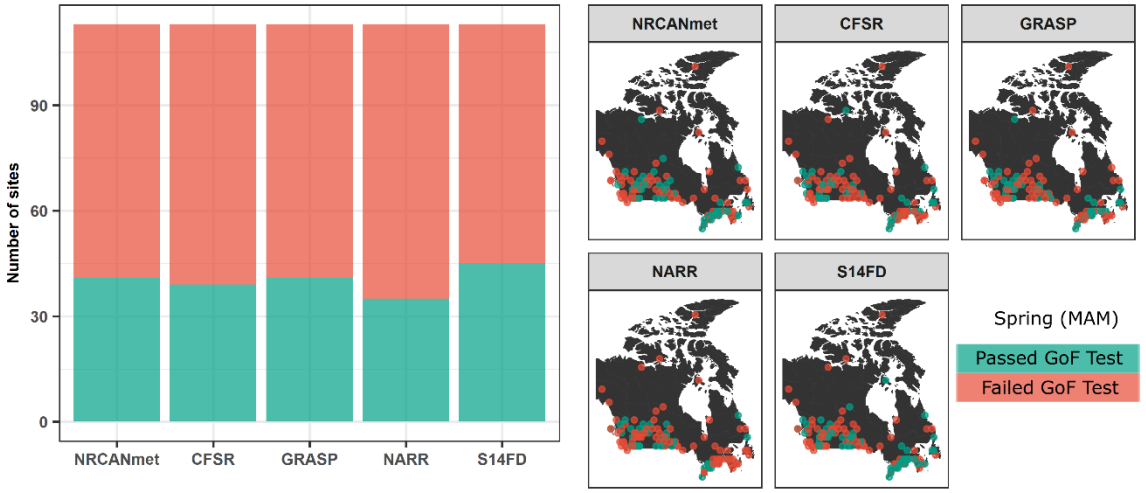
Number of sites
90
60
30
0
NRCANmet
CFSR
GRASP
NARR
S14FD
NRCANmet
CFSR
GRASP
NARR
S14FD
Spring (MAM)
Passed GoF Test
Failed GoF Test

(b)

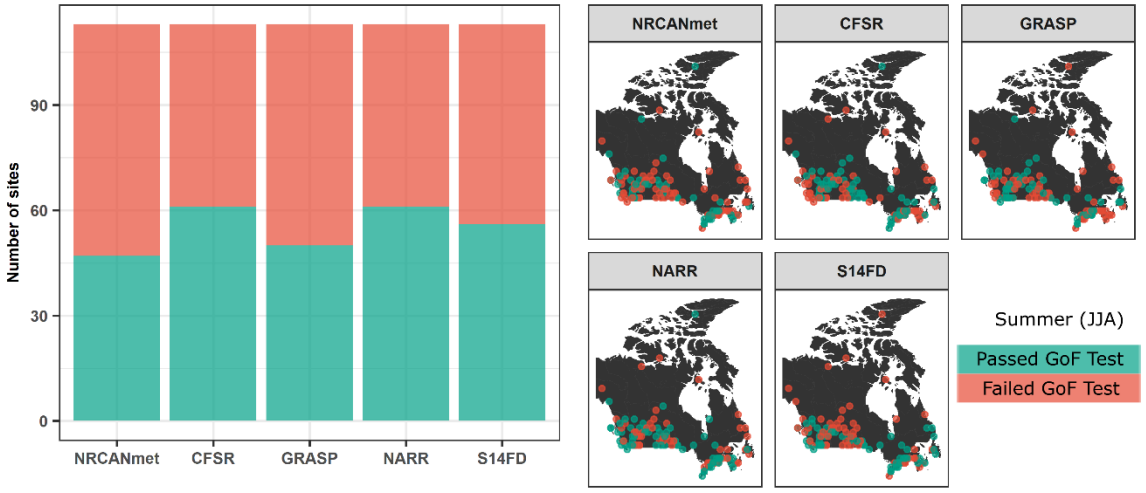

(c)

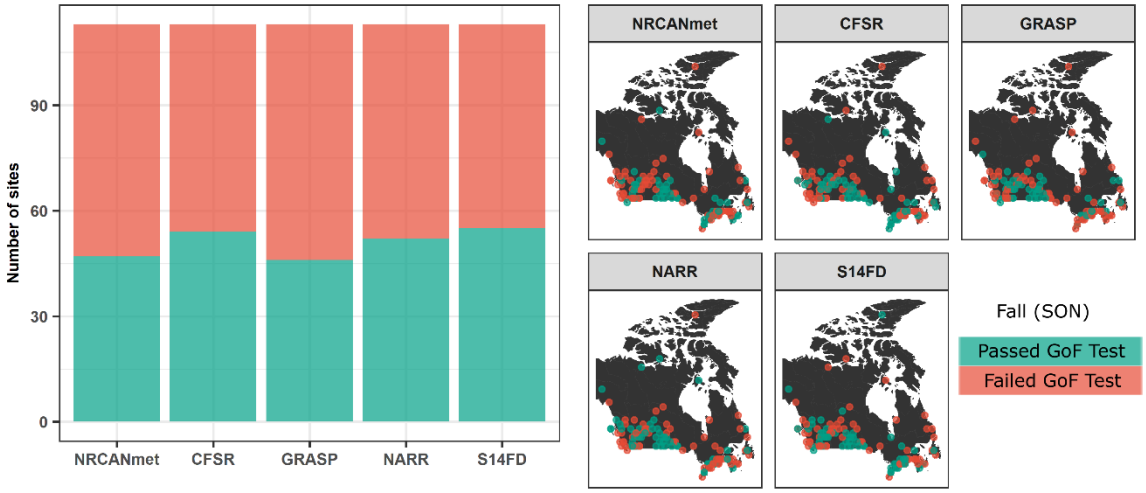

(d)

Figure 15 – Sites where the copula Goodness of Fit (GoF) test is passed/failed at 5% significance level for seasonally aggregated data (a) Winter (DJF) (b) Spring (MAM) (c) Summer (JJA) and (d) Fall (SON).

4.4.3 Hydrological Model Assessment

The comparison of simulated streamflow across the three input scenarios reveal that while univariate bias correction increases the accuracy of model outputs by a large degree,

multivariate bias correction further improves the accuracy in almost all cases. Here, we assume that streamflow simulations from AHCCD driven hydrological model is the 'observation' in order to assess how removing univariate and multivariate biases would enhance the overall performance of the model. Seasonal mean flows are significantly underestimated in winter and overestimated in spring (Figure 16a). In both cases, the pattern that emerges is that the model output of QDM scenario exceeds the target, going slightly above the observation if the original bias was underestimated or slightly below the observation if the original bias was overestimated. However, MBCr bridges this gap and brings the simulated values almost equal to the observations in almost every case. The pattern is repeated for seasonal maximum flows as well (Figure 16b) as a significant correction occurs in winter and spring where originally the biases are large. Additionally, if the original bias was observed to be insignificant, as in the case of fall, both bias correction scenarios do not disturb the final output. In both magnitude driven results, it is apparent how the predominant wet bias in CFSR is converted into high streamflow values as well.

KGE` metric is negative for almost all cases in winter and spring indicating poor performance for raw input data (Fig 16c). In all cases except for NARR in winter, KGE` of MBCr driven model output improves over the QDM driven model output. The highest values in comparison across datasets is observed for NRCANmet in each season, followed by NARR. The largest difference between QDM and MBCr is observed in the calculation of POD of extreme flows (Fig 16d). In most cases, the POD of extreme flows for MBCr scenario doubles as compared to QDM case. This observation captures the underlying importance of multivariate bias correction. Since extreme flows are not only related to high

precipitation events, but also to temperature, especially in high elevation areas, it becomes important to capture 'warm and wet' events within the input data which potentially cause high flows.

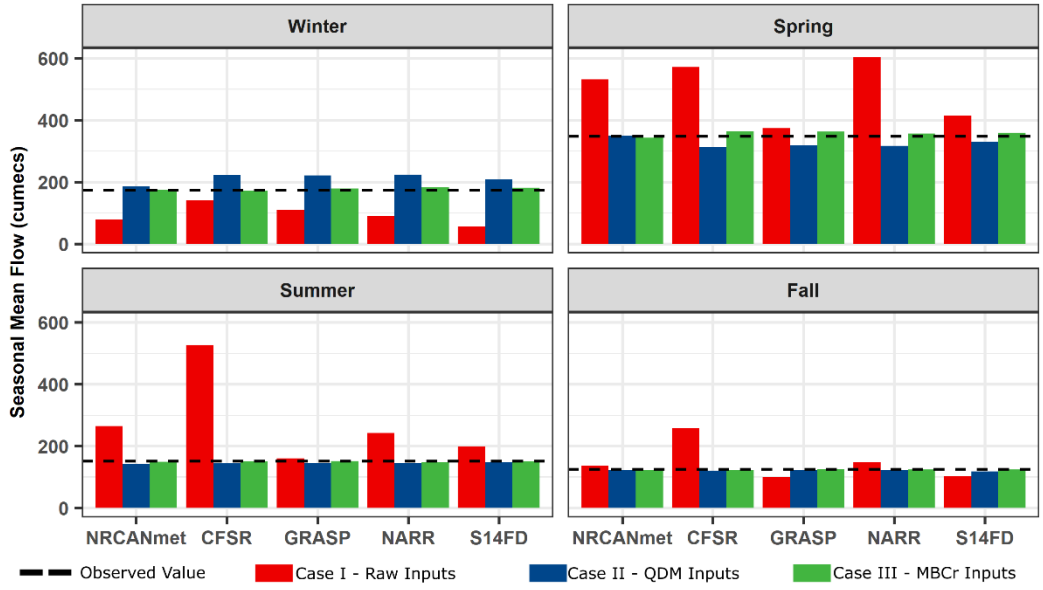

(a)

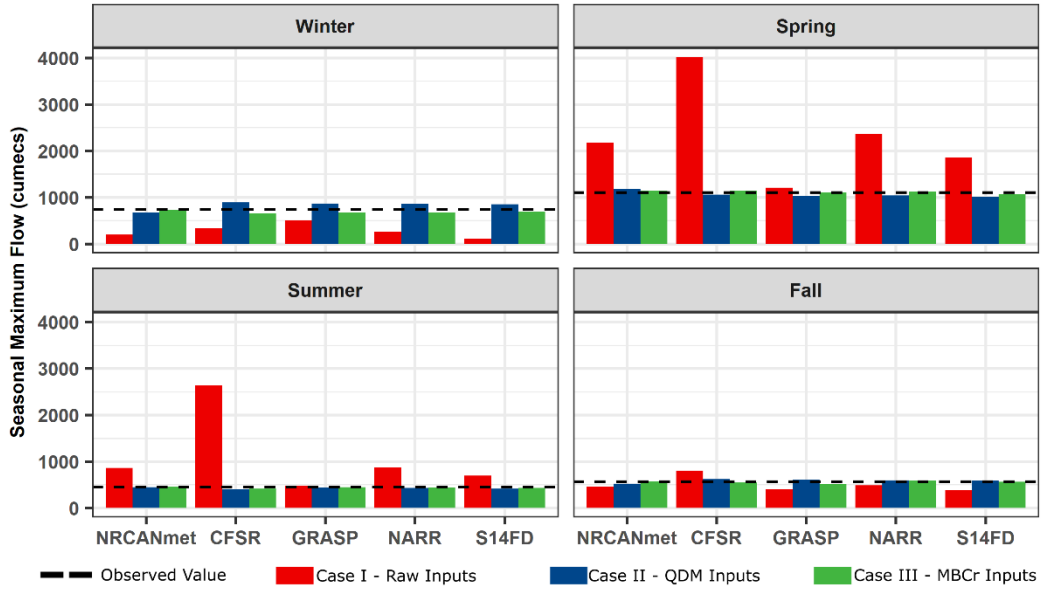

(b)

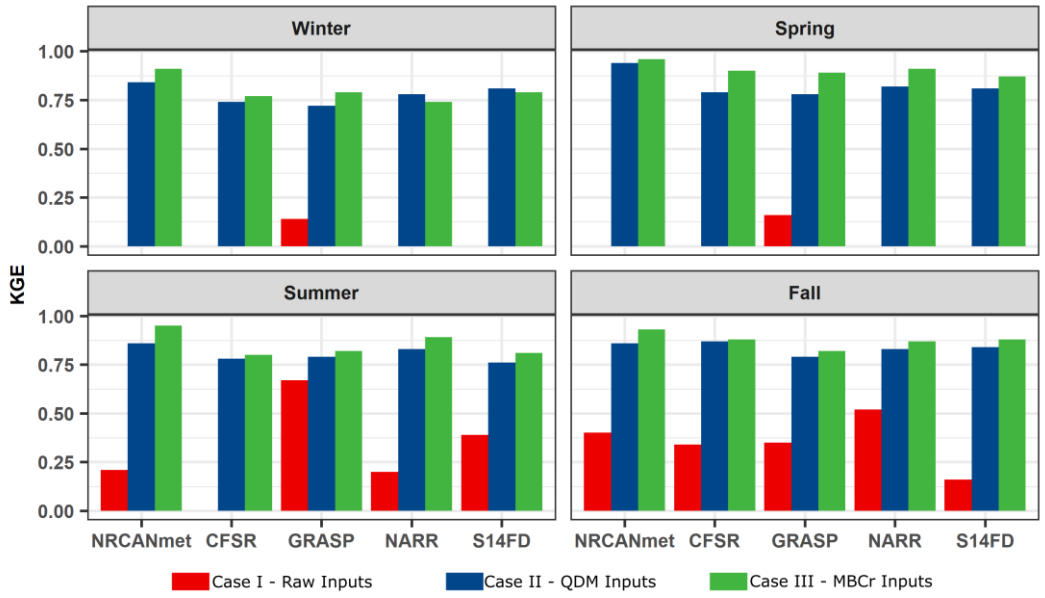

(c)

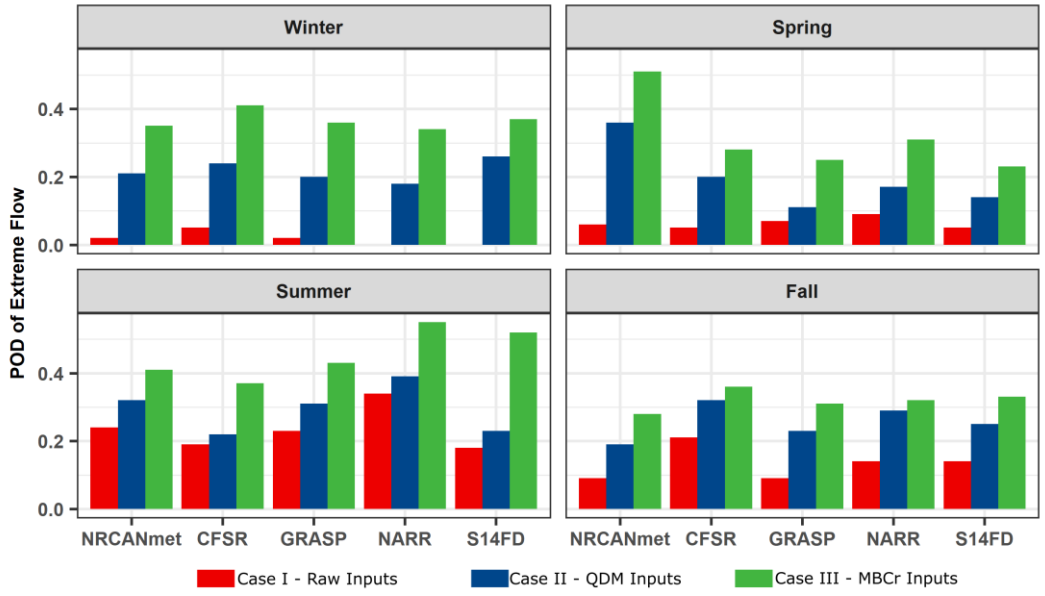

(d)

Figure 16 – Comparison between simulated streamflow across each dataset under three input scenarios across different seasons. The figures represent the (a) Seasonal Mean Flow (b) Seasonal Maximum Flow (c) KGE` and (d) POD. For Figure 5c, wherever KGE` value

is missing, it means that the value is negative. The negative value is not shown simply to keep the scale of the figure readable.

4.5 Conclusions

The goal of the study is to evaluate the performance of gridded products in representing the covariability between temperature and precipitation over Canada with the point of view of using these datasets for identifying and modelling compound events. Five gridded datasets are compared with ground-based observations considering both univariate and bivariate behaviours. The analysis is performed on daily temperature and precipitation data spanning over 31 years (1980-2010) at 113 station locations, most of which lie in the southern half of Canada. The overall characteristics of temperature and precipitation of each gridded dataset are assessed using Mean Bias Error (MBE). In addition, the frequency and magnitude of extreme precipitation represented by each gridded dataset are compared to the observed extremes. The bivariate performance is evaluated based on a formal goodness of fit test that verifies how well the gridded datasets capture the dependence between temperature and precipitation with respect to the dependence structure of the ground-based observation. To demonstrate the importance of bivariate bias correction, a semi-distributed hydrological model is forced with three sets of input data; original input data, input data bias-corrected using QDM – a univariate bias correction method and input data bias-corrected using MBCr – a multivariate bias correction method. The three sets of streamflow scenarios are then compared using metrics such as seasonal mean and maximum flows, KGE`, and Probability of Detection (POD) of extremes.

The minimum and maximum temperature biases across all gridded datasets are -7.9°C in fall (excluding an extreme outlier) to +7.6°C in winter. A cold bias exists at the majority of

the 113 locations for all datasets. The bias is the strongest west of the Rocky Mountains where all gridded products show colder conditions than ground-based observation, while warm bias is strongest over the Prairies. Overall, NRCANmet shows the closest temperature variability compared with the 'true' observation. One of the strengths of NRCANmet is its use of elevation as a predictor in thin-plate spline interpolation however, no clear relation is found between the observed bias and station elevations. The minimum and maximum biases for precipitation across all datasets are -3.8 mm/day to +6.2 mm/day in fall. In all datasets, sites with high wet biases are located on the windward side of the Rocky Mountains whereas the location of sites with dry biases varies between each dataset. There are significant biases in NRCANmet in several locations, however along with S14FD, it outperforms other products in representing precipitation.

We evaluated the performance of the gridded products in representing the dependence structures using copulas. The results show that in almost all cases (across seasons and datasets) the correct dependence structure is identified at less than 50% of the sites. Critical bivariate characteristics such as the upper tail dependencies between temperature and precipitation (warm-wet conditions) in the north and southwest regions of Canada are not captured by gridded datasets, which has important implications for flood risk analyses, especially in southwestern Canada. Similarly, hot-dry dependencies in the Prairies are not represented in gridded datasets, which can lead to drought underestimations in this region. Notably, the capability of NRCANmet to capture the individual characteristics of temperature and precipitation does not transfer over to the bivariate behaviour.

Using a hydrological model we showed how the biases in individual precipitation and temperature variability and their dependence structure propagates into streamflow

simulations. The first set of simulated streamflow generated from gridded input data (no adjustments applied) deviated heavily from the ground-based observation forced streamflow output. Especially, extreme streamflow was severely overestimated by almost all gridded datasets. In the second scenario after univariate bias correction of the input data all metrics (Mean, Maximum, KGE` and POD) shifted to acceptable ranges although the biases in extremes remained relatively significant. The Probability of Detection (POD) of extremes also remained quite poor. These improvements were further bolstered by the multivariate bias correction of the gridded data. The third scenario outperformed the other two, showing marginal improvements in summary statistics, and significant improvements in the representation of extremes particularly in POD.

The study shows that the surge in the analysis of compound events calls for a deeper analysis of existing datasets to verify their capabilities to identify joint events accurately. Without this verification, inferences based on such datasets particularly in the multivariate conditions are unreliable as the uncertainty increases with the addition of data and the covariability between different factors.

4.6 References

AghaKouchak, A., Cheng, L., Mazdiyasni, O., & Farahmand, A. (2014). Global warming and changes in risk of concurrent climate extremes: Insights from the 2014 California drought. Geophysical Research Letters, 41(24), 8847-8852.

Akaike, H. (1974). A new look at the statistical model identification. In Selected Papers of Hirotugu Akaike (pp. 215-222). Springer, New York, NY.

Balmaseda, M. A., Mogensen, K., & Weaver, A. T. (2013). Evaluation of the ECMWF ocean reanalysis system ORAS4. Quarterly Journal of the Royal Meteorological Society, 139(674), 1132-1161.

Bao, X., & Zhang, F. (2013). Evaluation of NCEP–CFSR, NCEP–NCAR, ERA-Interim, and ERA-40 reanalysis datasets against independent sounding observations over the Tibetan Plateau. Journal of Climate, 26(1), 206-214.

Bosilovich, M. G., Chen, J., Robertson, F. R., & Adler, R. F. (2008). Evaluation of global precipitation in reanalyses. Journal of applied meteorology and climatology, 47(9), 2279-2299.

Brunke, M. A., Fairall, C. W., Zeng, X., Eymard, L., & Curry, J. A. (2003). Which bulk aerodynamic algorithms are least problematic in computing ocean surface turbulent fluxes?. Journal of Climate, 16(4), 619-635.

Bürger, G., Schulla, J., & Werner, A. T. (2011). Estimates of future flow, including extremes, of the Columbia River headwaters. Water Resources Research, 47(10).

Burnham, K. P., & Anderson, D. R. (2003). Model Selection and Multimodel Inference: A Practical Information-theoretic Approach.,(Springer Science & Business Media: New York.).

Bush, E., & Lemmen, D. S. (Eds.). (2019). Canada's Changing Climate Report. Government of Canada= Gouvernement du Canada.

Cannon, A. J. (2016). Multivariate bias correction of climate model output: Matching marginal distributions and intervariable dependence structure. Journal of Climate, 29(19), 7045-7064.

Cannon, A. J., Sobie, S. R., & Murdock, T. Q. (2015). Bias correction of GCM precipitation by quantile mapping: How well do methods preserve changes in quantiles and extremes?. Journal of Climate, 28(17), 6938-6959.

Chen, J., Brissette, F. P., & Leconte, R. (2011). Uncertainty of downscaling method in quantifying the impact of climate change on hydrology. Journal of hydrology, 401(3-4), 190-202.

Chen, J., Brissette, F. P., Poulin, A., & Leconte, R. (2011). Overall uncertainty study of the hydrological impacts of climate change for a Canadian watershed. Water Resources Research, 47(12).

Choi, W., Kim, S. J., Rasmussen, P. F., & Moore, A. R. (2009). Use of the North American Regional Reanalysis for hydrological modelling in Manitoba. Canadian Water Resources Journal, 34(1), 17-36.

Craig, J.R., and the Raven Development Team, Raven User's and developer's manual (Version 2.9.2), URL: http://raven.uwaterloo.ca/ (Accessed xxx, 2019).

Daggupati, P., Shukla, R., Mekonnen, B., Rudra, R., Biswas, A., Goel, P., Prasher, S. and Yang, W., 2018. Hydrological responses to various land use, soil and weather inputs in northern Lake Erie basin in Canada. Water, 10(2), p.222.

Decker, M., Brunke, M. A., Wang, Z., Sakaguchi, K., Zeng, X., & Bosilovich, M. G. (2012).

Essou, G. R., Arsenault, R., & Brissette, F. P. (2016). Comparison of climate datasets for lumped hydrological modeling over the continental United States. Journal of hydrology, 537, 334-345.

Evaluation of the reanalysis products from GSFC, NCEP, and ECMWF using flux tower observations. Journal of Climate, 25(6), 1916-1944.

Environment and Climate Change Canada. “Government of Canada.” Canada.ca, Government of Canada, 19 Dec. 2018, www.canada.ca/en/environment-climate-change/services/top-ten-weather-stories.html.

Eum, H. I., Dibike, Y., Prowse, T., & Bonsal, B. (2014). Inter-comparison of high-resolution gridded climate data sets and their implication on hydrological model simulation over the Athabasca Watershed, Canada. Hydrological processes, 28(14), 4250-4271.

Faramarzi, M., Srinivasan, R., Iravani, M., Bladon, K. D., Abbaspour, K. C., Zehnder, A. J., & Goss, G. G. (2015). Setting up a hydrological model of Alberta: Data discrimination analyses prior to calibration. Environmental Modelling & Software, 74, 48-65.

Garnett, R. (2002). The Canadian Prairie drought of 2001: a four billion dollar shortfall?. CMOS Executive Office Bureau de la SCMO Suite112, McDonald Building University of Ottawa 150 Louis-Pasteur Ave., 30(2), 1.

Genest, C., Quessy, J. F., & Rémillard, B. (2006). Goodness-of-fit procedures for copula models based on the probability integral transformation. Scandinavian Journal of Statistics, 33(2), 337-366.

Genest, C., & Favre, A. C. (2007). Everything you always wanted to know about copula modeling but were afraid to ask. Journal of hydrologic engineering, 12(4), 347-368.

Genest, C., & Rémillard, B. (2008). Validity of the parametric bootstrap for goodness-of-fit testing in semiparametric models. In Annales de l'IHP Probabilités et statistiques (Vol. 44, No. 6, pp. 1096-1127).

Grimaldi, S., & Serinaldi, F. (2006). Asymmetric copula in multivariate flood frequency analysis. Advances in Water Resources, 29(8), 1155-1167.

Gupta, H. V., Kling, H., Yilmaz, K. K., & Martinez, G. F. (2009). Decomposition of the mean squared error and NSE performance criteria: Implications for improving hydrological modelling. Journal of hydrology, 377(1-2), 80-91.

Hao, Z., & AghaKouchak, A. (2014). A nonparametric multivariate multi-index drought monitoring framework. Journal of Hydrometeorology, 15(1), 89-101.

Haines, Brayden Jagger. "Quebec's Disastrous 2019 Floods Bring out Compassion from Local Volunteers." Global News, Global News, 5 May 2019, globalnews.ca/news/5240786/quebec-floods-2019-compassion-volunteers/.

Harris, I., Jones, P. D., Osborn, T. J., & Lister, D. H. (2014). CRU TS3. 22: Climatic Research Unit (CRU) Time-Series (TS) Version 3.22 of High Resolution Gridded Data of Month-by-month Variation in Climate (Jan. 1901-Dec. 2013). NCAS British Atmospheric Data Centre, 24th September, 2016.

Henn, B., Newman, A. J., Livneh, B., Daly, C., & Lundquist, J. D. (2018). An assessment of differences in gridded precipitation datasets in complex terrain. Journal of hydrology, 556, 1205-1219.

Hutchinson, M. F., McKenney, D. W., Lawrence, K., Pedlar, J. H., Hopkinson, R. F., Milewska, E., & Papadopol, P. (2009). Development and testing of Canada-wide interpolated spatial models of daily minimum–maximum temperature and precipitation for 1961–2003. Journal of Applied Meteorology and Climatology, 48(4), 725-741.

Iizumi, T., Okada, M., & Yokozawza, M. (2014). A meteorological forcing data set for global crop modeling: Development, evaluation, and intercomparison. Journal of Geophysical Research: Atmospheres, 119(2), 363-384.

Iizumi, T., Takikawa, H., Hirabayashi, Y., Hanasaki, N., & Nishimori, M. (2017). Contributions of different bias-correction methods and reference meteorological forcing data sets to uncertainty in projected temperature and precipitation extremes. Journal of Geophysical Research: Atmospheres, 122(15), 7800-7819.

Islam, S. U., & Déry, S. J. (2017). Evaluating uncertainties in modelling the snow hydrology of the Fraser River Basin, British Columbia, Canada. Hydrology and Earth System Sciences, 21(3), 1827-1847.

Janowiak, J. E., Gruber, A., Kondragunta, C. R., Livezey, R. E., & Huffman, G. J. (1998). A comparison of the NCEP–NCAR reanalysis precipitation and the GPCP rain gauge–satellite combined dataset with observational error considerations. Journal of Climate, 11(11), 2960-2979.

Kalnay, E., Kanamitsu, M., Kistler, R., Collins, W., Deaven, D., Gandin, L., Iredell, M., Saha, S., White, G., Woollen, J. and Zhu, Y., 1996. The NCEP/NCAR 40-year reanalysis project. Bulletin of the American meteorological Society, 77(3), pp.437-472.

Kling, H., Fuchs, M., & Paulin, M. (2012). Runoff conditions in the upper Danube basin under an ensemble of climate change scenarios. Journal of Hydrology, 424, 264-277.

Kobayashi, S., Ota, Y., Harada, Y., Ebita, A., Moriya, M., Onoda, H., Onogi, K., Kamahori, H., Kobayashi, C., Endo, H. and Miyaoka, K., 2015. The JRA-55 reanalysis: General specifications and basic characteristics. Journal of the Meteorological Society of Japan. Ser. II, 93(1), pp.5-48.

Kullback, S., & Leibler, R. A. (1951). On information and sufficiency. The annals of mathematical statistics, 22(1), 79-86.

Leonard, M., Westra, S., Phatak, A., Lambert, M., van den Hurk, B., McInnes, K., Risbey, J., Schuster, S., Jakob, D. and Stafford-Smith, M., 2014. A compound event framework for understanding extreme impacts. Wiley Interdisciplinary Reviews: Climate Change, 5(1), pp.113-128.

Makshtas, A., Atkinson, D., Kulakov, M., Shutilin, S., Krishfield, R., & Proshutinsky, A. (2007). Atmospheric forcing validation for modeling the central Arctic. Geophysical Research Letters, 34(20).

Mekis, É., & Vincent, L. A. (2011). An overview of the second generation adjusted daily precipitation dataset for trend analysis in Canada. Atmosphere-Ocean, 49(2), 163-177.

Mesinger, F., DiMego, G., Kalnay, E., Mitchell, K., Shafran, P.C., Ebisuzaki, W., Jović, D., Woollen, J., Rogers, E., Berbery, E.H. and Ek, M.B., 2006. North American regional reanalysis. Bulletin of the American Meteorological Society, 87(3), pp.343-360.

Motoya, K., Masuda, K., Takata, K., & Oki, T. (2002, December). Sensitivity of the Precipitation Gauge Correction for the Estimation of Global and Continental Water Balance. In AGU Fall Meeting Abstracts.

Onogi, K., Tsutsui, J., Koide, H., Sakamoto, M., Kobayashi, S., Hatsushika, H., Matsumoto, T., Yamazaki, N., Kamahori, H., Takahashi, K. and Kadokura, S., 2007. The JRA-25 reanalysis. Journal of the Meteorological Society of Japan. Ser. II, 85(3), pp.369-432.

Papalexiou, S. M., & Montanari, A. (2019). Global and Regional Increase of Precipitation Extremes under Global Warming. Water Resources Research.

Pelmorex Weather Networks Inc. “Update: 93 Deaths Now Connected to Quebec Heat Wave.” The Weather Network, www.theweathernetwork.com/news/articles/quebec-heat-wave-death-toll-hots-70-montreal-laval-july-2018-heatstroke/106337/.

Philips, David (2018). "Canada's Top Ten Weather Stories 2017 – CMOS Bulletin SCMO". CMOS BULLETIN SCMO. Canadian Meteorological and Oceanographic Society

Quesnel, H., & Thiessen, F. N. (1993). Ecosection Summaries for the Kootenay-Boundary Region. Forest Sciences and Recreation Sections, Ministry of Forests.

Rapaić, M., Brown, R., Markovic, M., & Chaumont, D. (2015). An evaluation of temperature and precipitation surface-based and reanalysis datasets for the Canadian Arctic, 1950–2010. Atmosphere-Ocean, 53(3), 283-303.

Rienecker, M.M., Suarez, M.J., Gelaro, R., Todling, R., Bacmeister, J., Liu, E., Bosilovich, M.G., Schubert, S.D., Takacs, L., Kim, G.K. and Bloom, S., 2011. MERRA: NASA’s

modern-era retrospective analysis for research and applications. Journal of climate, 24(14), pp.3624-3648.

Saha, S., Moorthi, S., Pan, H.L., Wu, X., Wang, J., Nadiga, S., Tripp, P., Kistler, R., Woollen, J., Behringer, D. and Liu, H., 2010. The NCEP climate forecast system reanalysis. Bulletin of the American Meteorological Society, 91(8), pp.1015-1058.

Schneider, U., Becker, A., Finger, P., Meyer-Christoffer, A., Rudolf, B., & Ziese, M. (2015). GPCC full data reanalysis at 0.58: Monthly land-surface precipitation from rain-gauges built on GTS-based and historic data, version 7.0. GPCC. Deutscher Wetterdienst/Global Precipitation Climatology Centre, accessed, 20.

Schoelzel, C., & Friederichs, P. (2008). Multivariate non-normally distributed random variables in climate research–introduction to the copula approach.

Seneviratne, S.I., Nicholls, N., Easterling, D., Goodess, C.M., Kanae, S., Kossin, J., Luo, Y., Marengo, J., McInnes, K., Rahimi, M. and Reichstein, M., 2012. Managing the risks of extreme events and disasters to advance climate change adaptation: Changes in climate extremes and their impacts on the natural physical environment.

Service, BC Wildfire. "Wildfire Season Summary." Province of British Columbia, Province of British Columbia, 22 July 2019, www2.gov.bc.ca/gov/content/safety/wildfire-status/about-bcws/wildfire-history/wildfire-season-summary.

Shafii, M., Basu, N., Craig, J. R., Schiff, S. L., & Van Cappellen, P. (2017). A diagnostic approach to constraining flow partitioning in hydrologic models using a multiobjective optimization framework. Water Resources Research, 53(4), 3279-3301.

Sklar, M. (1959). Fonctions de repartition an dimensions et leurs marges. Publ. inst. statist. univ. Paris, 8, 229-231.

Tencer, B., Weaver, A., & Zwiers, F. (2014). Joint occurrence of daily temperature and precipitation extreme events over Canada. Journal of Applied Meteorology and Climatology, 53(9), 2148-2162.

Uppala, S.M., Kållberg, P.W., Simmons, A.J., Andrae, U., Bechtold, V.D.C., Fiorino, M., Gibson, J.K., Haseler, J., Hernandez, A., Kelly, G.A. and Li, X., 2005. The ERA-40 re-analysis. Quarterly Journal of the Royal Meteorological Society: A journal of the atmospheric sciences, applied meteorology and physical oceanography, 131(612), pp.2961-3012.

Van Wagner, C., & Pickett, T. (1985). Equations and FORTRAN program for the Canadian forest fire weather index system (Vol. 33).

Vicente-Serrano, S. M., Beguería, S., & López-Moreno, J. I. (2010). A multiscalar drought index sensitive to global warming: the standardized precipitation evapotranspiration index. Journal of climate, 23(7), 1696-1718.

Vincent, L. A., Wang, X. L., Milewska, E. J., Wan, H., Yang, F., & Swail, V. (2012). A second generation of homogenized Canadian monthly surface air temperature for climate trend analysis. Journal of Geophysical Research: Atmospheres, 117(D18).

Wang, W., & Wells, M. T. (2000). Model selection and semiparametric inference for bivariate failure-time data. Journal of the American Statistical Association, 95(449), 62-72.

Wehner, M., Easterling, D. R., Lawrimore, J. H., Heim Jr, R. R., Vose, R. S., & Santer, B. D. (2011). Projections of future drought in the continental United States and Mexico. Journal of Hydrometeorology, 12(6), 1359-1377.

Werner, A. T., Schnorbus, M. A., Shrestha, R. R., Cannon, A. J., Zwiers, F. W., Dayon, G., & Anslow, F. (2019). A long-term, temporally consistent, gridded daily meteorological dataset for northwestern North America. Scientific data, 6, 180299.

Wong, J. S., Razavi, S., Bonsal, B. R., Wheater, H. S., & Asong, Z. E. (2017). Inter-comparison of daily precipitation products for large-scale hydro-climatic applications over Canada. Hydrology and Earth System Sciences, 21(4), 2163-2185.

Woo, M. K., & Thorne, R. (2006). Snowmelt contribution to discharge from a large mountainous catchment in subarctic Canada. Hydrological Processes: An International Journal, 20(10), 2129-2139.

Zhang, L. S. V. P., & Singh, V. P. (2006). Bivariate flood frequency analysis using the copula method. Journal of hydrologic engineering, 11(2), 150-164.

Zhang, X., Alexander, L., Hegerl, G.C., Jones, P., Tank, A.K., Peterson, T.C., Trewin, B. and Zwiers, F.W., 2011. Indices for monitoring changes in extremes based on daily temperature and precipitation data. Wiley Interdisciplinary Reviews: Climate Change, 2(6), pp.851-870.

Zscheischler, J., & Seneviratne, S. I. (2017). Dependence of drivers affects risks associated with compound events. Science Advances, 3(6), e1700263.

Chapter 5.

Projections of Temperature and Precipitation across Canada Based on Large Ensembles of Regional Climate Simulations and a Hierarchical Bayesian Approach

5.1 Introduction

The study of climatic extremes and the impacts associated with it in the future are primarily dependent on Global Climate Models (GCMs). These models are mathematical representations of natural processes and provide a host of climate variables as outputs. The models however are limited by gaps in our knowledge that lead to misspecification of natural processes (Wang et al. 2014) and therefore result in significant biases in GCM outputs, which make them inefficient for direct use in many applications (Giorgi et al. 2009). To overcome this limitation, Regional Climate Models (RCMs) are developed by downscaling GCMs to a finer resolution usually over a smaller spatial domain and bias correcting the data using various statistical methods.

Giorgi et al. (2009) reported that regionally downscaled climate products are not being utilized to their full potential, citing an example of the Fourth Assessment Report of the Intergovernmental Panel on Climate Change (IPCC), which mostly provided regional climate change information based on coarse resolution GCMs. They argued that one of the primary reasons of under-utilization of RCMs is a lack of integrated framework for regional models such as the Coupled Model Intercomparison Project (CMIP), which exists for

GCMs. To fulfill this gap, they created The Coordinated Regional climate Downscaling Experiment (CORDEX) framework, aimed at providing climate change information at the regional-to-local scale. Under the global umbrella of CORDEX, the North American Regional Climate Change Assessment Program (NARCCAP) was created to run a set of regional climate models over North America (conterminous United States and Canada). The Canadian Regional Climate Model (CanRCM4) is one of the RCMs created under this project. CanRCM4 is considered the latest generation of regional climate model for North America succeeding the CRCM. According to Whan and Zwiers (2016), CanRCM4 has not been evaluated in terms of biases in the climate data produced by the model. Therefore, they evaluated extreme indices based on daily maximum temperature, daily minimum temperature and daily precipitation in CanRCM4 and CRCM5 against several datasets including three observation and two reanalysis products. They reported the presence of significant biases over most of Canada, especially for temperature based indices in CanRCM4.

Several studies have done bias correction of CanRCM4 data over small regions in Canada for their individual use. Zhang et al. (2018) bias corrected CanRCM4 over northern Lake Erie basin to study the impact of climate change on streamflow. Qian et al. (2016) bias corrected CanRCM4 data over the Canadian Prairies to investigate yield changes in a crop model. Gaur et al. (2019) bias corrected CanRCM4 over 11 citywide regions across Canada to study the resilience of structures to climate change. This localized bias correction of climate data for individual studies, using different bias correction methods not only adds an extra dimension of uncertainty to climate change impacts, but also constrains the vision of a unified framework of regional climate modeling for which the CORDEX framework

was developed. Evidently, there is a lack of a high-resolution climate dataset, which can be used at a regional-to-local scale to predict reliable climate change impacts. To plug that gap, a bias corrected version of CanRCM4 over the North American continent has been created using a multivariate bias correction method (MBCn) (Cannon, 2018).

This study is aimed at a thorough evaluation of biases of CanRCM4 and its comparison to the bias corrected product. For this, projections of daily maximum temperature (Tasmax), daily minimum temperature (Tasmin) and daily precipitation are analysed across three large ensembles of 50 simulations each over Canada. The data used are the Canadian regional climate model (CanRCM4) and two versions of the Canadian Large Ensembles Adjusted Dataset (CanLEAD), which are multivariate bias corrected versions of CanRCM4. The CanLEAD products have been bias corrected with respect to EWEMBI (Lange, 2016) and S14FD (Iizumi et al. 2017) reanalysis products (hereafter referred to as CanLEAD1 and CanLEAD2, respectively). All three products will be collectively referred to as RCMs in the rest of the article for the sake of easy notation. The questions that this study aims to answer are:

- To what degree does multivariate bias correction affect biases of CanRCM4?
- How closely do the individual large ensemble simulations emulate observation data in terms of joint projections of temperature and precipitation?
- How do temperature and precipitation extremes vary across each dataset under different future warming scenarios?

Each of the above questions has been treated as a separate phase in this study as the datasets are used differently in each case in terms of temporal and spatial domains. In the first phase, temperature and precipitation from all three models is validated against a gridded

observation dataset (NRCANmet) for the period 1951-2000 using Mean Bias Error (MBE) and Mean Absolute Error (MAE) metrics. In the second phase, following Tebaldi (2009) a Hierarchical Bayesian model is setup over three spatial domains in southern Canada to analyse the joint distribution of temperature and precipitation among several other characteristics of each individual simulation of the large ensembles. In the third phase, extreme climate indices for both variables are generated in five 20-year periods across all datasets, a base period of 1986-2005 and four future warming periods corresponding to +1.5, 2.0, 3.0 and 4.0 °C above pre-industrial period (1850-1900) average temperature.

5.2 Data and Methods

The Canadian regional climate model (CanRCM4) is developed by CCCma of Environment and Climate Change Canada (ECCC). The model is developed according to the method proposed by Scinocca (2016) in which a regional climate model shares the same physical parametrizations as a global climate model, thus ensuring that the bias in simulations is a result of a different spatial resolution only and not any other factor. The global climate model which acts as the parent model to CanRCM4 is CanAM4, which is the atmospheric component of CanESM2 (Jeong et al. 2019). The RCM is a 50-member large ensemble simulation with all forcings over the historical period of 1950-2005 borrowing lateral boundary conditions from ERA-Interim reanalysis (Dee et al. 2011). The future period of 2006 to 2100 is simulated under RCP8.5 scenario (8.5 W/m^2 radiative forcing) by perturbing the initial conditions across the 50 branches of the ensemble.

Both CanLEAD products have been created using a multivariate bias correction technique proposed by Cannon (2018). The method uses an adapted N-dimensional probability density function transform to bias correct data in a way that not only corrects for univariate

bias but also retains the dependence structure of the underlying reference dataset with respect to which bias correction is performed. Figure 17 shows the iterative process of the *N*-pdft algorithm through which bias correction is achieved.

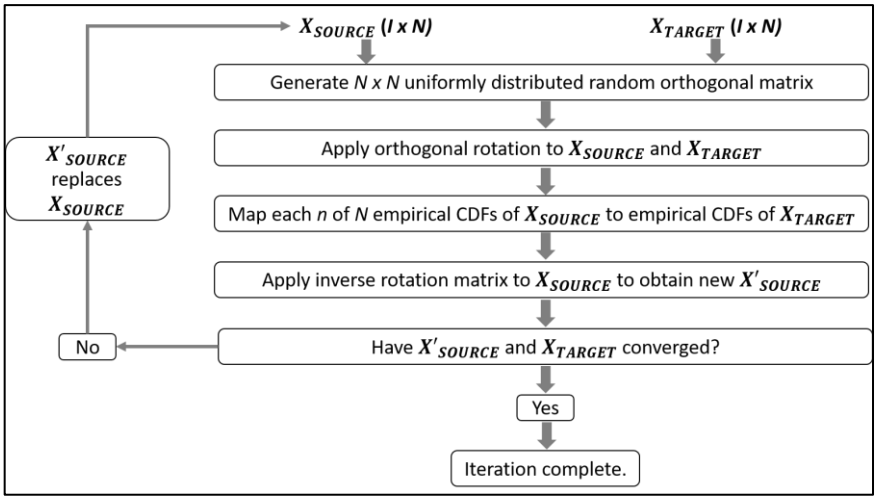

Figure 17 – The process of N-dimensional multivariate bias correction method (MBCn). X_{SOURCE} in this particular case refers to a matrix of CanRCM4 data with tasmax, tasmin and precipitation arranged in columns (N=3) and X_{TARGET} refers to the corresponding matrix of the reanalysis product with respect to which bias correction is done.

Besides evidence provided by Cannon (2018) in their study reporting the superiority of their bias correction method over traditional univariate quantile mapping methods, a few other studies have reported similar results as well. Meyer et al. (2019) reported that maintaining the dependence structure between air temperature and snowfall proved critical for identifying more precipitation occurring at sub-zero temperatures resulting in a different simulated snow volume. This of course affects snowmelt driven runoff in catchments, thus dictating the need for such bias correction methods in order to build reliable hydrological models based on any gridded product, be it reanalysis, RCMs and/or

GCMs. Zscheischler et al. (2019) used two hazard indicators, heat stress and fire risk indicator to study the effects of univariate and multivariate bias correction. They concluded that for hazards dependent on multiple correlated climate drivers, univariate bias correction as opposed to MBCn, leads to increases in the bias and uncertainty of associated impacts. Moreover, the upcoming protocol of the Inter-Sectoral Impact Model Inter-comparison Project (ISIMIP), the ISIMIP3BASD (v1.0) uses MBCn in both downscaling and bias correction. Bias correction of CanRCM4 was done with respect to two reanalysis datasets. EWEMBI reanalysis was created for the purpose of bias correcting in phase 2b of the ISIMIP project. The data are available at a horizontal resolution of 0.5° over the globe from 1979-2013. Further details about EWEMBI are available in (Lange, 2016). S14FD was created as a hybrid of Japanese Reanalysis Data JRA-55 (Kobayashi et al. 2015) and gridded observations. The dataset is available at a resolution of 0.5° over the globe from 1958-2013 at daily time step.

Station data from the National Climate Data Archives (NCDA), Environment and Climate Change Canada is interpolated using Australian National University Splines (ANUSPLIN) to create NRCANmet gridded dataset over Canada at a resolution of 300 arc second (~0.083° or ~10km) (Hutchinson et al. 2009). The dataset provides tasmax, tasmin and precipitation at daily time step from 1950 to 2013. NRCANmet is one of the most widely used gridded products in Canada for running hydrological models and statistical downscaling and has been evaluated by several studies in the past revealing is strengths and shortcomings. Werner et al. (2019) compared NRCANmet along with two other gridded products to station observations from the Agricultural and Rural Development Act (ARDA) network over western Canada. They reported a large dry bias in NRCANmet,

which was most prominent in fall, and least in summer. They also reported a dry bias in extreme precipitation based on several extreme climate indices. For tasmax, they reported a warm bias in winter and cold bias in all other seasons while tasmin showed a cold bias in all seasons, most prominent in winter. Eum et al. (2014) compared NRCANmet and North American Regional Reanalysis (NARR) (Mesinger et al. 2006), Canadian Precipitation Analysis (CaPA) (Mahfouf et al. 2007) and their impact on hydrological modelling over Athabasca basin in western Canada. They reported lowest biases in NRCANmet precipitation compared to other gridded products although the differences with compared to observation were still significant. They also reported a small cold bias in all seasons except winter at higher elevations and a warm bias at lower elevations in the basin. Wong et al. (2017) compared seven gridded products over Canada against Adjusted and Homogenized Canadian Climate Data (AHCCD) stations (Mekis & Vincent, 2011; Vincent et al. 2012). They reported a dry bias in NRCANmet, which ranged from -7.8% in the west (Pacific Maritime terrestrial ecozone) to -38.7% in the north (southern Arctic ecozone). Although their overall conclusion stated that NRCANmet (along with WFDEI) performed relatively well compared to other gridded product.

Table 6 – Observation and Projection data used in this study.

Dataset	Source	Time Period	Variables	Spatial Resolution
NRCANmet	Interpolated station data using ANUSPLIN package	1950-2013	1. Precipitation (mm/day) 2. Daily Maximum Temperature (°C)	~0.08° over North America

			3. Daily Minimum Temperature (°C)	
CanRCM4	Regional Climate Model	1950-2100	1. Precipitation Flux (kg m^{-2} $s^{-1)}$ 2. Daily Maximum Temperature (°K) 3. Daily Minimum Temperature (°K)	0.44° over North America
CanLEAD1	Bias corrected CanRCM4 w.r.t. EWEMBI reanalysis			0.5° over North America
CanLEAD2	Bias corrected CanRCM4 w.r.t. S14FD reanalysis			0.5° over North America

All datasets are interpolated to a 0.5° x 0.5° rectangular grid using bilinear interpolation following which 8,124 grids situated over Canada are extracted for further analysis. The variables across all models are converted to standard units of mm/day for precipitation and °C for tasmax and tasmin. The following section provides details regarding how the datasets are used at different temporal and spatial scales in each of the three phases in this study.

Phase 1

Figure 18 summarises the analysis process of phase 1. Every model simulation, including observation data are temporally averaged from 1951-2000 to decadal scale across four seasons – Winter (DJF), Spring (MAM), Summer (JJA) and Fall (SON). Then, error

metrics are computed at every grid point. The error metrics computed are Mean Bias Error (MBE) and Mean Absolute Error (MAE) defined according to the following equations:

$$MBE = \frac{\sum_{i=1}^{n}(y_i - x_i)}{n} \qquad (12),$$

$$MAE = \frac{\sum_{i=1}^{n}|x_i - y_i|}{n} \qquad (13),$$

where (x_i) represents the observation data i.e. NRCANmet, (y_i) represents the RCM data and n is the total number of data records. Consequently, in case of MBE, a positive bias value will point towards a warm or wet bias for temperature and precipitation, respectively, while a negative value will denote cold and dry bias.

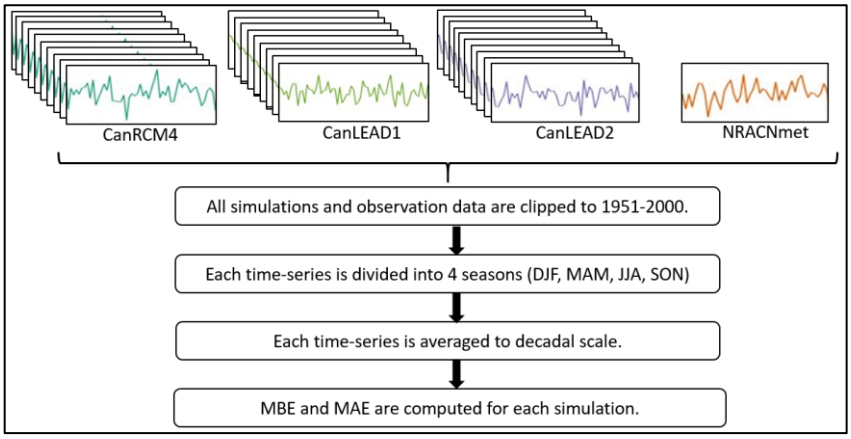

Figure 18 – The process followed in the first phase in which RCMs are validated with respect to observation data.

Phase 2

Figure 19 summarises the analysis process of phase 2. To evaluate each ensemble simulation with respect to observations and assess the capability of each model to jointly project temperature and precipitation in future, a Hierarchical Bayesian model is setup. The

models is similar to the one used by Tebaldi (2009) with a few differences in terms of the sampler used and choice of prior distributions for the parameters. All details of the model are provided in Appendix-A2.

The results in this phase are aimed at evaluating the agreement/disagreement of the individual simulations towards the central tendency of the model and the contribution of individual simulations to the ensemble average. Joint projections of temperature and precipitation are presented including the shift in the bivariate distribution from the end of the 20th century to the end of the 21st century. Other than that, trends in temperature and precipitation are also explored to assess the climate change signal.

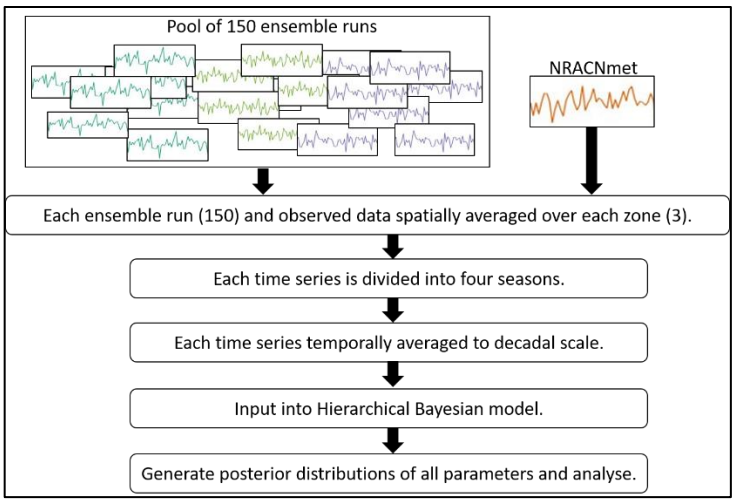

Figure 19 – The process followed in the second phase in which a Hierarchical Bayesian model is used to explore the joint distributions of temperature and precipitation.

The hierarchical Bayesian model is not evaluated at every grid point keeping in mind the computational complexity, time constraints and interpretability of results. Therefore, the model is run over three spatial domains in southern Canada (Figure 20). The domains have been created by merging terrestrial ecozones of Canada as defined by Wiken (1986). The

Western zone comprises of Montane Cordillera and the Pacific Maritime ecozones. The zone represents major mountainous region of Canada as well as a major population center on the west coast. The Central zone is defined by merging the Boreal Plains and the Canadian Prairies, which represents majority of the agricultural land in Canada. The Eastern zone is defined by merging Atlantic Maritime and Mixedwood Plains ecozones, which is another major population center. These zones in total represent over 28.6 million people, which is 90.51% of Canada's population as per 2006 figures reported by Statistics Canada (Statistics Canada). All grids lying within each zone are spatially averaged to get a single time-series of daily precipitation and daily average temperature (arithmetic mean of tasmax and tasmin) for each ensemble simulation.

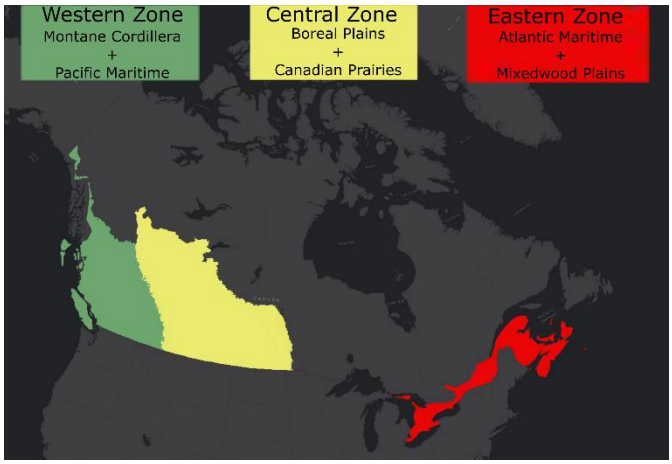

Figure 20 – Spatial domains defined during the third phase of the study. The zones are created by combining terrestrial ecozones of Canada as defined by Wiken (1986). The labels on the top show the name of each zone as used in this study (Western, Central and Eastern) and the two ecozones merged to create them in each case. The zones aim at capturing major population centers (east and west zones) and major agricultural land (central zone).

..

The major assumptions of the hierarchical framework are:

- The true observed temperature and log-precipitation is a joint Gaussian process and the data at hand is noise of that underlying true process.
- Both temperature and precipitation are linearly dependent on time with an elbow provided after the year 2000 to account for changes due to increased GHG emissions.
- Temperature and precipitation projections have an additive bias which is assumed to remain constant over time.

The posterior distributions in this study are sampled using the No-U-Turn Sampler (NUTS) (Hoffman and Gelman, 2014), which is an extension to the Hamiltonian Monte Carlo (HMC) sampler (Neal, 2011) using Stan platform (Stan Development Team, 2018). Several studies have reported the superiority of the NUTS-HMC sampler and it has become the standard MCMC sampler for Hierarchical Bayesian models. Some of its advantages include its ability to generate independent samples in presence of highly correlated parameters and sampling of posterior distributions more effectively (McElreath, 2018).

The data used for each zone includes 6 values (for 6 decades of 1951-2010) of observed temperature and precipitation obtained from NRCANmet and 15 values (for 15 decades of 1951-2100) of temperature and precipitation from 150 ensemble simulations for each season and each zone. This results in total 12 models i.e. 4 seasons and 3 zones.

Phase 3

Figure 21 summarises the analysis process of phase 3. Each ensemble simulation is divided into five 20-year periods. The first period, which is representative of the current climate

and serves as the baseline is selected as 1986-2005. The four subsequent periods are defined as that 20-year span in which the average daily temperature first rises to +1.5°C, +2.0°C, +3.0°C and +4.0°C respectively, above the pre-industrial (PI) average temperature. Since CanESM2 is approximately 0.79°C warmer than PI during 1986-2005 (Jeong et al. 2019), so the four periods of warming then correspond to an increase in temperature by 0.71°C, 1.21°C, 2.21°C and 3.21°C respectively, with respect to the baseline of 1986-2005. Extreme climate indices are first calculated in the baseline period across all simulations as well as the observation dataset to validate the accuracy of representation of extremes. Then, the same indicators are calculated for future warming scenarios across each RCM.

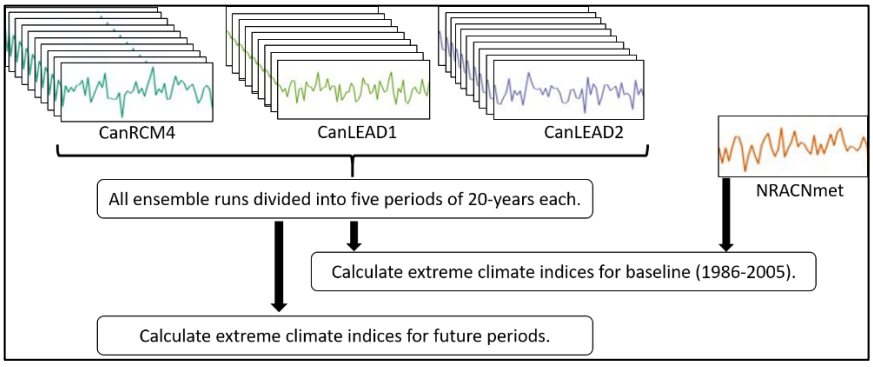

Figure 21 – The process followed in the third phase in which extreme climate indices are calculated.

Seven extreme climate indices are used in this study, three for temperature and four for precipitation (Table 7). The indices are taken from the CLIMDEX project defined by Expert Team on Climate Change Detection and Indices (ETCCDI) (Zhang et al. 2011).

Table 7 – Extreme Climate Indices used in this study. In all cases below, a wet day refers to a day when the daily precipitation is at least 1mm/day.

Category	Extreme Climate Index	Definition

Temperature extremes	Monthly maximum value of daily maximum temperature (TXx)	Maximum of the daily maximum temperature of a particular month.
	Monthly maximum value of daily minimum temperature (TNx)	Maximum of the daily minimum temperature of a particular month.
	Warm Spell Duration Index (WSDI)	Annual count of days with at least 6 consecutive days when tasmax > 90th percentile centered on a 5-day window in the base period.
Precipitation extremes	Consecutive Dry Days (CDD)	A Dry Spell is a sequence of days where daily precipitation is less than 1-mm per day.
	Consecutive Wet Days (CWD)	A Wet Spell is a sequence of days where daily precipitation is at least 1-mm per day.
	Annual total precipitation on wet days (PRCPTOT)	Sum of daily precipitation of all wet days in a year.
	R99p	Sum of daily precipitation on all days in a year in which precipitation exceeds the 99th percentile of precipitation on wet days in the base line period.

The indices have been chosen to analyse changes in magnitude as well as frequency of extreme events. TXx and TNx cover magnitude of extremes in tasmax and tasmin, respectively while PRCPTOT and R99p analyses the magnitude of overall and extreme precipitation. WSDI, CDD and CWD account for frequency measures of extreme temperature and precipitation.

5.3 Results

5.3.1 Phase 1 Results

MAE and MBE of tasmax for the three RCMs are computed seasonally over 1951-2000 with respect to NRCANmet (Figure 22). A significant warm bias can be observed in CanRCM4 in all seasons except fall, with magnitudes of up to 9°C. These biases are corrected by the CanLEAD products to a large degree, most prominently in winter and the least in summer. Warm bias in all three seasons can be observed in almost all of inland Canada, with only the extreme north, the western mountainous regions and the eastern coastal regions having a cold bias. Cold bias, although limited to smaller spatial domains, has a larger magnitude with some grids on the west coast near the Gulf of Alaska having up to -13°C bias in summer in CanRCM4. In fall, warm bias in CanRCM4 is limited to small pockets in northern regions reaching a magnitude of 4°C and cold bias of up to -9°C in the west. The effect of elevation can be easily detected as the western mountainous regions stand out in every map having a predominantly cold bias in CanRCM4 and small warm bias in both CanLEAD products. To summarise the overall results down to a single quantifiable number, Table 8 shows the spatially averaged MAE of the three products

across all seasons. CanLEAD2 has a much lower MAE in all seasons except fall, in which the MAE of CanLEAD2 is higher than CanRCM4.

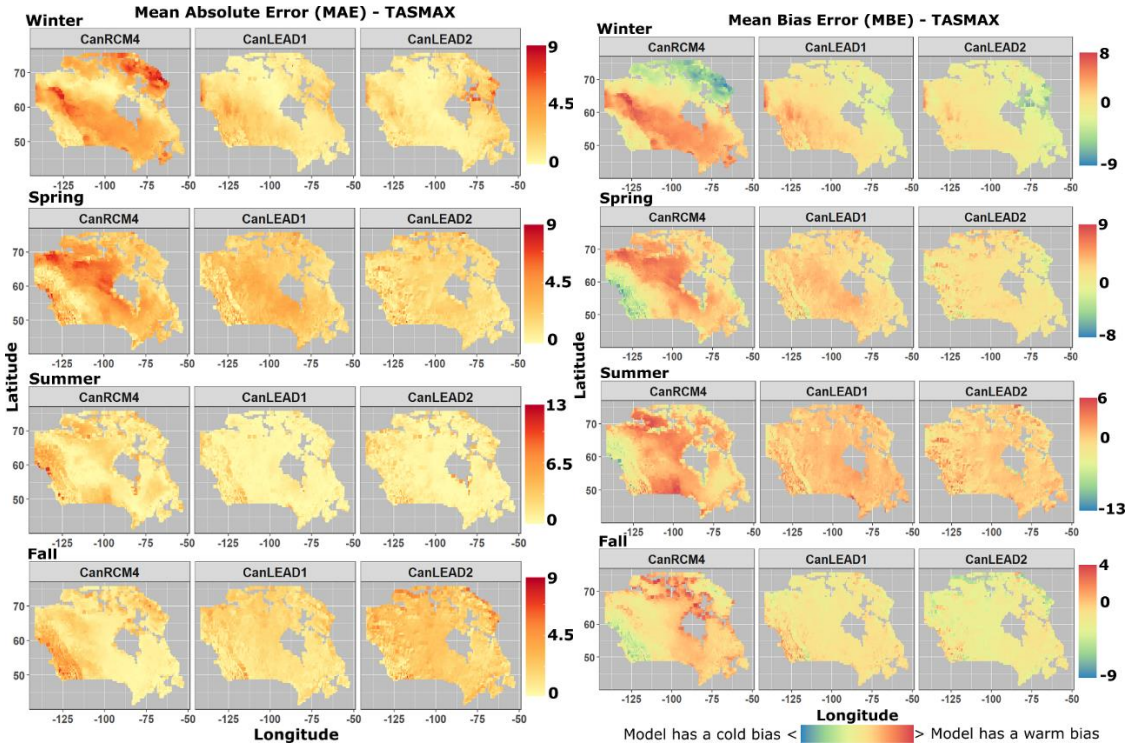

Figure 22 – Seasonal MAE (left) and MBE (right) for daily maximum temperature. The figures reported are for the period 1951-2000 calculated with respect to NRCANmet.

Table 8 – Spatially averaged MAE (Tasmax) for each product across seasons, providing an overview of accuracy with respect to observation.

Season	*CanRCM4*	*CanLEAD1*	*CanLEAD2*
Winter	3.21	1.43	1.13
Spring	3.59	2.70	1.79
Summer	1.99	0.85	1.02
Fall	1.60	1.70	2.56

The overall magnitude of bias in tasmin is higher than that of tasmax although spatially, the two variables exhibit similar behavior (Figure 23). The spatial pattern of cold bias observed in tasmax in extreme north and southwest is repeated for tasmin as well, and similarly warm bias dominates much of inland regions. In winter, warm bias goes up to 14°C for CanRCM4 in small areas around the Hudson Bay and near the Gulf of St Laurence in the east, which are corrected in the CanLEAD products. Warm bias is most dominant spatially in spring and summer and although the magnitude of bias is decreased by the CanLEAD products, the spatial patterns remain similar. In fall, CanLEAD products are predominantly colder with CanLEAD2 having a higher magnitude of cold bias. For MAE, the pattern is similar to the one observed for tasmax with CanLEAD2 having least error in winter and spring but the most in fall (Table 9).

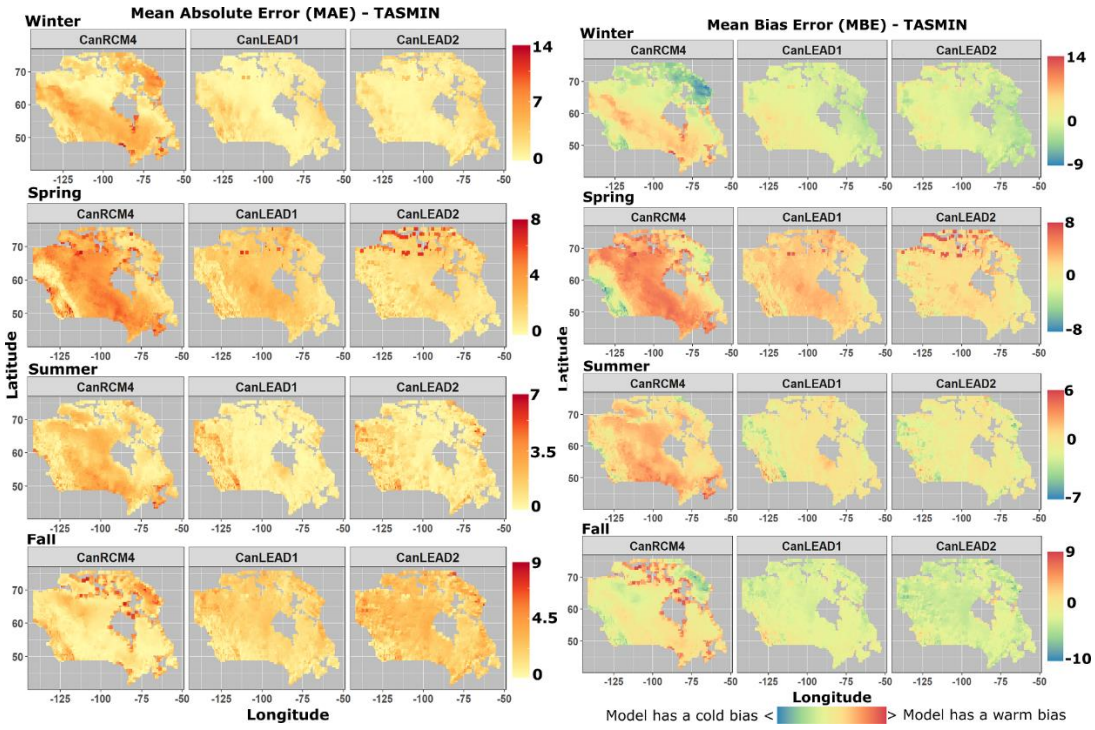

Figure 23 – Seasonal MAE (left) and MBE (right) for daily minimum temperature. The figures reported are for the period 1951-2000 calculated with respect to NRCANmet.

Table 9 – Spatially averaged MAE (Tasmin) for each product across seasons, providing an overview of accuracy with respect to observation.

Season	*CanRCM4*	*CanLEAD1*	*CanLEAD2*
Winter	3.51	1.36	1.41
Spring	3.56	2.20	1.57
Summer	1.59	0.71	0.87
Fall	1.73	2.10	2.84

Precipitation biases show a spatially homogenous trend with only the extreme eastern and western coastal regions showing high bias values (Figure 24). In all seasons, the windward side of the western mountain regions have a wet bias. Winter, spring and fall have a slight dry bias for majority of the country and summer has a wet bias, which is most dominant in CanRCM4. The magnitude of wet bias however is much higher with a particular grid in the west acting as extreme outlier with bias reaching up to 11 and 12 mm/day in winter and fall, respectively. The dominance of dry bias in rest of the country should also be seen from the perspective of the observation data. As reported earlier, NRCANmet is generally drier than historical station records, which means that the true magnitude of dry bias in these climate models would in fact be higher. In that respect, both CanLEAD products perform better as the magnitude of dry bias is reduced in all cases as compared to CanRCM4. The spatially averaged MAE reveals that significant improvement is achieved in spring and summer using the bias correction technique where CanRCM4 errors are large in magnitude (Table 10).

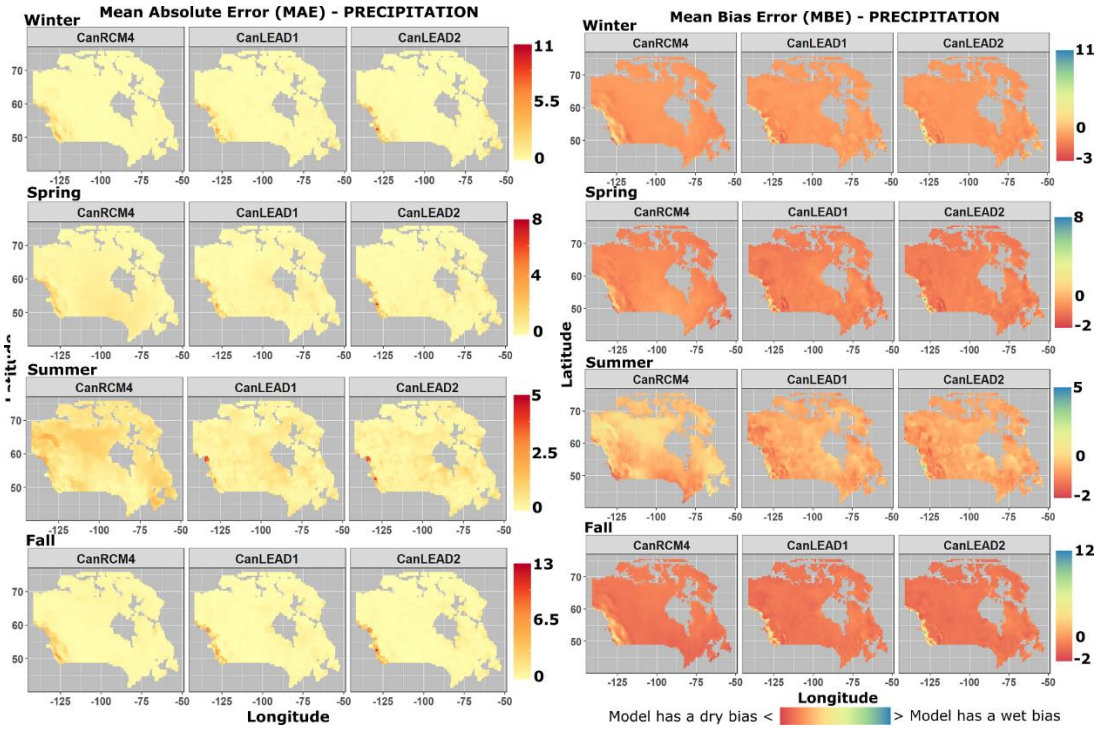

Figure 24 – Seasonal MAE (left) and MBE (right) for daily precipitation. The figures reported are for the period 1951-2000 calculated with respect to NRCANmet.

Table 10 – Spatially averaged MAE (Precipitation) for each product across seasons, providing an overview of accuracy with respect to observation.

Season	*CanRCM4*	*CanLEAD1*	*CanLEAD2*
Winter	0.22	0.26	0.25
Spring	0.47	0.30	0.26
Summer	0.72	0.37	0.35
Fall	0.39	0.34	0.33

5.3.2 Phase 2 Results

The hierarchical models for the eastern zone reveal that both CanLEAD products imitate observations more closely than CanRCM4, except in summer for which all three models are comparable (Figure 25). In all three seasons except summer, majority of the CanRCM4 simulations have a warm bias, with the highest magnitude of bias in winter, exhibited by a small number of simulations. The spread of the blue bars in Figure 25 also reveal that CanRCM4 tends to have a larger uncertainty bound than both CanLEAD products, especially in winter. This pattern is reversed however in the case of precipitation (Figure 26). All simulations of CanRCM4 exhibit very similar biases for precipitation thus the blue bars in Figure 26 cluster into small areas. In winter, CanRCM4 shows very good agreement with the true historical posterior density but in all other seasons, CanLEAD1 has the least bias. Figures 25-28 also show the trends in temperature and precipitation with respect to time. The marginal density of temperature in Figure 25 shifts to the right, most prominently in winter and summer, an effect that is revealed more clearly in the trend bars of Figure 27. The introduction of elbow at the year 2000 also reveals a big acceleration in warming which jumps from under 0.3°C/decade before the elbow to over 0.7°C/decade after. For precipitation, the magnitude of trend is highest in winter at +0.03 mm/decade in winter whereas a small negative trend is observed in fall. Finally, the joint distributions of temperature and precipitation in figure 28 reveal the warming and wetting trend in all seasons for the eastern zone except in summer.

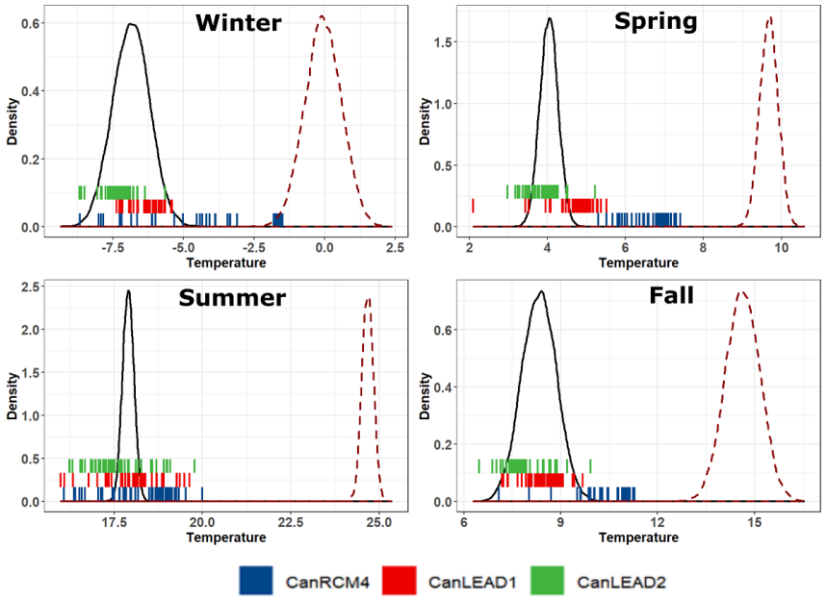

Figure 25 – Temperature bias in each simulation of the ensemble with respect to the posterior density of the *true* temperature (see Appendix-A2 for details) for each season in the eastern zone. The solid black posterior density corresponds to the temperature of decade centered at 1995 whereas the dashed red posterior corresponds to temperature of the decade centered at year 2095, thus indicating temporal shift in the density. The bars at the bottom represent the posterior means of the temperature projected by each ensemble simulation from the models (blue for CanRCM4, red for CanLEAD1 and green for CanLEAD2). The magnitude of the bias can be assessed by the distance of each bar from the center of the solid black posterior (since biases are assumed to remain constant, the spread of the ensemble will be same around the future posterior). The agreement/disagreement of the ensemble simulations within each model can be assessed by the spread of the bars themselves. The figure also shows evidence of how many ensemble simulations from each model contribute more to the true posterior (ones that are closer to the true temperature distribution).

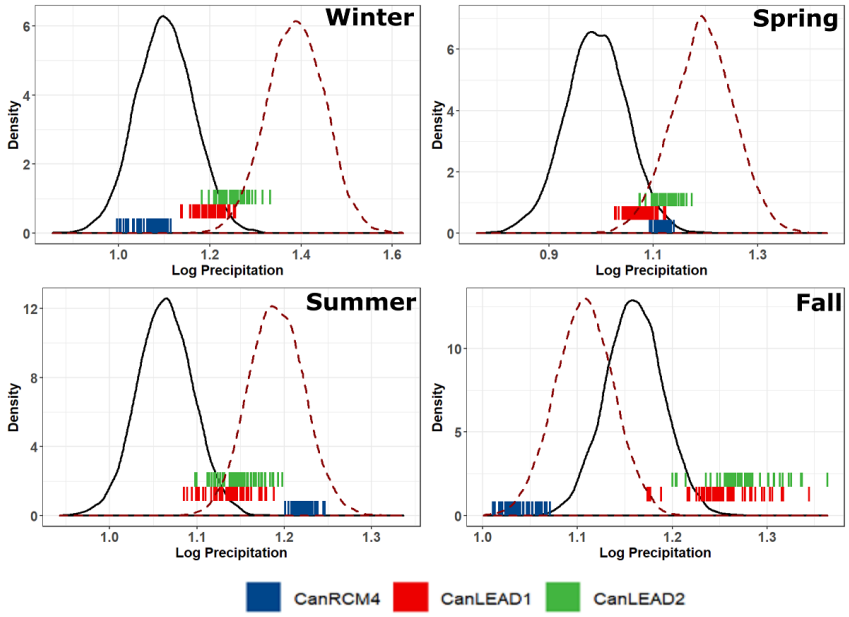

Figure 26 – Precipitation bias (logarithm scale) in each simulation of the ensemble with respect to the posterior density of the *true* log precipitation (see Appendix-A2 for details) for each season in the eastern zone. See caption of Figure 25 for more details.

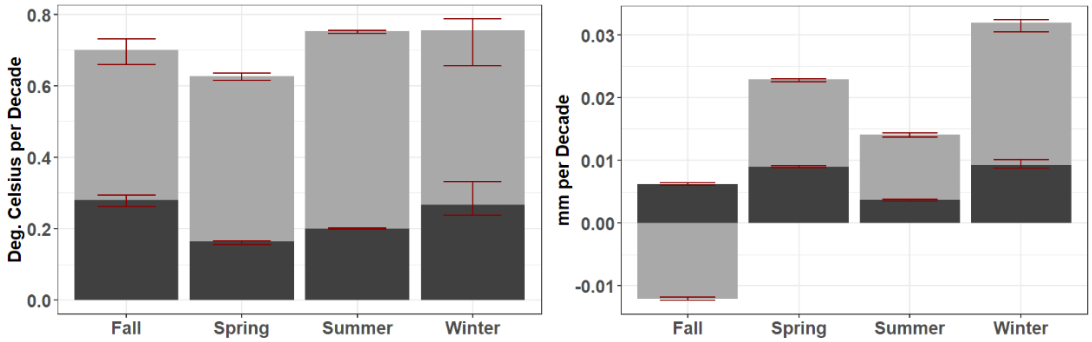

Figure 27 – The trends in temperature (left) and precipitation (right) for each season for the eastern zone. The dark grey bar signifies the trend before the year 2000 and the cumulative height is the trend after an elbow is introduced (which means the light grey bar corresponds to the increase in trend after an elbow is introduced). The red bars show the credible interval of the posterior distribution of the trends.

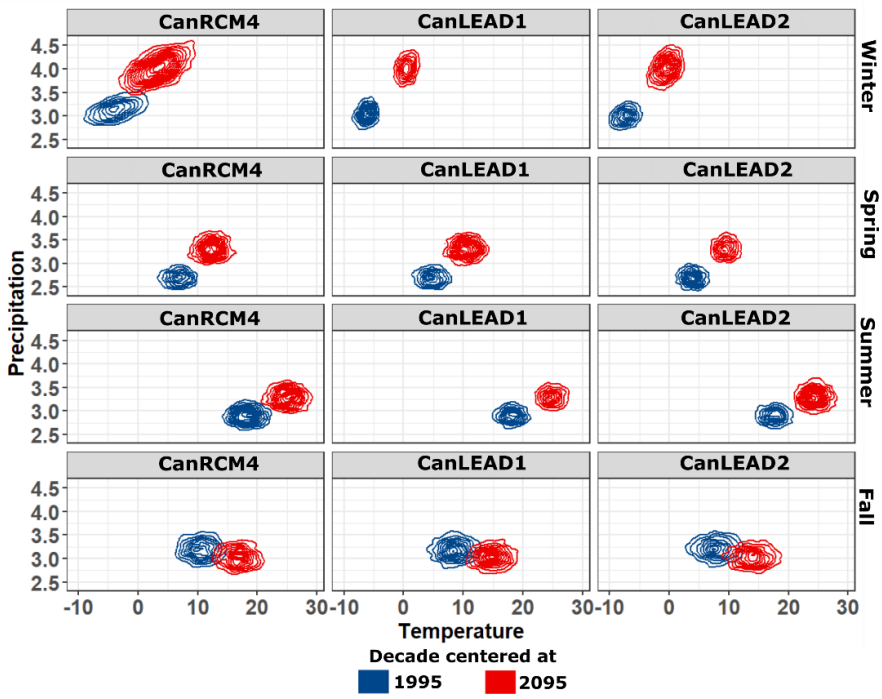

Figure 28 – Shift in the joint distribution of temperature and precipitation in each season for Eastern zone. The two distributions correspond to the decades centered at 1995 and 2095 respectively. A shift in the horizontal direction signifies change in warming/cooling over the decades while a shift in the vertical direction reflects a drying/wetting phenomenon.

There is very little variation in temperature biases across the three models in central zone (Figure 29). In all seasons except summer, majority of the model simulations remain within the historical posterior. In summer, the biases in the simulations are higher with respect to the spread of the posterior, but it should be noted that the posterior itself is quite narrow. For precipitation in central zone, all simulations from the CanRCM4 ensemble show very little bias in winter, fall, and relatively tight uncertainty bounds in terms of spread of the biases for each simulation with respect to CanLEAD products (Figure 30). In spring and summer, biases in CanRCM4 are large and while both CanLEAD products also lie outside the historical posterior mostly, they perform better than CanRCM4. Temperature shows

warming trends of over 0.75°C/decade in all seasons except spring in which the trend is much lower at 0.5°C/decade (Figure 31). The acceleration in warming post 2000 is even greater for the central zone, especially in winter with a seven-fold increase in warming trend. The highest positive trend for precipitation is recorded at just over 0.04 mm/decade while a negative trend is observed in summer. Figure 32 shows the joint distributions of temperature and precipitation in the central zone. While all seasons show a warming and wetting trend except in summer, which shows warming and drying trend.

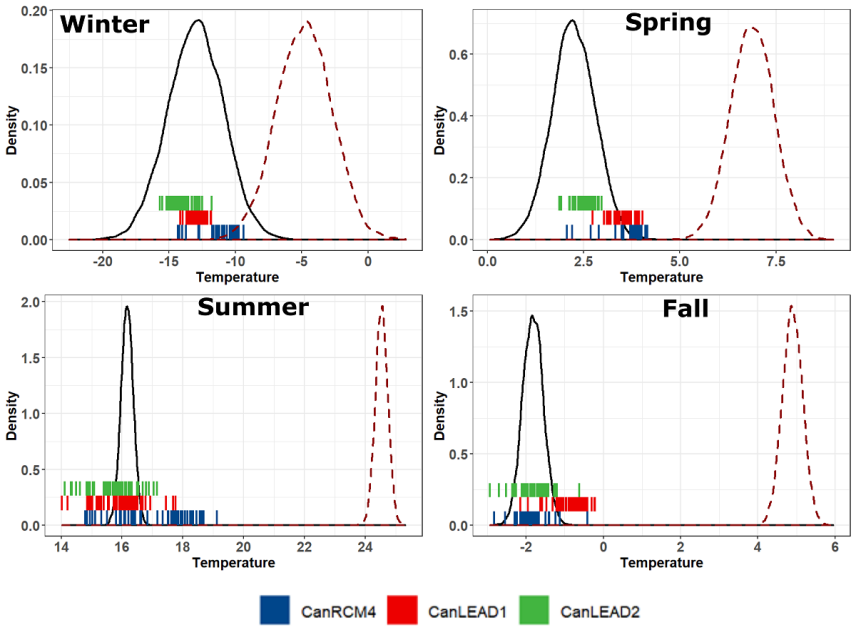

Figure 29 – Temperature bias in each simulation of the ensemble with respect to the posterior density of the *true* temperature (see Appendix-A2 for details) for each season in the central zone. See caption of Figure 25 for more details.

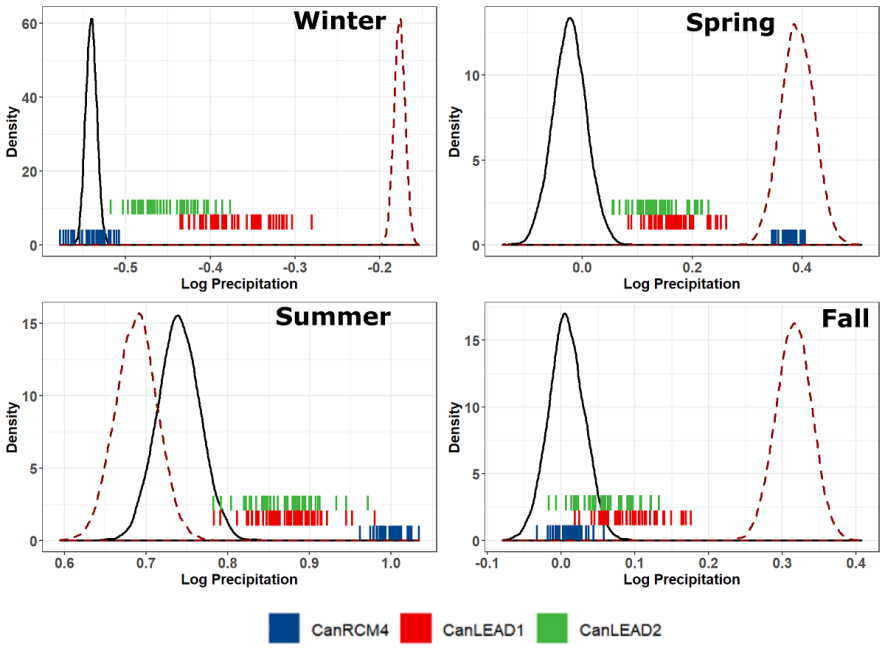

Figure 30 – Precipitation bias (logarithm scale) in each simulation of the ensemble with respect to the posterior density of the *true* log precipitation (see Appendix-A2 for details) for each season in the central zone. See caption of Figure 25 for more details.

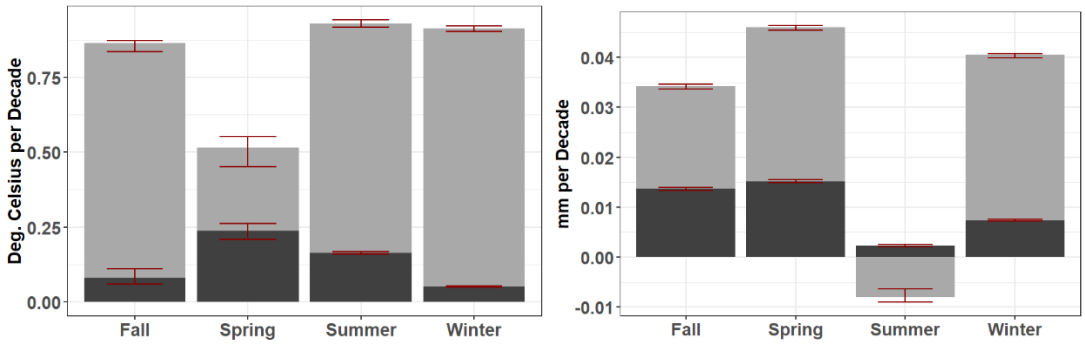

Figure 31 – The trends in temperature (left) and precipitation (right) for each season for the central zone. See caption of Figure 27 for more details.

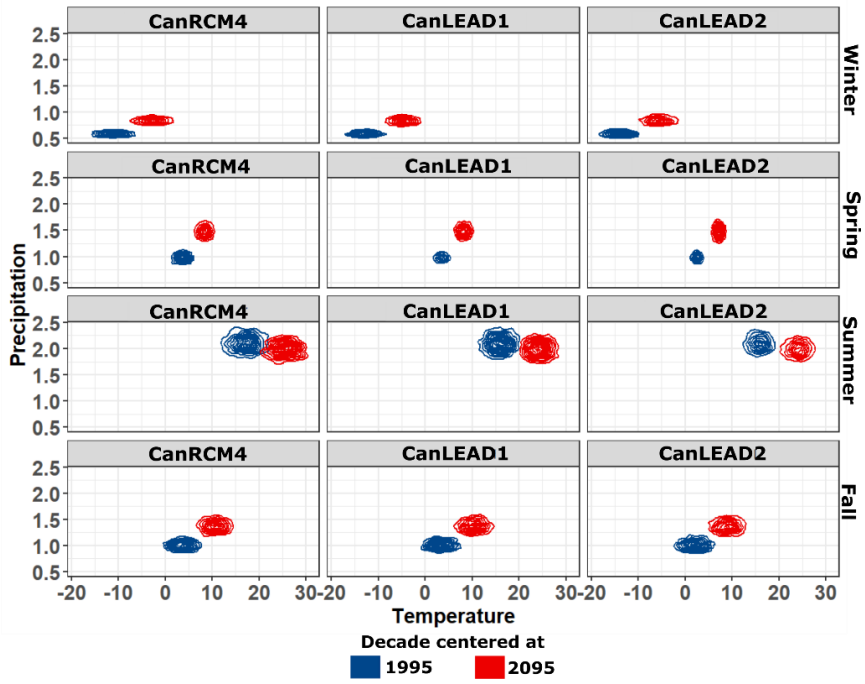

Figure 32 – Shift in the joint distribution of temperature and precipitation in each season for Central zone. The two distributions correspond to the decades centered at 1995 and 2095 respectively. A shift in the horizontal direction signifies change in warming/cooling over the decades while a shift in the vertical direction reflects a drying/wetting phenomenon.

For winter season in western zone, all models have relatively small bias (Figure 33). Majority of CanRCM4 simulations have a cold bias in spring and summer whereas CanLEAD products exhibit better agreement with the historical posterior. In fall, CanLEAD1 has a higher warm bias in majority of its simulations as compared to other two models and in fact, a higher percentage of CanRCM4 ensemble lies within the posterior as compared to CanLEAD products. CanRCM4 has relatively large wet bias in all seasons as compared to both CanLEAD products including similar behavior to the previous two zones where the uncertainty range of biases in CanRCM4 is very narrow (Figure 34). Except in summer, all simulations of all three models lie outside and to the right of the historical

posterior indicating a wet bias. Warming trends are similar to the ones observed in central zone, with all seasons except spring having over 0.75°C/decade trend in temperature (Figure 35). However, none of the seasons in the western zone exhibits a drying trend as seen in previous two cases. The least positive trend is observed in summer at almost 0.005mm/decade and the highest in fall at over 0.025mm/decade. As evident from the marginal trends, the joint contours of temperature and precipitation exhibit a wetting and warming towards the end of the 21st century in all seasons (Figure 36).

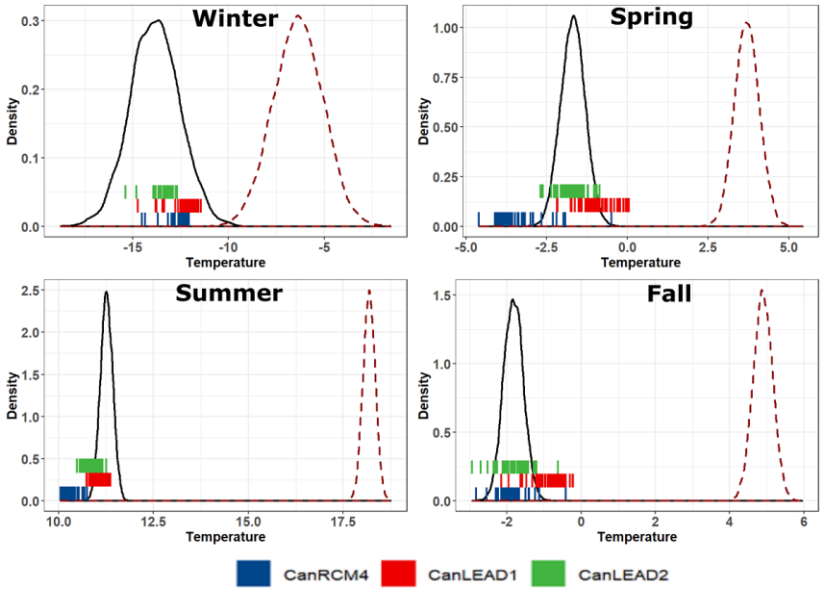

Figure 33 – Temperature bias in each simulation of the ensemble with respect to the posterior density of the *true* temperature (see Appendix-A2 for details) for each season in the western zone. See caption of Figure 25 for more details.

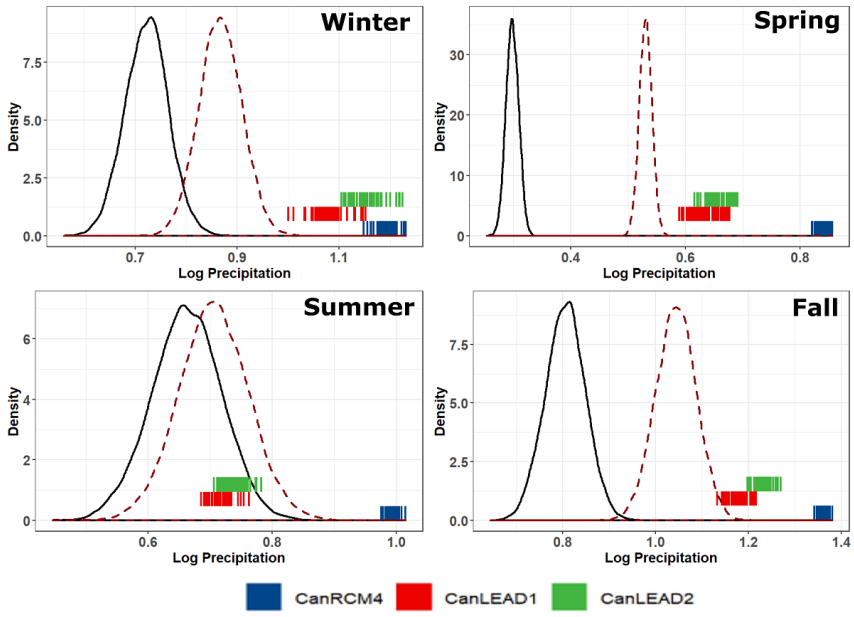

Figure 34 – Precipitation bias (logarithm scale) in each simulation of the ensemble with respect to the posterior density of the *true* log precipitation (see Appendix-A2 for details) for each season in the western zone. See caption of Figure 25 for more details.

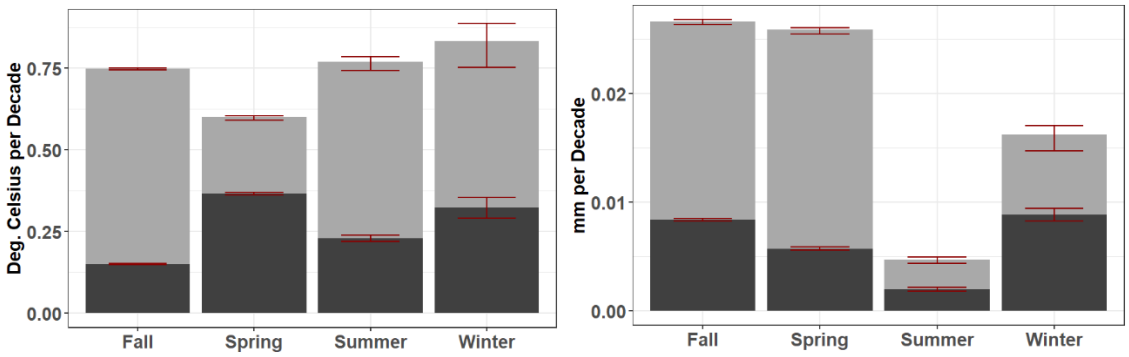

Figure 35 – The trends in temperature (left) and precipitation (right) for each season for the western zone. See caption of Figure 27 for more details.

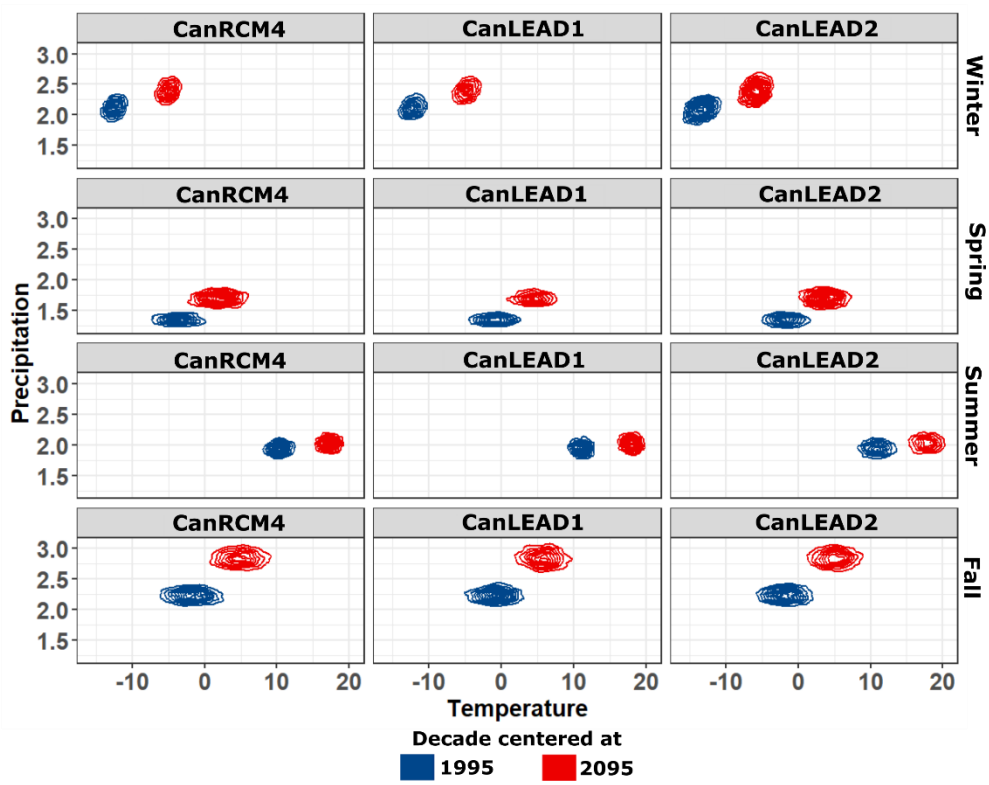

Figure 36 – Shift in the joint distribution of temperature and precipitation in each season for Western zone. The two distributions correspond to the decades centered at 1995 and 2095 respectively. A shift in the horizontal direction signifies change in warming/cooling over the decades while a shift in the vertical direction reflects a drying/wetting phenomenon.

5.3.3 Phase 3 Results

For both TXx and TNx extreme indices, CanLEAD2 exhibits the closest behavior to observed data (Figures 37 and 38). While in case of TXx, CanLEAD1 overestimates the magnitude the most, for TNx it is CanRCM4 with an average overestimation of 3°C. For both indices, an increasing trend is observed over the five warming periods with the mean TXx (in CanLEAD1) shifting from 10.39°C to 13.2°C while average TNx changes from 0.6°C to 3.8°C from baseline to the last period, respectively. The trend for tasmin driven index is higher than that of tasmax driven index indicating that changes in the diurnal

temperature range are driven more by changes in the daily minimum temperature, which is similar to results reported by other studies (Vincent et al. 2006; Zhang et al. 2000). Spatial maps for the baseline period created by averaging the indices over terrestrial ecozones reveal that the Canadian Prairies, southern Ontario and Atlantic Maritime are most susceptible to warming in both daily maximum and minimum temperature.

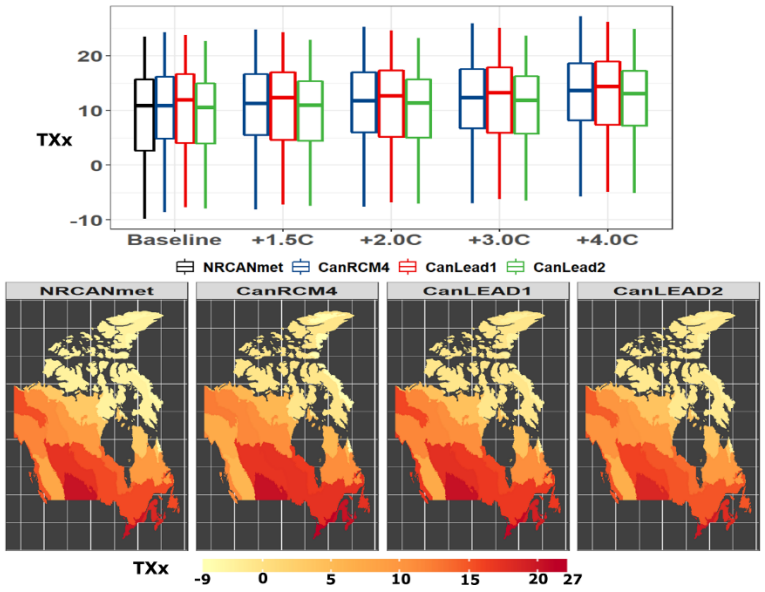

Figure 37 – Monthly maximum value of daily maximum temperature (TXx). The boxplots represent the distribution of the average TXx in every 20-year period at each grid from the whole ensemble thus capturing the complete spatial and ensemble variability. The maps represent spatially averaged TXx values within each terrestrial ecozone for the baseline period (1986-2005). The maps for the models are generated by taking the average of the index across the 50-run ensemble.

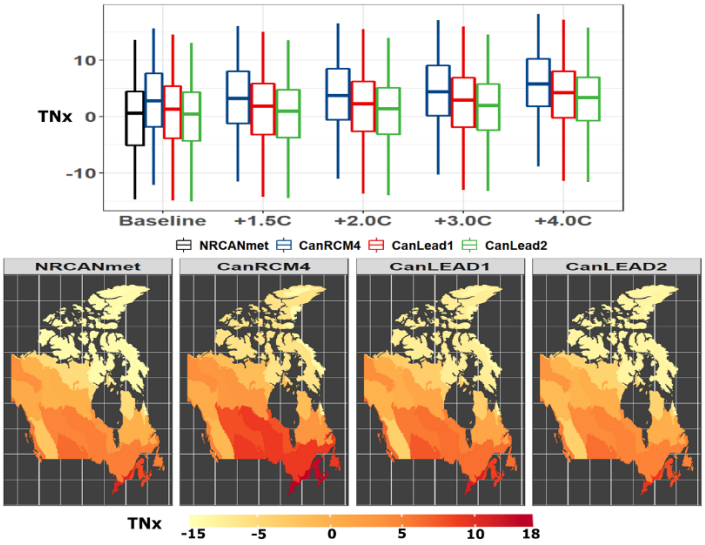

Figure 38 – Monthly maximum value of daily minimum temperature (TNx). The boxplots represent the distribution of the average TNx in every 20-year period at each grid from the whole ensemble thus capturing the complete spatial and ensemble variability. The maps represent spatially averaged TNx values within each terrestrial ecozone for the baseline period (1986-2005). The maps for the models are generated by taking the average of the index across the 50-run ensemble.

A significant increase is observed in WSDI, especially in the period corresponding to overall +4°C warming (Figure 39). In the baseline, the CanLEAD products tend to underestimate the duration of warm spells as compared to observation whereas CanRCM4 mimics the behavior quite well. In future warming periods, the pattern is repeated such that CanRCM4 projects higher WSDI consistently while CanLEAD1 projects the lowest WSDI in each period.

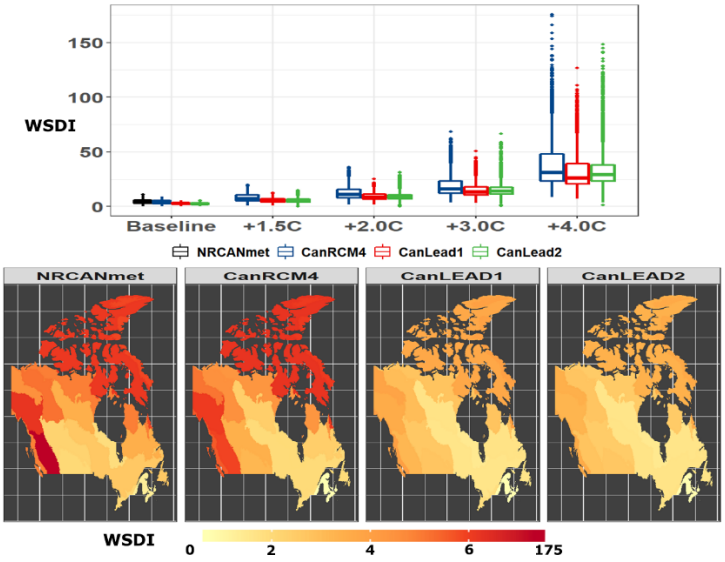

Figure 39 – Warm Spell Duration Index (WSDI). The boxplots represent the distribution of the average WSDI in every 20-year period at each grid from the whole ensemble thus capturing the complete spatial and ensemble variability. The maps represent spatially averaged WSDI values within each terrestrial ecozone for the baseline period (1986-2005). The maps for the models are generated by taking the average of the index across the 50-run ensemble.

CanLEAD2 proves better at capturing consecutive dry days in the baseline, especially in matching the extremes of the distribution of the observed data, which is largely underestimated by CanRCM4 (Figure 40). A slight decreasing trend is observed in the average number of CDD through the five periods most of which tends to be concentrated in the northern regions, the Canadian Prairies and over the western mountain regions.

On the other hand, consecutive wet days show a slight increasing trend over the five periods (Figure 41). During the baseline, whereas CanRCM4 captures the extreme of the distribution better than CanLEAD products, but it overestimates the average. CanLEAD1 captures the average CWD well but there is a large degree of underestimation in CanLEAD2. This trend carries over into the future periods as well with a consistent

overestimation by CanRCM4 and underestimation by CanLEAD1. The extremes in the distribution of CWD are entirely concentrated on the windward side of the western mountains, specifically in the Pacific Maritime ecozone on the western coast.

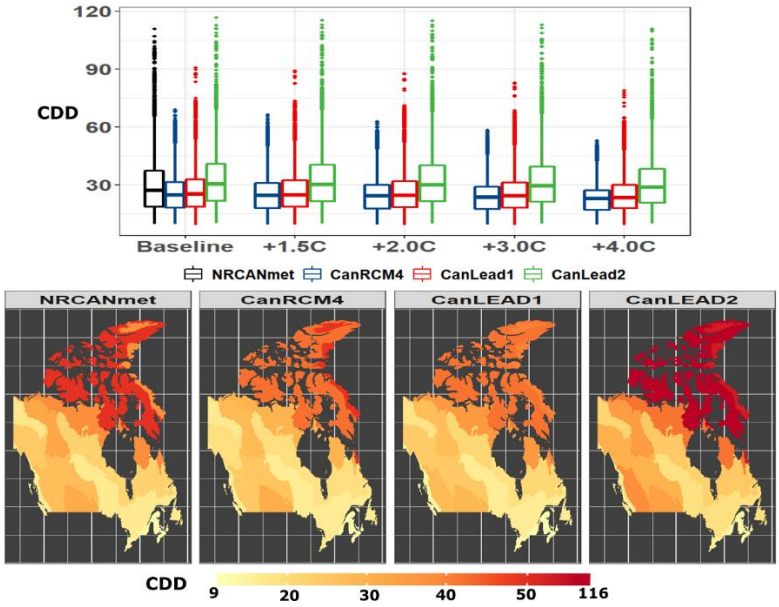

Figure 40 – Consecutive Dry Days (CDD). The boxplots represent the distribution of the average CDD in every 20-year period at each grid from the whole ensemble thus capturing the complete spatial and ensemble variability. The maps represent spatially averaged CDD values within each terrestrial ecozone for the baseline period (1986-2005). The maps for the models are generated by taking the average of the index across the 50-run ensemble.

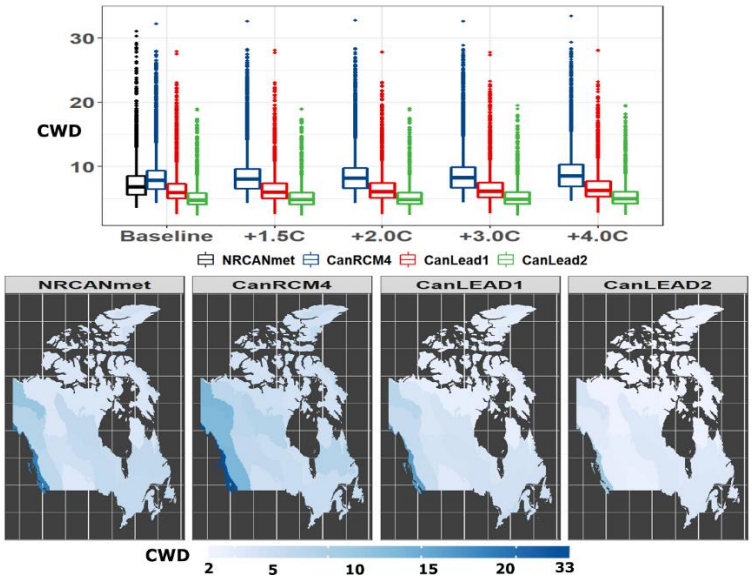

Figure 41 – Consecutive Wet Days (CWD). The boxplots represent the distribution of the average CDD in every 20-year period at each grid from the whole ensemble thus capturing the complete spatial and ensemble variability. The maps represent spatially averaged CWD values within each terrestrial ecozone for the baseline period (1986-2005). The maps for the models are generated by taking the average of the index across the 50-run ensemble.

Both PRCPTOT and R99p exhibit similar behavior. There is an approximately consistent 10% increase in the average of both indices for the first three future warming scenarios but the rate almost doubles in the last period (Figures 42 and 43). In the baseline, whereas CanLEAD2 has some outliers, it proves better in capturing the average annual total precipitation and the total of extreme precipitation. CanRCM4 overestimates the average annual total precipitation by ~130mm as compared to ~102mm and ~92mm by CanLEAD1 and 2, respectively. On the other hand, the overestimation in total of extreme precipitation (R99p) across the three models is ~43mm, ~31mm and ~27mm. While majority of the grids show an increase in percentage change from the baseline, CanLEAD1 shows a decrease of

about -1.1% in total annual precipitation and -2.5% in total of extreme precipitation around the Canadian Prairies region

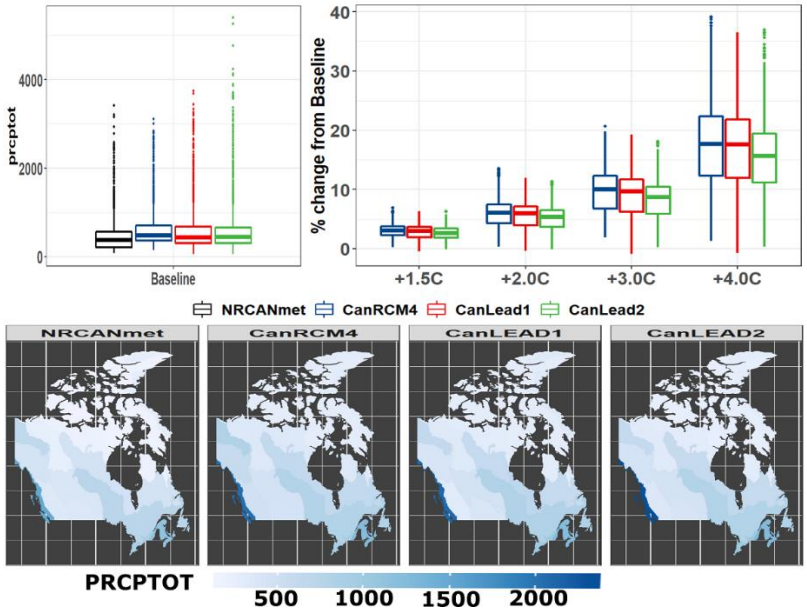

Figure 42 – Annual total precipitation on wet days (PRCPTOT). The top-left boxplot represents the value of PRCPTOT in the base line. The top-right boxplots represent the % change in PRCPTOT with respect to the baseline in each warming scenario. The maps represent spatially averaged PRCPTOT values within each terrestrial ecozone for the baseline period (1986-2005). The maps for the models are generated by taking the average of the index across the 50-run ensemble.

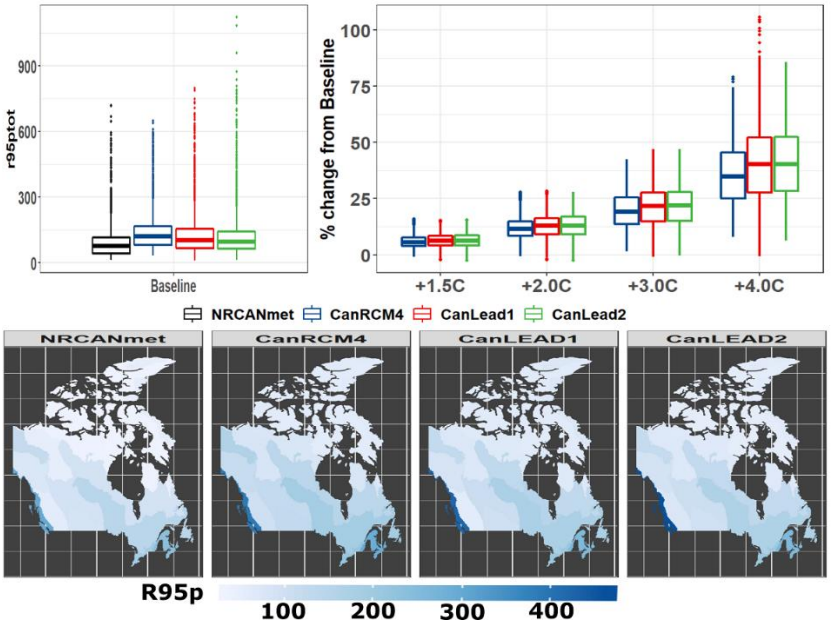

Figure 43 – Annual total of extreme precipitation on wet days (R95p). The top-left boxplot represents the value of PRCPTOT in the base line. The top-right boxplots represent the % change in R95p with respect to the baseline in each warming scenario. The maps represent spatially averaged R95p values within each terrestrial ecozone for the baseline period (1986-2005). The maps for the models are generated by taking the average of the index across the 50-run ensemble.

5.4 Conclusions

A new large ensemble, Canadian Large Ensembles Adjusted Dataset (CanLEAD) is created providing climate change information at the regional scale over the North American continent. The dataset is created using an adapted N-dimensional probability density function transform for the multivariate bias correction (MBCn) of The Canadian Regional Climate Model (CanRCM4). This study is aimed at evaluation of biases in daily maximum temperature, daily minimum temperature and daily precipitation from CanRCM4 and two versions of CanLEAD, bias corrected to EWEMBI and S14FD reanalysis data respectively. Biases are evaluated against NRCANmet gridded observation data over Canada from 1951-

2000. Further, a Hierarchical Bayesian framework is used to evaluate biases in each simulation of the large ensembles, identify climate change signal within the ensemble and to assess the joint distributions of temperature and precipitation projected by the models across three spatial domains over southern Canada. Finally, extreme indices are used to study compare the magnitude as well as frequency of extreme events across the models over five 20-year periods. In baseline period of 1986-2005, extreme indices are evaluated against indices generated from NRCANmet followed by an assessment of changes in the extremes in four future warming scenarios corresponding to +1.5°C, +2.0°C, +3.0°C and +4.0°C respectively, above the pre-industrial (PI) average temperature.

CanRCM4 showed significant warm biases in winter (DJF), spring (MAM) and summer (JJA) with magnitudes reaching up to 9°C for tasmax in spring and 14°C for tasmin in winter. Both CanLEAD products showed much lower biases in these three seasons with CanLEAD2 performing marginally better than CanLEAD1 in most cases. For precipitation too, in all three seasons, CanLEAD2 had the lowest bias with the exception of an extreme outlier grid on the west coast. In fall (SON), the corrected products had a higher mean absolute error than CanRCM4 for all three variables however, biases within NRCANmet should also be considered while evaluating these results since it has been reported as being dry and warm by previous studies, especially over western Canada. The hierarchical framework revealed further intricacies within the ensembles. Results show that a higher percentage of CanLEAD2 ensemble agrees with the overall central tendency of the observation relatively better compared to the other two models in most cases. However, in this case too, the CanLEAD products seemed to struggle in fall season. Trends revealed that the highest warming in all three zones is observed in summer and winter seasons, with

central and western Canada having a higher warming trend (over 0.75°C/decade) than eastern Canada. Precipitation trends were relatively small, with the highest trend observed in spring in central Canada at just over 0.4mm/decade. Negative trends were observed in precipitation for eastern Canada in summer and eastern Canada in fall whereas western Canada had positive trends in all seasons. The joint distributions of temperature and precipitation in all zones also revealed similar patterns as a warming and wetting trend was observed in most cases. The upper tail extremes of daily maximum and daily minimum temperature (TXx and TNx respectively) were best captured by CanLEAD2 with respect to NRCANmet whereas the corrected products underestimated the duration of warm spells. For precipitation extremes, whereas CanLEAD1 captured the average frequency of consecutive dry days better, CanLEAD2 captured some extreme regional outliers that exist in NRCANmet as well. Consecutive wet days were overestimated by CanRCM4 and underestimated by both CanLEAD products with respect to observation. The magnitude of total annual precipitation and total extreme precipitation (R95p) was overestimated to some degree by all models but least bias was found in CanLEAD2. For future trends in extremes, magnitude of temperature extremes rises steadily across all warming scenarios all over Canada with the highest magnitudes observed in central and southeastern Canada. The duration of warm spells increases exponentially over the warming periods, with the biggest spike projected in the last period of average +4.0°C warming above PI. A slight reduction in the number of dry days and an increase in wet days is projected. Total annual precipitation and extreme precipitation both increase consistently at a rate of approximately 10% for the first three warming periods but doubles in the last period. However, a small negative trend is also observed around the Canadian Prairies.

CanLEAD product offers a bias corrected large ensemble climate data for the analysis of climate change impacts at a regional scale over North America. It can be concluded from results of this study that with respect to NRCANmet, CanLEAD (especially CanLEAD2, which is bias corrected with respect to S14FD) can be used as a reliable alternative to the existing CanRCM4 ensemble. Moreover, the use of multivariate bias correction method for creating CanLEAD makes it ideal for use in the analysis of compound events, which rely on multiple statistically dependent climate variables. The ability of the CanLEAD dataset to identify compound events with respect to observation data and its comparison to the existing CanRCM4 should further be explored in future works.

5.5 References

Cannon, Alex J. "Multivariate quantile mapping bias correction: an N-dimensional probability density function transform for climate model simulations of multiple variables." Climate dynamics 50.1-2 (2018): 31-49.

Dee DP, Uppala SM, Simmons AJ, Berrisford P, Poli P, Kobayashi S, Andrae U, Balmaseda MA, Balsamo G, Bauer P, Bechtold P, Beljaars ACM, van de Berg L, Bidlot J, Bormann N, Delsol C, Dragani R, Fuentes M, Geer AJ, Haimberger L, Healy SB, Hersbach H, Hólm EV, Isaksen L, Kållberg P, Köhler M, Matricardi M, McNally AP, Monge-Sanz BM, Morcrette J-J, Park B-K, Peubey C, de Rosnay P, Tavolato C, Thépaut J-N, Vitart F (2011) The ERA-Interim reanalysis: configuration and performance of the data assimilation system. Q J R Meteorol Soc 137:553–597. doi: 10.1002/qj.828

Eum, H. I., Dibike, Y., Prowse, T., & Bonsal, B. (2014). Inter-comparison of high-resolution gridded climate data sets and their implication on hydrological model simulation over the Athabasca Watershed, Canada. Hydrological processes, 28(14), 4250-4271.

Gaur, A., Lacasse, M., & Armstrong, M. (2019). Climate Data to Undertake Hygrothermal and Whole Building Simulations Under Projected Climate Change Influences for 11 Canadian Cities. Data, 4(2), 72.

Gelman, A., & Rubin, D. B. (1992). Inference from iterative simulation using multiple sequences. Statistical science, 7(4), 457-472.

Gelman, A., Carlin, J. B., Stern, H. S., Dunson, D. B., Vehtari, A., & Rubin, D. B. (2013). Bayesian data analysis. Chapman and Hall/CRC.

Giorgi F, Jones C, Asrar G (2009) Addressing climate information needs at the regional level: the CORDEX framework. WMO Bull 58:175–183

Hoffman, M. D., & Gelman, A. (2014). The No-U-Turn sampler: adaptively setting path lengths in Hamiltonian Monte Carlo. Journal of Machine Learning Research, 15(1), 1593-1623.

Hutchinson, M. F., McKenney, D. W., Lawrence, K., Pedlar, J. H., Hopkinson, R. F., Milewska, E., . . . Climatology. (2009). Development and testing of Canada-wide interpolated spatial models of daily minimum–maximum temperature and precipitation for 1961–2003. 48(4), 725-741.

Iizumi, T., Takikawa, H., Hirabayashi, Y., Hanasaki, N., & Nishimori, M. (2017). Contributions of different bias-correction methods and reference meteorological forcing data sets to uncertainty in projected temperature and precipitation extremes. Journal of Geophysical Research: Atmospheres, 122(15), 7800-7819.

Jeong, D. I., Cannon, A. J., & Zhang, X. (2019). Projected changes to extreme freezing precipitation and design ice loads over North America based on a large ensemble of Canadian regional climate model simulations. Natural Hazards and Earth System Sciences, 19(4), 857-872.

Lange, S. (2016). EartH2Observe, WFDEI and ERA-Interim data Merged and Bias-corrected for ISIMIP (EWEMBI), GFZ Data Services.

Mahfouf, J. F., Brasnett, B., & Gagnon, S. (2007). A Canadian precipitation analysis (CaPA) project: Description and preliminary results. Atmosphere-ocean, 45(1), 1-17.

McElreath, R. (2018). Statistical rethinking: A Bayesian course with examples in R and Stan. Chapman and Hall/CRC.

Mekis, É., & Vincent, L. A. J. A.-O. (2011). An overview of the second generation adjusted daily precipitation dataset for trend analysis in Canada. 49(2), 163-177.

Mesinger, F., DiMego, G., Kalnay, E., Mitchell, K., Shafran, P.C., Ebisuzaki, W., Jović, D., Woollen, J., Rogers, E., Berbery, E.H. and Ek, M.B., 2006. North American regional reanalysis. Bulletin of the American Meteorological Society, 87(3), pp.343-360.

Meyer, Judith, et al. "Effects of univariate and multivariate bias correction on hydrological impact projections in alpine catchments." Hydrology and Earth System Sciences 23.3 (2019): 1339-1354.

Neal, Radford M. "MCMC using Hamiltonian dynamics." Handbook of markov chain monte carlo 2, no. 11 (2011): 2.

Qian, B., Wang, H., He, Y., Liu, J., & De Jong, R. (2016). Projecting spring wheat yield changes on the Canadian Prairies: effects of resolutions of a regional climate model and statistical processing. International Journal of Climatology, 36(10), 3492-3506.

Scinocca, J. F., et al. "Coordinated global and regional climate modeling." Journal of Climate 29.1 (2016): 17-35.

Stan Development Team. 2018. RStan: the R interface to Stan. R package version 2.17.3. http://mc-stan.org

Statistics Canada, Environment Accounts and Statistics Division, Spatial Environmental Information System and Censuses of Population, 1981, 2001 and 2006.

Tebaldi, C., & Sansó, B. (2009). Joint projections of temperature and precipitation change from multiple climate models: a hierarchical Bayesian approach. Journal of the Royal Statistical Society: Series A (Statistics in Society), 172(1), 83-106.

Vincent, L. A., & Mekis, E. (2006). Changes in daily and extreme temperature and precipitation indices for Canada over the twentieth century. Atmosphere-Ocean, 44(2), 177-193.

Vincent, L. A., Wang, X. L., Milewska, E. J., Wan, H., Yang, F., & Swail, V. J. J. o. G. R. A. (2012). A second generation of homogenized Canadian monthly surface air temperature for climate trend analysis. 117(D18).

Whan, K., & Zwiers, F. (2016). Evaluation of extreme rainfall and temperature over North America in CanRCM4 and CRCM5. Climate Dynamics, 46(11-12), 3821-3843.

Wang, C., Zhang, L., Lee, S. K., Wu, L., & Mechoso, C. R. (2014). A global perspective on CMIP5 climate model biases. Nature Climate Change, 4(3), 201.

Werner, A. T., Schnorbus, M. A., Shrestha, R. R., Cannon, A. J., Zwiers, F. W., Dayon, G., & Anslow, F. (2019). A long-term, temporally consistent, gridded daily meteorological dataset for northwestern North America. Scientific data, 6, 180299.

Wong, J. S., Razavi, S., Bonsal, B. R., Wheater, H. S., & Asong, Z. E. (2017). Inter-comparison of daily precipitation products for large-scale hydro-climatic applications over Canada. Hydrology and Earth System Sciences, 21(4), 2163-2185.

Zhang, X., Vincent, L. A., Hogg, W. D., & Niitsoo, A. (2000). Temperature and precipitation trends in Canada during the 20th century. Atmosphere-ocean, 38(3), 395-429.

Zhang, Xuebin, Lisa Alexander, Gabriele C. Hegerl, Philip Jones, Albert Klein Tank, Thomas C. Peterson, Blair Trewin, and Francis W. Zwiers. "Indices for monitoring changes in extremes based on daily temperature and precipitation data." Wiley Interdisciplinary Reviews: Climate Change 2, no. 6 (2011): 851-870.

Zhang, B., Shrestha, N., Daggupati, P., Rudra, R., Shukla, R., Kaur, B., & Hou, J. (2018). Quantifying the impacts of climate change on streamflow dynamics of two major rivers of the Northern Lake Erie Basin in Canada. Sustainability, 10(8), 2897.

Zscheischler, Jakob, Erich M. Fischer, and Stefan Lange. "The effect of univariate bias adjustment on multivariate hazard estimates." Earth System Dynamics 10.1 (2019): 31-43.

Chapter 6.

Non-Stationary Return Periods of Compound Extreme Events over Canada: A Large-Ensemble Pooling Approach

6.1 Introduction

Analysing risks associated with compound events has become a priority in climate change research. A leading example of this shift in focus from univariate to multivariate aspect of climate can be seen in reports by Intergovernmental Panel on Climate Change (IPCC). In the IPCC Fifth Assessment Report (AR5) released in 2014, mentions of compound extremes can be found whereas they are missing from the previous IPCC Fourth Assessment Report released in 2007. A simple trend of articles published with the keyword "compound extremes" over the last two decades also reveals the same (Figure 1). The reason behind this surge in interest can be attributed to many factors including better understanding of climate processes, increase in models with multivariate capabilities and an increase in computational abilities to run such models. This has lead to insights into extreme events from a new perspective in which the impact of a particular event is not just attributed to one climate variable (temperature, precipitation, humidity, soil moisture, fluvial flooding, storm surges etc.) but to different combinations of variables involved.

Temperature and precipitation are primary variables involved in any climate change impact assessment. Comprehensive research has been done involving the two variables in a

univariate setting, which include analysing long-term trends (Hansen et al. 2007; New et al. 2001) or specifically looking at extremes of the respective variables (Sillmann et al. 2013a; Sillmann et al. 2013b). However, our knowledge of the joint variability of temperature and precipitation is not comprehensive as is evident in the statement *"Understanding compound impacts from concomitant temperature and precipitation stress",* listed as a knowledge gap in the IPCC AR5 Regional Aspects (Africa) report (Niang et al. 2014). The motivation of studying these two variables jointly is rooted in our knowledge of large-scale atmospheric processes that are driven by underlying physical principles. Correlation between temperature and precipitation has been studied extensively at global as well as regional scales (Adler et al. 2008; Trenberth and Shea, 2005; Zhao and Khalil, 1993). Clausius-Clapeyron relation has been used to study scaling rates of extreme precipitation with respect to temperature following the principle that atmospheric moisture would increase at a rate of approximately $7\%K^{-1}$ (Allen and Ingram, 2002). Further, several studies have provided evidence regarding interactions between temperature and precipitation that have lead to extreme events. AghaKouchak et al. (2014) analysed the climatic conditions leading to the 2014 California drought and reported that the particular event would be underestimated under a univariate analysis considering only precipitation as extreme temperature played a significant role as well. Zscheischler and Seneviratne (2017) reported that in some cases, a hot and dry event with a return period of 100-years under univariate settings is reduced to just 16 years if negative correlation between temperature and precipitation is considered.

Such evidence gathered from historical occurrences of compound extremes leads to the question of how temperature and precipitation covariability will affect future extreme

events. Projections of future climate are generated from General Circulation Models (GCMs) which are mathematical models representing major climate systems and their interactions. GCMs have coarse resolution (~100-500km) and therefore cannot provide reliable estimates of climate data at regional scales. To fill this gap, regional climate models are created to downscale GCMs to finer resolutions over different regions. Both GCMs and RCMs are commonly further downscaled and/or bias corrected using statistical techniques using statistical methods (Najafi et al. 2010). Until recently, downscaling and bias correction of GCMs has been done using univariate bias correction methods, which only preserve traits of each variable separately but not the dependence between them making the analysis of compound events using such data unreliable (Rocheta et al. 2014). In response, multivariate bias correction algorithms have been developed which aim towards correcting univariate biases as well as preserving dependence (Bürger et al. 2011; Cannon, 2016; Piani and Haerter, 2012; Vrac and Friederichs, 2015). Cannon (2018) proposed a multivariate bias correction algorithm (MBCn) which conserves all aspects of the multivariate distribution between variables while correcting for univariate biases as well.

Using the MBCn algorithm, the Canadian Regional Climate Model (CanRCM4) large ensemble (50-member) has been bias corrected to produce a new dataset called Canadian Large Ensembles Adjusted Dataset (CanLEAD). The dependence structure of temperature and precipitation in CanRCM4 and CanLEAD with respect to a gridded observation product, NRCANmet, is evaluated over Canada. The full bivariate distribution in each dataset is explored using copulas (Sklar, 1959) following which, joint return periods of extreme events are calculated under a non-stationary framework using an approach that pools information from the entire ensemble. The primary aim of the study is to evaluate

changes in precipitation under future warming scenarios. We analyze the return periods of two compound extreme events, warm-wet events when the two variables exhibit a positive correlation and warm-dry events in the presence of negative correlations. Return periods of these joint events are calculated under a non-stationary framework that pools information from the entire ensemble. Return periods are first calculated under the assumption of independence between temperature and precipitation, followed by calculation considering correlation which allows for quantification of how increasing temperature might affect precipitation patterns in the future over Canada.

6.2 Data and Methods

6.2.1 Data

The Canadian Regional Climate Model (CanRCM4) 50-member large ensemble and its corresponding bias corrected version Canadian Large Ensembles Adjusted Dataset (CanLEAD) are used in this study. The details of these data and the bias correction method can be found in section 5.2 along with details of the observation data used for validation.

Daily maximum temperature (Tasmax), daily minimum temperature (Tasmin) and daily precipitation are used in this study from all 50 members of each ensemble (50 x 3 = 150 sets of data). CanRCM4 is regridded to the rectangular grid of CanLEAD using bilinear interpolation and all units across the models are converted to °C for temperature and mm/day for precipitation.

NRCANmet is used as the observation dataset against which the bivariate structure of temperature and precipitation is evaluated over the historical period of 1951-2000. NRCANmet was created from station data of National Climate Data Archive (NCDA),

Environment and Climate Change Canada using Australian National University Splines (ANUSPLIN) interpolation method with latitude, longitude and elevation as predictors. The data are available at a resolution of ~0.083° over Canada at daily time-step from 1950-2013. NRCANmet has been widely used in studies over Canada for hydrological modeling as well as downscaling of global and regional climate models. Inter-comparison studies involving station data and other gridded products have revealed NRCANmet having predominantly dry and cold biases in central and western Canada, but it performs better compared to other gridded products. (Bonsal et al. 2013; Eum et al. 2012; Eum et al. 2014; Mahfouf et al. 2007; Shrestha et al. 2012; Werner et al. 2019; Wong et al. 2017). Considering all factors such as time-span, spatial extent and biases, NRCANmet was chosen as the observation dataset for this study. NRCANmet (Tasmax, Tasmin and Pr) is also interpolated to a rectangular 0.5° x 0.5° grid. Finally, 8124 grid points over Canada are extracted from all the models.

6.2.2 Validation of Dependence Structure

Consider two pairs of data, each consisting of two dependent variables (x, y) and (x', y'). Following an effective univariate bias correction of (x', y') with respect to (x, y) respectively, one would ideally observe a reduction in the biases of the corresponding pairs of marginals (x, x') and (y, y'). Further, assume that a model is forced using this data such that model output is a function of the marginals, $O = f(x, y)$ and $O' = f(x', y')$. Indeed, one would observe some bias between O and O', however it cannot be assessed how much of that bias can be attributed to biases in the marginals and how much to bias in the dependence within the pairs of data. Hydrological models can be used for such evaluations because the model output is not only dependent on temperature and precipitation

individually, but also on how temperature and precipitation behave together. This was reported by Meyer et al. (2019) in which a hydrological model was forced using data corrected with QDM and MBCn approaches, respectively. They observed a difference in simulated snow volume as the MBCn forced model predicted more precipitation at sub-zero temperatures and thus affected snowmelt runoff even though the marginals of the input data were exactly similar in both cases.

In case of climate model outputs (from both GCMs and RCMs), focus has always been on univariate validation. However, as stated earlier, a univariate approach does not reveal all sources of bias in the data. As such, analysing the magnitude of biases in marginals and the dependence structure separately would encapsulate a complete characterization of the differences between datasets. Copulas are an ideal tool for this case. Fro details on copulas, refer to sections 3.3.1 and Appendix-A1.

Validation of the dependence structure between temperature (mean of tasmax and tasmin) and precipitation is performed for 1951-2000. Other methods, such as comparing linear correlation (Pearson) and rank correlation (Spearman or Kendall) could be used as well, however, they cannot capture all underlying multivariate aspects such as dependence in tails. Moreover, since the MBCn algorithm aims at bias correcting all aspects of the multivariate distribution rather than just correlations (Cannon, 2016), copulas provide a robust tool for verification. This section describes the copula fitting and verification process across the datasets. The following operations are iterated at each grid point:

1. The observed and simulated data (each 50-member ensemble) are aggregated to seasonal scale from 1951-2000 and the trend is removed. Therefore, every model

ensemble has 50 data points for average temperature and accumulated precipitation of winter (DJF), spring (MAM), summer (JJA) and fall (SON), respectively.

2. A suitable copula is selected for the observation time series (NRCANmet) from the Archimedean family using Maximum Pseudo Likelihood (MPL; Genest et al. 1995). See Appendix-A4 for further details on MPL. This copula is considered the 'ground truth' for the dependence between temperature and precipitation at each location. It should be noted however, that NRCANmet itself is an interpolated product, which does not guarantee a true reflection of the dependence.
3. Once a suitable copula is selected using the observation data, the fit of the copula is tested on the simulated datasets using a formal goodness of fit (GOF) test proposed by Genest et al. (2006). The goodness of fit test is based on calculating two variants of the Cramér–von Mises statistic (Genest and Favre, 2007) and calculating the p-values using a bootstrapping procedure. See Appendix-A5 for further details on the GOF test. This process is repeated for every member of the large ensemble for each model.

The crucial takeaway from the results of this validation will be identifying the areas where the observation dataset shows dependence in tails, such as high correlations for warm-wet or warm-dry conditions but the models fail to capture this behavior, which could lead to implications for projecting climate change impacts in the future. See Appendix-A3 for more details on identification of tail dependency using copulas.

6.2.3 Non-stationary Return Periods

The approach followed for calculating return periods is similar to the one used by Zscheischler and Seneviratne (2017). However, here the approach is extended to a method

that pools information from the entire 50-member ensemble of each model and accounts for non-stationarity in the dependence structure.

Pooling Approach

The following steps are performed for each ensemble, at every grid point, prior to the calculation of return periods:

1. Each ensemble run is aggregated from 1951-2100 to seasonal average temperature and accumulated precipitation resulting in a series of 150 data points in each season.
2. Each individual run is then divided into blocks of three years and all data within one block are pooled across the ensemble (Figure 44).
3. This results in 50 time-series (150 years split into 3-year blocks) of 150 data points each (3 data points from each ensemble run).

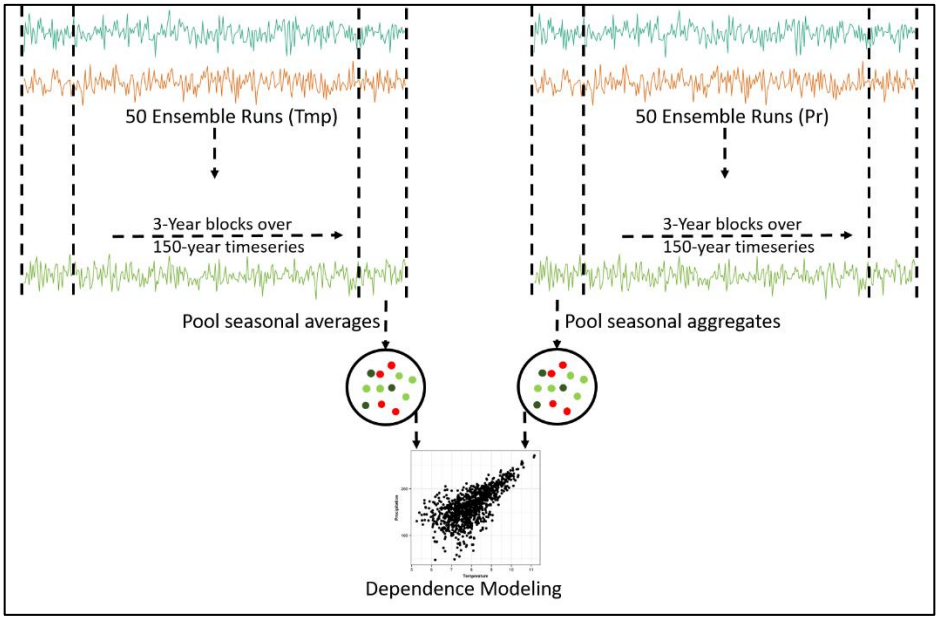

Figure 44 – Pooling approach for calculating return periods of compound events from the ensemble. Tasmax and Tasmin are first averaged to obtain daily mean temperature for each

individual run of the ensemble. Then, temperature (Tmp) is seasonally averaged and precipitation (Pr) is seasonally aggregated from 1951-2000 to obtain a time-series of 150 data points. The ensemble is divided into blocks of 3 years each and each variable is pooled across the ensemble thus obtaining a pooled sample of 150 points representing the climatology of each block. Then, copulas are used to characterize the dependence structure.

This approach provides several advantages. Firstly, the whole ensemble can be easily incorporated into the analysis ensuring no loss of information from the model. Secondly, pooling the estimates across 3-year blocks provides series of 150 samples which allows a robust estimation of the bivariate structure. Also, non-stationarity in the ensemble can be easily detected using this method as changes in the marginals as well as the dependence can be quantified with respect to time. Finally, pooling data from relatively small 3-year blocks across the ensemble ensures that no trend exists within each block, which makes it possible to fit a stationary distribution to data.

Return Period Calculation

As mentioned earlier, two scenarios are analysed in this study, warm-wet events and warm-dry events. Here, events are analyzed at seasonal scales, such as a warm season occurring simultaneously with a wet season. The warm-wet scenario corresponds to a positive correlation exhibited by temperature and precipitation and an extreme compound event is defined as a season in which the average temperature and accumulated precipitation exceed their 90^{th} quantiles, respectively. Similarly, warm-dry scenario corresponds to a negative correlation between the two variables and an extreme compound event is defined as a season in which average temperature (T) exceeds its 90^{th} quantile and accumulated precipitation (P) falls below its 10^{th} quantile (or –P exceeds its 90^{th} quantile). The joint

return period can be defined in two ways. First, when either of the two variables exceed their respective quantiles (OR scenario) and second, when both the variables simultaneously exceed their respective quantiles (AND scenario) (Salvadori, 2004). Here, only the AND case is of interest and discussed further.

Continuing the nomenclature used in equation (1), given two continuous random variables *x* and *y* with marginal distribution functions F_X and F_Y, joint distribution function F_{XY}, and copula $\boldsymbol{C}$, the AND joint return period can be written as:

$$R = \frac{\mu}{P(X \geq x, Y \geq y)} = \frac{\mu}{1 - F_X(x) - F_Y(y) + \boldsymbol{C}(F_X(x), F_Y(y))} \qquad (14),$$

Simplifying the equation, μ can be replaced with 1 which is the average inter-arrival time between events and $F_X(x)$ and $F_Y(y)$ can be replaced with u and v respectively.

$$R = \frac{1}{1 - u - v + \boldsymbol{C}(u, v)} \qquad (15),$$

Under the independence assumption, the copula is simply reduced to the multiplication of the respective marginal quantities.

$$R' = \frac{1}{1 - u - v + (u * v)} \qquad (16),$$

Since the 90th percentile thresholds are considered for both T and P, it corresponds to $u = v = 0.9$ which leads to the return period for the independent case, $R' = 100$ years. Since the quantiles in each block are always kept constant, i.e. 0.9, the return periods from block-to-block become independent of the magnitude of the respective marginals. In this way, any change in the return period from block 1 to a future block *N*, can be attributed solely to the change in the dependence structure between temperature and precipitation, rather

than the change in their magnitude. Return periods are also calculated for de-trended NRCANmet data at each grid for a stationary period of 1951-2000 to approximately compare model projections against observation derived return periods.

Since each individual run of the ensemble cannot be expected to exhibit the same dependence structure between the two variables, this uncertainty is captured through a Bayesian framework. According to Bayes' theorem

$$P(\theta|D) \propto P(D|\theta).P(\theta) \qquad (17),$$

Here, the left term of the equation is the posterior density which signifies the probability of the parameter vector θ, given the data. The term $P(D|\theta)$ is the likelihood of the model which signifies the probability of the data D conditioned on the parameter vector and $P(\theta)$ is the prior belief of the model parameters. In this case, the vector θ consists of five parameters, the mean and standard deviation of each marginal and the copula parameter (derived from Kendall's correlation coefficient). Since the return period calculation is independent of the marginal magnitude, the primary entity of interest here is the uncertainty in the copula parameter. Once the posterior estimates are obtained using an MCMC simulation implemented using Stan framework (Stan Development Team, 2018), the lower (2.5^{th} quantile), the median, and the upper (97.5^{th} quantile) of the copula parameter are obtained and the corresponding return levels are calculated for each case. This provides an uncertainty range for the return period of the event in question. See Appendix-A6 for further details on the Bayesian framework.

The results of return periods are presented at a coarser scale for easier interpretation and representation, by taking regional averages of return periods over terrestrial ecozones of Canada defined by Wiken (1986) (Figure 45).

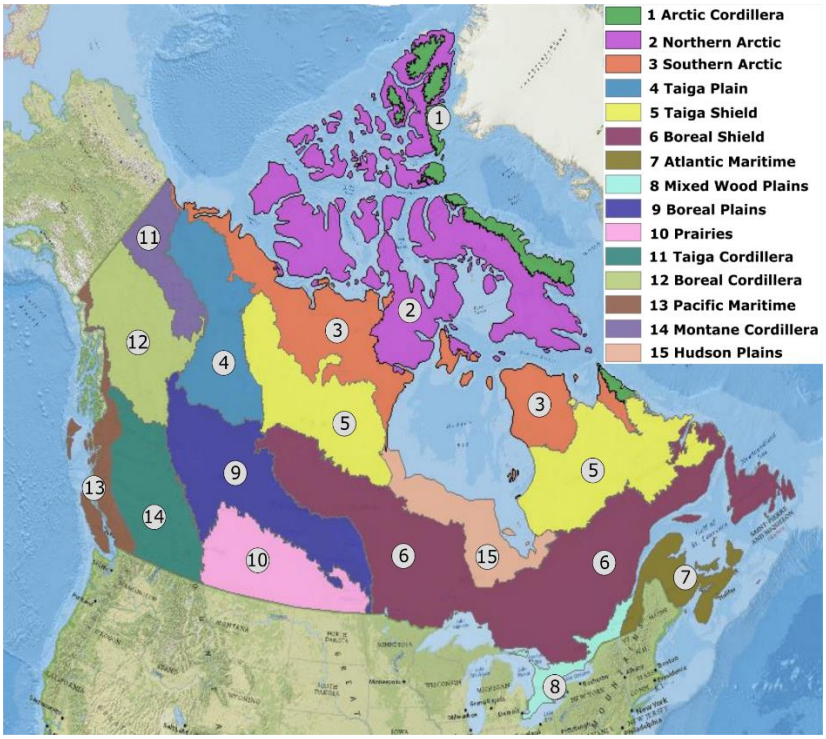

Figure 45 – Terrestrial ecozones of Canada used to present spatially averaged results of joint return periods.

6.3 Results

It should be noted that 'warm-wet' or 'warm-dry' events are in reference to the climatology of each specific region. Since the study area comprises all Canadian ecozones, the climate of different regions varies greatly from the north to the south and from the west to the east coast. As an example, if a copula model finds tail dependence between 'warm-wet' events in northern Canada in winter; it can be interpreted that whenever a *relatively warm* event happens in that region during winter, there is a high probability that it will be accompanied

by a *relatively wet* event as well. In the case of temperature and precipitation, inferences about future conditions can be drawn and are especially useful because the confidence in future temperature projections is much higher than in precipitation projections (Bush and Lemmen, 2019). Thus, an inevitable increase in the occurrence of warm events in the future will consequently lead to an increase in the occurrence of wet events in case of 'warm-wet' dependency and in the occurrence of dry events in the case of 'warm-dry' dependency.

6.3.1 Results of Dependence Structure Validation

The characterization of dependence structure in historical observation data (1951-2000, NRCANmet) is done using copulas, identifying the best model using Maximum Pseudo Likelihood (MPL) and verifying the fit of the model using GOF test.

Canadian Prairies exhibit warm-dry dependencies throughout the four seasons indicating that negative correlation between temperature and precipitation in this region is largely independent of seasonal shifts with only minor changes in the strength of dependence season to season (Figure 46). While this dependence is mostly limited to the Prairie region in spring, it extends over the Rocky Mountains during winter which goes back to one of the first studies conducted over Canada by Isaac and Stuart (1992) who reported that while the rest of the Canadian landmass had positive correlations between the two variables, the Rockies and the plains to its east (Prairies) received majority of its precipitation at lower temperatures indicating drier and warmer periods. Another clear pattern is the dominance of warm-wet dependence in northern Canada which remains persistent in all seasons except in summer. These historical patterns reveal that as warm events in winter increase, as confirmed by several other studies (Graham et al. 2017; Vincent et al. 2007), they tend to be associated with increased precipitation. Correlation generally breaks down in spring and

fall in southeastern and middle regions of Canada as statistically significant results (at 5% significance level) are not found at majority of locations. Other places of interest, such as high population centers in southeastern and southwestern Canada show sensitivity to seasonal changes. Southeastern Canada shows warm-wet dependence in winter which switches to warm-dry in summer and fall, while in spring, dependence is mostly insignificant. This indicates a potential of Rain-on-Snow events which usually happen when rainfall occurs during unusually warm days in winter, over frozen ground and thus immediately turning into runoff, which increases flood risks. Indeed, this has been observed in southeastern Canadian cities such as Quebec, Ottawa and Toronto in late winter and early spring (Buttle et al. 2016).

In all seasons, the ability of the models to capture the dependence with respect to observations can be deemed satisfactory. The patterns are also consistent across seasons with the CanLEAD products performing relatively better than CanRCM4, while CanLEAD2 is marginally better than CanLEAD1 in most cases. This means that future projections of the joint behavior of the two variables should be reliable, according to these models. However, as mentioned earlier, NRCANmet is itself an interpolated gridded observation and its own biases with respect to the *ground truth*, such as Adjusted and Homogenized Canadian Climate Data (AHCCD; Mekis and Vincent, 2011; Vincent et al. 2012) would add to the uncertainty of the results.

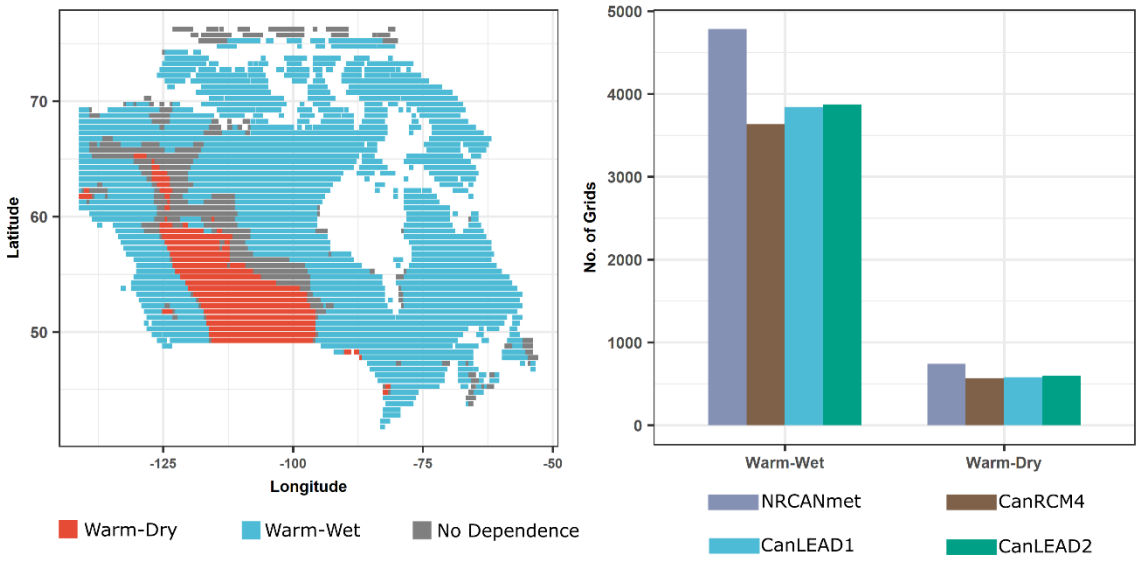
Latitude
70
60
50
-125
-100
-75
-50
Longitude
Warm-Dry
Warm-Wet
No Dependence
No. of Grids
5000
4000
3000
2000
1000
0
Warm-Wet
Warm-Dry
NRCANmet
CanRCM4
CanLEAD1
CanLEAD2

(a)

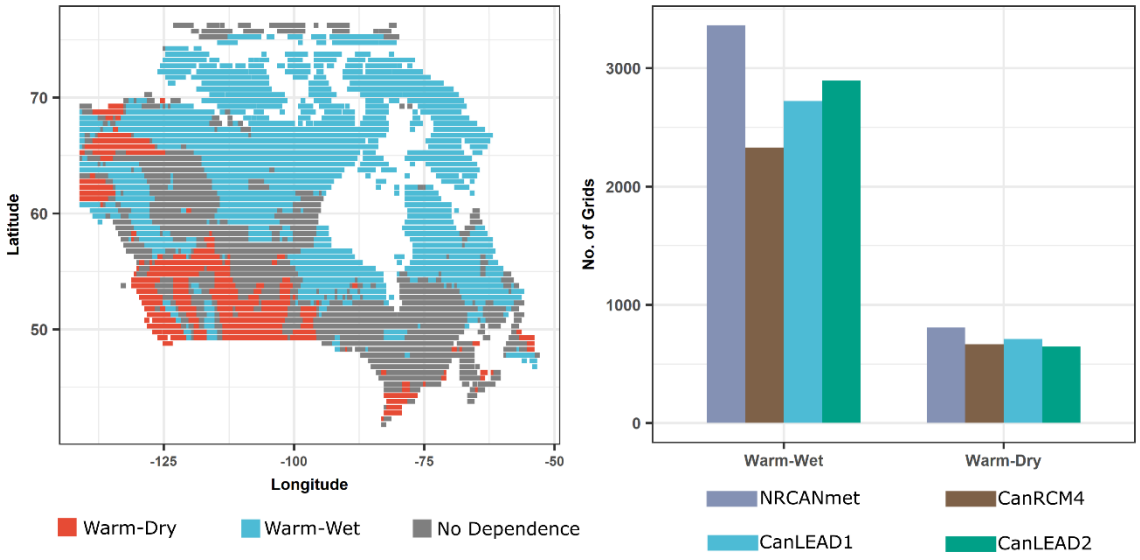
Latitude
70
60
50
-125
-100
-75
-50
Longitude
Warm-Dry
Warm-Wet
No Dependence
No. of Grids
3000
2000
1000
0
Warm-Wet
Warm-Dry
NRCANmet
CanRCM4
CanLEAD1
CanLEAD2

(b)

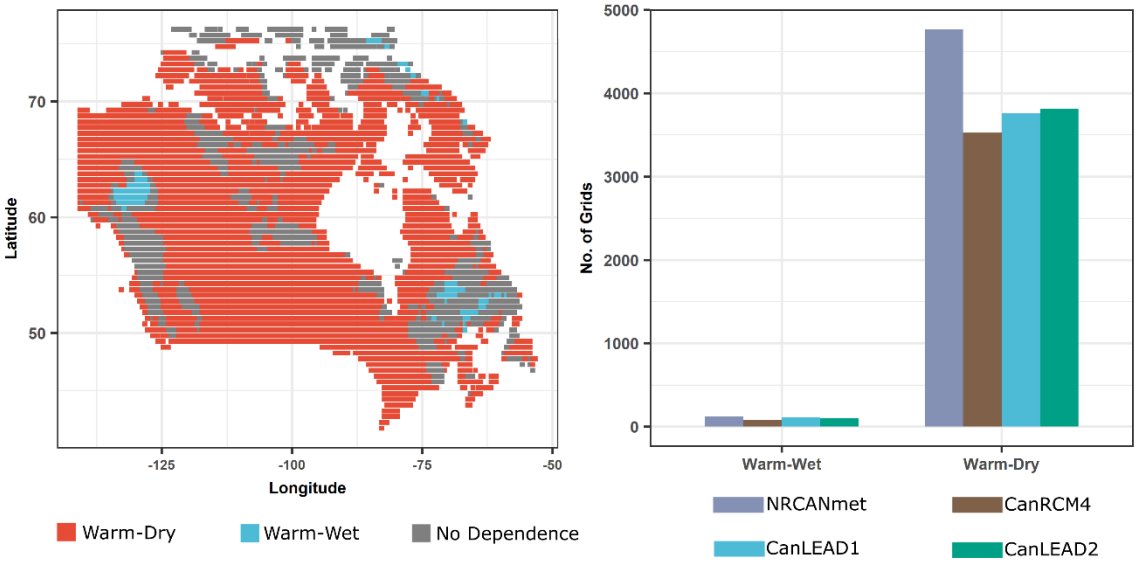

(c)

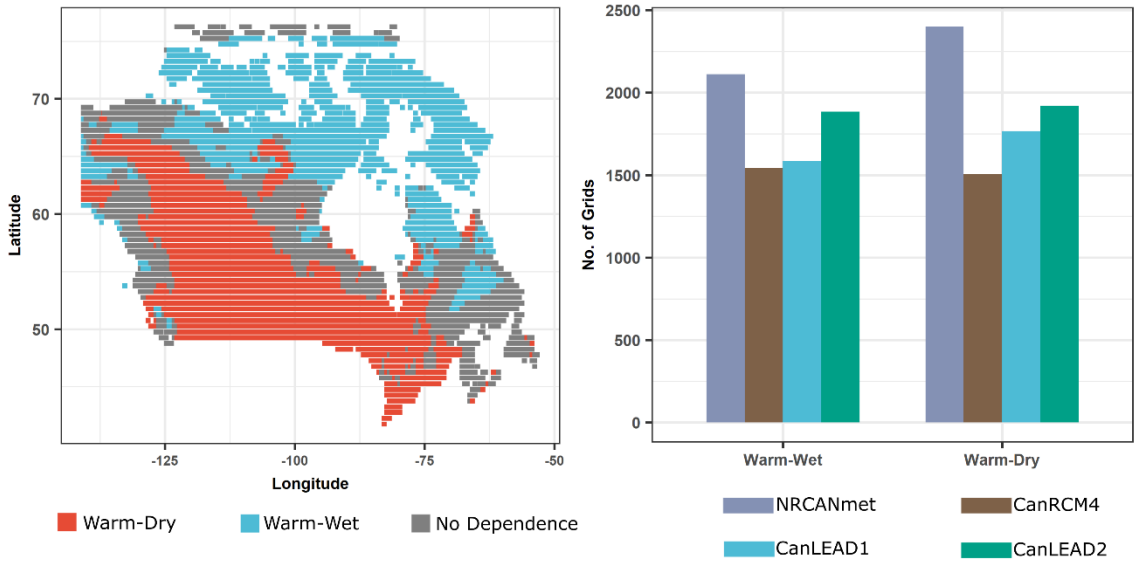

(d)

Figure 46 – Results of validation of dependence structure for (a) winter (b) spring (c) summer and (d) fall. The spatial plot shows the dependence structure exhibited by NRCANmet at each grid. The warm-wet and warm-dry scenarios are based on the type of copula selected for each grid using MPL. The grids with grey color signify no significant correlation at 5% significance

level. The bar plot shows the comparison between the number of grids where each model (result averaged over ensemble) captures the joint behavior based on the GOF test.

6.3.2 Results of Non-stationary Return Periods

A pattern that stands out from the Bayesian model is the systemic reduction in uncertainty of dependence structure in the CanLEAD products (Figure 47). The posteriors of the copula parameters for both CanLEAD products were less spread out in every case, indicating that each member of the large ensemble is more agreeable in identifying the dependence structure. Relatively wider posterior estimates of the copula parameter from CanRCM4 show that disagreements exist between the correlation structures exhibited by one member of the ensemble to the other. This can be traced back to the multivariate bias correction method which generated CanLEAD since each run was corrected with respect to a reference dataset while CanRCM4 ensemble is the result of varying initial conditions of physical parametrizations.

In winter, regions in northern Canada (zone 1, 2 and 3) show a significant effect of dependency between temperature and precipitation for calculating return periods of joint exceedance of their respective 90th quantiles (Figure 47a). On an average, all three models show that a 100-year event under the assumption of independence has in fact a return period of 50-60 years when dependence is considered. The return period calculated from observation data for a stationary period of 1951-2000 agrees with all models, however CanLEAD2 is better able to mimic the observations. Going into the future, these zones show sharp positive trends for all models indicating that the return periods are increasing. This signifies that the concordance between high temperature and high precipitation events

is projected to decrease in the future as by the end of 21st century, a ~ 60-year event becomes a ~75-year event. The Prairie region exhibits a behavior of similar pattern but for warm-dry events (Figure 47b). For historical periods, the dependency is quite strong in all models as well as the observation and a 100-year event under independence becomes a 65-year event in the joint modelling framework. However, a significant positive trend in the return periods is noted and the event becomes rare into the future indicating a reduction in the concordance of warm-dry events for this region in winters. Dependency between the variables is generally low in south-eastern Canada in winter and no significant trends are observed in the non-stationary return periods.

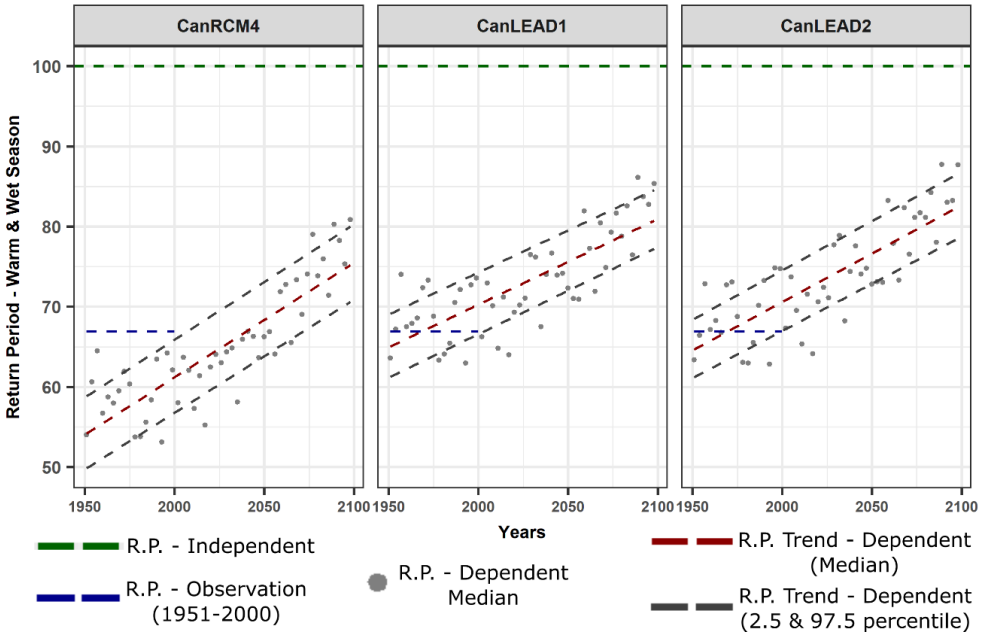

(a)

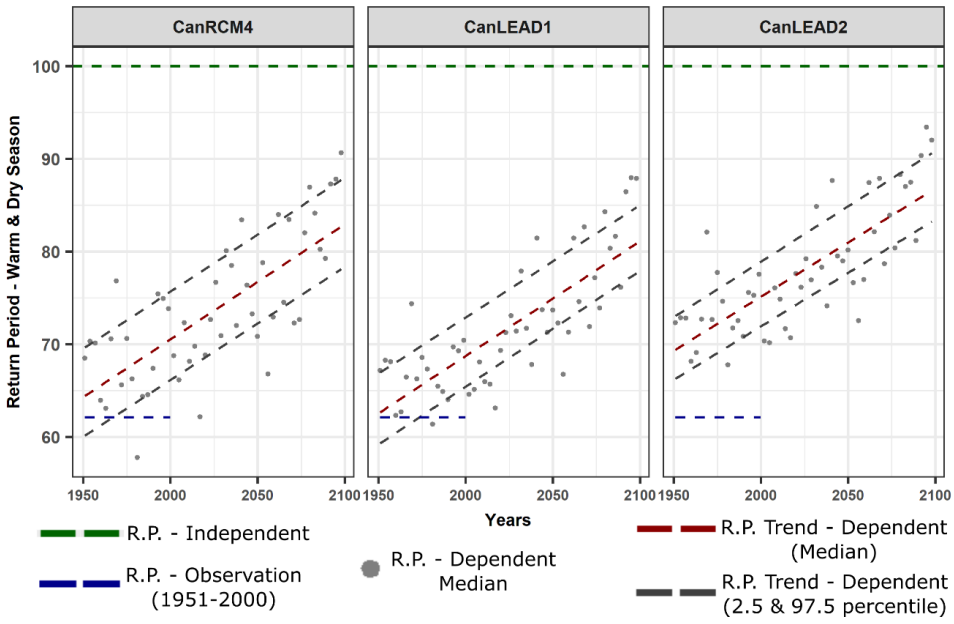

(b)

Figure 47 - The return periods calculated under different scenarios for a temperature-precipitation compound event in winter season for (a) southern Arctic and (b) Prairies. The horizontal green line at the top shows the reference 100-year return level for the joint probability of exceeding the 90th quantiles of temperature and precipitation respectively, under the assumption of independence. The horizontal blue line represents the return period of the same event calculated using NRCANmet over the de-trended stationary period of 1951-2000. The grey points represent the return periods calculated from the models using the non-stationary pooling approach. The slanted lines represent the trend of the non-stationarity in return period (trend lines fitted to the points). The red line represents the median return period and the grey lines represent the 2.5th and 97.5th quantiles of the return period. The calculation of this uncertainty range is based on the posterior samples of the copula parameter obtained from the Bayesian model.

Dependency in spring and fall is low across all zones according to the model projections, however a comparison with the observation derived return periods reveal that the models under-estimate the strength of dependence. Significant differences between the model

derived and observation derived return periods are found for the 1951-2000 period in several zones. For example, CanLEAD2 shows that for 1951-2000, a warm-dry event has an average return period of about 85 years whereas according to NRCANmet, the same event has a return period of less than 70 years (Figure 48). Comparing this to the result of validation in the historical period, it can be concluded that even though the models were able to capture the correlation being generally positive or negative, they did not reproduce the strength of the correlation (primarily the tails) with respect to the observation data in this case. Summarizing the rest of the spring season results, a 100-year event under independence assumption reduces to approximately 80-year event in most zones. However, significant negative trends are found for warm-dry events in south-eastern Canada and Prairie regions indicating a potential increase in the frequency of compound extremes.

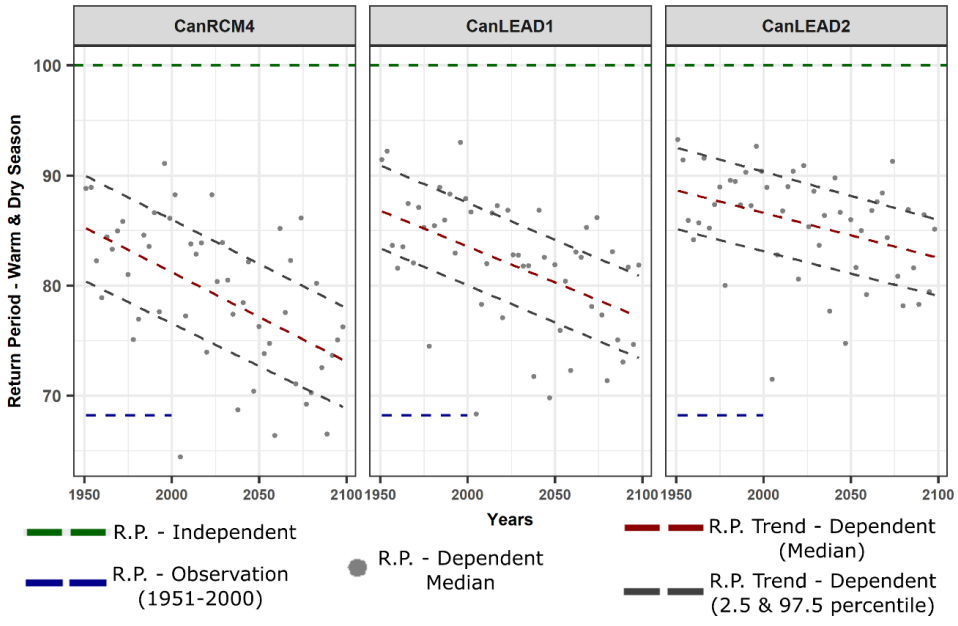

(a)

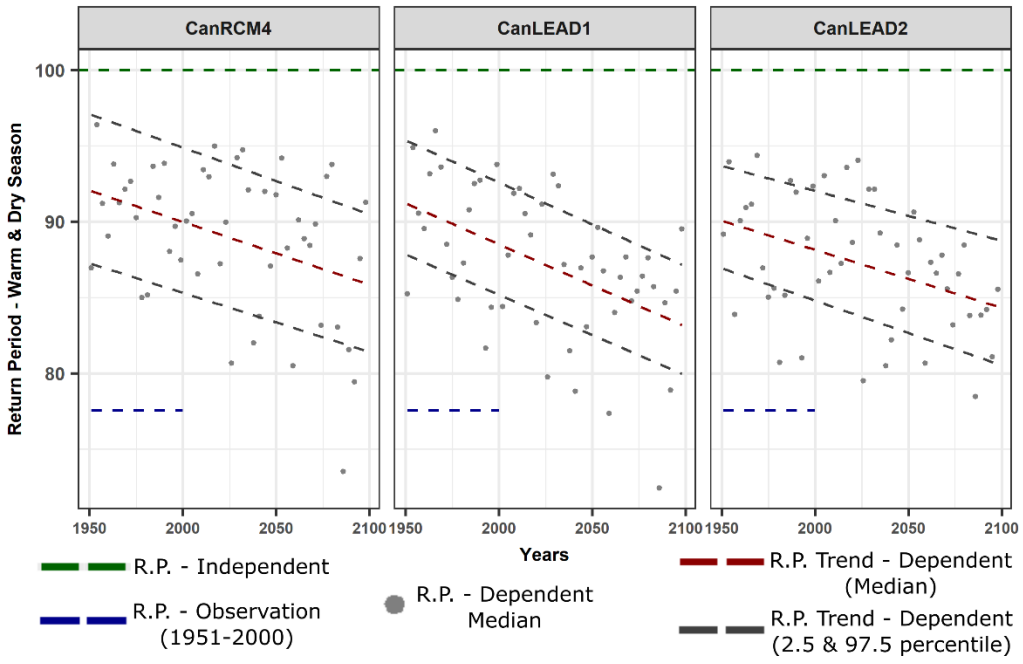

(b)

Figure 48 - The return periods calculated under different scenarios for a temperature-precipitation compound event in spring season for (a) Prairies and (b) Atlantic Maritime. See caption of Figure 47 for further details.

Results of summer season remain consistent with the previous validation results, as warm-dry conditions dominate all regions. The effect of considering dependence is strongest in the summer with significantly reduced return periods of compound events. Moreover, strong negative trends are found in majority of the regions indicating that dependence between warm-dry events is projected to increase in the future and the events will become even more frequent. Figure 49 is a good example of regional differences between results. In zone 8 (Mixedwood Plains), the return periods calculated with the model data and observation data are a good match whereas the strength of dependence is being overestimated by all models in zone 9 (Boreal plains).

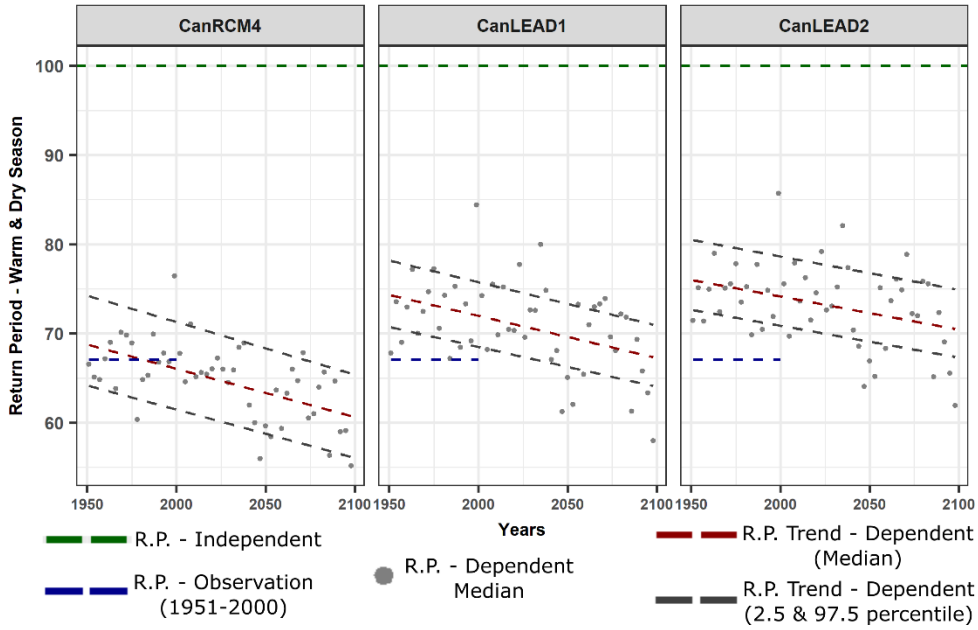
CanRCM4
CanLEAD1
CanLEAD2
Return Period - Warm & Dry Season
100
90
80
70
60
1950
2000
2050
2100
Years
R.P. - Independent
R.P. - Observation (1951-2000)
R.P. - Dependent Median
R.P. Trend - Dependent (Median)
R.P. Trend - Dependent (2.5 & 97.5 percentile)

(a)

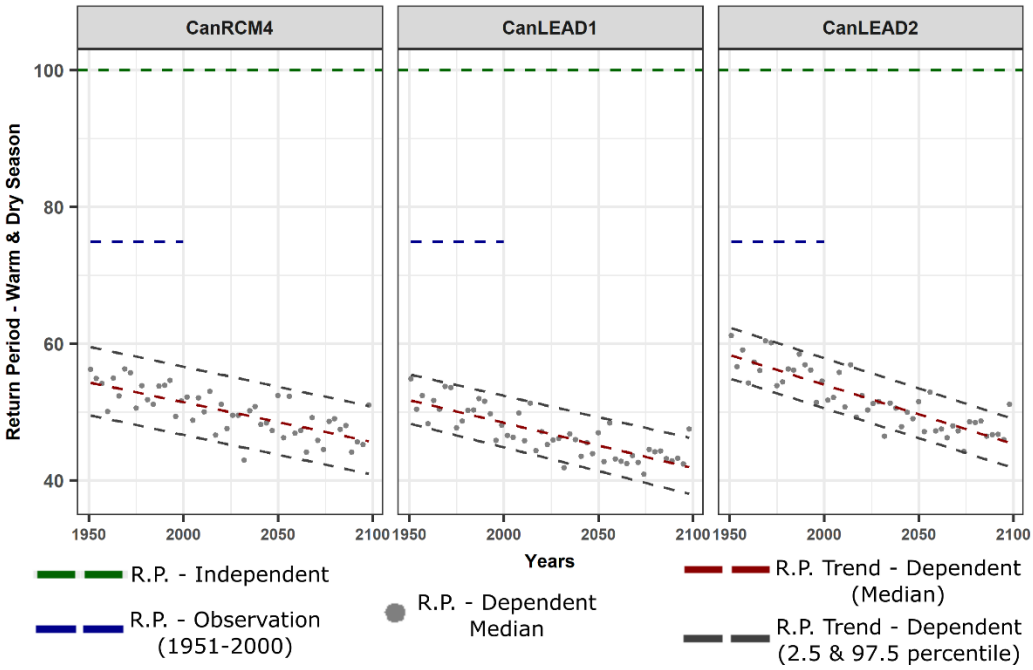
CanRCM4
CanLEAD1
CanLEAD2
Return Period - Warm & Dry Season
100
80
60
40
1950
2000
2050
2100
Years
R.P. - Independent
R.P. - Observation (1951-2000)
R.P. - Dependent Median
R.P. Trend - Dependent (Median)
R.P. Trend - Dependent (2.5 & 97.5 percentile)

(b)

Figure 49 - The return periods calculated under different scenarios for a temperature-precipitation compound event in spring season for (a) Mixedwood Plains and (b) Boreal Plains. See caption of Figure 47 for further details.

All results are independent of the magnitude of the individual variables. It implies that, while we already have strong confidence in a significant warming trend in the future over Canada (while trends in precipitation vary by region), these results further raise concern as the change in dependence alone is adding an additional component of potential future changes to the climatology of these regions.

Take for example, the Canadian Prairies where warming and drying trends are apparent in previous studies but only when treated individually (Zhang et al. 2000). If the dependence is taken into consideration, warm-dry extreme events become even more prominent because of the strength of negative correlations in the region and significant reduction in future return periods.

More results for this section can be found under Appendices - Figures.

6.4 Conclusions

The likelihood of compound extreme events caused by the joint occurrence of extreme temperature and extreme precipitation is analysed using three large ensembles of regional climate model simulations (50-members) over Canada. Seasonal dependencies between average temperature and accumulated precipitation were analysed from The Canadian Regional Climate Model (CanRCM4) and two of its multivariate bias corrected counterparts, Canadian Large Ensembles Adjusted Dataset (CanLEAD). The ability of the models to capture tail dependence between ‘warm-wet’ and ‘warm-dry’ events is evaluated

against gridded observation, NRCANmet from 1951-2000 using copulas. Joint return periods of extreme compound events are calculated using a pooling approach across each ensemble. The return periods calculated by considering the dependence between temperature and precipitation are compared to return periods under the assumption of independence to reveal the importance of considering relationships between climate variables in the context of compound extremes. The method isolates univariate sources that could affect future changes to concurrent events and reveals the changes to be expected solely based on change in the bivariate structure of temperature and precipitation. The uncertainty in dependence across the ensemble is captured using a Bayesian framework by estimating posterior densities of the marginal and copula parameters for every case.

Results reveal that all three ensembles can capture the dependence with respect to observation data over most regions of Canada, with CanLEAD products performing marginally better than CanRCM4. However, further results reveal that while the models do capture the general direction of correlation, they are not as accurate in reproducing the strength of dependence, which impacts inferences drawn from multivariate models, such as copulas. Warm-wet dependencies dominate almost all over Canada during winter except over the Rockies and the Prairies. Strong correlations observed during winter and summer over almost all of Canadian land mass generally break down in spring and fall with large areas in southeastern and central Canada showing insignificant results in these two seasons.

Return periods calculated using copulas show the importance of considering dependence as the frequency of compound events significantly reduces in comparison to independence assumption. For example, a 100-year warm-dry event calculated independently is reduced to a ~60 year event when calculated using copulas. The results also reveal significant

positive and negative trends in the joint return periods into the future, which vary by season and by region. Overall, it is very likely that warm-dry events will become more frequent in summers in the future while regions that already show warm-wet dependence generally show a negative trend, indicating breakdown of dependence between the two events. Posterior estimates of the copula parameters also reveal that CanLEAD ensembles have a better homogeneity in the dependence structure across the ensemble as compared to CanRCM4 which can be attributed to the multivariate bias correction method used to produce the ensembles.

This study highlights the projected changes in compound extremes using reliable regional climate change projections. It also highlights the advantages of the ensemble pooling approach for multivariate analysis of future projections which naturally lead to several advantages. These results can be used to further enhance the mitigation efforts to prepare for an inevitably warming climate and how its joint variability with precipitation will affect different regions over Canada.

6.5 References

Adler, R. F., Gu, G., Wang, J. J., Huffman, G. J., Curtis, S., & Bolvin, D. (2008). Relationships between global precipitation and surface temperature on interannual and longer timescales (1979–2006). Journal of Geophysical Research: Atmospheres, 113(D22).

AghaKouchak, A., Cheng, L., Mazdiyasni, O., & Farahmand, A. (2014). Global warming and changes in risk of concurrent climate extremes: Insights from the 2014 California drought. Geophysical Research Letters, 41(24), 8847-8852.

Akaike, H. (1974). A new look at the statistical model identification. In Selected Papers of Hirotugu Akaike (pp. 215-222). Springer, New York, NY.

Allen M, Ingram W (2002) Constraints on future changes in climate and the hydrologic cycle. Nature 419:224–232

Bonsal, B. R., Aider, R., Gachon, P., & Lapp, S. (2013). An assessment of Canadian prairie drought: past, present, and future. Climate Dynamics, 41(2), 501-516.

Bürger, G., Schulla, J., & Werner, A. T. (2011). Estimates of future flow, including extremes, of the Columbia River headwaters. Water Resources Research, 47(10).

Bush, E., & Lemmen, D. S. (Eds.). (2019). Canada's Changing Climate Report. Government of Canada= Gouvernement du Canada.

Buttle, J.M., Allen, D.M., Caissie, D., Davison, B., Hayashi, M., Peters, D.L., Pomeroy, J.W., Simonovic, S., St-Hilaire, A. and Whitfield, P.H., 2016. Flood processes in Canada: Regional and special aspects. Canadian Water Resources Journal/Revue canadienne des ressources hydriques, 41(1-2), pp.7-30.

Cannon AJ (2016) Multivariate bias correction of climate model output: matching marginal distributions and inter-variable dependence structure. J Clim 29(19):7045–7064.

Cannon, Alex J. "Multivariate quantile mapping bias correction: an N-dimensional probability density function transform for climate model simulations of multiple variables." Climate dynamics 50.1-2 (2018): 31-49.

Bürger G, Schulla J, Werner AT (2011) Estimates of future flow, including extremes, of the Columbia River headwaters. Water Resour Res 47(10):1–18

Dee DP, Uppala SM, Simmons AJ, Berrisford P, Poli P, Kobayashi S, Andrae U, Balmaseda MA, Balsamo G, Bauer P, Bechtold P, Beljaars ACM, van de Berg L, Bidlot J, Bormann N, Delsol C, Dragani R, Fuentes M, Geer AJ, Haimberger L, Healy SB, Hersbach H, Hólm EV, Isaksen L, Kållberg P, Köhler M, Matricardi M, McNally AP, Monge-Sanz BM, Morcrette J-J, Park B-K, Peubey C, de Rosnay P, Tavolato C, Thépaut J-N, Vitart F (2011) The ERA-Interim reanalysis: configuration and performance of the data assimilation system. Q J R Meteorol Soc 137:553–597. doi: 10.1002/qj.828

Dutra, E., Balsamo, G., Calvet, J.C., Minvielle, M., Eisner, S., Fink, G., Pessenteiner, S., Orth, R., Burke, S., van Dijk, A.I. and Polcher, J., 2015. Report on the current state-of-the-art Water Resources Reanalysis.

Eum, H. I., Gachon, P., Laprise, R., & Ouarda, T. (2012). Evaluation of regional climate model simulations versus gridded observed and regional reanalysis products using a combined weighting scheme. Climate Dynamics, 38(7-8), 1433-1457.

Eum, H. I., Dibike, Y., Prowse, T., & Bonsal, B. (2014). Inter-comparison of high-resolution gridded climate data sets and their implication on hydrological model simulation over the Athabasca Watershed, Canada. Hydrological processes, 28(14), 4250-4271.

Favre, A. C., El Adlouni, S., Perreault, L., Thiémonge, N., & Bobée, B. (2004). Multivariate hydrological frequency analysis using copulas. Water resources research, 40(1).

Frieler, K., Lange, S., Piontek, F., Reyer, C.P., Schewe, J., Warszawski, L., Zhao, F., Chini, L., Denvil, S., Emanuel, K. and Geiger, T., 2017. Assessing the impacts of 1.5 C global warming–simulation protocol of the Inter-Sectoral Impact Model Intercomparison Project (ISIMIP2b). Geoscientific Model Development.

Gelman, A., & Rubin, D. B. (1992). Inference from iterative simulation using multiple sequences. Statistical science, 7(4), 457-472.

Genest, C., Ghoudi, K., & Rivest, L. P. (1995). A semiparametric estimation procedure of dependence parameters in multivariate families of distributions. Biometrika, 82(3), 543-552.

Genest, C., & MacKay, J. (1986). The joy of copulas: bivariate distributions with uniform marginals. The American Statistician, 40(4), 280-283.

Genest, C., & Rivest, L. P. (1993). Statistical inference procedures for bivariate Archimedean copulas. Journal of the American statistical Association, 88(423), 1034-1043.

Graham, R. M., Cohen, L., Petty, A. A., Boisvert, L. N., Rinke, A., Hudson, S. R., Nicolaus, M., and Granskog, M. A. (2017), Increasing frequency and duration of Arctic winter warming events, Geophys. Res. Lett., 44, 6974– 6983, doi:10.1002/2017GL073395.

Hansen, James, and Sergej Lebedeff. "Global trends of measured surface air temperature." Journal of geophysical research: Atmospheres 92, no. D11 (1987): 13345-13372.

Hao, Z., & AghaKouchak, A. (2013). Multivariate standardized drought index: a parametric multi-index model. Advances in Water Resources, 57, 12-18.

Harris, I., Jones, P. D., Osborn, T. J., & Lister, D. H. (2014). CRU TS3. 22: Climatic Research Unit (CRU) Time-Series (TS) Version 3.22 of High Resolution Gridded Data of Month-by-month Variation in Climate (Jan. 1901-Dec. 2013). NCAS British Atmospheric Data Centre, 24th September, 2016.

Hoffman, M. D., & Gelman, A. (2014). The No-U-Turn sampler: adaptively setting path lengths in Hamiltonian Monte Carlo. Journal of Machine Learning Research, 15(1), 1593-1623.

Joe, H. (2014). Dependence modeling with copulas. Chapman and Hall/CRC.

Kobayashi, S., Ota, Y., Harada, Y., Ebita, A., Moriya, M., Onoda, H., Onogi, K., Kamahori, H., Kobayashi, C., Endo, H. and Miyaoka, K., 2015. The JRA-55 reanalysis: General specifications and basic characteristics. Journal of the Meteorological Society of Japan. Ser. II, 93(1), pp.5-48.

Leonard, M., Westra, S., Phatak, A., Lambert, M., van den Hurk, B., McInnes, K., Risbey, J., Schuster, S., Jakob, D. and Stafford-Smith, M., 2014. A compound event framework for understanding extreme impacts. Wiley Interdisciplinary Reviews: Climate Change, 5(1), pp.113-128.

Mahfouf, J. F., Brasnett, B., & Gagnon, S. (2007). A Canadian precipitation analysis (CaPA) project: Description and preliminary results. Atmosphere-ocean, 45(1), 1-17.

Mehrotra R, Sharma A (2016) A multivariate quantile-matching bias correction approach with auto and cross dependence across multiple time scales: implications for downscaling. J Clim 29(10):3519–3539.

Mekis E, Vincent LA (2011). An overview of the second generation adjusted daily precipitation dataset for trend analysis in Canada. Atmosphere-Ocean 49(2): 163-177

Meyer, Judith, et al. "Effects of univariate and multivariate bias correction on hydrological impact projections in alpine catchments." Hydrology and Earth System Sciences 23.3 (2019): 1339-1354.

Miguez-Macho, G., Stenchikov, G. L., & Robock, A. (2004). Spectral nudging to eliminate the effects of domain position and geometry in regional climate model simulations. Journal of Geophysical Research: Atmospheres, 109(D13).

Najafi, M. R., Moradkhani, H., & Wherry, S. A. (2010). Statistical downscaling of precipitation using machine learning with optimal predictor selection. Journal of Hydrologic Engineering, 16(8), 650-664.

Neal, Radford M. "MCMC using Hamiltonian dynamics." Handbook of markov chain monte carlo 2, no. 11 (2011): 2.

Nelsen, R. B. (2007). An introduction to copulas. Springer Science & Business Media.

New, Mark, Martin Todd, Mike Hulme, and Phil Jones. "Precipitation measurements and trends in the twentieth century." International Journal of Climatology: A Journal of the Royal Meteorological Society 21, no. 15 (2001): 1889-1922.

Niang, I., O.C. Ruppel, M.A. Abdrabo, A. Essel, C. Lennard, J. Padgham, and P. Urquhart, 2014: Africa. In: Climate Change 2014: Impacts, Adaptation, and Vulnerability. Part B: Regional Aspects. Contribution of Working Group II to the Fifth Assessment Report of the Intergovernmental Panel on Climate Change [Barros, V.R., C.B. Field, D.J. Dokken, M.D. Mastrandrea, K.J. Mach, T.E. Bilir, M. Chatterjee, K.L. Ebi, Y.O. Estrada, R.C. Genova, B. Girma, E.S. Kissel, A.N. Levy, S. MacCracken, P.R. Mastrandrea, and L.L.White (eds.)]. Cambridge University Press, Cambridge, United Kingdom and New York, NY, USA, pp. 1199-1265.

Piani, C., & Haerter, J. O. (2012). Two dimensional bias correction of temperature and precipitation copulas in climate models. Geophysical Research Letters, 39(20).

R Core Team (2019). R: A language and environment for statistical computing. R Foundation for Statistical Computing, Vienna, Austria. URL https://www.R-project.org/.

Rocheta, E., Evans, J. P., & Sharma, A. (2014). Assessing atmospheric bias correction for dynamical consistency using potential vorticity. Environmental Research Letters, 9(12), 124010.

Salvadori, G. (2004). Bivariate return periods via 2-copulas. Statistical Methodology, 1(1-2), 129-144.

Salvadori, G., & De Michele, C. (2007). On the use of copulas in hydrology: theory and practice. Journal of Hydrologic Engineering, 12(4), 369-380.

Scinocca, J.F., Kharin, V.V., Jiao, Y., Qian, M.W., Lazare, M., Solheim, L., Flato, G.M., Biner, S., Desgagne, M. and Dugas, B., 2016. Coordinated global and regional climate modeling. Journal of Climate, 29(1), pp.17-35.

Schneider, U., A. Becker, P. Finger, A. Meyer-Christoffer, B. Rudolf, and M. Ziese. 2016. GPCC Full Data Reanalysis Version 7.0: Monthly Land-Surface Precipitation from Rain Gauges built on GTS based and Historic Data. Research Data Archive at the National Center for Atmospheric Research, Computational and Information Systems Laboratory.

Shrestha, R. R., Dibike, Y. B., & Prowse, T. D. (2012). Modelling of climate-induced hydrologic changes in the Lake Winnipeg watershed. Journal of Great Lakes Research, 38, 83-94.

Sillmann, J., V. V. Kharin, F. W. Zwiers, X. Zhang, and D. Bronaugh, 2013a: Climate extremes indices in the CMIP5 multi-model ensemble. Part 1: Model evaluation in the present climate. J. Geophys. Res., doi:10.1002/jgrd.50203

Sillmann, J., V. V. Kharin, F. W. Zwiers, X. Zhang, and D. Bronaugh, 2013b: Climate extremes indices in the CMIP5 multi-model ensemble. Part 2: Future projections. J. Geophys. Res., doi:10.1002/jgrd.50188.

Sklar M (1959). Fonctions de repartition an dimensions et leurs marges. Publ. inst. statist. univ. Paris 8: 229-231.

Stackhouse Jr., P. W., Gupta, S. K., Cox, S. J., Mikovitz, C., Zhang, T., and Hinkelman, L. M.: The ASA/GEWEX surface radiation budget release 3.0: 24.5-year dataset, Gewex news, 21, 10–12, 2011.

Stan Development Team. 2018. RStan: the R interface to Stan. R package version 2.17.3. http://mc-stan.org

Trenberth, K. E., & Shea, D. J. (2005). Relationships between precipitation and surface temperature. Geophysical Research Letters, 32(14).

Vincent, L. A., van Wijngaarden, W. A., & Hopkinson, R. (2007). Surface temperature and humidity trends in Canada for 1953–2005. Journal of Climate, 20(20), 5100-5113.

Vincent, L. A., Wang, X. L., Milewska, E. J., Wan, H., Yang, F., & Swail, V. (2012). A second generation of homogenized Canadian monthly surface air temperature for climate trend analysis. Journal of Geophysical Research: Atmospheres, 117(D18).

von Storch, H., Langenberg, H., & Feser, F. (2000). A spectral nudging technique for dynamical downscaling purposes. Monthly weather review, 128(10), 3664-3673.

Vrac, M., & Friederichs, P. (2015). Multivariate—intervariable, spatial, and temporal—bias correction. Journal of Climate, 28(1), 218-237.

Weedon, G. P., Balsamo, G., Bellouin, N., Gomes, S., Best, M. J., & Viterbo, P. (2014). The WFDEI meteorological forcing data set: WATCH Forcing Data methodology applied to ERA-Interim reanalysis data. Water Resources Research, 50(9), 7505-7514.

Werner, A. T., Schnorbus, M. A., Shrestha, R. R., Cannon, A. J., Zwiers, F. W., Dayon, G., & Anslow, F. (2019). A long-term, temporally consistent, gridded daily meteorological dataset for northwestern North America. Scientific data, 6, 180299.

Wiken EB (1986). Terrestrial ecozones of Canada, Ecological Land Classification Series No. 19. Environment Canada, Ottawa.

Wong, J. S., Razavi, S., Bonsal, B. R., Wheater, H. S., & Asong, Z. E. (2017). Inter-comparison of daily precipitation products for large-scale hydro-climatic applications over Canada. Hydrology and Earth System Sciences, 21(4), 2163-2185.

Zhang, X., Vincent, L. A., Hogg, W. D., & Niitsoo, A. (2000). Temperature and precipitation trends in Canada during the 20th century. Atmosphere-ocean, 38(3), 395-429.

Zhang, L. S. V. P., & Singh, V. P. (2006). Bivariate flood frequency analysis using the copula method. Journal of hydrologic engineering, 11(2), 150-164.

Zhao, W., & Khalil, M. A. K. (1993). The relationship between precipitation and temperature over the contiguous United States. Journal of climate, 6(6), 1232-1236.

Zscheischler, J., & Seneviratne, S. I. (2017). Dependence of drivers affects risks associated with compound events. Science Advances, 3(6), e1700263.

Chapter 7. Conclusion

7.1 Concluding Remarks

At the outset of this thesis, three primary research gaps were stated and objectives were formulated in order to address them. Here, we discuss those gaps, the corresponding objectives and assess to what extent this study achieved those objectives.

7.1.1 Characterizing past dependence using historical data

As stated during the formulation of the objective, a complete characterization of the temperature-precipitation joint behavior was missing over Canada, especially in terms of the complete bivariate structure. In Chapter 3, using adjusted and homogenized observation data, a bivariate analysis is conducted over Canada using a set of multivariate distribution functions called copulas, which capture all aspects of statistical dependence between two (or more) variables. The copula analysis is performed for 1950-2010 on annual, seasonal and monthly aggregates to assess how (if) dependence structure changes with respect to the temporal scale. Further, taking advantage of very long historical records at a few locations (1910-2017), a non-stationary approach is applied to investigate changes in the dependence structure over time which help reveal joint trends of temperature and precipitation over southern Canada. Finally, the theoretical assumptions of Clausius-Clapeyron relationship are tested for extreme precipitation (95^{th}, 99^{th} and 99.9^{th} percentiles) to quantify extreme precipitation scales with rise in temperature. Removing stations with more than 20% missing data and considering only those locations which capture both temperature and precipitation, a total of 113 stations are included in the analysis. Results are presented over spatial regions defined by Canada's terrestrial ecozones (Wiken, 1986).

Northern Canada and Canadian Prairies stand out as regions with strongest positive and negative dependencies, respectively. The presence of upper tail dependence in the north directs towards prevalence of *relatively* warm and wet events while tail dependence in the Prairies indicates warm-dry dependence. Non-stationary approach reveals significant trends in almost all zones for temperature (average 1.5°C) and 10% to 35% changes in precipitation which are consistent with the previous studies (Zhang et al. 2000). The response of extreme precipitation to temperature shows that the scaling rate varies significantly from the theoretical value of $7\%K^{-1}$. This does not come as a surprise as several other studies have reported similar results citing reasons such as latent heat feedback from ground, and the availability of moisture in the air itself which could either push the scaling rate above 7% K^{-1} or below it (see Section 2.1.4 for more details).

This study helped establish a baseline, or a *ground truth*, even if limited in scale due to availability of reliable data, of what trends and patterns can be expected from the joint behavior of temperature and precipitation over different regions in Canada.

7.1.2 To what extent have the gaps been filled?

The second step in the study is to assess what solutions exist for temporal and spatial gaps in climate data and exam them from not just a univariate viewpoint (which is commonly conducted), but also from a bivariate perspective. Five gridded climate datasets are selected for this study, NRCANmet, CFSR, GRASP, NARR and S14FD; see Chapter 4 for details. These datasets provide a continuous time-series of temperature and precipitation at individual grids over Canada (and some globally). Since we already established a source of truth in Chapter 3, 113 individual grids are chosen from these datasets which are closest to the AHCCD observation stations and analysed from 1980-2010. MBE metric is used to

assess univariate biases in each dataset which provides the magnitude as well as direction of bias at seasonal scale (warm/cold and dry/wet bias). The magnitude of extreme temperature and precipitation is analysed with respect to observation using extreme climate indices and frequency of extreme events is compared following Papalexiou and Montanari (2019). Using copula goodness of fit tests, the gridded data are evaluated to check if they are able to reproduce the bivariate structure exhibited by the observation data. Finally, to assess the impacts of not preserving the dependence structure on real world applications, a hydrological model setup using Raven hydrological framework is forced with three sets of data over Kootenay basin in southeastern British Columbia (Craig, 2015). Forcing data include the original raw data, data bias corrected using a univariate bias correction approach which corrects individual variables but does not preserve the dependence and a multivariate bias correction approach which corrects all aspects of the bivariate distribution along with univariate biases.

Results reveal that NRCANmet, which is a direct interpolation of station data over Canada (and thus considered an observation dataset, as opposed to other gridded data in this study) can capture temperature better than other products but its ability to capture precipitation is just as good as S14FD. Generally, all datasets have cold biases for temperature whereas precipitation biases differ by regions. Bivariate analysis reveals that all datasets equally struggle to capture the dependence between temperature and precipitation with the correct identification at less than 50% sites in almost all cases. This shows that capturing individual variables does not guarantee that a dataset would be able to represent bivariate properties equally well.

Comparison of all three sets of hydrological model outputs reveal that although univariate bias correction vastly improves over the raw inputs, it is further refined using multivariate bias correction, with the largest increase in performance recorded in probability of detection of extreme streamflow.

This study has helped reveal that the spatiotemporal datasets widely used in hydrological applications may not be performing at par with the underlying observed datasets, especially in outcomes that depend on the joint behavior of two or more variables. Propagation of biases from both univariate as well as multivariate biases can be studied using respective bias correction methods and they can further be utilized to improve the quality of data used in applied research.

7.1.3 Characterizing future dependence using climate projections

Having set a ground truth of how temperature and precipitation interact with each other and analysing the alternatives at hand for filling in large gaps in time and space in data, the next step is to analyse projections of climate change over Canada. A 50-member large ensemble regional climate model, CanRCM4 developed by CCCma is used for this purpose. To make the projections more robust, two additional climate simulations (CanLEAD), which are multivariate bias corrected counterparts of CanRCM4, are considered. This is to evaluate whether preserving dependence between climate variables should be prioritized in order to reliably project compound events in the future.

In Chapter 5, a comprehensive univariate evaluation of all three projected datasets is conducted against NRCANmet from 1951-2000. The choice of NRCANmet, even though it performs at par with other gridded products in Chapter 4 is based on several factors including spatial and temporal scales and mainly because it is one of the most widely used

observation datasets over Canada. Following a grid by grid analysis over all of Canada using MBE and MAE, a hierarchical Bayesian framework is setup over three regions in southern Canada to explore biases in individual members of each large ensemble and to generate joint distributions of future temperature and precipitation change. Finally, projections of extreme climate indices are calculated across five 20-year periods, a baseline period of 1986-2005 and four future warming scenarios corresponding to +1.5°C, +2.0°C, +3.0°C and +4.0°C warming above the pre-industrial period of 1850-1900.

In chapter 6, the evaluation is extended to a bivariate setting where a similar approach to chapter 4 is used. Copula goodness of fit tests are used to evaluate whether the projected datasets capture the bivariate structure exhibited by NRCANmet (while recognizing the limitation of NRCANmet in exhibiting the 'true' dependence structure). Next, the joint return periods of warm-wet and warm-dry events are calculated across all datasets from 1951-2100 using a non-stationary ensemble pooling approach, while also quantifying uncertainty across the ensemble using a Bayesian approach. The joint return periods calculated considering dependence are compared to return periods calculated under the assumption of independence to quantify the importance of considering dependence. Moreover, the methodology used completely isolates changes in the dependence structure by keeping univariate magnitude constant.

Results from chapter 5 reveal that multivariate bias correction increases the reliability of projections in most cases with respect to the observations. Significant warm and wet biases in CanRCM4 are reduced by both products with CanLEAD2 (bias corrected with respect to S14FD) outperforming CanLEAD1 (bias corrected with respect to EWEMBI) in majority of the cases. Note that this also traces back to chapter 4, where S14FD is able to

perform at par with NRCANmet and proved even better at capturing precipitation. Using the hierarchical Bayesian framework, strong warming trends are found over all three regions, with the greatest warming in winter and summer. However, precipitation trends are mostly insignificant even though extreme indices of precipitation reveal significant trends in future warming periods. This follows the results reported by CCCR (Bush and Lemmen, 2019) as well that state with *medium confidence* that annual precipitation would increase but *high confidence* that daily precipitation extremes will increase in the future. There is common consensus among models that temperature extremes will increase in the future with higher increases in the lower tail (Tasmin) of temperature as compared to upper (Tasmax). A 4.0°C warmer world also results in an exponential increase in warm spells as well as extreme precipitation events over vast regions of Canada as compared to other warming scenarios.

Bivariate evaluation of the models with respect to observation in chapter 6 shows that all models capture more than 70% of grids accurately, with CanLEAD2 again showing better results than the other two models. Spatially, almost entire Canada shows a higher warm-dry dependence in summer and this dependence remains insensitive to seasonal changes in the Canadian Prairies. Northern Canada on the other hand shows a predominantly warm-wet dependence which reverberates the results of chapter 3. The effect of considering dependence between temperature and precipitation is revealed clearly as joint return periods are significantly reduced compared to the same joint event under the assumption of independence. Results also show that warm-dry events are projected to become more common in the future with sharp decreasing trends in their return periods in most regions of Canada. Another interesting outcome is the reduction in the uncertainty of dependence

structure across the ensemble in the CanLEAD products as compared to CanRCM4 as the Bayesian framework returns wider posterior estimates of copula parameter for the latter model. This is most likely the effect of preservation of the multivariate structure during bias correction of CanLEAD.

In summary, we analysed temperature and precipitation jointly spanning almost two centuries, 1910-present for historical data and until the end of 21st century for future periods. Results from this study can be used to form a foundational understanding of the joint behavior of two of the most important climatic drivers and their combined impacts under climate change to develop appropriate adaptation and resilience plans for cities, communities and infrastructure.

7.2 Potential Limitations and Future Recommendations

The author realizes that no study is a perfect encapsulation of all desired information that one might want to convey about a given objective, methodology or data and this is no exception. As such, the following section reflects upon the findings of this study, identifying potential limitations and how they could be overcome in the future.

7.2.1 Aggregation and Loss of Information

Every time, any data are aggregated to any scale, be it temporally or spatially, it leads to loss of information. Although in case of climate data, it is in fact desirable to look at temporal aggregates to look at patterns because of signal-to-noise ratio, especially in precipitation. Spatially however, aggregating climate data becomes a limitation since temperature to some extent, and precipitation to a larger extent, varies significantly with topography. As such, spatial aggregation might ‘smooth’ out outliers which could lead to

under-estimation of the impacts associated with the particular entity. There are several methods to resolve such issues such as working with standardized anomalies however they have their own drawbacks such as harder interpretation of end results. In an ideal world, spatial aggregations would not be required however, it leads to excessive amounts of data, requirement of time and resources as well as a huge amount of results which become harder to interpret and communicate. Since this study was pan-Canadian, some compromises with spatial scales had to be made. Site-specific analysis should of course always use all available data to aid their decision-making.

7.2.2 A Model is as Good as the Underlying Data

AHCCD (Mekis and Vincent, 2011; Vincent et al. 2012) data used in chapter 3 is the most reliable observation dataset of temperature and precipitation available in Canada. Even then, the station selection criteria of at least 80% data availability leads to an average 3000 days of missing data over a period 50 years. There are several methods of treating missing data and the author realizes that each one of them can alter the final outputs of a model. The problem is exasperated when multivariate models are involved since now the uncertainty is not just arising out of each variable involved, but also out of the change in dependence structure that might happen due to missing data.

Further, based on author's personal observations as well as recommendations from other prominent literature on copulas (from other fields as well such as econometric modelling where copulas were first widely used; see Genest et al. 2013), the model selection criteria for copula is robust. Especially, in cases where dependencies are relatively weak (< 0.3 Kendall's rank correlation), multiple copula families might prove to be a 'good fit' given the generically weak dependence between the variables. In cases like these, several metrics

such as maximum likelihood methods supplemented with information criterions and goodness of fit tests should be used in conjunction to select an appropriate model. Moreover, Grønneberg and Hjort (2014) investigated the use of AIC as a copula selection criterion and questioned its underlying assumptions. They propose another version of this criterion, named the Copula Information Criterion (CIC), specifically tailored for copulas which could be used instead of AIC and BIC metrics in future studies. Researchers should also pay close attention to ties in ranks of data when fitting copulas as it can introduce strong biases in Maximum Pseudo Likelihood (MPL; Hofert, 2018).

7.2.3 Multivariate Analysis using Future Projections

Although this study shows that multivariate bias correction methods improve upon the results from an existing regional climate model to some extent, but further investigation is required. For example, comparison of a multivariate bias corrected product to a univariate bias corrected product would truly identify the extent to which the additional step of correcting the dependence structure affects results because it would completely isolate the effects of the multivariate correction from the univariate correction. That said, the author recommends that since multivariate bias correction already corrects for univariate biases within itself, the principle of *"err on the side of caution"* should be followed, especially when analysing multivariate or compound extremes in the future. The precedent has already been set with the upcoming protocol of ISIMIP, the ISIMIP3BASD (v1.0) using MBCn in both downscaling and bias correction (Lange, 2019).

7.3 References

Bush E, Lemmen DS (2019) Canada's Changing Climate Report; Government of Canada, Ottawa, ON pp 444

Craig, J.R., and the Raven Development Team, Raven User's and developer's manual (Version 2.9.2), URL: http://raven.uwaterloo.ca/ (Accessed xxx, 2019).

Genest, C., Gendron, M., & Bourdeau-Brien, M. (2013). The advent of copulas in finance. In Copulae and Multivariate Probability Distributions in Finance (pp. 13-22). Routledge.

Grønneberg, S., & Hjort, N. L. (2014). The copula information criteria. Scandinavian Journal of Statistics, 41(2), 436-459.

Hofert, M. (2018). Elements of copula modeling with R. Springer.

Lange, S.: Trend-preserving bias adjustment and statistical downscaling with ISIMIP3BASD (v1.0), Geosci. Model Dev., 12, 3055–3070, https://doi.org/10.5194/gmd-12-3055-2019, 2019.

Mekis E, Vincent LA (2011). An overview of the second generation adjusted daily precipitation dataset for trend analysis in Canada. Atmosphere-Ocean 49(2): 163-177

Papalexiou, S. M., & Montanari, A. (2019). Global and Regional Increase of Precipitation Extremes under Global Warming. Water Resources Research.

Vincent, L. A., Wang, X. L., Milewska, E. J., Wan, H., Yang, F., & Swail, V. (2012). A second generation of homogenized Canadian monthly surface air temperature for climate trend analysis. Journal of Geophysical Research: Atmospheres, 117(D18).

Wiken EB (1986). Terrestrial ecozones of Canada, Ecological Land Classification Series No. 19. Environment Canada, Ottawa.

Zhang, X., Vincent, L. A., Hogg, W. D., & Niitsoo, A. (2000). Temperature and precipitation trends in Canada during the 20th century. Atmosphere-ocean, 38(3), 395-429

Appendices - Methods

A1 – Copula CDFs

CDF functions of some widely used copulas are provided in the following equations (Genest 1987, Joe 2014, Nelsen 2007). In all equations, *u* and *v* are the probability integral transforms of variables *X* and *Y*, θ and δ are the copula parameters and τ is the Kendall's rank correlation coefficient between X and Y variables.

Clayton Copula:

$$C(u,v) = \left(u^{-\theta} + v^{-\theta} - 1\right)^{-\frac{1}{\theta}}) \qquad -(i)$$

$$\tau = \frac{\theta}{\theta + 2} \qquad -(ii)$$

Gumbel Copula:

$$C(u,v) = \exp\left(-\left[(-\log(u))^{\theta} + (-\log(v))^{\theta}\right]^{\frac{1}{\theta}}\right) \qquad -(iii)$$

$$\tau = 1 - \theta^{-1} \qquad (12)$$

Joe Copula:

$$C(u,v) = 1 - \left([1-u]^{\theta} + [1-v]^{\theta} - [1-u]^{\theta}[1-v]^{\theta}\right)^{\frac{1}{\theta}} \qquad -(iv)$$

$$\tau = 1 + 2(2-\theta)^{-1}[digamma(2) - digamma(2/\theta + 1)] \quad -(v)$$

Frank Copula:

$$C(u,v) = -\theta^{-1}\log\left(1 + \frac{\left(e^{-\theta u}-1\right)\left(e^{-\theta v}-1\right)}{\left(e^{-\theta}-1\right)}\right) \quad -(vi)$$

$$\tau = 1 + 4\theta^{-1}[D_1(\theta) - 1] \quad -(vii)$$

$$D_k(x) = kx^{-k}\int_0^x t^k(e^t-1)^{-1}dt \quad -(viii)$$

BB1 Copula:

$$C(u,v) = (1 + [(u^{-\theta}-1)^{\delta} + (v^{-\theta}-1)^{\delta}]^{1/\delta})^{1/\theta} \quad -(ix)$$

$$\tau = 1 - \frac{2}{[\delta(\theta+2)]} \quad -(x)$$

BB6 Copula:

$$C(u,v) = 1 - \left(1 - \exp\left\{-\left[\left(-\log\left(1-u^{-\theta}\right)\right)^{\delta} + \left(-\log\left(1-v^{-\theta}\right)\right)^{\delta}\right]^{\frac{1}{\delta}}\right\}\right)^{\frac{1}{\theta}} \quad -(xi)$$

BB7 Copula:

$$C(u,v) = 1 - \left(1 - \left[\left(1-u^{-\theta}\right)^{-\delta}\left(1-v^{-\theta}\right)^{-\delta} - 1\right]^{-\frac{1}{\delta}}\right)^{\frac{1}{\theta}} \quad -(xii)$$

BB8 Copula:

$$C(u,v) = \frac{1 - \left(1 - \omega^{-1}\left[1-(1-\delta u)^{\theta}\right]\left[1-(1-\delta v)^{\theta}\right]\right)^{\frac{1}{\theta}}}{\delta} \quad -(xiii)$$

$$\omega = 1 - (1-\delta)^{\theta} \quad -(xiv)$$

The densities of the rotated copulas are defined as:

Rotated-90 copula:

$$C^{90}(u,v) = C(1-u,v) \qquad -(xv)$$

Rotated-180 copula or Survival Copula:

$$C^{180}(u,v) = C(1-u,1-v) \qquad -(xvi)$$

Rotated-270 copula:

$$C^{270}(u,v) = C(v,1-u) \qquad -(xvii)$$

A2 - Hierarchical Bayesian Framework

The following framework is used in Chapter 5.

The following equations describe the model setup.

$$O_d^T \sim Normal(\mu_d^T, \sigma^T), where\ d = 1\ to\ 6 \qquad -(xviii)$$

Equation i here denotes that the observed temperature O_d^T of each decade is normally distributed around a *true* mean μ_d^T and scale σ^T.

$$M_{d,n}^T \sim Normal(\mu_d^T + \delta_n^T, \quad \rho_n^T), where\ d = 1\ to\ 15\ and\ n = 1\ to\ 150 \qquad -(xix)$$

Equation ii denotes that the temperature projected by each model $M_{d,n}^T$ is normally distributed around the true mean plus an additive bias that is unique to each ensemble simulation and a scale ρ_n^T. Each simulation has its unique bias, which remains consistent across the 15 decades.

$$\mu^T = m^T d + c^T \quad ; \qquad \mu^T = m^T d + c^T + m'^T(d' - d), where\ d = 1{:}6\ and\ d' = 1\ to\ 15 \qquad -(xx)$$

In equation iii, it is assumed that the mean temperature follows a linear trend with time with slope m^T until the year 2000, after which an elbow is provided with slope m'^T to account for accelerated warming projected by all climate models to account for increase in GHG emissions.

$$O_d^P \sim Normal(\mu_d^P + r^o(O_d^T - \mu_d^T), \quad \sigma^P) \qquad -(xxi)$$

Equation iv states that temperature and log-transformed precipitation follow a joint Gaussian distribution. The correlation coefficient between temperature and precipitation arises out of the linear slope of observed data r^o.

$$M_{d,n}^P \sim Normal(\mu_d^P + r_n^m\left(M_{d,n}^T - \mu_d^T - \delta_n^T\right) + \delta_n^P, \rho_n^P), where\ d = 1\ to\ 15\ and\ n = 1\ to\ 150 \qquad -(xxii)$$

The same assumption is held for precipitation projected by the ensemble simulations with an additional bias δ_n^P, which is unique to each simulation. The correlation coefficient between temperature and precipitation of each simulation arises out of the slope parameter r_n^m (equation v).

$$\mu^P = m^P d + c^P \quad ; \qquad \mu^P = m^P d + c^P + m'^P(d' - d), where\ d = 1{:}6\ and\ d' = 1\ to\ 15 \qquad -(xxiii)$$

The mean of precipitation is also said to follow a linear trend with time with slope m^P accounting for the trend before the year 2000 and m'^P after 2000 when an elbow is introduced to the trend.

The following table defines the specification of prior distributions in a hierarchical framework.

Table 11 – Prior distributions for the parameters of the Bayesian framework.

Parameter	Description	Prior Distribution
$\boldsymbol{\sigma_d^T}$	Scale of observed temperature	Estimated from data. Different for each zone and season.
$\boldsymbol{\sigma_d^P}$	Scale of observed log-precipitation	Estimated from data. Different for each zone and season.
$\boldsymbol{r^o}$	Correlation between observed temperature and precipitation.	$\sim Normal(r', \gamma_o)$
$\boldsymbol{r_n^m}$	Correlation between each simulation's projected temperature and precipitation	$\sim Normal(r', \gamma)$
$\boldsymbol{\delta_n^T}$	Bias term for temperature projection of each simulation.	$\sim Normal(\Delta^T, \varphi_n^T)$
$\boldsymbol{\delta_n^P}$	Bias term for precipitation projection of each simulation.	$\sim Normal(\Delta^P, \varphi_n^P)$
$\boldsymbol{\rho_d^T}$	Scale of projected temperature of each decade.	$\sim Cauchy(a^T, b^T)$
$\boldsymbol{\rho_d^P}$	Scale of projected precipitation of each decade.	$\sim Cauchy(a^P, b^P)$

All parameters defined in the distributions of priors are given weakly informative priors (or hyperpriors).

Table 12 - Hyperpriors for the parameters of the Bayesian framework.

(Hyper) Parameters	**Description**	**Prior Distribution**
$\boldsymbol{c^T}$, $\boldsymbol{m^T}$, $\boldsymbol{m'^T}$, $\boldsymbol{c^P}$, $\boldsymbol{m^P}$, $\boldsymbol{m'^P}$	Slope and intercept parameters of linear trend for temperature and precipitation.	$\sim Normal(0,100)$
$\boldsymbol{r'}$	Parameter for mean of correlation between temperature and precipitation.	$\sim Normal(0,100)$
$\boldsymbol{a^T}$, $\boldsymbol{a^P}$, Δ^T, Δ^P	Parameters for mean of prior distributions of projected temperature and precipitation scales.	$\sim Normal(0,100)$
$\boldsymbol{\gamma}$, $\boldsymbol{\varphi_n^T}$, $\boldsymbol{\varphi_n^P}$, $\boldsymbol{b^T}$, $\boldsymbol{b^P}$	Parameters for scale of all prior distributions.	$\sim Cauchy(0,10)$

To deal with convergence issues with MCMC sampling of hierarchical models, thinning technique was used under which 10,000 samples were taken from each parameter's posterior distribution and only every 10th sample was saved. This technique has been known to reduce autocorrelation of samples within the chain producing a higher Effective Sample Size (ESS) (Gelman et al. 2013). The posterior distributions are diagnosed using the ratio of effective samples to total samples (N_{eff}/N) and the Gelman-Rubin Diagnostic

($\hat{R}$) metrics (Gelman and Rubin, 1992). The $\hat{R}$ diagnostic calculates variance within multiple MCMC chains started from different randomly sampled starting points. If the variance between the chains after all iterations is still relatively large, it denotes that the chains have not converged to a *true* posterior. (Stan Development Team, 2018) recommends $\hat{R}$ of less than 1.1 and N_{eff}/Nat least 0.001.

The metrics are summarized across all models and all parameters in figure 50. The maximum $\hat{R}$ observed was 1.08 (calculated across five parallel MCMC chains) and the minimum N_{eff}/Nratio was 0.08 indicating that all chains have converged.

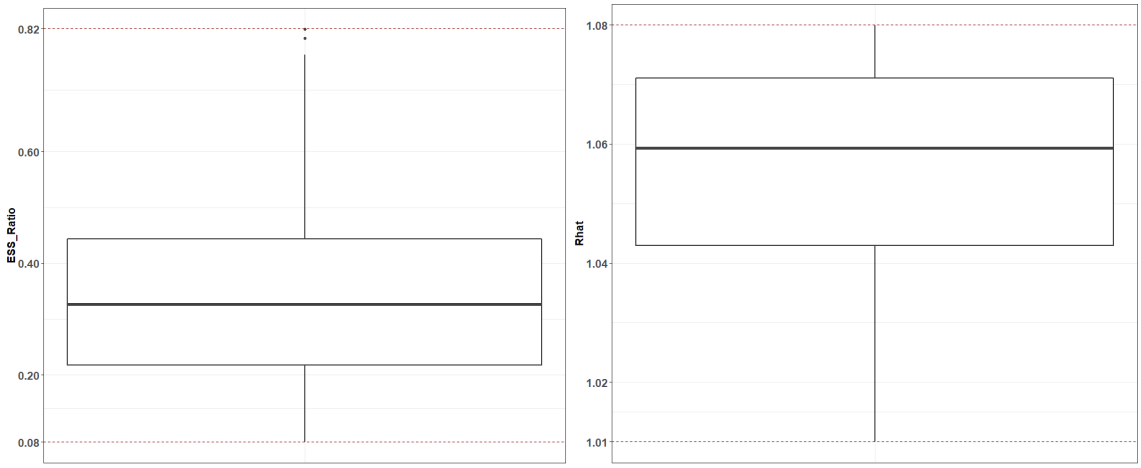

Figure 50 – Distribution of N_{eff}/N ratio (left) and $\hat{R}$ (right) for MCMC chains across all models. The dashed horizontal lines indicate the maximum and minimum range of the metrics.

A3 - Tail Dependence in Copulas

The Archimedean family provides some one-parameter copulas that can capture dependence in tails (extremes) of the marginals. For example, Clayton copula can be used to model lower tail dependence (correlation between lower tails of marginals), while Gumbel and Joe copula can be used to model upper tail dependence (correlations between

upper tails of marginals). Using these copulas, we can capture correlation in warm-wet events (upper tails) or cold-dry events (lower tails) however, the correlation between warm-dry events and cold-wet events cannot be modeled using the copulas as is. Simply put, if temperature and precipitation are plotted on x and y axis respectively, there can be four quadrants in which tail dependence can arise (moving clockwise from top left, the four quadrants would correspond to cold-wet, warm-wet, warm-dry and cold-dry events).

In this case, the concept of rotated copulas can be used. If the density of a regular (non-rotated copula) can be written as $C^0 = C(u, v)$, where u and v are random uniformly distributed variables, then the corresponding rotated version can be written as $C^{90} = C(1-u, v)$, $C^{180} = C(1-u, 1-v)$ and $C^{270} = C(u, 1-v)$, where the superscript of C refers to the angle by which the copula is rotated. Thus, taking all rotations into account, every scenario of tail dependence between the two variables can be captured using three copulas each (Figure 51). In this study, we are only focusing on the right hand side quadrants, i.e. warm-wet and warm-dry events since the primary goal is to assess the behavior of precipitation under future warming.

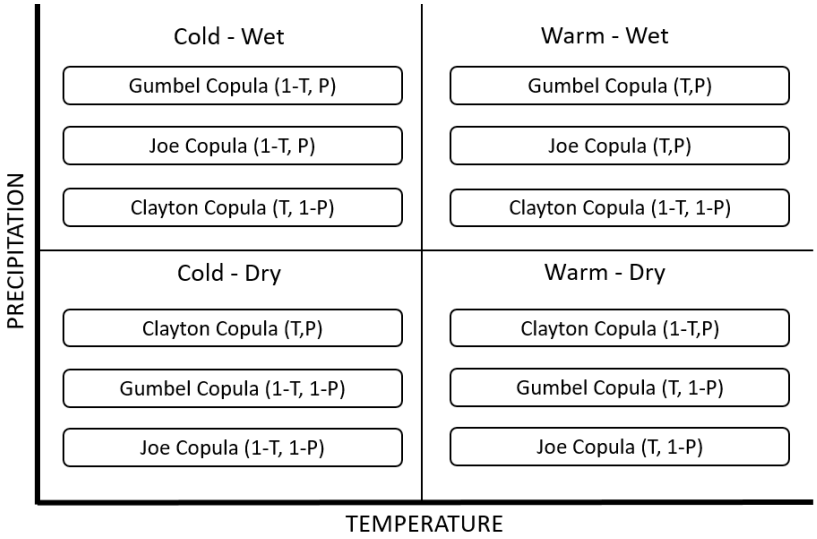

Figure 51 – The four quadrants represent the four combinations in which temperature and precipitation extremes can be correlated. Each quadrant shows the type of copula that can be used to capture the particular behavior.

A4 - Maximum Pseudo-Likelihood

As explained by Genest et al. (1995), if parametric models of marginals are used to calculate the likelihood, the copula parameter becomes dependent on the form of the marginal, which is undesirable when only dependence structure is being analysed. Thus, a semi-parametric method was proposed in which parametric marginal distributions are replaced by empirical rank-based marginals. Given two continuous random variables x and y of length n, the empirical CDF of the variables can be calculated using the following equation

$$u = \frac{R_x}{n+1}, \qquad v = \frac{R_y}{n+1} \qquad -(xxiv)$$

Where R_x and R_y are the ranks of x and y respectively. As is evident from the above equations, parametric marginals will no longer play a role in further estimation of the copula parameter, which is obtained by maximizing the log-likelihood function defined by

$$L(\theta) = \sum_{i=1}^{n} \log\{C_\theta[u_i, v_i]\} \qquad -(xxv)$$

Often, information criterions such as Akaike Information Criterion (AIC; Akaike, 1974) are used in conjunction with maximum likelihood methods. The primary advantage of information criterions is the introduction of a penalty term, which is a function of the number of parameters in the model and is subtracted from the maximum likelihood in order

to avoid over-fitting. In this case, since we only use one-parameter copulas, the penalty term would remain constant across different models and thus provide no additional benefit.

A5 - Goodness of Fit Test

The goodness of fit test, proposed by Genest et al. (2006), is based on calculating two variants of the Cramér–von Mises statistic (Genest and Favre, 2007).

$$S_n = \int_0^1 |K_n(t)|^2 \, K_{\theta_n}(t) dt \qquad -(xxvi),$$

$$T_n = \sup_{0 \le t \le 1} |K_n(t)| \qquad -(xxvii),$$

where $K_n(t) = \sqrt{n}\{K_n(t) - K_{\theta_n}(t)\}$. Here, K_n refers to the empirical distribution of the data and K_{θ_n} refers to the theoretical distribution of samples taken from the selected copula. This method is an improvement over the previous work of Genest and Rivest (1993) and Wang and Wells (2000). The enhancements over previous approaches include the extension of the goodness of fit test beyond the Archimedean family of copulas and the estimation of p-values of the statistic. Genest et al. (2006) reported that the comparison of raw values of the statistics S_n and T_n may be inappropriate in model selection in some cases. To rectify this drawback, they proposed a bootstrapping procedure to estimate p-values under the null hypothesis, $H_0 : C_\theta \in C_{\theta_n}$ where C_θ is the underlying empirical copula and C_{θ_n} is a parametric family of copulas in consideration. The procedure is based on identifying the asymptotic null distribution from which the empirical statistics S_n and T_n are obtained (Genest and Rémillard, 2008). Following similar works by Henze (1996) and Stute et al. (1993), they proposed generating n independent observations from the

parametric family C_{θ_n} and calculating the statistics S_n^* and T_n^* for the sample. The process is repeated for a large number of times to obtain distributions of the statistics following which p-values are estimated according to the following equation

$$\frac{1}{N}\sum_{k=1}^{N} 1\left(S_{n,k}^* > S_n\right) \qquad -(xxviii),$$

for every $k \in \{1 \ldots N\}$, where N is the number of times the procedure is repeated. In this study, each copula is evaluated at N = 1000 iterations.

A6 - Bayesian Framework

The following model is used in Chapter 6, section 6.3.3. The following section describes the Bayesian model for a single scenario and is applied as is to every case. Let T denote the seasonally averaged temperature and P, the log-transformed seasonally accumulated precipitation. Both variables are assumed to follow a Gaussian distribution.

$$T \sim N(\mu_T, \sigma_T) \qquad -(xxix)$$

$$P \sim N(\mu_P, \sigma_P) \qquad -(xxx)$$

Here, μ_* and σ_* are the mean and standard deviation of temperature and precipitation, identifiable by their respective subscripts. The cumulative density functions of the respective copula are defined according to the equations in Appendix-A1. The copula parameter θ is transformed from the Kendall's correlation coefficient τ.

The Bayesian model parameter set thus consists of five primary parameters. The four parameters belonging to the marginal distributions are given weakly informative priors whereas τ is given a uniform prior between [-1, 1] (Table 13).

Table 13 – Prior distributions for the parameters of the Bayesian model.

Parameter	Description	Prior Distribution
$\boldsymbol{\mu_T}$	Mean of temperature	$Normal(0, 100)$
$\boldsymbol{\mu_P}$	Mean of log-precipitation	$Normal(0, 100)$
$\boldsymbol{\sigma_T}$	Standard Deviation of temperature	$HalfCauchy(0, 10)$
$\boldsymbol{\sigma_P}$	Standard Deviation of precipitation	$HalfCauchy(0, 10)$
$\boldsymbol{\tau}$	Kendall's Correlation Coefficient	$Uniform(-1,1)$
$\boldsymbol{\theta}$	Transformation of τ	Constrained by τ

The resulting posterior distributions, which do not have a closed form, are obtained using MCMC simulations with the help of the No-U-Turn Sampler (NUTS) (Hoffman and Gelman, 2014), which is an extension to the Hamiltonian Monte Carlo (HMC) sampler (Neal, 2011) using Stan platform (Stan Development Team, 2018) in R programming language (R Core Team, 2019). The only variable of interest is the copula parameter θ since the analysis is independent of the magnitude of the marginals. However, MCMC chain convergence is verified for all parameters using the Gelman-Rubin Diagnostic ($\hat{R}$) metric (Gelman and Rubin, 1992). Following the diagnostic check of the model, the uncertainty in the copula parameter is quantified by obtaining the 2.5th, 50th and 97.5th quantile of the posterior, respectively. These values are further used in the return period calculation, thus presenting a range of return periods for a particular event, which quantifies the uncertainty in the dependence structure across the ensemble.

Appendices - Figures

Figures for Chapter 3

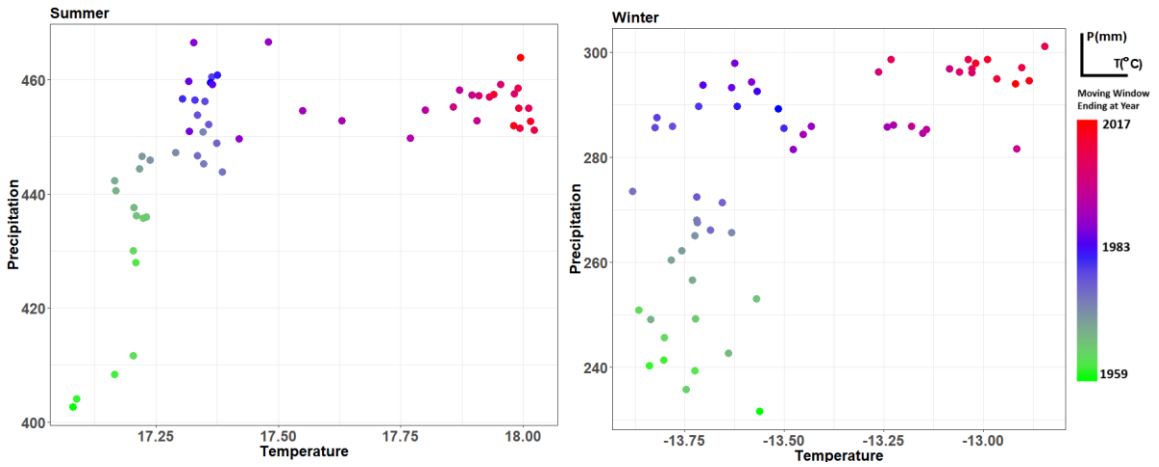

Figure 52 - The shift in the peak copula density over a moving window of 50 years applied from 1910 to 2017 for Zone 6 – Boreal Shield.

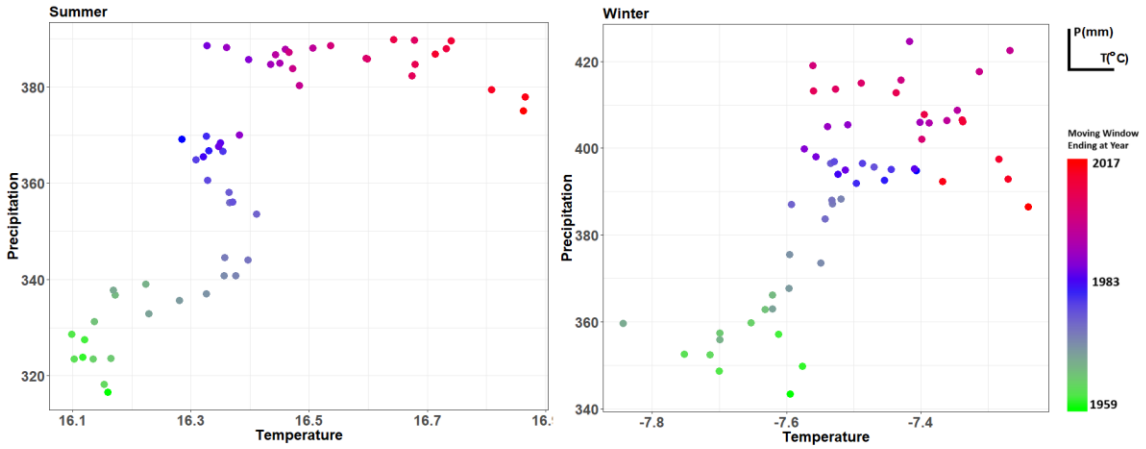

Figure 53 – The shift in peak copula density over a moving window of 50 years applied from 1910 to 2017 for Zone 7 – Atlantic Maritime.

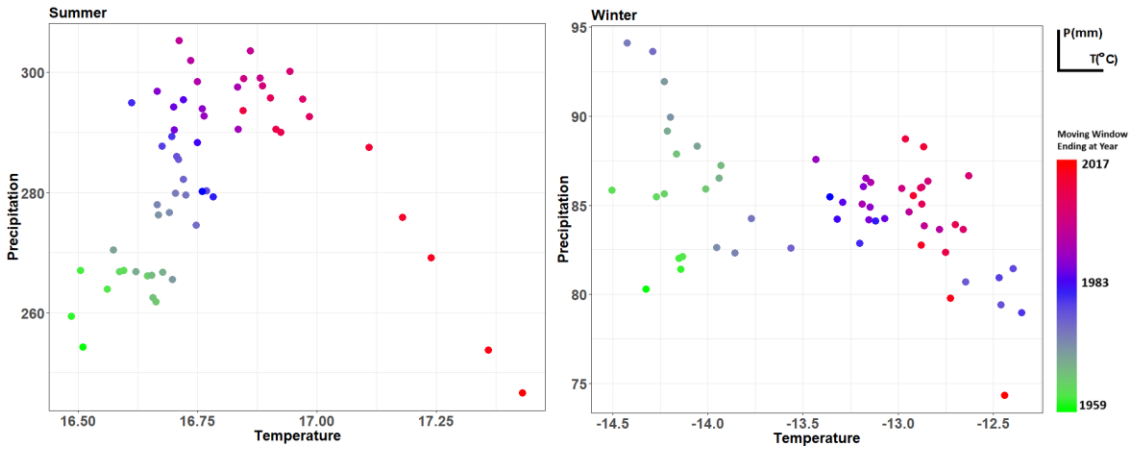

Figure 54 –The shift in peak copula density over a moving window of 50 years applied from 1910 to 2017 for Zone 7 – Boreal Plains.

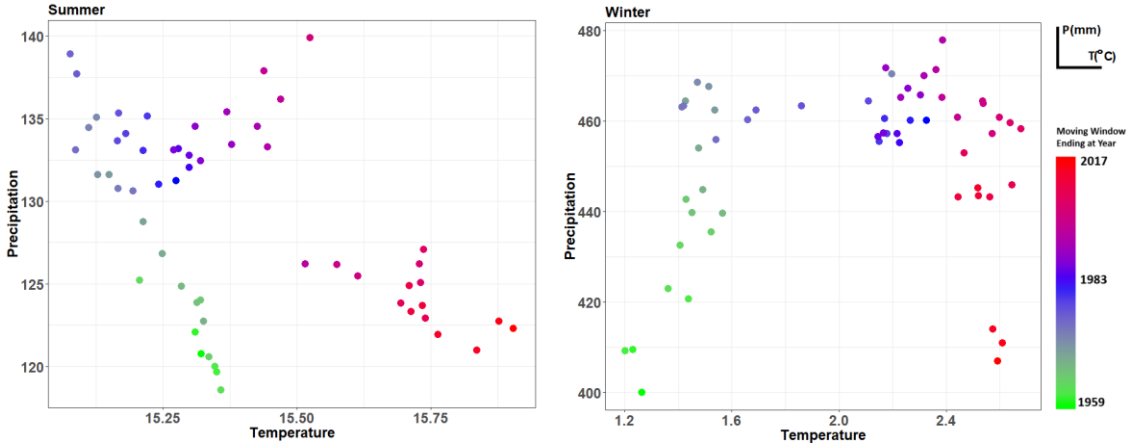

Figure 55 – The shift in peak copula density over a moving window of 50 years applied from 1910 to 2017 for Zone 12 – Boreal Cordillera.

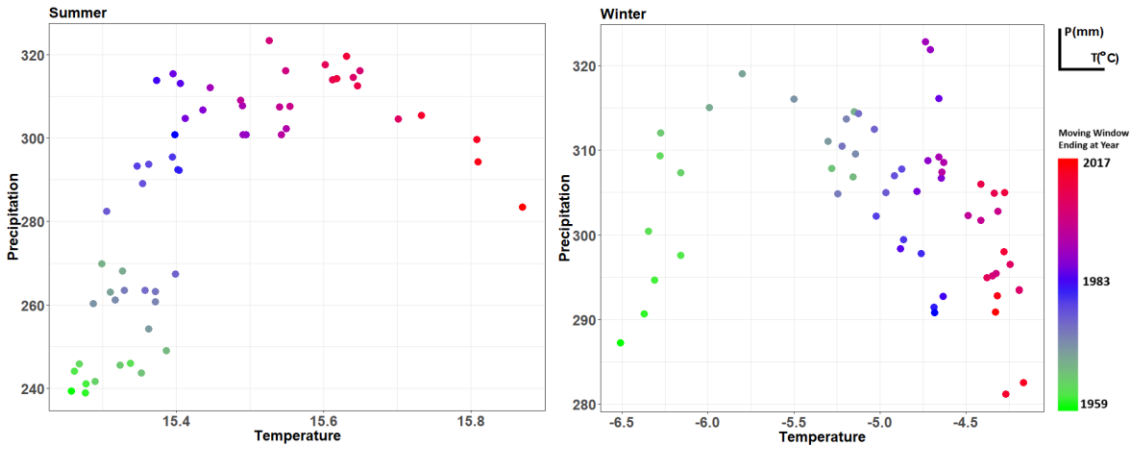

Figure 56 –The shift in peak copula density over a moving window of 50 years applied from 1910 to 2017 for Zone 12 – Pacific Maritime.

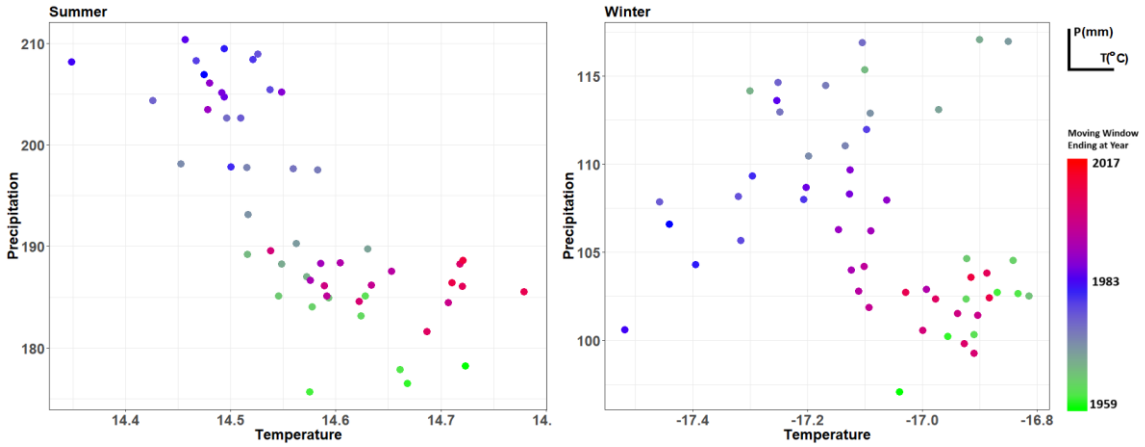

Figure 57–The shift in peak copula density over a moving window of 50 years applied from 1910 to 2017 for Zone 12 – Montane Cordillera.

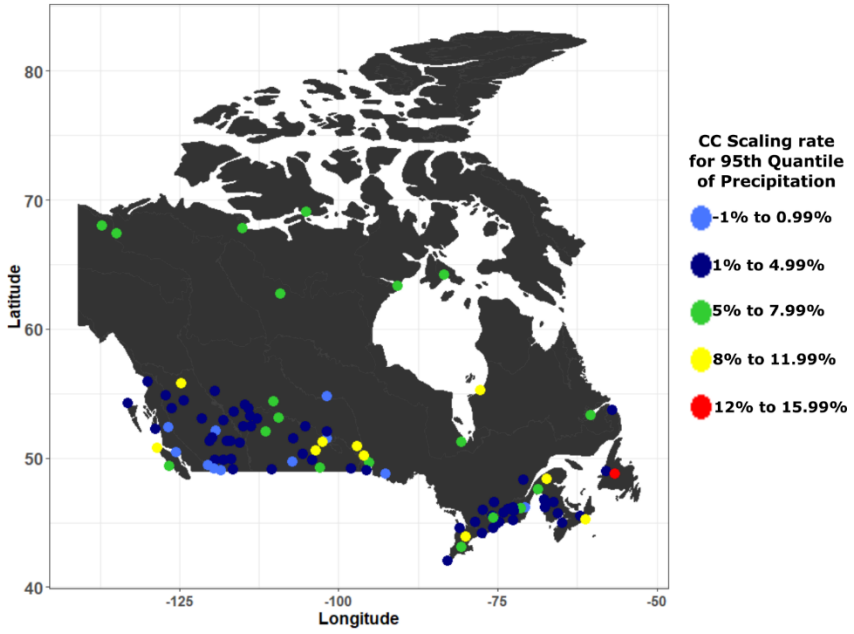

Figure 58 – CC scaling rates for individual stations for 95th quantile of daily extreme precipitation.

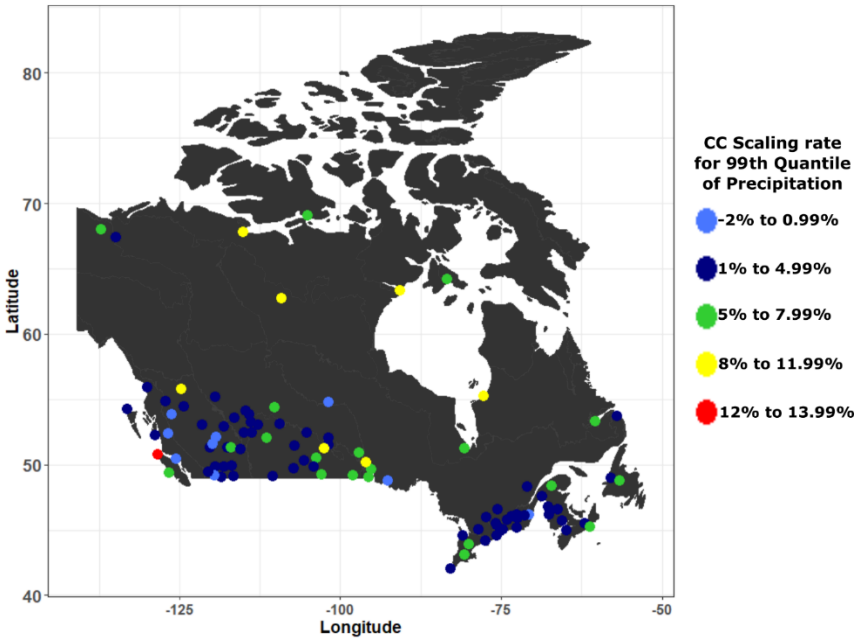

Figure 59 – CC scaling rates for individual stations for 99th quantile of daily extreme precipitation.

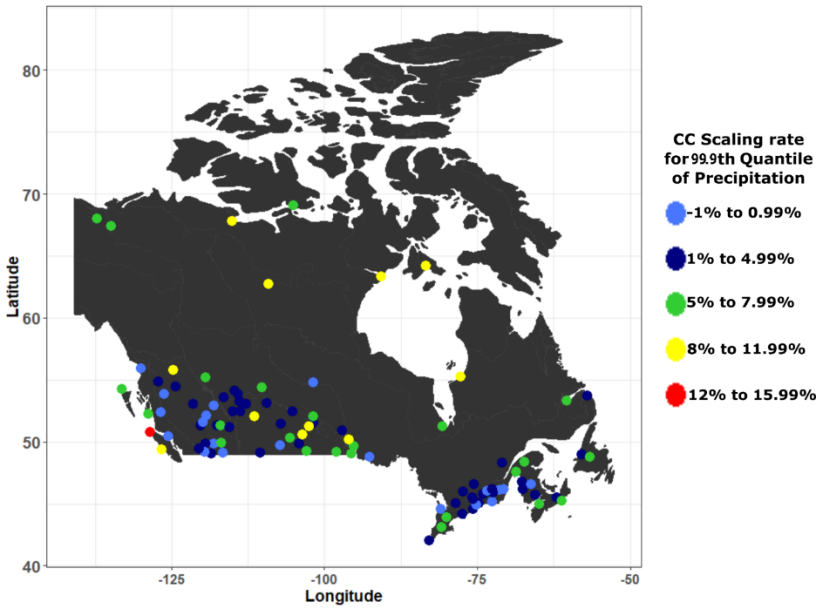

Figure 60 – CC scaling rates for individual stations for 99.9th quantile of daily extreme precipitation.

Figures for Chapter 6

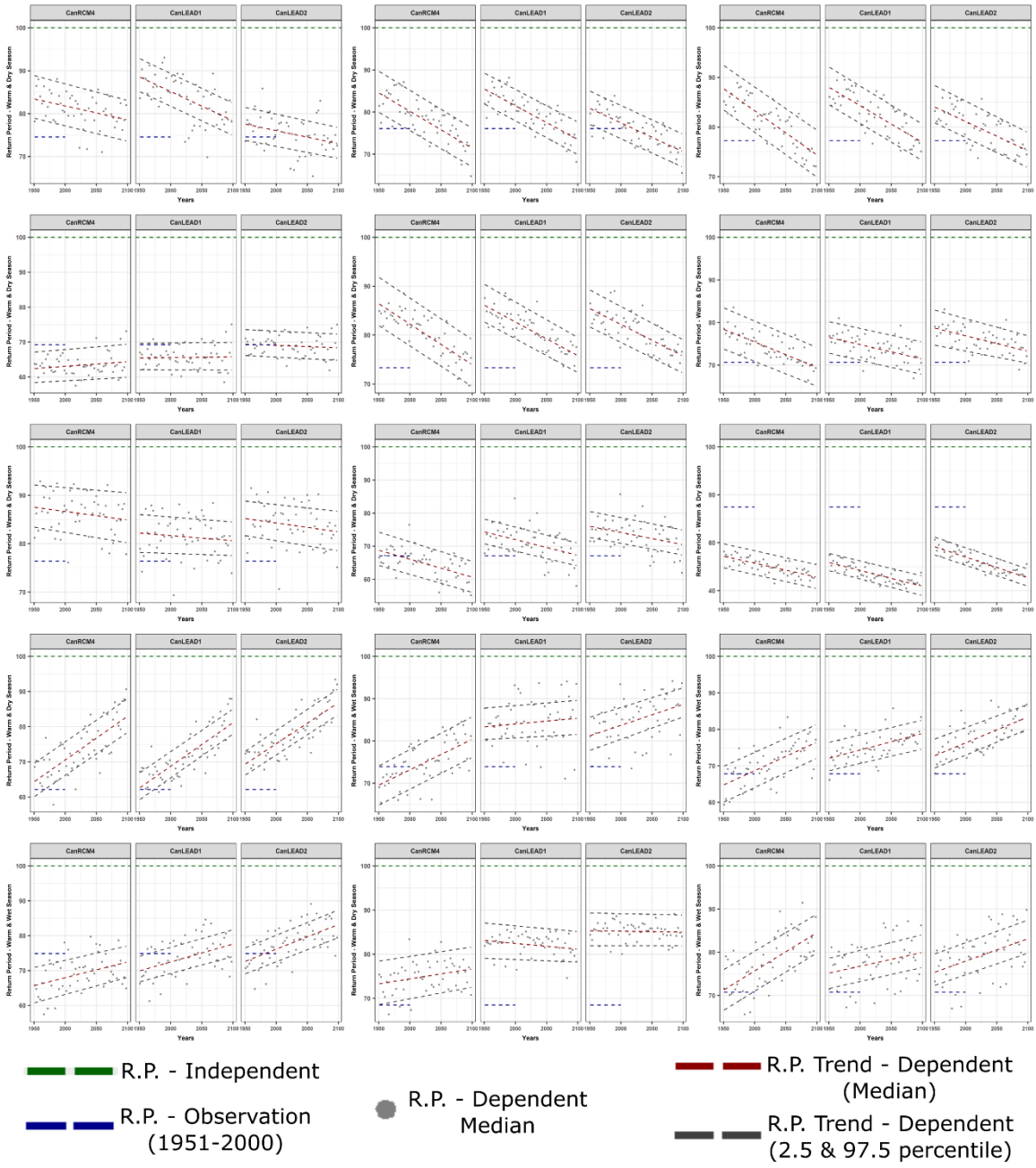

Figure 61- The figure shows the return periods calculated under different scenarios for a temperature-precipitation compound event in winter season for each zone (1-15, sorted row-wise). The horizontal green line at the top shows the reference 100-year return level for the joint probability of exceeding the 90th quantiles of temperature and precipitation respectively, under

the assumption of independence. The short blue line represents the return period of the same event calculated from NRCANmet over the de-trended stationary period of 1951-2000. The grey points represent the return periods calculated from the models using the non-stationary pooling approach. The slanted lines represent the trend of the non-stationarity in return period. The red line represents the median return period and the grey lines represent the 2.5th and 97.5th quantiles of the return period. The calculation of this uncertainty range is based on the posterior samples of the copula parameter obtained from the Bayesian model.

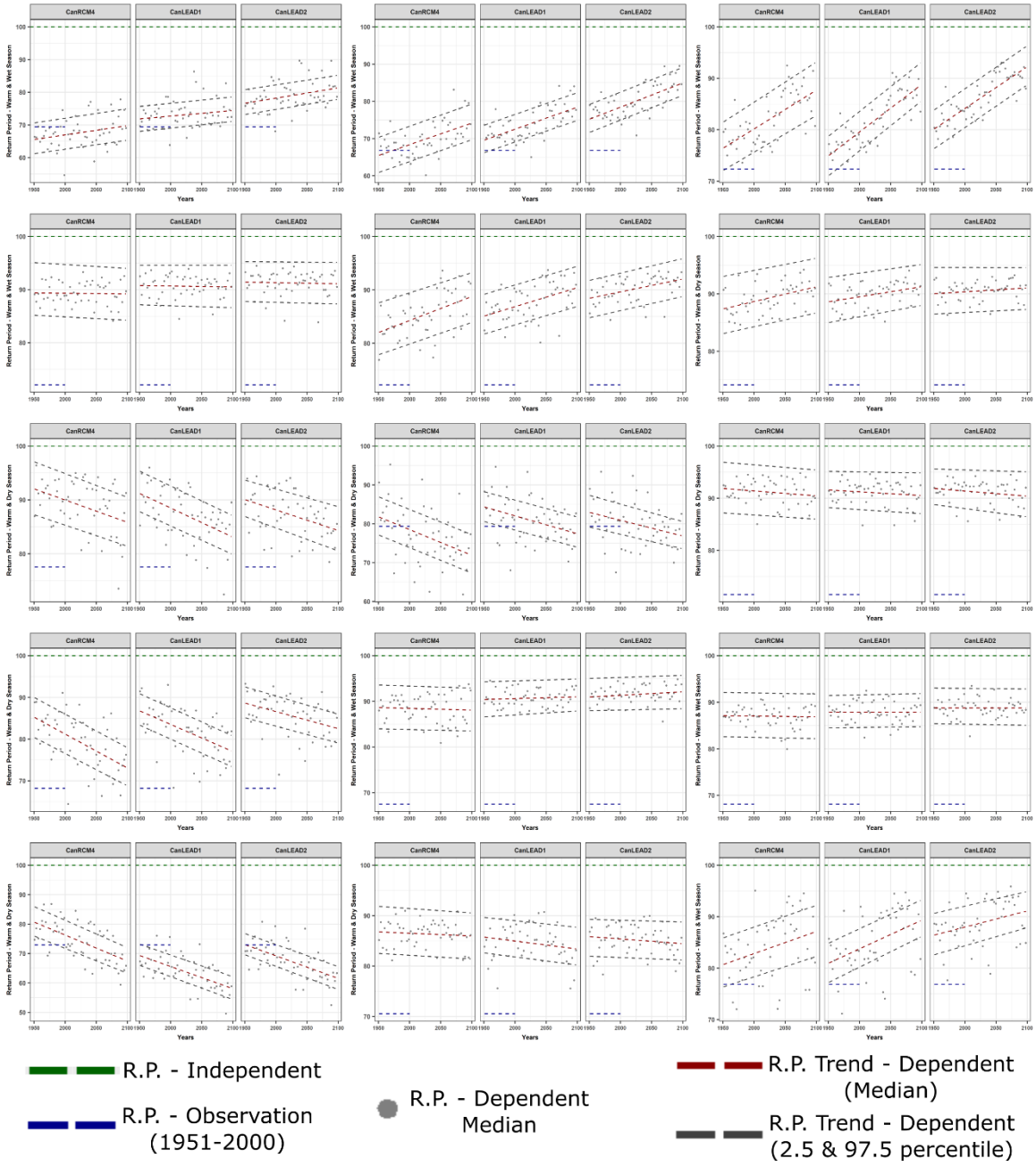

Figure 62 - The figure shows the return periods calculated under different scenarios for a temperature-precipitation compound event in spring season for each zone (1-15, sorted row-wise). See caption of figure 61 for further details.

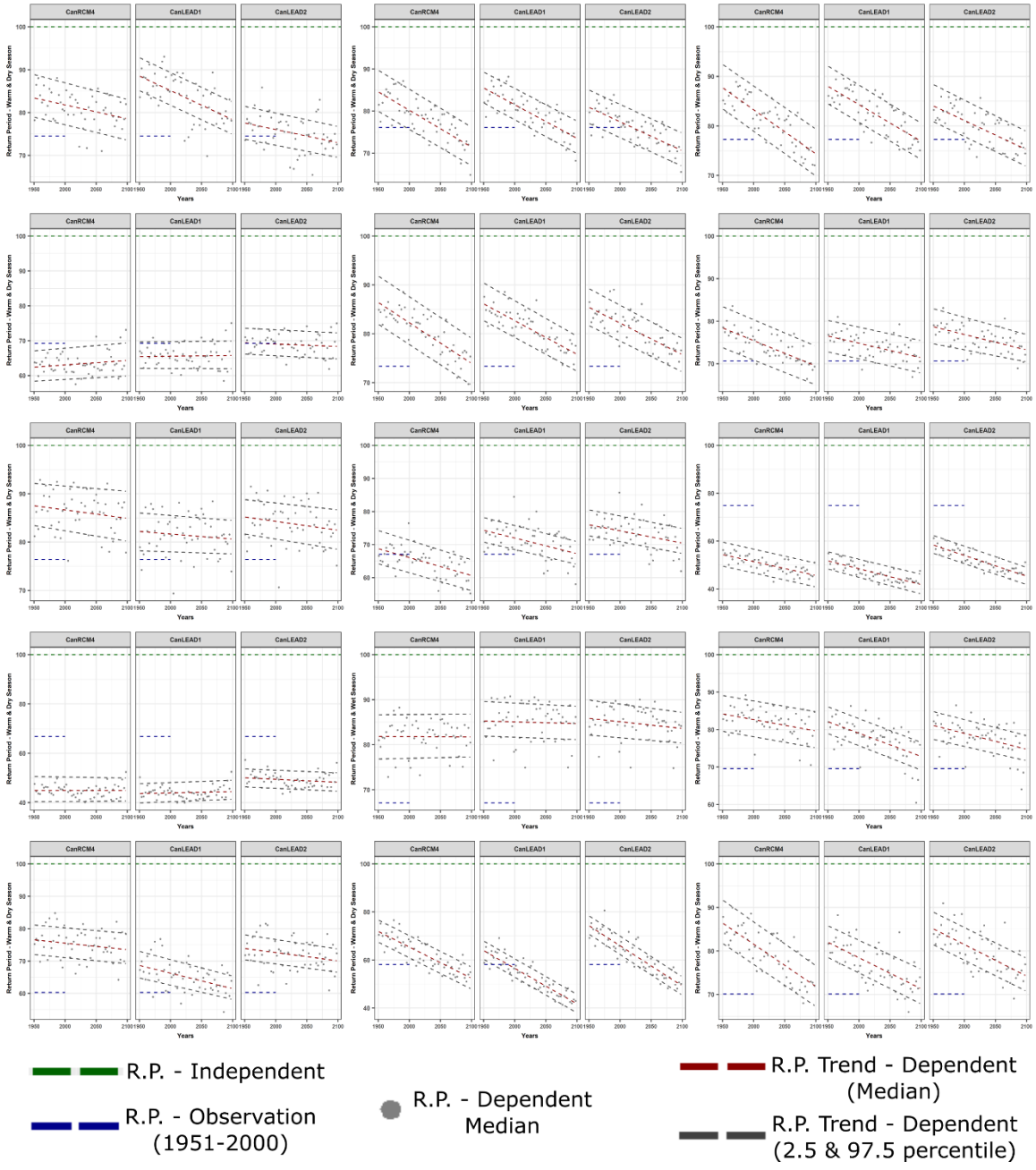

Figure 63 - The figure shows the return periods calculated under different scenarios for a temperature-precipitation compound event in summer season for each zone (1-15, sorted row-wise). See caption of figure 61 for further details.

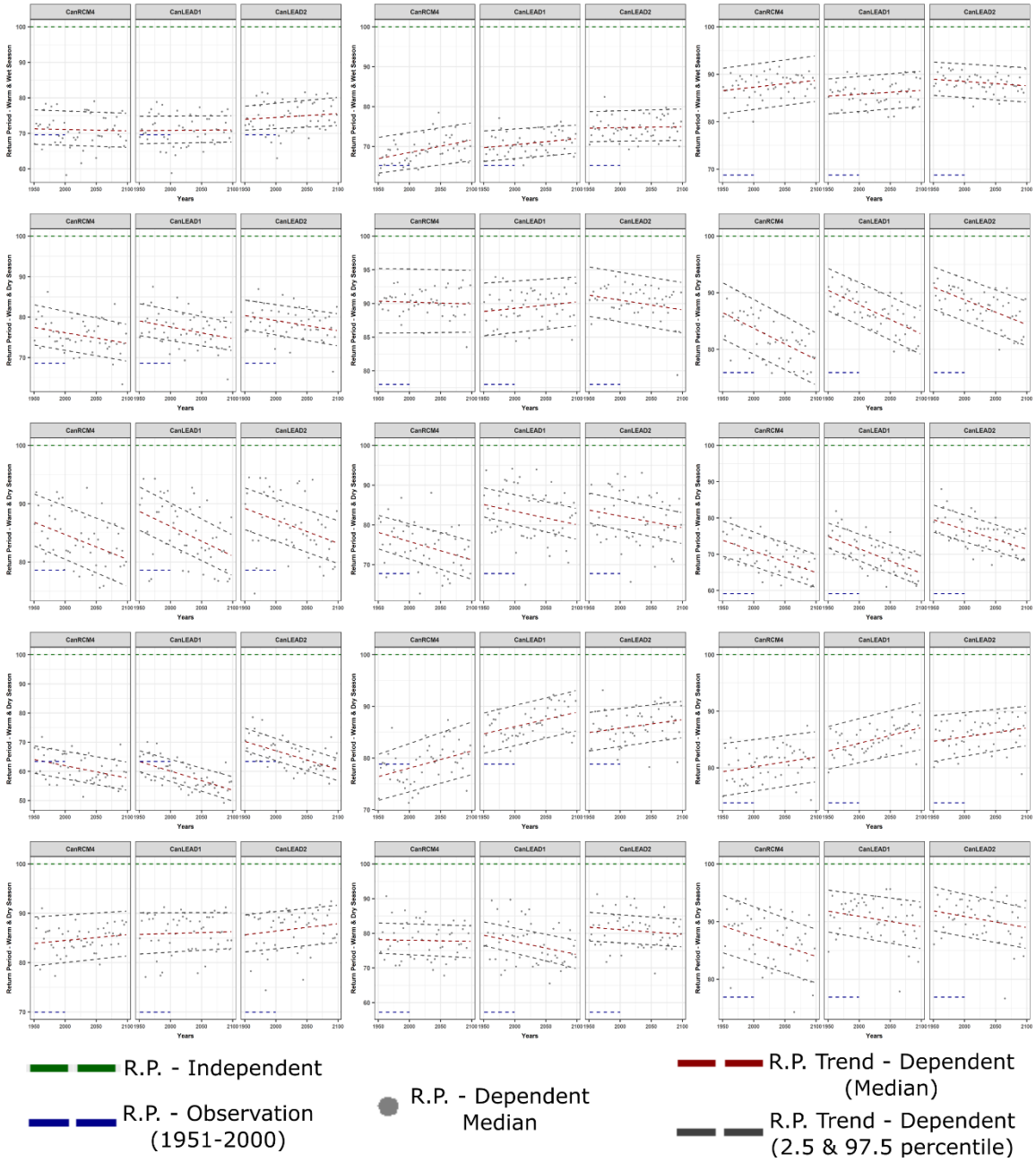

Figure 64 - The figure shows the return periods calculated under different scenarios for a temperature-precipitation compound event in fall season for each zone (1-15, sorted row-wise). See caption of figure 61 for further details.

Appendices - Codes

Most of the code for this dissertation was written in R programming language. Some prominent sections of the code (excluding initial stages of data cleaning) are available at the following location https://github.com/HarrySng/Front_End.

HARSIMRENJIT SINGH

EDUCATION

M.E.Sc. - Environmental and Water Resources Engineering (2019). Western University, London, ON.

B.Tech. - Civil Engineering (2014). Guru Nanak Dev Engineering College, Ludhiana, India.

RESEARCH

Publications

1. ***Characterizing the Dependence Structure between Temperature and Precipitation over Canada***
    - Status: Accepted - Theoretical and Applied Climatology.
    - Analyzed non-linear interactions between temperature and precipitation at 108 locations over Canada using copulas under a stationary as well as non-stationary framework.

2. ***Inter-comparison of Gridded Datasets over Canada: A Univariate and Bivariate Perspective***
    - Status: Submitted – Journal of Hydrology.
    - Comparison of five gridded products over Canada including characterization of bivariate structure using copula goodness of fit test.
    - Presented the importance of preserving correlation structure by comparing outputs from RAVEN hydrologic model forced with univariate and multivariate bias correction of input data.

3. ***Projections of Temperature and Precipitation across Canada Based on Large Ensembles of Regional Climate Simulations and a Hierarchical Bayesian Approach***
    - Status: Submitted for internal review.
    - Used three large ensembles (CanRCM4) and two CanLEAD products (multivariate bias corrected versions of CanRCM4) to study extreme climate indices across four future warming scenarios.
    - Performed validation of joint projection of temperature and precipitation from ensembles against NRCANmet using a Hierarchical Bayesian model.

4. ***Non-Stationary Return Periods of Compound Extreme Events over Canada: A Large-Ensemble Pooling Approach***
    - Status: Submitted for internal review.
    - Use of non-stationary copulas to generate joint return periods for compound events.
    - Accounted for uncertainty across ensemble using block maxima pooling and uncertainty in correlation structure using Bayesian methods.

5. ***Projection of rain-on-snow events over Liard Basin in Canada***
    - Status: Results generated. Manuscript in progress.
    - Comparison of rain-on-snow events across several climate models, including outputs from a VIC model.

6. ***Analyzing extremes in univariate and multivariate bias corrected CMIP5 ensembles***

- Status: Results generated. Manuscript in progress.
- Univariate and Multivariate bias correction of 10 CMIP5 ensembles and subsequent analysis of effect of bias correction methods on compound indices.

Conference Presentations

1. **American Geophysical Union, Fall 2018:**
   - *Characterizing the Dependence Structure between Temperature and Precipitation over Canada*
2. **International Union of Geodesy and Geophysics, Montreal, 2019:**
   - *Validating gridded datasets over Canada: A univariate and bivariate perspective.*

COMPUTING EXPERTISE

1. *Data Analytics*
   - Analyzed over 30 TB of data in two years of M.E.Sc. research projects.
   - Expert knowledge of majority climate data tools, libraries and packages.

2. *Programming*
   - Professional expertise in R, Python, MATLAB, Shell scripting and SQL.
   - Intermediary knowledge of Julia, JAVA and C++.
   - Written over 300 scripts in previous two years of research.
   - Familiar with Git version control.

3. *Cluster Computing*
   - In depth knowledge of high performance computing (HPC) on Sharcnet as well as AWS platforms.
   - Helped colleagues in several side-projects on code optimization and efficient resource usage.

4. *GPU Computing*
   - Setup a CUDA enabled NVIDIA TITAN-V GPU for research team on Linux workstation.
   - Reduced script run times drastically (up to 80 times for low memory, high iteration matrix operations) using PyCUDA.

5. *Server Administration*
   - Setup a Linux workstation for research team from scratch including parallel login capabilities, testing/production environment setups and security protocols.

6. *Database Administration*
   - 1.5 years of experience in handling Oracle Relational Database Systems (RDBMS).

7. *Web Development*
   - Deployed three R based web application for presenting results during M.E.Sc.
   - Experience with web hosting services and tools including intermediary knowledge of CSS.

STRENGTHS

- Western University's engineering heat runner up and top 20 Finalist in "3 Minute Thesis" competition.
- University gold medalist and provincial bronze medalist in public speaking event (India).
- Participant in Model United Nations (Environmental Committee) organized by Ryan International Schools in New Delhi, India, 2008.
- Experience of working in a projectized environment. Completed a certified course in Project Management (PMP) and taking the Certified Associate in Project Management (CAPM) examination in Dec'19.

PROFESSIONAL EXPERIENCE

Graduate Teaching Assistant (Sep'18 – Dec' 19)
Western University, London, ON.

Jr. Solution Engineer (May'15 – Sep'17)
ANR Software Pvt. Ltd., Noida, India